# CORRELATING MATERIAL PROPERTIES TO MATRIX CONSTITUTION IN PORCINE ARTICULAR CARTILAGE

A DISSERTATION SUBMITTED TO THE UNIVERSITY OF OXFORD


IN PARTIAL FULFILMENT OF THE REQUIREMENTS FOR THE DEGREE OF

**DOCTOR OF PHILOSOPHY**

**Monica Armengol**

Wolfson College

Department of Engineering Science

Univeristy of Oxford

Trinity Term 2014

Supervisors:

Prof. Richie Gill

Dr. Philippa Hulley

Prof. Andrew Price

Dr. Hua Ye

# ABSTRACT


**CORRELATING MATERIAL PROPERTIES TO MATRIX CONSTITUTION IN PORCINE ARTICULAR CARTILAGE**

**Monica Armengol** **Doctor of Philosophy**
**Wolfson College** **Trinity Term 2014**

Osteoarthritis (OA) is one of the most common musculoskeletal diseases, mainly affecting people over the age of 60. This disease has multiple symptoms which include wear and loss of articular cartilage and debilitating pain. Its initiation and progression is not well understood and, at the moment, there is no cure. It is important that efforts are made to understand OA because as global life expectancy increases, diseases which affect the ageing population will become more predominant. However, before it is possible to understand what happens to cartilage in the diseased state, the interaction of cartilage structure, mechanical properties and external stimuli in healthy cartilage must be characterised first.

The knee joint is commonly affected by OA. Knee OA is often unicompartmental (UKOA), occurring in either the medial or lateral compartment alone. The location of the lesions in UKOA has been observed to be very repeatable among patients. We believe that this could be explained by variations in cartilage properties over articular surfaces coupled with loading patterns.

The distribution of material properties, glycosaminoglycans(GAG) concentration and cartilage thickness in healthy cartilage on six porcine tibial plateaux were examined. Approximately 1000 measurements were taken of *in-situ* mechanical properties of articular cartilage-on-bone through indentation using a novel mechanical testing machine on whole specimens. The Whole Articular Surface Indentation Machine (WASIM) possesses 5 degrees of freedom (DOF) and allows the interchange of several probes such as an indenter (hemisphercal with 1.35 mm radius), high resolution laser and ultrasound (US). The three dimensional geometry of articular surfaces were obtained by laser scanning. Routines were developed to analyse this topography, automatically calculate the surface normals and then rotate the specimen relative to the indenter; normal indentation was performed at every test point (displacement controlled, 10 percent per second (pps) strain rate). GAG concentrations in cartilage plugs (4 mm) were obtained using DMMB and an imaging method which combined a cationic contrast agent with fluoroscopy.

Mechanical properties (elasticity modulus) were found to vary between 1 and 40 MPa depending on the spatial location of the test points on the articular surface. The differences in elasticity moduli between regions on the tibial plateaux correspond to the position of the meniscus and load-bearing areas. Central areas on each tibial compartment were found to have the highest stiffness, while peripheral areas, as well as

areas uncovered by the meniscus were found to have a lower stiffness. Concentrations of GAG were found to be between 1 and 20 $\mu$g/mg depending on the location of test points. Overall, results showed heterogeneous distribution of elastic modulus, GAG concentration and cartilage thickness in terms of their spatial location over the tibial plateaux. Repeatable patterns were observed between all of the six tested specimens. These patterns were correlated to the position of the menisci, which lead to grouping parameters in regions. Region analysis showed inverse correlations ($r$) between GAG concentration and elastic modulus (-0.1$<r<$-0.6), and direct correlation between GAG concentration and cartilage thickness (0.1$<r<$0.6) across specimens. Finally, an analysis of the gradient changes in the mechanical properties over the tibial plateaux showed that steep gradients (i.e. relatively large changes in stiffness) occurred in locations that are associated with UKOA lesion locations in human joints.

This work provides insight into the variation, distribution and correlation of mechanical properties, GAG concentration and cartilage thickness in healthy cartilage. Additionally, a testing device which can automatically scan and rotate uneven surfaces to allow normal indentation was introduced. This machine has the potential to measure mechanical properties and biological composition at the same test points in whole specimens, and therefore create distribution maps of different parameters.

Further work needs to be carried out on healthy human articular cartilage to assess whether similar patterns are found. Also, implementation of these methods can be used to assess deterioration at different stages of disease.

# ACKNOWLEDGEMENTS

I would like to thank my supervisors Prof. Richie Gill, Prof Andrew Price, Dr. Phillipa Hulley and Dr. Hua Ye. Prof. Gill, was always very thorough and determined to produce good science. Prof. Price, always made sure not to forget the big picture and the practical applications of the work. Dr Hulley, thank you so much for your patience, for the commitment, for showing me the world of biology and biochemistry and your optimism and continuous encouragement. Dr. Hua, my link to Engineering Science, thank you for wise words when I needed them. I will be eternally grateful to you all for the opportunity you gave me. For believing in me and for all the help you provided along the way.

I would also like to thank Dr. Elise Pegg and Dr. Stephen Mellon, for always being incredibly generous with their time and willingness to always share their knowledge. Thank you so much for your friendship, I wouldn't have been able to do it without you.

I would also like to thank Dr. Cameron Brown, for his help with the indentation machine.

Thank you for all those people that supported me in one way or another, and who made the whole experience better; thank you to Isuara, Annie, Jennifer, Catriona, Anneke, Mona, Anthony, Raj, Mike and Rafael. Special thank you to Barbara and Jo who always made sure I was ok and helped wherever and whenever they could.

Thank you to my parents, who have always inspired me and raised me to believe I could do anything and accomplish whatever I wanted. You will always be an inspiration to me.

Last but not least, thanks to God for helping me complete this work successfully.

# Contents

# List of Figures

# List of Tables

# LIST OF ABBREVIATIONS

| | |
|---|---|
| ACL | Anterior Cruciate Ligament |
| ANOVA | Analysis of variance statistical test |
| AOI | Area of Interest |
| BMI | Body mass Index |
| ChS | Chondroitin Sulphate |
| CS | Coordinate System |
| CT | Computer Tomography |
| CV | Coeficient of Variation |
| CA4+ | Contrast Agent with 4 Positive Charges |
| DMMB | 1,9-Dimethylmethylene Blue |
| DOF | Degrees Of Freedom |
| ECM | Extracellular Matrix |
| GAG | Glycosaminoglycans |
| ICP | Iterative Closest Point |
| JSW | Joint Space Width |
| MMR | Modified Michigan Regions |
| MR | Michigan Regions |
| MRI | Magnetic Resonance Imaging |
| NDORMS | Nuffield Department of Orthopaedics Rheumatology and Musculoskeletal Sciences |
| OA | Osteoarthritis |
| OOEC | Oxford Orthopaedic Engineering Centre, located at Botnar Research Centre in the Nuffield Orthopaedic Centre, Oxford University. |
| P - h | Force-Displacement |
| PG | Proteoglycans |
| ROI | Region Of Interest |
| $R^2$ | Coeficient Of Determination |
| SD | Standard Deviation |
| SSE | Sum Square Error |
| UKOA | Unicompartmental Knee OA |
| US | Ultrasound |
| $\mu$CT | micro Computer Tomography |
| WASIM | Whole Articular Surface Indentation Machine |
| WHO | World Health Organization |
| 2D/3D | Two/Three dimensional |

# LIST OF SYMBOLS

| | |
|---|---|
| a | Radius of contact |
| $A_c$ | Area of contact |
| b | Constant from unloading curve determined by curve fitting |
| $E^*$ | Effective elastic modulus |
| $E_1$ | Elastic modulus of the sphere |
| $E_2$ | Elastic modulus of the indenter |
| $E_{adj}$ | Adjusted elastic modulus |
| $\epsilon$ | Constant dependent of indenter geometry |
| h | Displacement |
| $h_{max}$ | Maximum displacement |
| $h_c$ | Contact displacement |
| $h_c$ | Displacement at contact |
| $h_f$ | Final displacement |
| $h_r$ | Residual displacement |
| $I$ | Found as subscript meaning: at/of the indenter |
| LSF | Least-square fit |
| m | Constant from unloading curve determined by curve fitting |
| $\hat{N}$ | Normal vector |
| $\hat{N}_{1_{XZ}}$ | X, Z components of Normal vector 1 ($\hat{N}_{1_{XZ}} = \left\{ \begin{array}{c} X_{N_1} \\ Z_{N_1} \end{array} \right\}$) |
| $\hat{N}_{XY}$ | X,Y components of the Normal vector ($\hat{N}_{XY} = \left\{ \begin{array}{c} X_N \\ Y_N \end{array} \right\}$) |
| $\hat{N}_1$ | Normal vector $\hat{N}$ rotated by $\Theta$ |
| $\hat{N}_2$ | Normal vector $\hat{N}_1$ rotated by $\Phi$ |
| $O_i$ | Origin at i |
| P | Force |
| $\Phi$ | Pitch angle |
| $P_{max}$ | Maximum force |
| Q | A given point |
| R | Radius of indenter |
| S | Stiffness |
| $T$ | Found as subscript meaning: at/of the pitch |
| $\tau$ | Time required to reach 65% of maximum attenuation |
| $\Theta$ | Yaw angle |
| $\nu$ | Poisson's ratio |
| $\nu_1$ | Poisson's ratio of the sphere |
| $\nu_2$ | Poisson's ratio of the indenter |
| $W$ | Found as subscript meaning: at/of the WASIM |
| $Y$ | Found as subscript meaning: at/of the Yaw |
| $\hat{X}$, $\hat{Y}$ and $\hat{Z}$ | Unit vector in X, Y, Z axis |

# Chapter 1

# INTRODUCTION

According to the World Health Organization 2012 [4], between the years 2000 and 2050 the world population over the age of 60 will double (from 11% to 22%). This growth in ageing population, due to medical advances and improvement in general quality of life, will translate into an increase in the demand for treatments and medical attention for diseases associated with advanced age.

Osteoarthritis (OA) is a very common disease estimated to affect approximately 10% of men and 18% of women over the age of 60 [5]. Moreover, OA was classified as the 10th leading global cause of non-fatal disease burden in 1990 [6]. OA of the knee, in particular, is a major cause of mobility impairment; up to 40% of the population over the age of 70 suffer from OA of the knee. Almost 80% of these patients have some degree of limitation of movement and 25% cannot perform major daily activities of life [7]. In the future, as the population ages and life expectancy increases, OA is likely to become a larger public health problem and it is predicted to become the fourth leading cause of global disability by the year 2020 [5].

OA most commonly becomes symptomatic when the disease is in an advanced stage. Therefore, by the time it is clinically relevant, the most common option the patient has for pain relief is a joint replacement [8, 9]. In 2007, Kurtz *et al.* projected an increase in total knee arthroplasties of 673% by 2030 [10]. To place this in context, in 2007 there were approximately 66,000 primary knee replacements in the UK according

to the National Joint Registry [11], therefore, according to Kurtz *et al.*, 444,000 knee replacements will be carried out in the year 2030. Considering the cost of the operation and treatment, as well as the years of disability that lead up to surgery [8], the exponential increase in the demand for hip and knee replacements will not be viable for economies and societies. Thus it is important to develop methods to identify and treat OA at the early stages when it is more likely to control its progression.

The solid portion of the extracellular matrix (ECM) is composed of PG and collagen. Both structures interact to provide cartilage with its mechanical properties. Nevertheless, proteoglycan (PG) plays a key part in compression [12, 13, 14], while when compression is applied perpendicular to the surface in healthy cartilage the role of collagen is minor [15, 16].Moreover, proteoglycan (PG) degradation has been identified as a change that occurs in early stages of OA [17]. Literature suggests that cartilage adapts to external stimulus [18, 19, 20, 21] throughout life. A heterogeneous distribution of mechanical properties and thickness has been reported in articular cartilage [19, 22]. Moreover, a relationship between mechanical properties and GAG concentration in articular cartilage has been found [23, 24] and GAG concentrations change in response to external stimuli [20]. These facts suggest that there may be a difference in the response to load between regions over the tibial plateau. Moreover, it is possible that if there is a sudden shift in loading to areas not adapted to high load, it could initiate a process of cartilage deterioration. Such sudden shifts occur as a result of injury to the soft tissue that support the joint, for example, the cruciate ligaments.

Researchers have reported that in isolated medial and lateral unicompartmental knee OA (UKOA), the wear of cartilage and lesions have distinct patterns and these are highly repeatable [25, 19, 22]. In isolated medial knee OA, erosion of cartilage at the tibial plateau occurs in reproducible patterns with the lesion localized anteromedially. Similarly, isolated OA in the lateral compartment exhibits a reproducible pattern and the disease progresses with a more posterior lesion [25]. Taking into account heterogeneity of articular cartilage, it is probable that these patterns occur as a combination of variations in mechanical properties, cartilage structure and external stimuli.

An understanding of the distribution of variables (mechanical properties, GAG concentration and cartilage thickness) over the healthy tibial plateau is fundamental in order to understand the interactions between them that could be involved in the initiation of OA pathways.

***Research Proposal***

Hirsch [26] was one of the first authors to study the correlation between the matrix structure and mechanical properties. In 1944, he observed that macroscopically damaged cartilage was softer than normal cartilage and had less GAG [26]. Years later, Kempson *et al.* demonstrated the correlation between GAG and stiffness, and studied topographical variation of stiffness in the femoral head [27]. The variation of material properties throughout the articular cartilage were acknowledged by some authors [23, 28, 29, 30, 31]. However, Maroudas *et al.* found insignificant topographical differences in GAG content in the femoral head [32]. In 2001, Appleyard *et al*, studied the performance of a handheld indenter [28], measuring the dynamic shear modulus, static force and thickness of bovine tibial plateau in 18 locations over six knees [28]. In this thesis protocols were developed to test mechanical properties using a novel indentation testing device with the specific advantages of 5 degrees of freedom and the ability to automatically indent normal to the surface at any position on a whole articular surface. To the author's knowledge there are no studies that map distribution of thickness, GAG content and elastic modulus in a porcine tibial plateau. Additionally, this thesis presents a method to produce these measurements in a non-destructive way with a contrast agent that binds directly to PG, rather than using an inverse proportionality. Finally, repeatable patterns in degradation lesions have been observed in the femoral head [27, 31] and in the knee [25], however these authors did not provide an explanation. Based on the results of my research an explanation of the repeatable patterns of OA lesions is proposed, based on matrix and mechanical property distribution.

The aim of this work was to explore the detailed distribution of cartilage biological (GAG concentration), mechanical (elastic modulus) and physical (cartilage thickness) properties over the tibial plateaux. It was hoped that by studying the interaction between these properties some insight into the initiation of OA and specifically UKOA

lesion location could be obtained.

The specific aims of this theses were to:

- Set up WASIM and develop routines necessary to carry out mechanical tests.
- Establish the distribution of mechanical properties (elastic modulus) and articular cartilage matrix constitution (GAG concentration) over whole tibial plateaux.
- Assess correlations between measured variables.
- Analyse whether the interaction between measured variables could be associated with known UKOA lesion location in human knees.

***Structure***

Chapter 2 gives an overview of the anatomy of the knee, osteoarthritis, imaging methods and contains a literature review of previous studies that have examined matrix and material properties of cartilage. Chapter 3 describes the unique testing machine used to obtain the mechanical properties and the routines developed to measure them. Chapter 4 describes the methodology followed to carry out the experiments. Chapter 5 presents the analysis of elastic modulus, cartilage thickness and GAG concentration distribution with statistical analysis of their distribution over six tibial plateaux. Chapter 6 examines the correlations between measured variables as well as the correlation of their distributions over all tested specimens. This chapter also provides insight into how the distribution of material properties and if changes in the distribution could be associated with UKOA lesion location. Lastly, in Chapter 7 the general conclusions of the thesis are provided along with an outline of future work.

# Chapter 2

# BACKGROUND

In this chapter a brief review of the knee anatomy and its components and the different methods commonly used for mechanical testing of soft tissue is presented. Additionally, OA characteristics at different stages of the disease and common methods for OA detection are discussed.

## 2.1 Knee Internal Structure and Anatomy

The knee is the largest joint in the body. It is formed by three bones: the femur, the tibia and the patella (knee cap). It is held together by the collateral and cruciate ligaments which provide stability. Tendons bind muscles to bone and connect the knee bones to the leg muscles to allow movement.

The knee is commonly divided into three compartments: the medial compartment, on the side closer to the centreline of the body, the lateral compartment on the outside half of the body and the patellofemoral compartment, which is the area behind the knee cap. The medial compartment is slightly bigger than the lateral compartment in humans, and it has an slightly concave shape. On the other side, the lateral compartment is flat or convex. These compartments are separated by the tibial eminence where the cruciate ligaments attach to the tibial plateau (Figure 2.1).

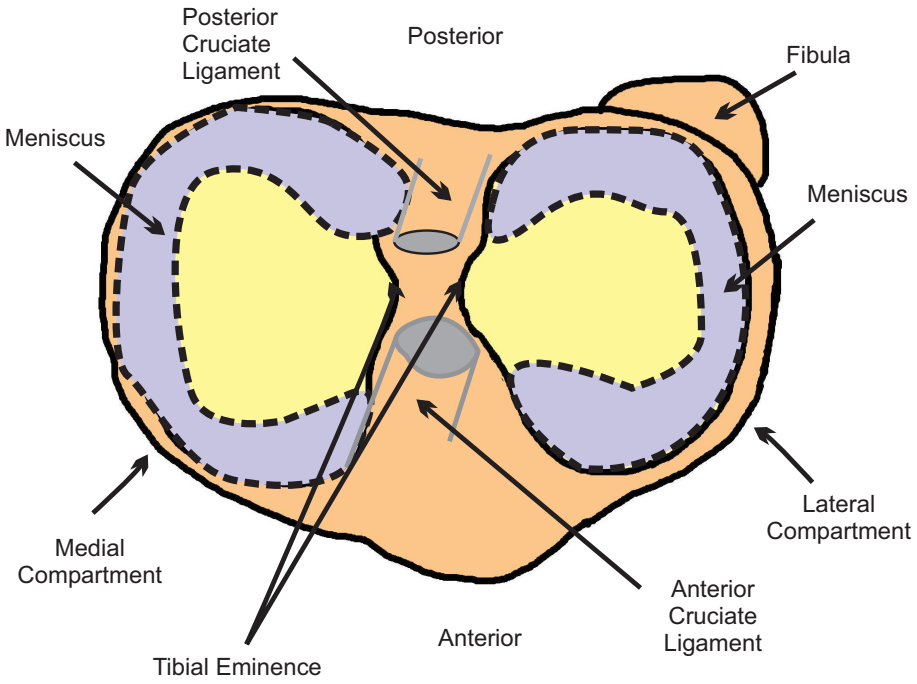


**Figure 2.1:** Axial view of human tibial plateau.

## 2.2 Soft Tissue

The 'soft tissue' are the different structures that surround the bones in the body, these include tendons, ligaments, fat, skin, cartilage, meniscus. This section introduces four soft tissues relevant to the knee; the menisci, ligaments and tendons, and the main focus of this thesis, the articular cartilage.

### 2.2.1 Menisci

The menisci are semi-lunar shaped fibrocartilaginous structures that, in humans, are found between the cartilage of the knee joint [33]. The meniscus mechanical properties allow load bearing, distribution and absorption [3, 33, 34]. Fukubayashi and Kurosawa, found that the medial meniscus provides stability to the joint while the lateral meniscus plays an important role in load bearing [3]. They demonstrated that upon removal of the meniscus, the cartilage contact area decreases while cartilage contact pressure significantly increases [3].

Biochemically, the meniscus has a similar composition to cartilage. It consists of a combination of interstitial water, which constitutes 60-70% of the total weight and a solid structure predominantly composed of collagen, proteoglycan (PG), and meniscal

cells called fibrochondrocytes [33].

### 2.2.2 Ligaments and Tendons

Ligaments and tendons are fibrillar connective tissues. Tendons and ligaments are very similar in structure and composition, the main differences between them are their location and function. Ligaments connect bones while tendons tend to be stiffer and connect bones to muscles [35]. These soft tissues consist of 60-70% water (total weight), with a high content of an organized collagen fibril network and PG [33].

Mechanically, the main function of tendon is to transform the muscle contraction into movement [35]. Ligaments, on the other hand, limit movement in certain directions or planes [35] to provide stability of joints.

### 2.2.3 Cartilage

Cartilage is found in different forms in the body. These forms are classified according to their composition as articular (or hyaline) cartilage, elastic cartilage and fibrocartilage [36, 37]. Elastic cartilage is responsible for maintaining the shape of structures, and it is composed of elastic fibres which provide flexibilty. It is normally found in the ear and the trachea [36]. Fibrocartilage is the strongest type of cartilage and it is normally found between joints with limited movement such as invertebral disks [36]. Finally, articular cartilage is found at the ends of the adjacent bony segments that form synovial joints [36].

Articular cartilage is a smooth, glossy and semi-transparent material. As a biomaterial, articular cartilage is heterogeneous, anisotropic and multiphasic [38]. Biochemically, articular cartilage, is composed of cells called chondrocytes (5-10%) and the extracellular matrix (ECM) (90-95%) [33, 39]. About 70-85% of the total weight of the ECM is water, the remaining 15-30% is a combination of proteoglycan (PG) and collagen (type II) [36]. Mechanically, it gives the synovial joint surface load distribution properties and low friction [36].

Articular cartilage is avascular, alymphatic and aneural, the levels of oxygen in cartilage are very low compared to other tissues such as bone and muscle [40, 41]. Therefore,

it receives most of its nutrients from the synovial fluid and the capillary beds of the subchondral bone [41].

Articular cartilage has mechanical properties which facilitate almost frictionless movement providing synovial joints with very low wear. Additionally, hyaline cartilage allows load distribution and is resilient to compressive load [42].

#### 2.2.3.1 Articular Cartilage Zones or Layers

In cross-section four distinct layers can be found in articular cartilage (Figure 2.2) [40, 43, 44, 45]. These layers have significantly different properties. A number of authors have reported on the depth variation in properties of articular cartilage [45, 46, 47, 48, 49, 50, 51, 52].

1. **Superficial or Tangential Zone:**

   The top zone, which is in contact with the synovial fluid, represents about 10-20% of the total cartilage thickness [40]. The superficial layer has proportionally higher amounts of collagen (aligned parallel to the surface) relative to PG compared to the other layers [52, 53]. This zone contains the highest amount of water, compared to the other layers, and has a relatively larger number of chondrocytes. The chondrocytes have a flattened shape due to osmotic pressure [54]. This layer also synthesizes an endemic protein called superficial zone protein (SZP) [54], which appears to have important lubrication properties [55].

   The superficial layer of the articular cartilage contains the least amount of PG compared to deeper zones [24, 45], and it has the lowest compressive modulus [46]. This zone has the smallest Poisson's ratio so undergoes the smallest expansion when subjected to compressive strains [45, 51, 56, 57].

   The superficial zone architecture provides it with the ability to act as a physical barrier to large molecules [43]. This zone is the most exposed to compressive strain and load [58], however this zone has the highest tensile modulus of articular cartilage [56, 59, 60]. Early features of OA, such as GAG loss [32, 48] are normally apparent in this zone exclusively [48, 59]

2. **Transitional or Middle Zone:**

   This is the largest layer in the articular cartilage. It is located between the superficial and deep zones and it represents 40-60% of total cartilage volume [40]. The middle zone contains PGs and collagen fibrils randomly arranged [53, 43, 52]. A low density of chondrocytes are found in the middle zone and they have a spherical shape [40].

3. **Radial or Deep zone:**

   This zone constitutes about 30% of total cartilage volume [40]. The collagen fibrils in this zone have the greatest diameter and are orientated perpendicular to the subchondral bone [53, 55, 61]. These provide the highest resistance to compressive loads in articular cartilage [62]. The main function of this zone is load distribution throughout articular cartilage [55]. This zone has the greatest amounts of PG and the lowest concentration of water [55]. Chondrocytes found in this zone are organized in columns perpendicular to the cartilage surface [52, 63].

4. **Tidemark:**

   The tidemark separates all previous zones from the subchondral bone. The tidemark indicates the transition to calcified tissue [40].

#### 2.2.3.2 Articular Cartilage Components

The components that constitute articular cartilage play an important role in preserving its properties over a lifetime, despite constant repetitive static and dynamic loads [38, 39].

1. **Chondrocytes**

   Chondrocytes are a highly specialized type of cell only found in articular cartilage. They constitute approximately 5-10% of the volume of adult human articular cartilage [36]. Chondrocytes do not have a blood supply and rely on anaerobic respiration in order to survive in an environment with almost no oxygen [63]. The most important nutrients are obtained from synovial fluid [63].

   Chondrocytes play an important role in the repair and maintenance of the artic-

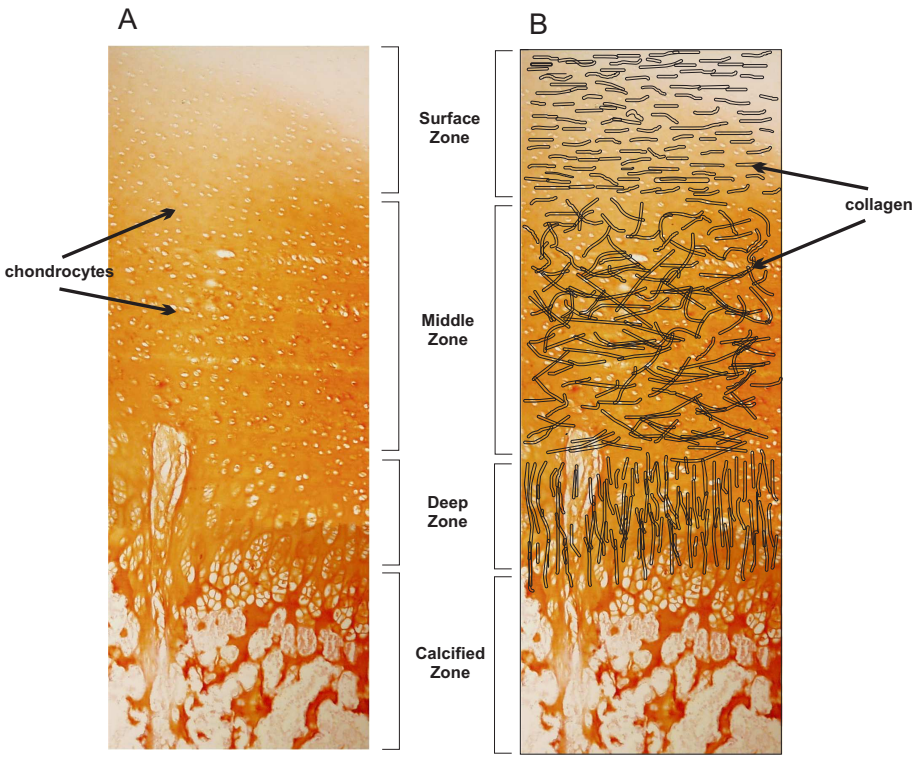


**Figure 2.2:** Optical micrograph of cross-section of normal porcine articular cartilage. A. Organization of cells throughout the articular cartilage zones. B. Sketch of the alignment of collagen fibrils superimposed on the cross-sectional view.

ular cartilage. They are tied to a lacuna, which restricts their movement within the ECM. Nevertheless, these cells have the capacity to respond to their environment to maintain the equilibrium within the ECM [64] by reacting to internal and external stimuli [63, 64, 65, 66].

2. **Collagen**

Collagen is a fibrous protein that constitutes about 50-80% of the dry weight and 15-22% of the wet weight of the organic component of articular cartilage [36, 43]. Although cartilage contains many types of collagen, type II accounts for 90-95% of the total collagen forms in the tissue [36, 43, 67]. The mechanical properties of collagen have been studied by many authors [43, 44, 68, 69, 70]. Collagen fibrils are highly organised through the depth of the articular cartilage (Figure 2.2). In the superficial zone, the fibrils are parallel to the subchondral bone. In the deep zone fibrils are oriented perpendicular to the surface and in the middle, the orientation of the fibrils is variable [43, 61, 68]. The fibril alignment and meshwork distribution play an important role in the mechanical properties of articular cartilage, such as resistance to load, and Poisson's ratio

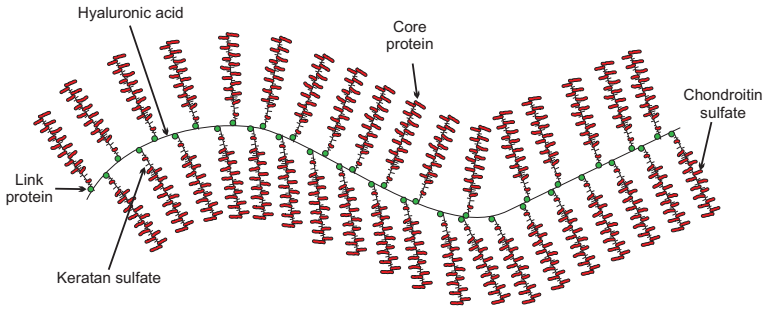


**Figure 2.3:** Aggrecan to illustrate proteoglycan structure

[36, 62, 68, 70, 71].

3. **Proteoglycan (PG)**

   Proteoglycans (PG) constitutes the second largest portion of organic material [36, 43]. PG constitutes approximately 30% of the dry weight of the tissue [36]. PGs are composed of a protein core to which a significant amount of glycosaminoglycans (GAG) (chondroitin sulfate and keratan sulfate) are attached. These structures are polysaccharide chains covalently bound due to their negative change forming aggrecans which exhibit a "bottle brush-like structure" [36, 43, 72] (Figure 2.3). The most common PGs present in articular cartilage are the ones able to form aggregates, which make up to 80-90% of the total amount of PGs [72].

   PG provides cartilage with important mechanical characteristics. The fixed negative charge present in GAG, produce strong repulsive forces between each other, forcing the aggregated molecules to spread out [43, 73, 74]. In solution, this process is magnified and quantified as fixed charged density (FCD) [43], and is responsible for the majority of the swelling. Moreover, this expansion is restrained by the collagen meshwork, creating interstitial pressure within the articular cartilage. This process is an essential contributor to compressive stiffness and load distribution when the tissue is under compression[41, 43, 62, 73].

4. **Tissue Fluid**

   The interstitial space of articular cartilage is occupied by water and positively charged ions (to balance PGs negative charge), gases and small proteins [36, 43, 75]. Water constitutes about 60-85% of the wet weight of articular cartilage

[12, 43, 76, 77, 78] and the proportion of water decreases with the cartilage depth (80-85% in the superficial layer to 65% in the deep layer) [75, 79].

Water is constantly interacting with the macro-structures that surround it. It can be found within the collagen framework, interacting with the PG (repulsion forces) and some is flowing freely within the ECM [43, 75, 79], these interactions define the mechanical properties of cartilage.

## 2.3 Soft Tissue Measurements

### 2.3.1 Poisson's Ratio

Poisson's ratio refers to the ratio between deformation in the perpendicular direction (transversal) and the parallel direction (axial) to the applied load [80, 81]. It can be measured in compression or in tension. In compression it is a negative ratio while in tension its positive, although most of the time it is expressed as an absolute value. Mathematically, it is expressed by Equation 2.1

$$\upsilon = \frac{\frac{\Delta w}{w}}{\frac{\Delta l}{l}} = -\frac{\epsilon_{lat}}{\epsilon_{axi}} \tag{2.1}$$

where $\Delta w$ is the fraction change in the lateral direction, $w$ is the original length of the lateral direction and $\epsilon_{lat}$ refers to the strain in the lateral direction. Similarly, $\Delta l$ is the fraction of change in the axial direction, $l$ is the original length in the axial direction and $\epsilon_{axi}$ is the axial strain [33] (Figure 2.4).

Values of Poisson's ratio (in absolute values) can be found between 0 and 0.5. A Poisson's ratio of zero denotes an extremely compressible material, while a Poisson's ratio of 0.5 indicates an incompressible material [81].

The Poisson's ratio has been determined in many ways. Authors often have used an optical method [68, 82, 83], consisting of a microscope attached to a digital camera, which observes the tissue during unconfined compression [45, 68, 82, 83]. Another frequently used method is curve fitting parameters to experimental results of biphasic indentation analysis obtained through creep [30, 84].

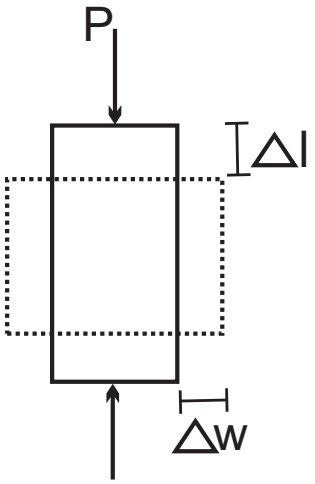


**Figure 2.4:** Poisson's ratio graphical description. P is the force applied, $\Delta l$ and $\Delta w$ are the change in length, and $l$ and $w$ are the original length of each side

Although many studies take Poisson's ratio as a constant value across the tibial plateau, Jurvelin *et al.*, showed that Poisson's ratio values vary topographically [83] and Chegini *et al.*, determined that Poisson's modulus is depth-dependent being the lowest in the superficial layer [56].

A negative correlation between Poisson's ratio and both collagen-to-PG content [83] and the elastic modulus [68] have been reported. Poisson's modulus is also influenced by the orientation of the collagen fibrils in the articular cartilage [68].

### 2.3.2 Permeability

Permeability refers to the fluid flow within and out of the porous tissue [81]. Permeability is associated with the pore size and inversely associated with the resistance of the fluid to flow in and out of the material [81]. Therefore, a material with low permeability normally has small pores with a major resistance to fluid flow. This was described by Mow *et al.* who introduced permeability into their biphasic model as a regulator of fluid velocity [85].

Permeability is not an intrinsic material parameter, on the contrary it has been observed that it is strain dependent [82, 86] and it is correlated with water content [12, 87].

### 2.3.3 Elastic Modulus (E)

The elastic modulus (Young's modulus) refers to the stiffness of a material or the capacity of a material to deform reversibly or non-permanently when a force is applied [88]. Mathematically it is described by the relationship between stress and strain.

Studies on the stiffness of articular cartilage have shown: (1) topographical variations of stiffness over the articular cartilage [26, 27, 68, 83, 89, 90, 91, 92, 93], (2) correlations between stiffness and articular cartilage ECM structure [26, 27, 94, 95] and (3) topographical variations associated with loading patterns [24, 26, 96, 97].

### 2.3.4 Cartilage Thickness

Healthy articular cartilage thickness is reported to be between 1 and 6 mm [40, 98, 99], however it varies between species. Additionally, topographical variations of cartilage thickness within the same joint have been confirmed by many researchers [24, 27, 94, 97, 100].

One of the reasons why thickness has been widely studied is because of its relevance for the calculation of material properties such as stiffness during indentation. However, Lyyra *et al.*, found that when cartilage was thicker than 2 mm, thickness was not relevant in stiffness calculations [101].

There are many ways in which cartilage thickness has been determined; one of the most common methods is using a needle probe [1, 101, 102, 103] or optical methods [103]. In clinical applications radiographic imaging is traditionally used [104, 105], and more recently ultrasound technology has been employed [106, 107].

- **Radiography Imaging:** Medical imaging radiography resources such as Magnetic Resonance Imaging (MRI), Computer Tomography (CT), fluoroscopy and x-ray, have the potential to non-invasively obtain the morphology of cartilage. In MRI, a clear image of soft tissues and bone surface is obtained, therefore cartilage thickness can be measured directly from the image [104]. In CT, fluoroscopy and x-rays, soft tissues are not easily observed [105], however cartilage thickness can be determined using one of two methods: (1) Thickness can be deduced by

measuring the distance between bones of a joint (empty space is occupied by the cartilage). This method is better known as joint space width (JSW). (2) Adding specific contrast agents to the articular cartilage, can allow the observation of soft tissue in the image.

These methods are widely used in the clinical setting, mainly because they are non-invasive and non-destructive methods, therefore they can be performed repeatedly on the same joint [104].The disadvantages are that these methods have a high cost and in some cases, involve exposure to radiation.

- **Needle Probe:** This method consists of attaching a sharp needle to a testing device, which normally has a load cell. The needle must be placed perpendicular to the cartilage surface. The device is capable of detecting the force signals obtained at the cartilage surface and in the tidemark [1]. The difference in displacement between these two measurements corresponds to the thickness (Figure 2.5).

  The puncture of the articular cartilage by needle probe might cause damage to the matrix, altering its internal structure. Nevertheless it has been used by many researches [1, 101, 102, 103] to measure material properties *in vitro*. The way to overcome these problems is to carry out the mechanical tests prior to measuring the thickness. Obviously this method is restricted to *in vitro* testing and normally, it can only be performed once at an specific location on the sample.

- **Ultrasound (US):** Ultrasound consists of a transducer or probe which acts as both the emitter and receiver of pulses. Pulses sent at high frequencies are emitted into the tissue, and travel through the medium in almost a straight line. Due to different acoustic impedances, part of the pulses are echoed back to the probe. The difference between the emitted and receiving pulse allows the reconstruction of an image [1] (Figure 2.5). The measurement of cartilage thickness with US has been done by using A-mode (amplitude modulation) [1, 105, 106, 108, 109] or B-mode (brightness modulation) [1, 106, 107] US at frequencies that go between 7.5 to 12.5 MHz [1, 105, 108, 110]. The cartilage thickness is measured by calculating

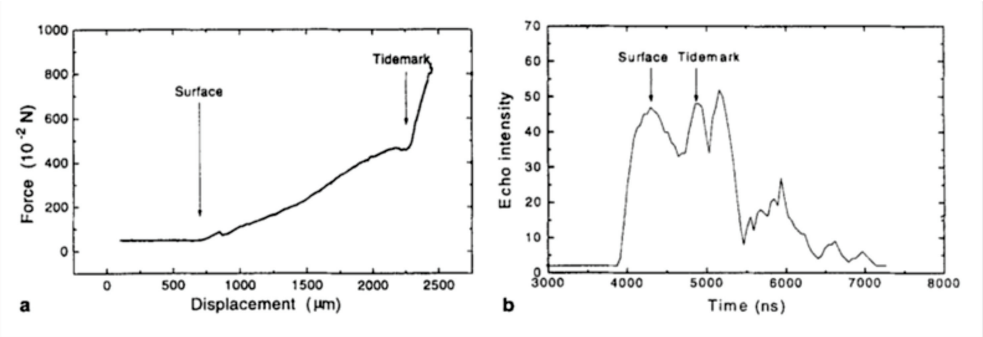


**Figure 2.5:** Results obtained from needle probe measurement and ultrasound measurements. Arrows indicate peaks that mark cartilage surface and tidemark. This figure was reproduced with permission of Elsevier [1].

the time delay between echoes assuming the speed of sound through cartilage is constant. The first echo corresponds to the cartilage surface and another one corresponds to the tidemark [1].

This method is a non-destructive and cost-effective technique [105, 110]. The accuracy of the method is dependent upon the perpendicular positioning of the probe to the articular surface, therefore it has mostly been used *in vitro*. Also there might be errors in the calculation due to the assumption of the speed of sound through cartilage [1].

- **Optical:** The optical method consists of measuring cartilage thickness in plugs or slices with the aid of a microscope and sometimes staining [1, 108]. Once again the section or plug should be taken perpendicular to the surface [1]. Obviously this is a method used exclusively in *in vitro* settings. Nevertheless, even in *in vitro* settings, damage to ECM structures may alter cartilage properties [1].

Even though the methods presented for the measurement of cartilage thickness are quite different, Jurverlin *et al.*, found a correlation between the thickness measured using needle probe and optical methods (3.5% difference) [1]. Reports on thickness measurements carried out using an ultrasound probe show conflicting results [1, 107, 111, 112, 113].

## 2.4 Mechanical Testing of Soft Tissue

The mechanical properties of soft tissue are important to understand the behaviour of cartilage and its response to external stimuli. Common tests to obtain the material properties are compression and tensile tests.

### 2.4.1 Compression Tests

Static compressive loading is one of the most common mechanical tests performed on knee cartilage. These tests are particularly relevant because the knee joints are subjected to compressive forces when performing daily activities such as walking and running [33]. Thus common compression tests are confined compression and unconfined compression.

#### 2.4.1.1 Confined Compression

Confined compression is commonly used to measure material properties in articular cartilage [12, 45, 81, 90, 114]. The test set up consists of an impermeable well or a sealed chamber, where a cartilage plug is placed. The load is applied to the plug through a porous plate [36] (Figure 2.6). This type of test restricts the movement and the interstitial fluid flow uniaxially through the porous surface or filter [90]. Material properties in confined compression are normally obtained through time-dependent tests such as creep and relaxation [36].

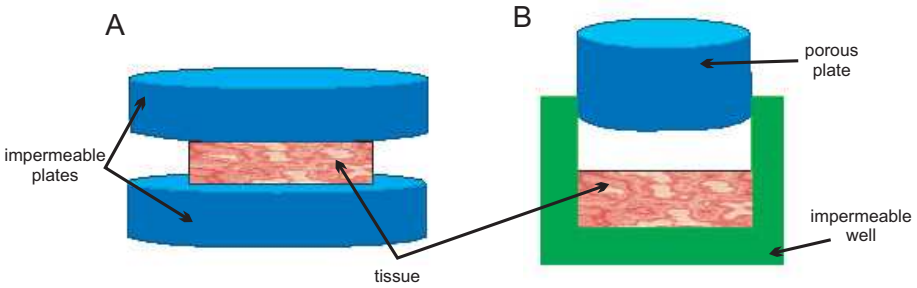


**Figure 2.6:** Schematic of A.unconfined and B.confined compression tests

Confined compression has been used to measure the equilibrium modulus [12], permeability [12], elastic bulk modulus [114] as well as other properties.

#### 2.4.1.2 Unconfined Compression

This test was initially used in the soil mechanics field and later was extended into other research areas. Unconfined compression involves compressing a cartilage plug through two impermeable plates (one placed at the bottom and the other at the top). This allows interstitial fluid to flow in the lateral direction [33]. This test is commonly used to obtain the Poisson's ratio [68, 83, 96]. Stress relaxation and creep tests are also commonly performed in this manner.

Many researchers use a combination of confined, unconfined and indentation tests [45, 90] to obtain soft tissue parameters (elastic modulus, aggregated modulus and Poisson's ratio).

### 2.4.2 Indentation

Indentation testing can also be used to measure material properties [47, 83, 115, 116, 117, 118, 119, 120]. The advantages of this method are: (1) unlike other mechanical tests (tensile and confined and unconfined compression), indentation does not require meticulous preparation and/or mounting of the sample [81, 121]. While in confined and unconfined compression undamaged plugs must be extracted from the articular cartilage, and in tensile tests, thin micro-slices must be obtained; in indentation tests the material properties can be measured *in situ* by testing the whole sample while attached to the subchondral bone [81] which is a great advantage [30]. This allows the measurement of material properties in a setting that resembles the normal environment [81], therefore better representing normal response [81]. (2) Indentation tests can be performed in different material volumes. They can test nano-scales [118, 122, 123, 124] and bulk materials [120, 125], by choosing a different tip size and the appropriate load. The load can go from kilo-newton to micro-newton by choosing the right instrumentation. (3) Indentation can be used in an *in vivo* setting during arthroscopy [28, 101, 126].

The output of a typical indentation test is displacement and force during a set amount of time. Normally, one of these parameters is controlled as an input and the other

becomes the output [33]. Therefore, there are two types of indentation tests:

- **Load Controlled Indentation:**

  A constant load or force is applied for a specific period of time and deformation is recorded. The time-dependent nature of articular cartilage allows creep stress behaviour to be observed. Normally, at least 1000 s are needed to obtain equilibrium measurements [36].

- **Displacement Controlled Indentation:**

  A constant displacement or displacement rate is applied for a period of time and force is recorded. The time-dependent nature of articular cartilage allows stress relaxation response to be observed.

Nevertheless, there are also problems related to indentation tests. One of the main difficulties with indentation tests is the data analysis, since it is dependent on the tip size, geometry and chosen material model [13, 45, 119, 121, 127, 128, 129]. Moreover, it has been observed that the materials properties (Young's modulus and Poisson's ratio) calculated through indentation are not always comparable to those determined by other compressive (confined and unconfined) tests. In 1977, Parsons *et al.*, pointed out the difficulty in comparing data from independent experiments [13]. Later, Korhonen *et al.*, observed that Young's moduli calculated through indentation tests were 30% higher than those measured through unconfined compression tests, however they attributed this difference to measuring the material properties in intact versus isolated cartilage samples [90]. Additionally, there have been contradictory results with Young's modulus dependence on the indenter's diameter. Jin *et al.*, and Simha *et al.*, found an increase in articular cartilage elastic modulus (tibial murine and patellar bovine) with decreasing indenter size [96, 127], however Simha *et al.*, repeated the experiment in urethane rubber and found size independence, therefore the authors concluded that the size dependency was a characteristic of cartilage due to its inhomogeneity, rather than related to indentation testing [127]. This result was also confirmed by Korhonen *et al.*, who showed that Young's modulus obtained by indentation testing was higher than that obtained by other compression tests [90]. Additionally, they confirmed a dependency on indenter size (except for the humeral cartilage where independence

of indenter size was found) [90]. Stolz *et al.*, proposed a theory on why the material parameters were dependent on the indenter size. The authors suggested that while millimetre size indentation measures bulk material parameters, nanoindentation measures the material properties of nanometre scale structures (PG and collagen organization) [130]. This explanation was consistent with Simha's findings, which established that indentation modulus obtained from large size tips (millimetre scale) was comparable with the modulus obtained from confined and unconfined compression [127]. Finally, indentation values extracted under different loading conditions are often not comparable [106, 121].

Aiming to overcome these problems related to indentation testing of soft tissues, Mow *et al.*, developed a method that determines all three intrinsic material parameters (aggregate modulus, permeability and Poisson's ratio) with a single indentation test [131]. This technique was later used by Athanasiou *et al.*, to compare interspecies parameters [30].

Data analysis is also a key part of indentation testing. As mentioned previously, the analysis of the raw data obtained from indentation results is complex, but essential to this test. The Oliver and Pharr method proposed in 1992 [132], is one of the most used methods to analyse indentation output. This method calculates the elastic modulus from the load-displacement (P - $h$) relationship. Soon after, Field and Swain, proposed a similar method for spherical intenders [133]. Later, many researchers have proposed other solutions to analyse indentation data based on $P$ - $h$ relationships based on these methods [128, 134, 135, 136].

### 2.4.3 Tensile

The layout of tensile testing consists on fixing both sides of a soft tissue sample and subjecting it to a predefined stress or strain [33, 137]. This type of test is commonly used to measure material properties of ligaments and tendons. In articular cartilage, tension tests are done over thin slices of articular cartilage. Tensile modulus is normally associated with collagen content and organization, however research into the tensile properties of articular cartilage are not consistent. Some authors have found correl-

ation between tensile properties of articular cartilage and collagen network [94, 71]. Moreover, Akizuki *et al.* concluded that tensile stiffness also depends on the interactions between the collagen mesh and the PG trapped inside [94]. Nevertheless, other authors have found no correlation between tensile modulus and cartilage composition or material properties [59].

## 2.5 Time Dependent Mechanical Tests in Soft Tissue

Experimental mechanical testing can be divided into destructive and non-destructive methods. A method is considered non-destructive when complete recovery is made after being subjected to strains or loads. A method is destructive when the deformation caused by large strains or loads, cause an irreversible state [33]. The two most common non-destructive time-dependent tests used for measurement of material properties are stress-relaxation and creep [33]

### 2.5.1 Creep

Creep consists in applying a constant load (step load) below the yield stress for prolonged periods of time to the tissue and measuring the resulting displacement [36] (Figure 2.7). In cartilage, the resulting displacement is typically quick growth, followed by a slowing down as the system approaches equilibrium (an inverse exponential growth). Biologically this corresponds to the fluid flow in the cartilage [36].

A creep test is a very commonly used to measure the mechanical properties of articular cartilage. It has been shown that this test can provide two different responses according to the time when the values is calculated: the instantaneous modulus and the equilibrium modulus [29, 120]. The instantaneous modulus can be calculated from milliseconds after initial load [29] to several seconds after load application [27]. Equilibrium, on the other hand, is not normally reached before 1000 s and can actually take many hours before it is achieved [103].

### 2.5.2 Relaxation

Stress relaxation involves applying a constant compressive or tensile strain and measuring the resisting force of the tissue [33, 138] (Figure 2.7). The displacement is normally ramp displacement at a constant rate followed by constant displacement. In cartilage, normally the result is described by a high initial peak resistance force, followed by a slow decrease that approaches equilibrium in an exponential decay. Mechanically, the initial high resistance is consistent with a damper, after which the energy is translated to a spring (damper and spring in series).

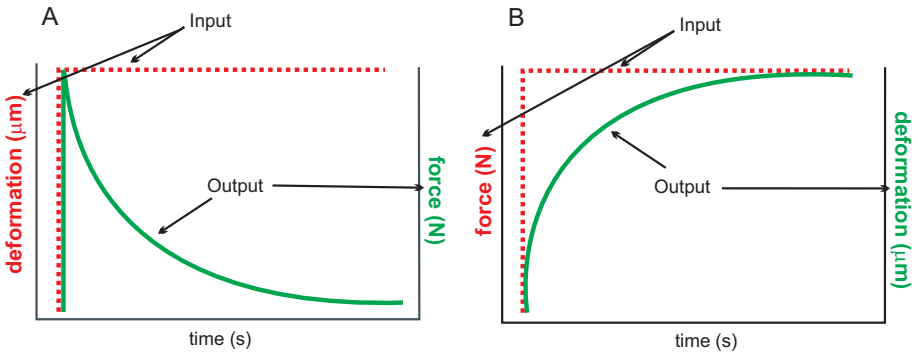


**Figure 2.7:** A. Stress-relaxation and B. creep tests

## 2.6 Osteoarthritis

OA is one of several musculoskeletal conditions. OA was estimated to be within the first ten most prevalent non-fatal diseases in the world [139] and it is estimated that about 70% of adults over the age of 65 show signs of OA [140, 141]. The prevalence of OA is higher in men than women before the age of 50, after which it becomes more prevalent in women [142]. OA can occur in any joint of the body, however it is common to find it in the knee, hip, hand, foot and spine [5, 143].

The aetiology of OA is not completely understood, however it is accepted that it is complex and multifactorial. Macroscopically, OA is characterized by the loss of articular cartilage in combination with changes in the subchondral bone, such as the development of osteophytes and pain [5, 9, 144]. Nevertheless, studies in athletes show that the development of osteophytes by itself is not a sign of OA [75, 145, 146].

OA was thought to be a disease related to wear-and-tear that was inevitable with age.

In fact, evidence suggests a high prevalence in OA in population over the age of 60 [5, 147, 148, 149]. Indeed some of these age-related processes have been investigated by Aigner *et al.*, who confirmed the diminution of the size of aggrecan molecules and increase in collagen cross-linking with age [150]. Additionally, increase in fibrillation and a decline in the anabolic response and regulative function of chondrocytes were also observed [150]. No correlation between water content and ageing was found [32, 47]. Martin *et al.*, admit that these age-related changes increase the vulnerability of the tissue to degradation, however the authors believe that these changes do not cause OA [147]. Age-related changes only increase the risk of suffering OA and accelerate the progression of the disease, they are not the cause [147, 151].

It is believed that a key factor in the development of OA is the degradation of articular cartilage, as a result of matrix structure alterations and biomechanical factors [9, 150, 152, 153, 154, 155]. Many studies have been carried out to understand this relationship. Pond and Nuki studied the development of OA in dogs by surgically rupturing the anterior cruciate ligament (ACL) [156]. This group repeated this experiment several times and in 1977 McDevitt *et al.*, concluded that the progression of surgically induced disease was very similar to the natural progression of OA [31]. In this study progressive degradation of the articular cartilage was observed. Initial degradation (at 1-3 weeks) was characterized by an increase in water content and localized decrease of PG [31]. In later stages degradation continued to spread throughout the tibial plateau in the form of fibrillation, decrease in cell density in the superficial zone, development of osteophytes were observed and increased loss of PG [31]. Hoch *et al.*, surgically induced degradation in articular cartilage in rabbits and observed a decrease in GAG content after 2 weeks of surgery [157]. However, after 6 months, the GAG content had recovered and values of stiffness were approaching normal values [157].

Early stage changes reported by McDevitt *et al.* [31] have been confirmed by other authors [12, 157, 158, 159, 160, 161, 162]. The decrease in PG was observed by Bollet and Nance in 1966 [158]. Later Mankin *et al.* stated that OA early stage degradation could be reproduced in normal cartilage by extracting PG from the tissue [159] or be induced by enzymatic digestion [130, 162] or by surgical procedures such as ACL

resection [31]. Inerot *et al.*, observed that PG in degraded cartilage had smaller size and less capacity to bind and form aggrecan compared to normal cartilage of the same age [72]. The capacity of forming aggrecan is important since it improves the ability to resist loads [12, 36]. Correlation between PG content and stiffness was confirmed experimentally [12, 47, 99, 163]. The increase in water content in early OA was observed by many scientists [59, 12, 157, 158, 159] and some suggested that it could be explained by alterations in ECM, such as damage to the collagen network [48]. However, findings regarding collagen are not consistent. Saarakkala *et al.*, found that in early stages of OA, collagen showed some changes to its orientation, however no changes in collagen concentration were detected [48]. Some authors have found a correlation between the ratio of collagen to PG with tensile modulus [94, 162]. On the contrary, other authors found no correlation between the mechanical properties of cartilage and collagen [47, 59, 164].

Most of these changes at early stages were limited to the superficial zone [159, 165]. Armstrong and Mow showed a correlation between water content and compressive modulus [12]. Additionally, several authors have found an inverse correlation between permeability and compressive modulus [12, 157, 166]. These changes in the biochemical composition of articular cartilage inevitably affects its biomechanical properties. Vansal *et al.*, confirmed a linear relationship between reduction in stiffness and increasing stage of OA [12, 47, 167, 168]. Alterations in the biomechanical balance of cartilage increase the deformation [12, 94, 169, 170] and affect its ability to resist load [167], making it more vulnerable to develop OA long term [59]. All these changes are observed long before any gross morphology change occurs [28, 167, 168, 171].

As the disease progresses the PG loss spreads to deeper zones of the cartilage, first to the transitional zone and finally to the deep zone [48, 67, 159, 172, 173]. In severe OA, the superficial zone of cartilage no longer exists [48]. At this stage it is believed that chondrocytes lose their ability to maintain the catabolic and anabolic equilibrium, and a breakdown process occurs [48, 72, 167]. Additionally, at this stage collagen degradation is evident [164, 168, 173]. As a consequence of this degradation, significant changes in the mechanical properties of the tissue such as a decrease in stiffness and tensile

strength and an increase in water content occurs [43, 115, 152, 162]. It is not clear when changes in the subchondral bone, such as stiffening begin, however they are apparent in late-stages of OA [9, 174].

Risk factors for development and progression of OA in the knee are obesity due to the high loads the knee is subjected to, any problems in the joints related to alignment, injuries in the joint, surgery and inadequate muscle strength [75, 154]. Also occupations involving frequent squatting or carrying heavy loads often are at higher risk [75, 145, 175].

## 2.7 Detection of OA

Traditionally OA has mainly been detected after pain symptoms occur, which is generally when macroscopic changes are perceptible [28]. In these cases, OA is confirmed by measuring cartilage thickness and observing the presence of osteophytes using radiography [141, 176]. Although this technique is widely used, there are many problems related to it; (1) Studies have shown that the development of osteophytes is not always related to OA [75, 148]. (2) When cartilage loss is detectable through JSW narrowing or similar macroscopic methods, the damage to the articular cartilage is advanced and essentially irreversible [28]. Once this is the case, very few treatment options will be available for the patient, the majority involving surgery [28].

In this context, it is important to study methods that are capable of detecting articular cartilage degradation in the early stages of the disease [177]. The following methods are some of the most commonly used methods for early detection of OA.

### 2.7.1 Delayed Gadolinium-Enhanced Magnetic Resonance Imaging of Cartilage

Delayed Gadolinium-Enhanced Magnetic Resonance Imaging of Cartilage (dGEMRIC) is a non-damaging method to detect GAG content *in-vivo* [141, 178]. This technique consists in the injection of gadolinium or gadopenentetate dimeglumine ($Gd - DTPA^{2-}$) into the cartilage [178]. The gadolinium distributes through cartilage in inverse amounts to GAG concentration due to its negative charge [23, 178].

This contrast agent is paramagnetic [23], therefore GAG content can be quantified by the concentration of the contrast agent in the cartilage, using the MRI parameter T1 [178, 179].

This technique has been tried and used *in vivo* [180, 181] and *in vitro* [23], however it has some disadvantages. MRI images have a high cost, the time taken to acquire an MRI is long, it is necessary to have an expert to operate the MRI to obtain the right sequence and it is necessary to use specialized software for the analysis of the data [141].

### 2.7.2 Quantitative CT Arthrography Using Anionic, Iodinated Contrast Agent

The quantitative CT Arthrography (qCTA) is a similar technique to dGEMRIC. It is also based on the detection of the spatial distribution of GAG through the use of a contrast agent [141, 182, 183]. Similar to dGEMRIC, the negative charge of the contrast agent (gadopentete or ioxaglate) makes it diffuse inversely to GAG content [141, 182, 183]. Bansal *et al.* points out that the contrast agent distributes better in degraded areas where GAG has been depleted [141].

Unlike dGEMRIC, this technique uses micro-computed tomography ($\mu$CT) to observe PG in the articular cartilage [183]. High resolution images of the tissue are obtained, allowing the 3D detailed reconstruction of PG [183].

This technique, in comparison with other similar techniques such as dGEMRIC, has the advantage of being cheaper and more accessible than a MRI [141]. Additionally, the obtained images are of a much higher resolution and faster acquisition [141]. The disadvantages are that it has only been used *in vitro* [182]. *In vitro* studies have demonstrated that the time needed for full penetration and diffusion and the dosage needed for acquisition of quality images are too high for *in vivo* use [182].

### 2.7.3 Histochemical and Biochemical Methods

The quantification of GAG through the use of dyes is an indirect method of detection of OA in early stages. The use of histochemical in combination with biochemical methods to detect GAG throughout the articular cartilage is attributed to Stockwell and Scott [184]. Since then histologically staining has become a well accepted technique for GAG quantification and it has been used by many authors for decades [20, 24, 29, 31, 48, 89, 185, 186, 187]. Two methods will be presented here:

- **Safranin O:** Safranin O is a cationic dye that, due to its electrostatic charge, binds to GAG polyanions [186, 188]. Safranin O is a commonly used dye for the quantification of PG, due to some of its properties such as specific binding, molecule size and stoichiometry [186]. The binding properties of Safranin O with keratan sulphate and chondroitin 6-sulphate were studied by Rosenberg [188]. In this study Rosenberg shows that Safranin O binds stoichiometrically to polyanions, in a relationship of one to one. Additionally, Safranin O does not bind with collagen or other matrix structures [186]. The molecule size of Safranin O allows it to penetrate and diffuse within the articular cartilage [186, 189]. All these characteristics makes Safranin O a commonly used dye to obtain accurate GAG concentrations in cartilage [186, 188].

- **1,9-Dimetrylmethylene Blue:** 1,9-dimetrylmethylene blue (DMB or DMMB) was first used as a histological stain [190], later the method was modified to allow spectrophotometric quantification of GAG in solution [191]. This method is based on the capacity of GAG to bind with the dye and the changes in the spectrum of DMMB dye [190, 191, 192]. The original method is described by Handley [191], and has been adapted many times for different purposes [193, 194].

In general these methods are highly labour intensive. Additionally the quantification of GAG through Safranin O stained samples needs the development of specialized software. The DMMB is a reliable and reproducible method, however DMMB solution tends to precipitate and the assay is highly photosensitive [194].

## 2.8 Correlation Between Biological Constitution and Mechanical Properties of Cartilage

Healthy cartilage is a material characterized by a smooth and lubricated surface that provides near frictionless properties to the joints. Additionally, the internal structure of articular cartilage, governed by the relationships between water content, PG and collagen mesh-work, gives cartilage the capacity to withstand load for a life time of use [36, 43, 72, 167, 195, 196, 197].

All these components have an important role in the biomechanical properties and maintenance of articular cartilage. The correlations between articular cartilage structures and bulk mechanical properties have been studied for many decades. The function of water molecules is vital as water causes expansion by interacting with the GAG and collagen structures [183, 198]. This expansion is constrained by the collagen mesh-work creating high interstitial fluid pressures which play a key role in the resistance to physical stress [12, 199, 200, 201]. A correlation between water content and both intrinsic compressive modulus [12] and GAG concentrations [196, 202] have been reported. Furthermore, Armstrong and Mow showed that permeability of the ECM is directly correlated with water content in equilibrium [12]. Ateshian and Wang, confirmed experimentally that interstitial fluid pressurization accounts for 90% of the load resistance, protecting articular cartilage from peak stresses and reducing deformation [199].

The role of PG as a regulator of interstitial fluid flow was recognized by different authors [12, 13, 14]. At physiological pH, PGs are negatively charged, attracting cations and repelling anions such that the interstitial fluid osmolarity increases substantially above that of the tissue's environment [203]. This osmotic disparity causes an influx of water that swells the tissue. The swelling is resisted by the fibrillar matrix and an osmotic pressure arises to counter this matrix stress [204, 205]. As well as showing a correlation between PG concentration with deformation under load [12, 13, 14] authors have also shown a relationship between PG content and stiffness [32, 47, 99, 109, 157, 206].

The three dimensional collagen network, which entraps the hydrated PG is one of the key factors that maintains the resilience of articular cartilage. Collagen fibrils surround hydrated PG restricting their movement. This directly influences the instantaneous stiffness of cartilage [207]. In order to investigate the role of each component separately (PG and collagen fibrils) under load, researchers have used enzymatic degradation to assess the effect on the mechanical properties [208, 209]. It was found that mechanical properties were significantly affected by a lack of PG in the matrix even when the collagen network was intact [208]. The authors explained that the absence or degradation of PG, reduced the water binding properties of the matrix and therefore the collagen network responded to compression as an unsupported structure resulting in a reduction of the compressive stiffness of the articular cartilage [208]. Enzymatic degradation of collagen fibrils produced secondary PG degradation, which also affected mechanical properties and permeability of the tissue [210, 209]. Thus PGs are key in maintaining the static compressive stiffness of articular cartilage [209, 211]. The collagen network, meanwhile, is responsible for the dynamic response of the matrix to both tension and compression [209, 211, 212, 213]. Computational modelling suggests the orientation of the collagen fibril networks stiffen the tissue while protecting it from excessive strains and distortions under physiological compression loads at transient periods [62, 214]. Collagen fibril networks are said to contribute directly by resisting tensile stresses and indirectly by augmenting the pore fluid pressure especially at higher, more physiological, loading rates [214]. Under compression the drastic increase in fluid pressurization in turn stiffens the tissue's transient response [215, 216]. The very low permeability causes near incompressibility during fast physiological loading cycles [207]. The collagen fibril architecture (horizontally oriented at the superficial zone, random in the transitional zone and perpendicular in the bone-cartilage interface [61, 217]), plays an important role on load resistance and rearrangement of collagen fibrils was observed in loaded regions [208, 217].

In addition, chondrocytes have the capacity to detect and respond to alterations in the articular cartilage by synthesizing ECM constituents [152, 157, 167]. The mechanism by which the communication happens is not fully understood but is thought to be a

combination of mechanical signals and environmental factors [157, 218, 219].

Many studies have been performed comparing characteristics of degraded cartilage with normal cartilage, aiming to understand the processes behind the development of OA. Maroudas *et al.*, found higher water content [32] and increased permeability [199] in degraded cartilage. It has been demonstrated that degenerated human cartilage was softer than normal cartilage and had less GAG [26, 27, 182, 220]. Damaged cartilage was found to have lower fixed charge density (FCD) and therefore more water content [26, 47, 158, 202]. After enzymatic damage to collagen *in vivo*, an increase in swelling and stiffness was observed [221].

## 2.9 Topographical Variations

Topographical variations in the distribution of material properties and matrix constituents distribution have been studied by many authors. Topographical variations of Poisson's ratio [45, 83], thickness [19, 24, 70], PG content [23, 27, 29, 70, 222], stiffness [27, 83, 90, 103] and collagen content [70, 223] have been reported.

The medial compartment has been reported to be thicker than the lateral compartment [70]. The tibial plateau has a greater PG content than the femoral condyle [24, 29, 157]. In contrast, the collagen content in the femoral cartilage is higher than in the tibia [29]. This is thought to be a consequence of the load pattern that the joint is subjected to. The tibial plateau receives large compressive stress while the femur receives the largest shear stress [187].

Many studies have detected significant differences in material properties in the tibial plateau between the areas covered by the meniscus and the uncovered areas [28, 70, 83, 89, 103, 224]. These studies demonstrated that the area uncovered by the meniscus showed high concentration of PG [225], and higher thickness [70, 225], while covered areas showed higher stiffness [28, 103].

Kempson *et al.*, found a systematic and repeatable pattern in stiffness distribution throughout the femoral head [27]. This author arrived at this result by comparing an indentation map of the femoral head to a known contact load [27]. More recently,

patterns on the distribution of mechanical properties were studied by Deneweth *et al.* [2]. Moreover, McDevitt *et al.*, observed that the OA lesion will always begin at the same area in the tibia plateau. This area was severely affected and then spread to other areas [31]. These findings were confirmed by Gulati *et al.*, who observed reproducible patterns in human tibial plateau for unicompartmental knee OA [25].

## 2.10 Effect of Loading

The joints are loaded continuously throughout the day while performing daily activities. The effect of the load on the articular cartilage is dependent on many factors, such as magnitude of the load, frequency and rates of loading [17, 81, 116, 154, 226]. Indeed, loading is necessary to maintain articular cartilage in good health [75]. Several authors have studied the effect of loading in dogs by subjecting them to treadmill running for different periods of time [20, 167, 185, 206, 227, 228]. Moderate exercise increases PG content in the transitional and deep zones [20, 229, 230], it increases stiffness in loaded and weight bearing areas [17, 20, 228, 231] and increases thickness of articular cartilage [228, 231]. Despite general agreement of these finding among several authors, Vasan *et al.*, who studied the effect of moderate exercise (1 hour a day for 8 months) on the femoral head, found a decrease of PG in weight bearing areas [167].

The importance of loading for the healthy development of articular cartilage was further proven by immobilization studies. Several studies were carried out to study immobilization in young beagle dogs [14, 17, 19, 227, 232, 233]. These studies immobilized canine limbs for 11 [17, 227, 232] and 15 [14] weeks using a splint [17, 227, 232]. Softening of articular cartilage [14, 232] and significant decreases of GAG concentration [14, 17, 227] in load bearing areas were observed, no decrease in cartilage thickness was reported [17]. On the contrary in runners increased thickness in weight bearing areas has been reported [17, 113]. Jortikka *et al.*, observed an increase in the size of PG's after immobilization and an increase in aggrecan size shortly after remobilization in a splinted joint [227]. On the contralateral side, a localized increase in PG was also observed [227]. Jortikka *et al.* also studied the reversibility of matrix changes after 50 weeks of remobilization and concluded that complete recovery of articular cartilage normal

properties was not achieved [227]. These studies show the long-term impact that small changes in loading patterns have in joints. Moreover, Palmoski *et al.*, demonstrated the importance of load bearing for matrix health, rather than solely movement in the knee [187]. In this study, Palmoski *et al.*, observed decrease of thickness, decrease in PG aggregation and increase of water content in dog joints that were mobilised, in the absence of load [187].

In contrast, strenuous exercise or high impact loading may be detrimental for articular cartilage [234]. Kiviranta *et al.* and Saamamen *et al.*, subjected dogs to running training consisting of 20 km/day for 15 weeks [233, 235]. They observed an increase in water content [233], reduced thickness [235], localized decrease in GAG concentration [235, 233] and decreased collagen content in load bearing areas [233]. Saamamen *et al.* also observed a size increase of aggregating PG, that the authors interpreted as an increased synthesis of new PG [233]. The studies continued by Arokoski *et al.* and Oettmeier *et al.*, who subjected dogs to even more "strenuous" loading (40 km/day for 15 weeks) [14, 185, 236]. Arokoski *et al.* demonstrated that the PG loss for these runner dogs was not limited to the superficial zone but it had extended to the intermediate zone in weight bearing areas [14, 185]. Localized increase of thickness in cartilage in weight bearing areas and increase of thickness of the subchondral bone were also reported [104, 185, 236]. Moreover, remodelling of the subchondral bone [236] and disorganization of collagen fibrils in the superficial layer was observed [14]. Studies did not observe any changes in collagen concentration [187]. The differences in thickness of cartilage and bone remodelling between 20 km/day runs and 40 km/day runs, suggests a dynamic nature of articular cartilage as it appears to adapt to new loading circumstances after only 15 weeks. Moreover, the localized variations presented in these studies, were probably due to the different types of loading to which the joints were subjected to during exercise [185, 236, 237].

Kujala *et al.*, studied the long term effect of strenuous exercise in top level athletes that were subjected to different types of loading during their younger years [238]. The group of athletes examined came from different sports, which are subject to different types of load: 28 long distance runners (cyclic loading), 31 soccer players (high impact

loads and sprains), 29 weight-lifters (high peak loads) and 29 shooters [238]. The study found that soccer players and weight lifters had a higher incidence of knee OA than other examined athletes [238]. This was partially explained by an increase in observed injuries in soccer players and increase body muscle index (BMI) in lifters at age 20, and also explained by the dynamic and highly loaded movements that soccer playing requires [238]. It was concluded that risk factors were injuries in knee joints, high body mass index, participation in jobs that involve persistent kneeling and squatting and heavy lifting [75, 238].

In conclusion, moderate exercise is beneficial to articular cartilage health. There is no evidence that activities such as running or jumping will cause OA, since they do not produce stress greater than 10 MPa [75]. Additionally, it has been reported that articular cartilage damage occurs at loads greater than 25 MPa [234, 239, 240]. People with previous injury or malalignment of the joints can also benefit from moderate exercise, however special care has to be taken in choosing the type of loading they will subject their joints to [75].

The rate at which the articular cartilage is loaded is of great importance. As mentioned previously, fluid pressurization plays a critical role in load resistance [241]. When load is applied slowly, the fluid movement allows the cartilage to deform, dissipating the applied force [75, 199]. On the contrary, in high impact loading the fluid does not have time to move and therefore the load is absorbed almost entirely by the solid part of the ECM [75]. This explains the distinction between the instantaneous and equilibrium moduli [103]. The dependency of mechanical properties in strain and stress rates been discussed in several articles [44, 130, 240, 242, 243]. Chen *et al.*, studied the effect of dynamic loading with different stress magnitude and observed that cell death in the superficial layer occurred at loads of 1 MPa applied for an hour and at 6 MPa applied for a minute (rate $9 \pm 6$ $\mu$m/h and $47 \pm 8$ $\mu$m/h [44]). Thibault *et al.*, also applied cyclic loading to cartilage plugs between 2 and 8 MPa and strain of 8-25%, and although the authors did not observe cell death, they did demonstrate damage to the collagen network, increased PG loss and increase permeability [69]. To put these studies into context, normal physiological loads are reported to be between 2 to 12

MPa [13, 241] and normal strains are between 5 to 20% [45, 58]. In this context Chen's findings show the impact that repetitive loading can have on cartilage.

It has been shown that cartilage can withstand peak forces of 2 to 30 MPa without any macroscopic damage [239, 240, 244, 245]. Newberry *et al.*, applied impact loading to articular cartilage and observed a significant decrease in stiffness 12 months after impact, but not immediately after impact [102]. However, Borrelli *et al.*, observed immediate changes such as significant reduction of PG content and increase in water content in impacted areas [246]. In human studies it has been observed that after a serious injury it takes several years for OA to develop [148, 247]. This could explain why OA prevalence in young people is so rare, but it also promotes the importance of seeking appropriate treatment and rehabilitation after an injury [75].

Large strains can also be an important factor in cartilage degradation. In fact, Patwari *et al.*, induced injuries by subjecting human cadavers to 65% strain in confined compression tests at a rate of 2 mm/s (400%/s) [154]. The study demonstrated that high peak stresses alone did not seem to be an important factor in decrease of GAG content [154]. Therefore, they concluded that peak strain might be a more determinant factor in cartilage degradation [154].

The subchondral bone also presents changes in response to load. An increase in PG synthesis in calcified areas with moderated runners was detected [17]. Newberry *et al.* also observed remodelling of the subchondral bone due to impact loading [102].

## 2.11 Summary

In this section components of knee anatomy such as menisci, ligaments, tendons and cartilage were presented. Articular cartilage was described in detail, including the zone/layer division and the different constituents of the tissue. Measurements and mechanical tests performed on articular cartilage were also described. Finally, OA was defined and the most common methods for its observation were presented. Literature shows that there is a correlation between biological matrix and mechanical properties of articular cartilage. In fact, when load is applied, it is the interactions between constitu-

ents in the structural matrix which gives articular cartilage its mechanical properties. Furthermore, at different stages of OA, it is possible to observe structural changes in the biological matrix. For example, in severe OA, it is possible to observe an increase in water content, increased permeability, and degraded PGs . The importance of moderate loading for knee health was also highlighted in studies by several authors. On the other hand, strenuous loading was reported to cause damage in articular cartilage.

# Chapter 3

# Whole Articular Surface Indentation Machine

In this chapter a novel and custom designed testing machine for whole articular surface indentation testing is introduced. Force and displacement were measured using the The Whole Articular Surface Indentation Machine (WASIM). From this both stiffness and elastic modulus were calculated. A set of routines to automate the measurement of mechanical properties and thickness were developed by the author and are presented here. These routines are highly adaptable for use with other probes with the WASIM, which will allow a range of other measurements to be carried out in future studies.

## 3.1 The WASIM

Indentation is a commonly used method for mechanical testing (Chapter 2, Section 2.4.2). Testing instruments used to acquire mechanical properties through indentation are diverse in size, functionality and complexity. Some of the factors that play a role in the design of an indentation device are the size of the sample to be indented, the type of mechanical test to be carried out and the flexibility of the machine in terms of movement and incorporation of new probes. Most indentation devices aim to achieve indentation normal (perpendicular) to the surface of a specimen; this is particularly relevant when working with large or whole specimens, since surfaces of biological samples tend to be have complex geometry. In these cases, the sample holder should possess freedom of

movement, in order to adjust the position of the sample. When performing mechanical tests on cartilage plugs, normal indentation and adjustment of the sample are not a significant issue since plug sample surfaces are assumed to be relatively flat.

Measurement of material properties on whole undamaged specimens includes many advantages already discussed in Chapter 2. In 1970 Kempson *et al.* tested a femoral head using a large indentation device that allowed translation and rotation about two axes (X and Y) in order to obtain indentation at any point on the femoral head [47]. Later, Mow *et al.* used an indentation device that could test whole bovine knees [248]. This device also allowed translation of the specimen in 3 DOF (X, Y, Z) and rotations around these three axes [248]. Additionally, the testing device had a needle probe for thickness measurements [248]. Both of these devices allowed the acquisition of material properties from whole undamaged specimens and due to their flexibility allowed indentation of uneven surfaces. However, neither of these two devices provided a mechanism for automated normal indentation to be obtained, on the contrary, in both of these devices normal alignment was achieved by manually adjusting the position of the sample.

Normal indentation, or the positioning of the indenter perpendicularly to the loading surface, allows more accurate measurements of the material properties. There are many reasons for this, some of them are: (a) When using a hemispherical indenter the initial contact should occur at the pole or tip of the indenter, otherwise the contact nature changes making the analysis considerably more complex. (b) Normal indentation cancels the gross shear effect and reduces friction. (c) Physiological loading occurs normal to the surface.

In the work presented here, a novel testing machine, designed through a collaboration between the OOEC (the host centre for this thesis's work) and Tiab Ltd. (Banbury, UK), was used as the main instrumentation for the measurement of material properties. The WASIM permits normal indentation because it has 5 degrees of freedom (DOF) that allows the rotation and translation of the specimen. Additionally, acquisition of the surface topography is possible. The WASIM was designed with flexibility to allow the attachment of interchangeable probes such as an indenter, ultrasound probe, a

spectroscope and others. This mechanism allows the use of various sized or shaped indenters, or even other probes such as a needle probe. These probes are attached to the load cell and along the Z axis of the WASIM coordinate system.

The WASIM is composed of a rigid steel frame (1060 x 970 x 1850 mm), a rectangular flat stage (± 30 $\mu$m flatness) translatable along the X and Y axes, and capable of pitch rotation. The stage can be positioned in (X, Y) coordinates with a repeatability of ± 5 $\mu$m using linear encoders (resolution 1 $\mu$m). In the middle of this stage there is a circular sample holder, which is capable of yaw rotation.

The stage possesses 3 DOF: X, Y and pitch. Additionally, the circular movement of the sample holder adds one DOF (yaw). Furthermore, an additional DOF is provided in the vertical axis (Z), to which a load cell and two lasers for distance measurements along the Z axis are attached (Figure 3.1).

These 5 DOF allow the rotation and translation of the sample such that normal alignment to the specimen can always be achieved. The apparatus has a fixed coordinate system (CS) established by a calibration routine which runs at each start-up cycle of the device. $X_W$, $Y_W$, $Z_W$ axes of the stage (WASIM coordinates ($CS_W$)) are orthogonal to each other. The indenter is positioned parallel to the $Z_W$ axis. The Yaw CS ($CS_Y$) is orthogonal to $CS_W$. Pitch CS ($CS_T$), rotates about the $Y_W$ axis, however $CS_T$ is not absolutely orthogonal to $CS_W$ (this was due to tolerance issues in its manufacture), therefore pitch rotations in the $CS_W$, resulted in a combination of rotation about $Y_W$ and translation in $X_W$.

Movement and ranges of each axis are below:

- ***X axis:*** Forward and backward movement of the stage. It can move ±100 ± 0.1 mm.
- ***Y axis:*** Sideways movement of the stage. Perpendicular to the X axis. It can move ±100 ± 0.1 mm.
- ***Z axis:*** Vertical movement of the Z axis stepper motor. This axis can move ±90 ± 0.1 mm.

- ***Yaw:*** Rotation of the sample holder around the Z axis. The possible rotation is ±180° ± 1 minute.
- ***Pitch:*** Rotation around the Y axis. The rotation is limited to -9° to +80° ±1 minute.

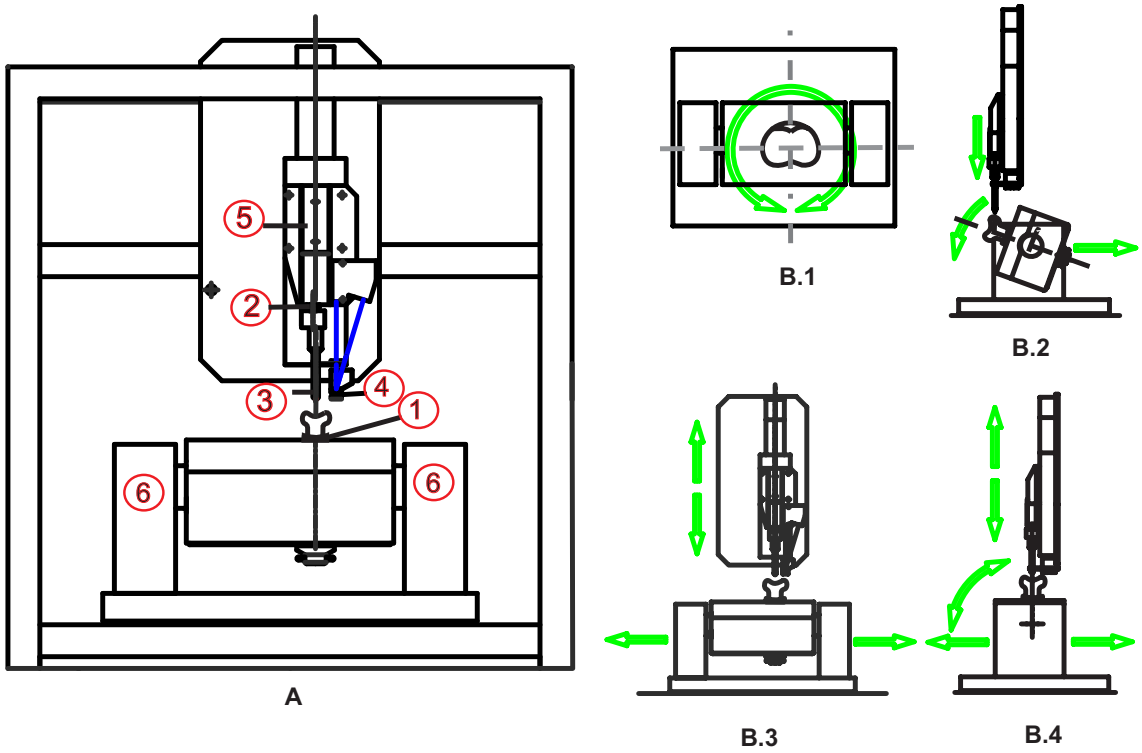


**Figure 3.1:** (A) Whole Articular Surface Indentation Machine (WASIM).(1) Sample Holder, (2) Load Cell, (3) Indenter, (4) Lasers, (5) Z axis Stepper-motor, (6) Houses the motors for X, Y, Z, pitch. (B) Indenter in WASIM Apparatus. B.1. Top View. Shows yaw movement of the sample. B.2. Lateral View. Shows pitch movement, as well as downward movement on the Z axis. B.3. Front View. Shows possible movement on the Y axis. B.4. Lateral View. Shows possible movement on the X axis

The highly accurate (repeatability of ±0.02% load) load cell (F256-Z3837 100 N, Novatech, Portsmouth, UK) measures loads between ± 100 N ± 0.05 N, i.e. both in tension and compression.

A hemispherical indenter (2.7 mm diameter) was mounted under the load cell for indentation testing. The distance measurement lasers consisted of a medium resolution laser (LK-G152, Keyence, Higashi-nakajima, Japan, repeatability 0.5 $\mu$m, spot diameter 120 $\mu$m and working range 150 mm ± 40 mm), and a high resolution laser (LK-G32, Keyence, Higashi-nakajima, Japan, repeatability 0.05 $\mu$m, spot diameter 30 $\mu$m and working range 30 mm ± 5 mm).

## 3.2 Set-Up Routines

A series of routines were written to set-up the WASIM to perform the measurement of the different parameters. These routines are outlined in Figure 3.2.

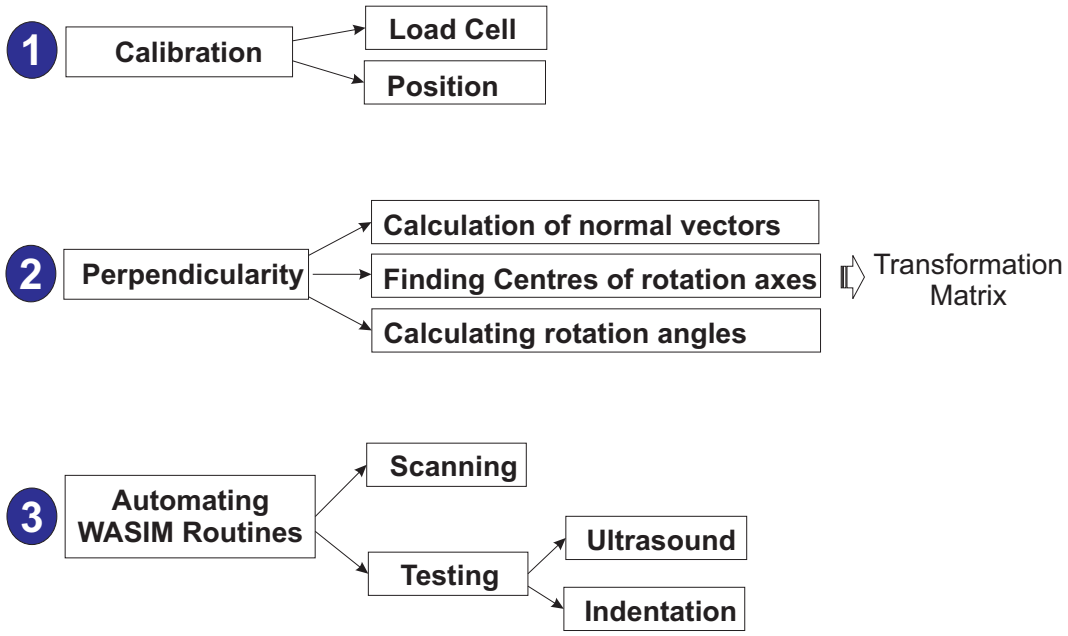


**Figure 3.2:** Flow chart showing routines developed to use WASIM

### 3.2.1 Calibration

Each time the WASIM was used, it was calibrated for position. Control systems were implemented for the Z-axis in order to control velocity while performing indentation. Additionally, the load cell was also calibrated. This assured the repeatability of measurements over time.

#### 3.2.1.1 Calibration of Position

The aim of the position calibration routine was to assure that a unique origin was found for each translation (X,Y,Z) and rotation (yaw and pitch) axis. The calibration routine for each axis consisted of finding the maximum range of motion in the positive and negative directions and setting a reference point to obtain the origin. This was repeated for each axis.

Reference positions such as the origin and minimum/maximum position at each axis, were marked on the WASIM with an indelible pen (as external marks). These external

marks were preserved on the WASIM throughout all tests.

In order to validate the calibration for each axis, WASIM was directed to each of the reference positions. If the WASIM did not reach external mark appropriately, the calibration routine was repeated.

#### 3.2.1.2 Calibration of Load Cell

The calibration of the load cell was carried out by collecting the data with different loads in both compression and tension, and obtaining the resulting output voltage.

In tension a series of calibration weights (1, 2, 5, 10 and 20 Kg) were applied to the load cell in an increasing sequence. The output voltage collected with each weight was recorded to form a calibration curve.

Following a similar procedure, the calibration of the load cell in compression was carried out. However, on this occasion the load applied was measured using a commercial balance (NVL20000, Ohaus Corporation, USA). Once again the output voltage was recorded at each measurement and a linear calibration curve formed.

#### 3.2.1.3 Calibration of Speed

When performing the first indentation tests it was noticed that force-displacement (P-h) curves showed peaks in both the unloading and loading curves. After investigation, it was found that this was due to the lack of speed control in the movement of the Z axis, which resulted in reaching the target position faster than requested in the input file, and instead oscillating around the position until it was time to move to the next position.

To resolve this problem a proportional integral controller (PI) was incorporated digitally. This type of controller allows an accurate and quick response of the stepper. The result was a significant reduction of peaks, obtaining a smooth signal without the need of any external filters.

### 3.2.2 Control Routines

The WASIM is controlled by a Tiab proprietary controller and software. The WASIM can be controlled in different ways. There is a user interface that allows the discrete movement of each stepper motor (X, Y, Z, yaw, pitch). Through the user interface it is also possible to upload a routine file. This routine file could be used to describe the position of each stepper motor at any given time step. The other way to interact with and control the WASIM was through custom written routines. These routines linked with the Tiab dynamic libraries to allow more advanced and dynamic interaction with the WASIM. The custom routines not only allowed the automated movement of the motors, but also the definition of different scenarios depending on the output of the hardware attached to the WASIM (i.e. load cell, laser readings). In the present work several custom routines were developed, in Matlab and C++, by the author to (1) control the movement of the stepper motors for normal indentation, (2) process the topographical maps to obtain coordinates for normal indentation, and (3) perform indentation in an automated manner. These are explained in the following sections.

### 3.2.3 Scanning of the Specimen

A scanning routine was developed in order to obtain the topographical map of the joint surface to be tested. The spot height of the laser beam was recorded at 200 Hz which allowed measurements to be made approximately every 100 microns.

This routine takes as inputs the area of the sample to scan in X and Y (e.g. 80 x 80 mm or 60 x 70 mm), the initial position of the laser spot in 3D coordinates, yaw, pitch and the file name for data storage. The scan area was used to calculate the number of points to be measured. Before beginning the scanning routine, the height of the laser was adjusted to the optimal operating position and the laser beam was centred on the sample. The initial position was taken as the centre of the raster scan.

The sample specimen was moved with a raster pattern based on the input X and Y values. Simultaneously, the laser beam measured the spot height (reflected light at each X, Y position) and recorded these values in an output file.

### 3.2.4 Finding Perpendicularity

Perpendicularity during indentation is important since inclination of the indenter will change the projected contact area and, therefore, affect the mechanical properties measurements [249, 250]. Similarly, perpendicularity is important while using the ultrasound in order to maximize the detection of the reflected energy.

The articular surface is an uneven surface, therefore in order to guarantee that the indentation and ultrasound measurements occur perpendicular to the surface, rotation angles had to be calculated. The position of the ultrasound and indenter attachment (probe attachment) are fixed in X and Y, and their movement was restricted to translation along the Z axis. Therefore, the specimen holder/stage must rotate in yaw and pitch so the area of interest (AOI) is perpendicular to the probe.

Below the steps taken to obtain perpendicularity at each testing point are outlined.

#### 3.2.4.1 Calculation of Normal Vectors

The cloud point data obtained from the scanning routine (Section 3.2.3) was reconstructed to create a 3D topographical map of the articular surface of each specimen by fitting a surface.

In order to make sure that testing at each location was performed perpendicular to the surface, a normal vector at each test point was calculated. To do this an AOI, centered at the test location and with a radius equal to that of the indenter, was selected at each test location. Points within the AOI were grouped into groups of four neighbour points. The normal vectors within the AOI were calculated using the cross product of the two diagonals formed by opposite corner points. The average of all normals within the AOI (approximately 8 normal vectors) was found, resulting in one normal vector for each test location. This allowed the calculation of the rotations and translations necessary to place the AOI perpendicular to the testing probes.

#### 3.2.4.2 Finding Origins

Rotations and translations necessary to make the AOI perpendicular to the probes, were calculated relative to the origin ($O$) of each of the four CS (Yaw (Y), Pitch (T) and Global WASIM (W) and indenter/US (I)). Before the beginning of the work presented here, the position of these origins in Global WASIM coordinates were unknown. Therefore work had to be carried out in order to identify the location of each origin.

- Yaw:

  The X and Y components of the yaw centre ($O_Y$) were calculated by taking four points on the sample holder with zero pitch at 0°, 90°, 180°, 270°. Two lines were formed between points opposite to each other: one from the point at 0° to the point at 180° and the other from the point at 90° to the point at 270°. $O_Y$ was determined by the intersection between these two lines. This procedure was repeated six times at four different angles. Results were averaged and the error was calculated. The Z component of $O_Y$ was set to zero, since it rotates about this axis.

- Pitch:

  As mentioned previously, the $CS_T$ is not completely orthogonal to the $CS_W$. Therefore, the pitch rotation is not about the $Y_W$ axis, but instead has an angle with respect to this axis. In order to understand the behaviour of the pitch rotation, several points on a custom made phantom (shaped as a half octahedron) were selected. The X,Y and Z position of each point were recorded at different pitch angles between -9° to +80°. Points were then rotated in yaw and the procedure was repeated. This was done with 30 different points at 15 different yaw angles.

  Using the obtained points, a plot outlining the trajectory of a given point at any X position as a function of the pitch angle was obtained (Figure 3.3). By curve fitting this trajectory, an equation for the trajectory was obtained, which made it possible to calculate the position of a given point within the sample holder area at any pitch angle.

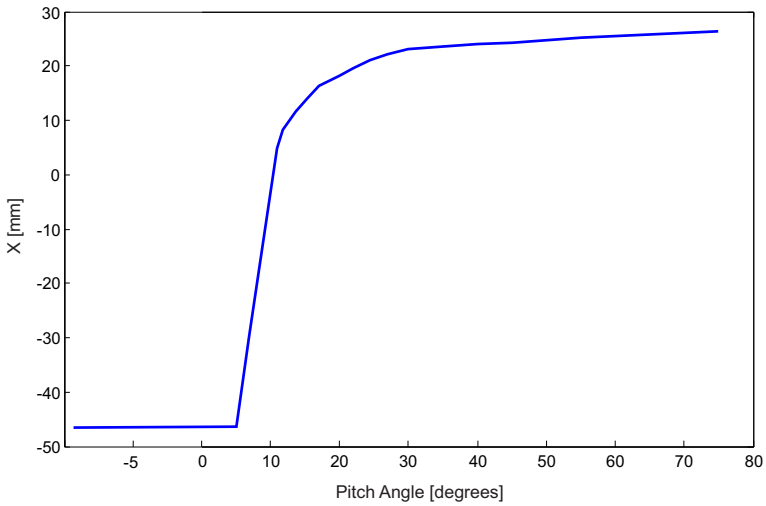


**Figure 3.3:** Curve describing trajectory of pitch angles in relation to the X axis

- Probe attachment:

  As mentioned previously, the indenter and ultrasound probe attachment is fixed in X and Y axes. The distance between this attachment ($O_I$) and the laser beam was measured. This allowed the alignment of the AOI with the probe attachment centre.

#### 3.2.4.3 Rotation Angles to align each AOI with probe

Rotation angles yaw and pitch ($\Theta$ and $\Phi$ respectively) were calculated to align the normal vector ($\hat{N}$) of each test location (Q) to the indenter/ultrasound probe position (I) (Figure 3.4).

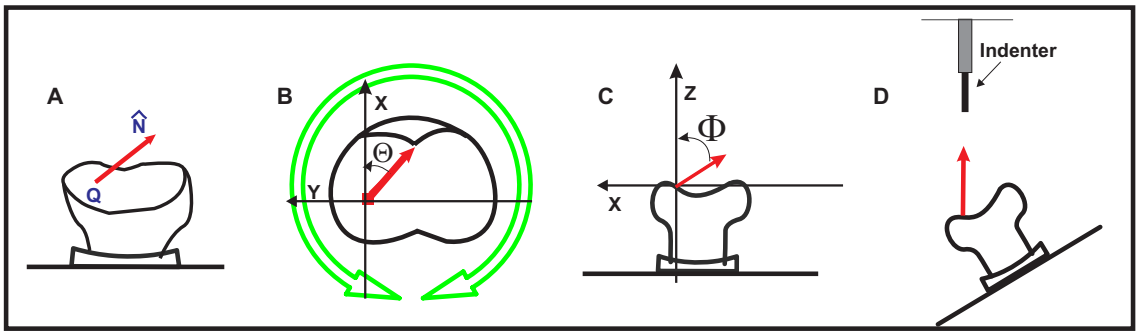


**Figure 3.4:** Rotations in yaw and pitch to achieve indentation normal to surface. (A) is the original orientation of the tibial plateau, where the normal vector of point Q is shown by the red arrow. (B) axial view of the tibial plateau, identifying yaw angle ($\Theta$) necessary for the alignment of the normal vector with the X axis. (C) View from YZ plane. Pitch angle ($\Phi$) is the necessary rotation to align the previously rotated normal vector with the Z axis. (D) Tibial plateau was rotated by $\Theta$ and $\Phi$, and has now been translated to be aligned with the probe position.

In this section, $\hat{N}$ corresponds to the original normal vector at a given point (Q). $\hat{N}$ is rotated in yaw (about the Z axis) by $\Theta$ to be aligned with X axis ($\hat{X}$), becoming $\hat{N}_1$.

Then, $\hat{N}_1$ was rotated in pitch (about the X axis) by $\Phi$ to be aligned with the Z axis ($\hat{Z}$) becoming $\hat{N}_2$. Calculation of $\Theta$ and $\Phi$ are presented below.

- ***Yaw Rotation:***

  The yaw angle was determined by the rotation of the sample holder. It consisted of the rotation that was necessary to align the normal vector of each testing point with the X axis. Yaw angle ($\Theta$) was calculated in 2D on the XY plane (Equation 3.1).

$$\Theta = cos^{-1}(\hat{N}_{XY} \quad . \quad \hat{X}) \tag{3.1}$$

  where $\hat{N}_{XY}$ is the subvector consisting only of X and Y components of the original normal vector $\hat{N}$, thus $\hat{N}_{XY} = \left\{ \begin{array}{c} X_N \\ Y_N \end{array} \right\}$ and $\hat{X}$ is defined by the 2D unit vector of the X axis.

  The use of Equation 3.1 required the verification of parallelism with $\hat{X}$, since the solution to this equation is always a positive angle. The verification consisted in validating that the projection of the X component of the normal vector ($\hat{N} * cos(\Theta)$) was aligned with the positive X axis ($\hat{X}$). This was achieved by forming the cross product between them. If result showed that vectors were not aligned, $\Theta$ was multiplied by -1 and verification was repeated.

  Once an angle $\Theta$ that aligned $\hat{N}$ with $\hat{X}$ was found, the required rotation matrix around the Z axis was calculated (Equation 3.2).

$$R_Y = \begin{bmatrix} cos(\Theta) & -sin(\Theta) & 0 \\ sin(\Theta) & cos(\Theta) & 0 \\ 0 & 0 & 1 \end{bmatrix} \tag{3.2}$$

  where $R_Y$ corresponds to the yaw rotation matrix around the Z axis.

  The multiplication of the rotation matrix $R_Y$ by $\hat{N}$ resulted in $\hat{N}_1$ (Equation 3.3)

$$\hat{N}_1 = R_Y * \hat{N} \tag{3.3}$$

- *Calculating Pitch Angle:*

  The pitch angle ($\Phi$) was determined by the rotation of the stage around the Y axis. Therefore $\Phi$ consisted of the rotation necessary for the normal vector rotated in yaw by $\Theta$ angle ($\hat{N}_1$) to be parallel to the Z axis. Rotation was performed in the XZ plane (Equation 3.4).

$$\Phi = cos^{-1}(\hat{N}_{1_{XZ}} \quad . \quad \hat{Z}) \tag{3.4}$$

  where $\hat{N}_{1_{XZ}}$ is the subvector consiting only of the X and Z components of $\hat{N}_1$, thus $\hat{N}_{1_{XZ}} = \begin{Bmatrix} X_{N_1} \\ Z_{N_1} \end{Bmatrix}$ and $\hat{Z}$ is unit vector of the Z axis in the XZ plane.

- *Rotating in Pitch Angle:*

  The rotation about Y axis was described by Equation 3.5:

$$R_T = \begin{bmatrix} [cos(\Phi) & 0 & -sin(\Phi) & 0 \\ 0 & 1 & 0 & 0 \\ sin(\Phi) & 0 & cos(\Phi) & 0 \\ 0 & 0 & 0 & 1 \end{bmatrix} \tag{3.5}$$

  This rotation was also verified for parallelism with $\hat{Z}$. However, given restrictions in terms of pitch rotations (-9° limit), if a negative angle was needed, the yaw angle was recalculated by rotating it 180° and the whole process was repeated.

  Then, the normal vector, which is parallel to Z axis, was obtained ($\hat{N}_2$) by multiplying the rotation matrix $R_T$ by $\hat{N}_1$ (Equation 3.6)

$$\hat{N}_2 = R_T * \hat{N}_1 \tag{3.6}$$

  Using calculated angles: $\Phi$ and $\Theta$, and the adjustment by the pitch trajectory

equation, the new position of the test point Q after rotations was obtained.

- *Translation to Probe Attachment Position:*

  Using the indenter origin ($O_I$), Q was translated in X and Y to align the AOI with the probe attachment position.

- *Adjustment of Initial Conditions and Limitations:*

  In order to translate the rotations angles ($\Theta$ and $\Phi$) into coordinates to be input, it is important to take into consideration two points: (1) the initial conditions in which the topographical scan were obtained in terms of initial pitch and yaw angles and (2) range of movement of the WASIM. The first consideration is important since the rotations in which the initial scan (therefore topographical map) were obtained, are considered to be zero rotation for the calculation of $\Theta$ and $\Phi$ angles. Here the initial rotations were taking into account (by adding the initial position (initial value) of the yaw and pitch angles to the final calculated $\Theta$ and $\Phi$ angles respectively) in order to input the correct angle into the WASIM. The second condition is regarding the final coordinate system that is obtained to achieve indentation perpendicular to the surface after multiplying the rotation and translation matrix by each point. These coordinates must be within the range of movement of the WASIM, otherwise it is not possible for that point to be tested. This consideration includes comparing the pitch angles, which is restricted to -9° to +80°, to required rotation angle. If the pitch angle was outside the movement range, both $\Theta$ and $\Phi$ were adjusted by turning $\Theta$ by 180°, verifying parallelism and recalculating $\Phi$.

  As a last step, 3D coordinates were compared against the range of motion of the stepper motors. In the case that the WASIM coordinates were outside the possible range of motion, in order to achieve normal indentation, the point was eliminated as a test location.

This procedure was repeated for every test location in each tibial plateau using an automated program. X, Y, Z coordinates, yaw and pitch angles for normal indentation at each point were recorded in a file referred to as the "transformation" file.

### 3.2.5 Automation of Measurements Perpendicular to the surface

A custom routine was developed in C++ by the author to allow automated measurements of mechanical properties (using indentation) and thickness measurements (using an ultrasound probe) at each testing points. The "transformation" file was used as input to this routine, as it contained the WASIM orientations needed to localize each location perpendicular to the testing probe (coordinates $Q_i$ in Figure 3.5).

The routine read each location and moved the stage (X, Y, yaw and pitch) to the required position established to be perpendicular to the AOI of point $Q_i$. Once this position was achieved, the probe (indenter or ultrasound) was lowered along the Z axis in regulated steps controlled by continuous monitoring of the load cell and estimated distance to the specimen surface. The closer the probe tip was to the specimen's surface the smaller distance increments were made. The movement stopped when the load cell registered a value above 0.5 N. This value was set as a threshold for contact between the indenter and the articular surface. When contact was established, the WASIM switched to either indentation mode or ultrasound mode depending on the input file.

In the case of choosing indentation, the controlling software allowed the indentation mode to be either force controlled or displacement controlled.

## 3.3 Parameters to be considered for Indentation Tests

As discussed in Chapter 2, Section 2.4.2, the use of indentation as a method to measure material properties is common and presents many advantages. These advantages involve an ability to measure the mechanical properties in whole specimens with similar settings to real conditions (subchondral bone, interstitial fluid). However, it has been suggested that the values obtained through indentation should be observed in relation to other measurements obtained using the same technique rather than as absolute values of the tissue. Some considerations taken into account during the selection of the indenter are presented as follows.

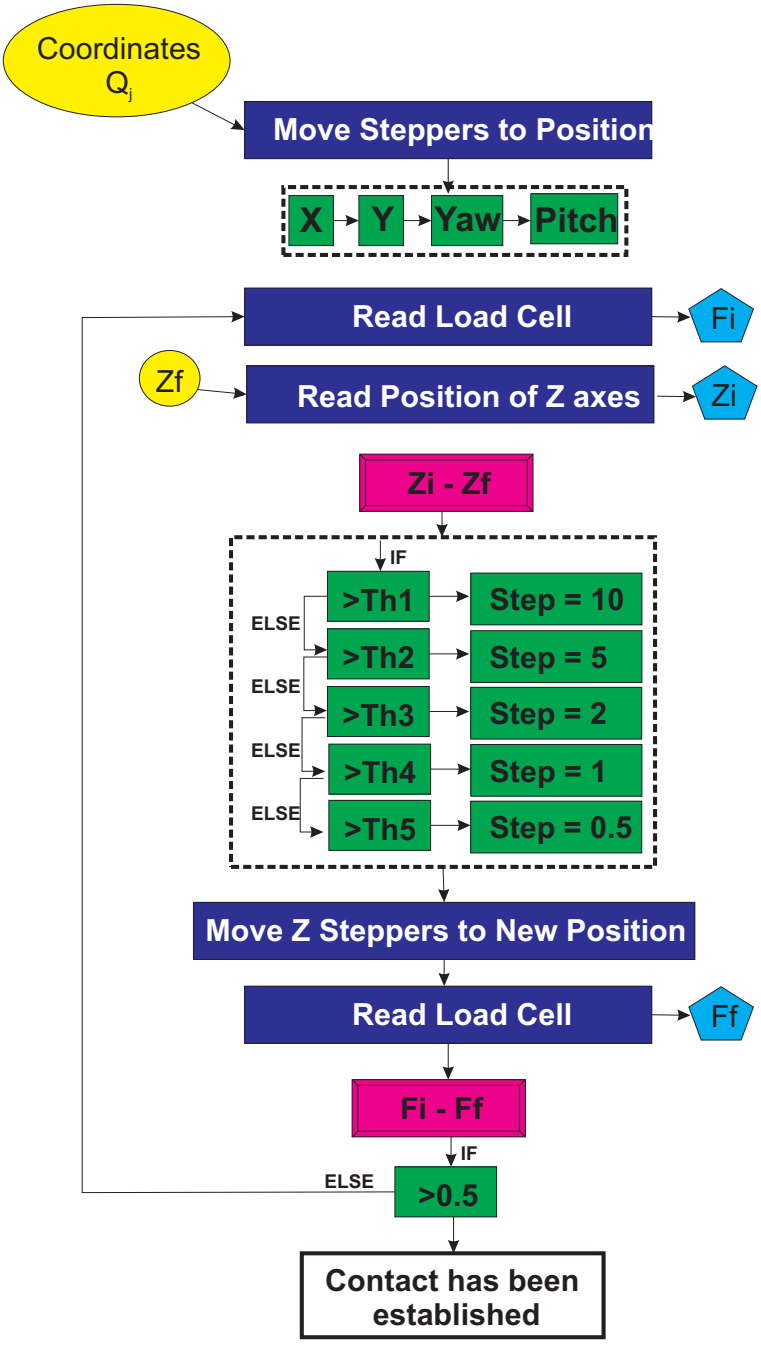


**Figure 3.5:** Flow chart showing process followed with each test point to establish contact between articular cartilage and probe. In the flow chart circles indicate inputs, polygons indicate outputs, double squares indicate conditionals. 'Th' is the different thresholds.

### 3.3.1 Indenter Choice

Indentation tests were performed using a hemispherical indenter of radius 1.35 mm. This indenter was chosen taking into consideration the following:

1. According to Stolz *et al* [130], the size of the indenter should be determined according to the structure to be measured. For example, nanometre scale indenters will reveal the stiffness of nanostructures such as collagen fibers and PG

chains. In contrast, millimetre and micrometre scale indenters will provide the aggregated mechanical properties of the articular cartilage.

2. Spherical indenters have been commonly used for the testing of soft tissue since they produce results that are more consistent and easier to model and interpret [130].

3. Spherical indenters are less sensitive to cartilage thickness [251] and depth penetration [252] than flat ended indenters.

4. Millimetre scale indenters have been commonly used for mechanical testing of soft tissue [47, 116, 127, 130, 253, 254]. Indenter tip size used by these authors ranges between 0.5 - 4 mm. Moreover, indenters used in arthroscopy tend to be on the millimetre scale [23].

5. The indenter radius must be smaller than the articular cartilage thickness but larger than the deformation which will be applied.

### 3.3.2 Preliminary Tests: Strain Rate and Thickness

In order to understand the effect of strain rate, indentation depth and total thickness of the specimen on the mechanical properties obtained through indentation tests, a series of preliminary tests on synthetic rubber materials and porcine specimens were carried out.

#### 3.3.2.1 Methodology

***Rubber Materials***

Two commercial ethylene propylene diene monomer (EPDM) synthetic rubber materials (EPDM 48 and EPDM 85, Just Roller Ltd, UK) were tested at different strain rates and penetration depths. Tests were performed on 2 mm and 10 mm thick sheets of both materials. These materials were chosen since their equivalent elastic modulus were within the range of those reported for articular cartilage [255] (i.e. 1-20 MPa).

The rubber materials were placed on a flat steel base and compression tests were carried out at rates at 0.01, 0.1, 1, 10, 20 and 40 percent per second (pps) using a hemispherical

indenter of radius 1.3 mm. Five locations on the rubber sheets were selected randomly and tested with 5 repetitions.

The experimental elastic modulus values were calculated following the procedure described in detail in Chapter 4, Section 4.2. These were compared with the elastic modulus of the commercial materials calculated from hardness values given on data sheets provided from standard tests [255]. The hardness was obtained using the shore A method and was converted into elastic modulus using an equation published in the literature [256]. Reported hardnesses were equivalent to elastic moduli of approximately 2.5 MPa and 18 MPa, for EPDM 48 and EPDM 85, respectively.

***Porcine Articular Cartilage***

Three porcine specimens were tested at 6 different points, using different strain rates (0.1, 1, 10, 20, 40 pps) and different penetration depths (100, 150, 200, 250 $\mu$m). Articular cartilage thickness at each location was measured after indentation tests were performed and compared to penetration depth. Tested points had a total thickness in the range 900 - 1200 $\mu$m.

#### 3.3.2.2 Results

***Strain Rates***

An apparent increase in stiffness values with strain rate increase was observed (Figure 3.6). This effect was most apparent between strain rates in the range of 0.01 pps to 1 pps in porcine articular cartilage and EPDM 48, and from 0.01 to 10 pps in EPDM 85. Beyond 10 pps, strain rate had a minimal effect on the elastic modulus. These observations were examined statistically using paired T-test on values of subsequent strain rates (i.e.0.01 vs 0.1 pps, 0.1 vs 1 pps, etc). Statistical analysis showed that small strain rates (0.01 vs 1 pps, 0.1 vs 1 pps) had a statistically significant difference in mean values in all (articular cartilage, EPDM 48 and EPDM 85) samples ($p_{85} < 0.003$, $p_{48} < 0.02$, $p_{AC} = 0.029$). Consecutive paired comparisons of higher strain rates (10 vs 20 pps, 20 vs 40 pps) showed no significant difference ($p_{85} > 0.06$, $p_{48} > 0.37$, $p_{AC} > 0.09$).

Viscoelastic materials typically respond differently to loads at different strain rates. As

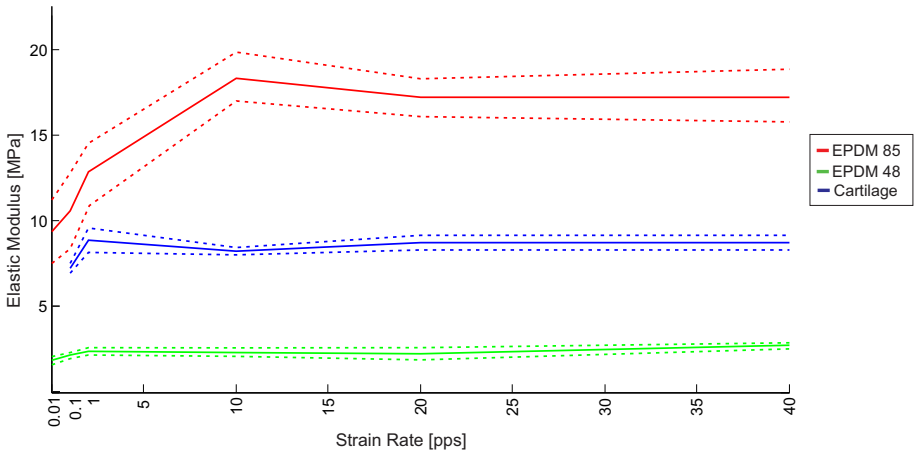


**Figure 3.6:** Elastic modulus calculated from indenting rubber synthetic materials and porcine specimens at different strain rates (0.01, 0.1, 1, 10, 20 and 40 pps)

highlighted in Chapter 2, Section 2.8, in articular cartilage this is related to the flow of interstitial fluid. However, the behaviour of cartilage under high strain rates (i.e. short-term or quick stimulus) can be captured by a linear elastic behaviour based on the assumption that there is no time for interstitial fluid to flow [207]. Slow rates allow interstitial fluid time to flow and therefore a time-dependent behaviour is observed. It has also been demonstrated that in whole specimens this movement of fluid occurs more slowly than in plugs [201].

In the work presented here indentation tests were performed under displacement controlled mode (as described in Chapter 2, Section 2.4.2). The strain rate results (Figure 3.6) indicate that at strain rates above 10 pps, the elastic modulus of porcine cartilage was constant, suggesting elastic material behaviour. This behaviour has been reported by a number of previous studies [207, 257, 258].

Therefore, the indentation test were performed at 10 pps to 10% thickness. This loading cycle was equivalent to 1 Hz, which is comparable to slow walking [130, 253]. Under these conditions the water movement is very small due to a high drag coefficient [259] and as was mentioned previously, this suggests elastic behaviour.

***Modulus Comparison***

The elastic modulus obtained from EPDM 48 at 10 pps was $2.33 \pm 0.19$ MPa, which was 8% lower than manufacturer specifications. The elastic modulus of EPDM 85 at 10 pps was $18.4 \pm 1.73$ MPa, which was 9% higher than manufacturer specifications. This can be partly attributed to the approximate method used to convert the shore A values in the manufacturer's specifications to the elastic modulus. The manufacturer measured shore A hardness, using a durometer. The hardness values were then converted to modulus by the manufacturer using published equation [256]. It was reported by the author [256] that this formula introduces an error of approximately 5% compared to experimental values. Additional differences between modulus values can be attributed to test settings, such as the shape of the indenter (shore A hardness was measured with a cone shaped indenter), strain rates (highly user dependent in shore A) and the use of different dwell times.

***Effect of Thickness***

Articular cartilage thickness is not homogeneous throughout the tibial plateau. In order to perform indentation within 10% of the total articular cartilage thickness advised by Buckle [260], it is useful to have thickness measurements prior to performing indentation tests. In the present work, provided that cartilage thickness could be measured prior to indentation, using an ultrasound probe, the percentage of displacement required could be calculated. Nevertheless, in cases where it was not possible to obtain an ultrasound measurement, a fixed displacement of 200 $\mu$m was applied, and cartilage thickness was measured *a-posteriori* using optical methods.

In such cases, if the depth of indentation went beyond this maximum of 10% of the total cartilage thickness, the results were adjusted by a ratio of depth to thickness [115, 130]. A theoretical solution for these cases was proposed by Hayes *et al.* [115] and, where appropriate, this was applied (Chapter 4, Section 4.2). Nevertheless, it has been reported that when cartilage is thicker than 2 mm this effect is considered negligible [47, 130].

The effect of indentation depth on the articular cartilage stiffness values beyond the threshold of 10% was examined. A slight increase in articular cartilage modulus was

observed when depth of penetration was increased (Table 3.1), however this increase was minimal (less than 2% even at 20% penetration depth).

**Table 3.1:** Elastic moduli values for articular cartilage at different penetration depths

| % Depth | 8.3 | 12.5 | 16.7 | 20.8 |
|---|---|---|---|---|
| E (MPa) | 8.00 | 8.04 | 8.07 | 8. 18 |

When testing the thin rubber sheets (2 mm thickness), an apparent increase in the overall stiffness values was observed, compared to stiffness values found on thick sheets (10 mm thickness), throughout all indentation depths tested (Figure 3.7).

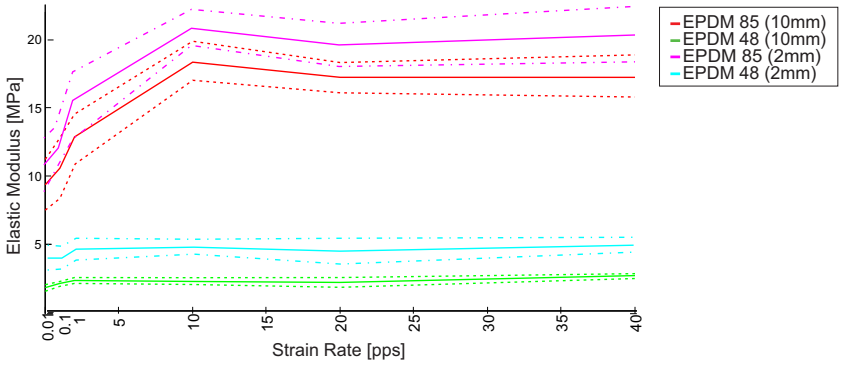


**Figure 3.7:** Comparison between elastic modulus measured on thin sheets vs thick sheets of synthetic rubber.

These results suggest that when measuring mechanical properties on whole specimens with cartilage thinner than 2 mm, it is possible that measurements show an increased elastic modulus due to the effect of the underlying material (i.e. subchondral bone when measuring articular cartilage-on-bone). The difference in modulus between rubber and steel (base on which the rubbers were tested), is greater than the difference between the modulus of cartilage and subchondral bone, thus it is possible that the offset in the absolute values introduced by the thickness, will be less than observed in the rubbers in these preliminary tests (Figure 3.7).

Articular cartilage-on-bone values provide a more realistic indication of the physiological response to load, however it is important to take into consideration the set-up of the test when analysing results.

## 3.4 Conclusions

In this chapter the WASIM was introduced. Moreover, several routines to control the behaviour of this machine were explained. The developed routines are adjustable with minimal modifications to be used with any other probe attached to the WASIM. This makes the WASIM an even more powerful tool for the analysis of whole specimens.

Additionally it was shown that there are several parameters to be considered when performing indentation. Some of these parameters are the size of the indenter, the strain rate at which the load is applied, and the indentation depth which should be calculated relative to cartilage thickness. It has been demonstrated in the literature and through preliminary experiments that the modification of these parameters will alter the measured mechanical properties. Therefore, care should be taken when comparing material properties obtained under different experimental conditions. The measurement of many points over the same tibial plateau allows the understanding of properties distribution under similar external stimuli through relative changes on the parameters over the surface, rather than focussing on absolute independent values.

# Chapter 4

# MATERIALS AND METHODOLOGY

In this chapter the materials and methods used in this thesis are explained in detail. The chapter is divided into sections: (1) Mechanical testing, (2) Calculation of Elastic modulus, (3) Measurement of cartilage thickness, (4) Determination of matrix constitution and (5) Tests of correlation between all variables measured.

The different steps followed for the determination of each variable are outlined in Figure 4.1.

## 4.1 Mechanical Testing

The aim of the mechanical tests was to determine the elastic modulus of articular cartilage at different locations on the tibial plateau. The mechanical testing consists of several steps; (1) Preparation of the sample, (2) Scanning of the sample, (3) Indentation testing and (4) Analysis of the data.

### 4.1.1 Preparation of the Samples

Six porcine tibial plateaux were dissected and dislocated. All the soft tissues, except for the cartilage, were removed. The tibial shaft was cut approximately 100 to 150 mm below the articular surface. The tibial plateau was mounted in the sample holder using bone cement (VersoCit-2 kit, Struers, UK). Once the bone cement was cured,

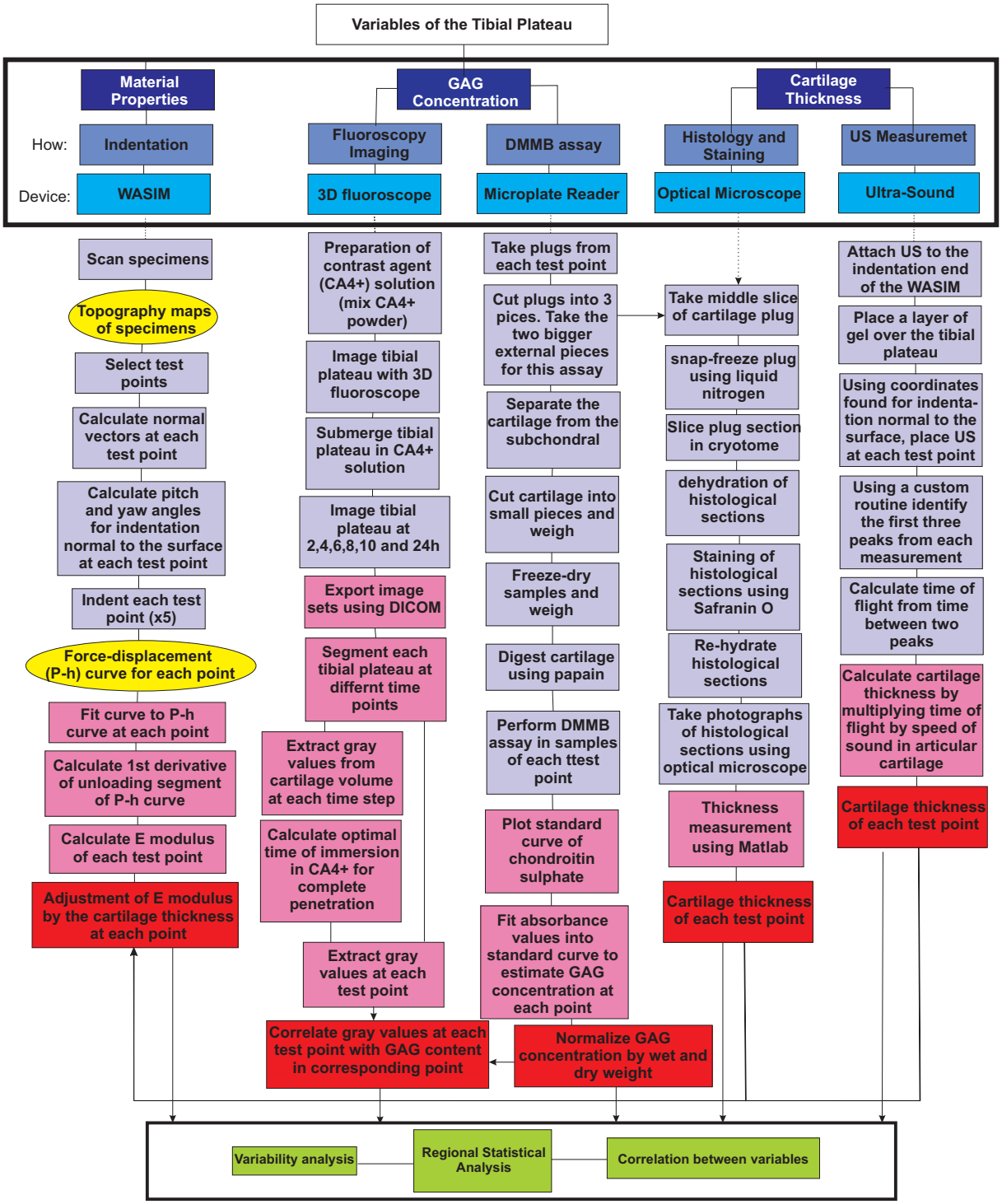


**Figure 4.1:** Methodology flowchart for the measurement of three variables of porcine articular cartilage. The 2nd row highlights the three measured variables (material properties, GAG concentration and cartilage thickness). The 3rd and 4th row identify how the variable was measured and the main device used for this purpose. Below that, in light purple, the main steps of the procedure for the variable measurement are outlined. Yellow ovals represent output from previous section. The pink squares represent the steps followed for the analysis of the data and the red squares were the obtained results. Finally, green squares at the bottom of the flowchart are analyses performed to final results.

the sample holder was mounted in the middle of the stage and the specimen was kept hydrated by keeping it in a bath of isotonic saline solution (0.15 M) before and after tests and by using a drip irrigation system during indentation tests (for more details

see Section 4.1.4). This system allowed tibial plateux to be hydrated constantly. Nevertheless, on some occasions small areas of the tibial plateau could not be hydrated due to the position of the tibia during indentation testing (maximum of 2-5 min). Other authors have reported constant hydration [261] or sample immersion in saline solution [12, 47, 262] while performing *in-vitro* mechanical tests. Dehydration of articular cartilage has been observed after periods of time of around 40 min [263]. Thus, it was assumed that the method of hydration was appropriate and the tissue preserved its integrity. However, continuous hydration might be advisable in the future.

### 4.1.2 Scanning of the Sample

A high resolution laser was used to perform a raster scan of the specimens. Scanning routine is outlined in Chapter 3, Section 3.2.3. Although dimensions of the raster scan could be adjusted according to the size of the specimen, an 80 x 80 mm square raster was used for all the samples used in this study. This size was considered appropriate since it was large enough to cover all tibial plateaux tested.

The process of scanning an area of this dimensions took approximately 1 hour. The output file obtained from this procedure was used to generate a topographical map of the surfaces.

### 4.1.3 Analysis of Topographical Map

Several custom routines were developed by the author during the period of this work to analyse the topographical maps. The objective was to obtain the transformation matrix necessary for indentation normal to the surface at each point.

1. ***Building a 3D Surface***

   Point cloud was meshed (using quad elements) and reconstructed into a 3D surface using Matlab (R2012a, The MathWorks, Inc., Natick, Massachusetts, USA). Resulting surface was smoothed by minimizing outlying data. A continuous surface representing the tibial plateau topography was obtained.

2. ***Selecting Testing Points***

   In the axial view of the surface, the user selected a minimum of 6 points on the

surface. An ellipse was fitted onto the selected points using a least-squared fit (LSF) and an equally spaced grid of points (6 mm spacing) was then fitted to the ellipse. This separation (6 mm) was chosen due to the 4 mm diameter of the osteotome used later to extract cartilage plugs centred at each testing point (Chapter 5).

Test points were generated using an algorithm that fitted points into a predetermined area (ellipse fitted to the tibial plateau). The first point was located in the central regions of the tibial plateau and following points were positioned in nearest point of the grid, keeping a symmetrical distribution. Once the next possible position reached the external border, the new position moved further from the centre.

The test points were obtained from the grid for each tibial plateau (Figure 4.2). The X, Y, Z, yaw and pitch position of each of these points was recorded in a file which will be referred to as the "Initial Testing Points" file.

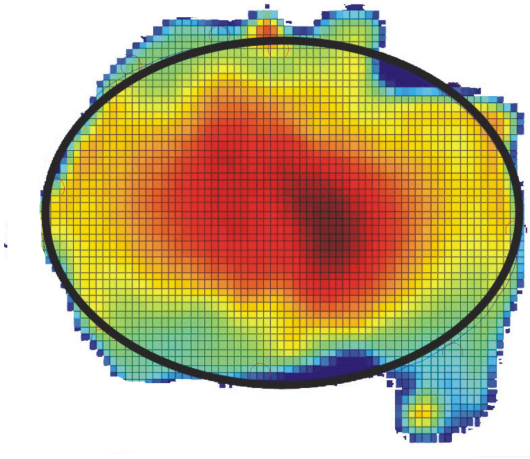

**Figure 4.2:** Ellipse is fitted into axial view of the tibial plateau

3. ***Measuring Surface Height***

A routine (C++) which interacted with the WASIM was developed to read the "Initial Testing Points" file. This automated routine allowed the re-measurement of the testing point height. The routine aligned each test point with the high resolution laser beam and measured the height of each testing point. The re-measured surface height was recorded in a file referred to as the "Selected Testing Points" file. This procedure allowed the direct reading of each testing point

height, rather than relying on the interpolated value. Additionally, manual filtering of testing points was performed to only take points inside the region of interest (ROI) (Figure 4.3).

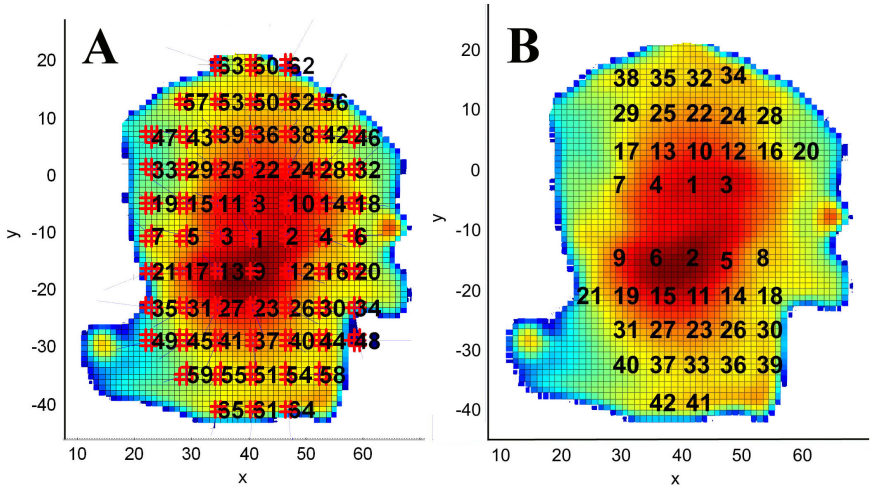


**Figure 4.3:** Testing points in the tibial plateau. A. All testing points, B. Selected testing points

### 4.1.4 Indentation Testing

Using the custom routine presented in Chapter 3, Section 3.2.5, mechanical properties at each test point were measured.

The average time for testing each whole tibial plateau (average 40 testing points) was 2 hours. This procedure was repeated five times for each point for each tibial plateau specimen.

Displacement and force were measured at a sampling frequency of 200 Hz throughout the test and recorded. Once the indentation process was completed for a given point, the indenter lifted to a position where it was clear of the surface and the process was repeated for the next point.

A drip irrigation system (Garland Big Drippa Watering Kit, Garland Products Limited, England), used normally for gardening was adapted, with the aim of keeping the tibial plateau hydrated while mechanical tests were carried out (Figure 4.4). A 10.25 L bag was filled with saline solution (0.15 M). The bag was held by a patient hospital rack (drip stand) and connected to a pipe of about 1.5 m. Four adjustable drippers were connected at intervals of 50 mm at the end of the pipe. These were positioned

circumferentially around the load cell. The drippers could be adjusted to regulate the release of saline solution and for testing they were set at approximately 2 drips per second. The circumferential position of the dripper ensured that all points of the tibial plateaux remained hydrated throughout testing.

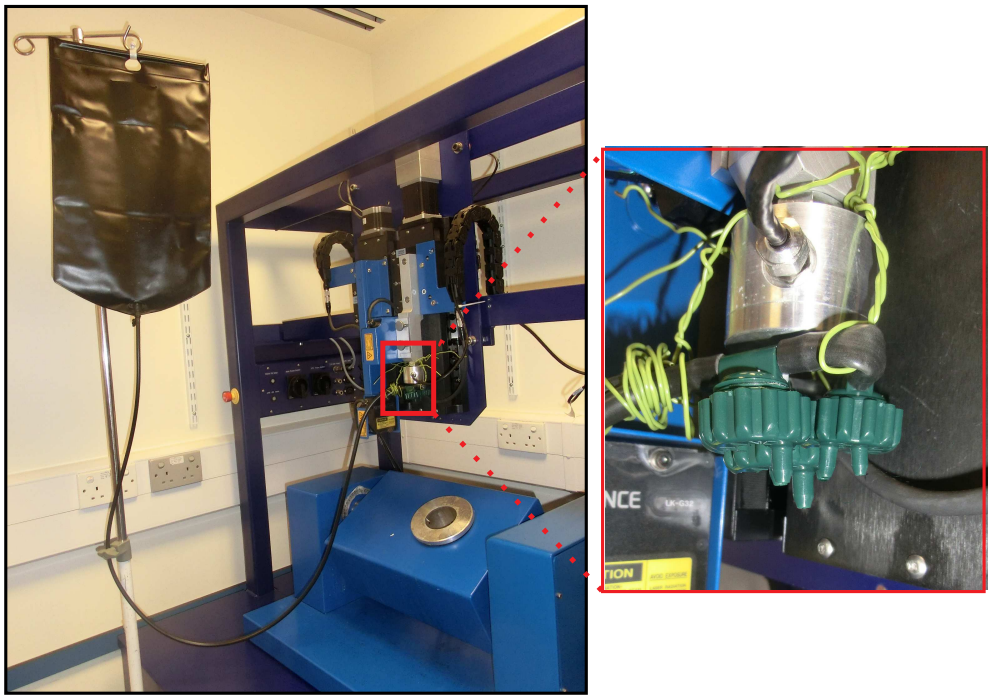

**Figure 4.4:** Drip Irrigation System for cartilage hydration

### 4.1.5 Calculating Stiffness

A custom Matlab routine was developed in the present work to plot the displacement (h) against force (P) for the indentation of each point. For each force-displacement ($P - h$) curve the following points were identified: (1) maximum load ($P_{max}$), (2) maximum displacement ($h_{max}$), (3) residual displacement when unloading was complete ($h_r$) and all points from the unloading curve.

Following the Oliver and Pharr method [132], the unloading curve was used to calculate the stiffness of the tested area. This method is based on the theory that the loading is elastic-plastic, while the unloading is elastic, therefore the stiffness can be described by the 1st derivative of the unloading curve (Equation 4.1) [132, 134].

$$S = \frac{dP}{dh} \tag{4.1}$$

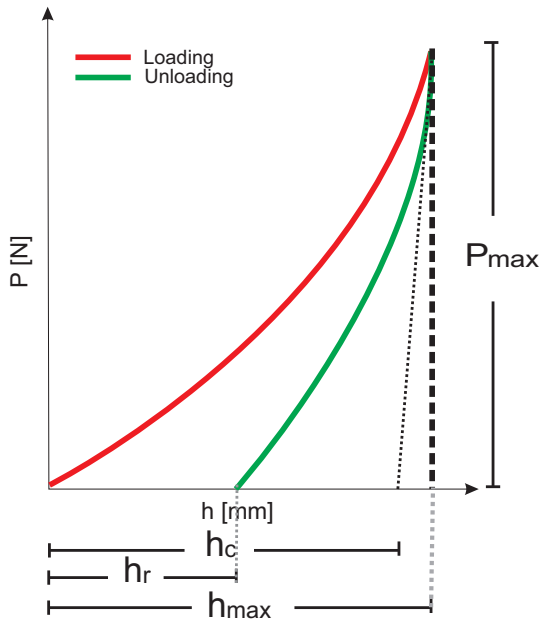


**Figure 4.5:** Force-displacement ($P-h$) curve. The following points were identified: (1) maximum load ($P_{max}$), (2) maximum displacement ($h_{max}$), (3) residual displacement when unloading was complete ($h_r$) and (4) contact depth.

There are two commonly used procedures to calculate the stiffness. The first is to fit a straight line to the superior portion of the unloading curve. In this method the slope of the line represents the stiffness. The problem with this method is how to choose the portion of the unloading curve that should be taken into consideration, since this will inevitably affect the result [132]. The second method is to fit the unloading curve to a power law equation known to describe the curve behaviour (Equation 4.2). The stiffness is then calculated by differentiating Equation 4.2 and evaluating it at $h_{max}$ and $P_{max}$.

$$P = B(h - h_f)^m \tag{4.2}$$

where $P$ is the load, $h$ is the displacement, $h_f$ is the final displacement when unloading is complete ($h_r$) in Figure 4.6, and $B$ and $m$ are constants determined by the curve fitting.

Hertzian contact theory [264] which describes the contact between two spheres, was used to model the contact between a hemispherical indenter and the cartilage of the whole tibial plateau. This can be approximated to contact between a sphere (sphere 1, with stiffness $E_1$) and a semi-half space (semi-half 2 space, with stiffness $E_2$) by making the radius of the articular surface tend to infinity [118, 264].

According to Hertzian contact theory, the load can be described by Equation 4.3.

$$P = \frac{4}{3}\sqrt{R}E^{*}h^{\frac{3}{2}} \tag{4.3}$$

Since there is special interest in the elastic part of the curve (unloading portion), Equation 4.3 becomes Equation 4.4.

$$P = \frac{4}{3}\sqrt{R}E^{*}(h - h_f)^{\frac{3}{2}} \tag{4.4}$$

where R is is the radius of the indenter and $E^{*}$ is the effective elastic modulus given by Equation 4.5

$$\frac{1}{E^{*}} = \frac{1-\nu_1^2}{E_1} + \frac{1-\nu_2^2}{E_2} \tag{4.5}$$

where $\nu$ is the Poisson's ratio ($\nu_1$ for the sphere and $\nu_2$ for the half space).

However, since the indenter is significantly more rigid than cartilage, the indenter can be assumed to be perfectly rigid ($E_1 \to \infty$). Therefore $E^{*}$ becomes

$$E^{*} = \frac{1-\nu_2^2}{E_2} \tag{4.6}$$

where $E_2$ is the cartilage elastic modulus.

Comparing Equation 4.2 with Equation 4.4, it can be deduced that $m = 1.5$, which would be taken as the initial value for curve fitting. Furthermore, the stiffness was determined by the differentiation of Equation 4.4 [134].

$$S = \frac{dP}{dh} = 2\sqrt{R}E * (h - h_f)^{\frac{1}{2}}|_{h=h_{max}} \tag{4.7}$$

The following assumptions of Hertzian contact theory were taken into account for analysis: (1) size of the indenter relative to the specimen, (2) deformation after load compared to radius of the indenter, (3) elasticity of the samples, (4) friction between

surfaces

Hertzian contact theory takes into account several assumptions: (1) The surfaces are continuous and non-conforming: This makes reference to smooth surfaces in the areas where contact takes place, and that the contact occurs in one point at first. (2) Size of the indenter is relatively small compared to the specimen, (3) Small deformations compared to the size of the indenter. (4) Both solids can be considered elastic half-space and (5) The surfaces are frictionless.

Both the indenter and the articular cartilage surface are smooth (roughness significantly smaller than the radius of the indenter). The radius of the indenter was approximately 10 times larger than the deformation of the specimen under maximum load. It was assumed that under the conditions of indentation tests (loads less than 20 MPa and deformation rate of 200 $\mu$m/s) both the steel indenter and the articular cartilage behaved elastically in the unloading part of the curve. Finally, normal indentation (indentation perpendicular to the surface) reduced the friction to a minimum and therefore it was assumed to be negligible.

## 4.2 Calculating Elastic Modulus

The elastic modulus was calculated taking into account the stiffness values for each test point (Chapter 4, Section 4.1.5) and the thickness at that point (Chapter 4, Section 4.3).

It was also important to take into account Hertz assumptions discussed in Chapter 4, Section 4.1.5. Additionally, some authors have observed that when the radius of the indenter is comparable to the thickness of the articular cartilage, an adjustment of the elastic modulus due to cartilage thickness must be carried out [47, 115]. This adjustment was performed following Hayes *et al.* suggestions [115].

1. ***Calculation of Elastic Modulus*** Sneddon [265] derived an equation that relates the depth of penetration of an indenter tip ($h$) with the load applied to it (P) (Equation 4.8).

$$P = \frac{4Eah}{1-\nu} \tag{4.8}$$

where $a$ is the contact radius between the cylindrical flat-ended punch and the surface at maximum load, E is the elastic modulus and $\nu$ is Poisson's ratio.

An extension of Sneddon's equation by Oliver *et al.* [266], adapted Equation 4.8, to include the projected contact area of an indenter ($A_c$ ). Equation 4.1 is equal to Equation 4.9.

$$S = \frac{dP}{dh} = 2E^* \sqrt{\frac{A_c}{\pi}} \tag{4.9}$$

where, S is the stiffness calculated in Chapter 4, Section 4.1.5 with the Oliver and Pharr method. $E^*$ was defined in Equation 4.6. Therefore, the elastic modulus of cartilage is obtained by making a substitution of Equation 4.6 into Equation 4.9 and rearranging Equation 4.9 to obtain E (Equation 4.10 )

$$E = \frac{1-\nu^2}{2} \sqrt{\frac{\pi}{A_c}} \frac{dP}{dh} \tag{4.10}$$

Equation 4.10 is valid for any indenter with a form of a body of revolution with a smooth surface [266]. Then $A_c = \pi a^2$ where $a$ can be calculated by the Field and Swann method [133].

$$a = \sqrt{2Rh_c - h_c^2} \tag{4.11}$$

where R is the radius of the indenter and $h_c$ is the contact displacement (contact depth).

To obtain $h_c$, Equation 4.2 (Chapter 4, Section 4.1.5) was used for data fitting. When Equation 4.7 (to determine stiffness) was evaluated at $P_{max}$, this $h_c$ was defined as:

$$h_c = h_{max} - \epsilon \frac{P_{max}}{S} \tag{4.12}$$

where $\epsilon$ is a constant which depends on the geometry of the indenter [132]. $\epsilon =$

0.75 for a paraboloid of revolution [132] (hemispheral indenter).

$A_c$ was defined as a function of $h_c$ and was obtained by replacing $h_c$ in Equation 4.11 with Equations 4.12 and then calculating the projected area $A_c$. Finally $A_c$ was input into Equation 4.10 to obtain the elastic modulus of cartilage.

2. ***Adjustment of Elastic Modulus by Cartilage Thickness***

   As mentioned previously Buckle [260] demonstrated that indentations should only be to a maximum of 10% the thickness of the sample been tested. However, studies have found that these alterations are negligible when cartilage is thicker than 2 mm [47, 115, 251, 267, 268, 269].

   If the cartilage at a given point was thicker than 2 mm then the elastic modulus of cartilage was obtained through Equation 4.10. However, if the cartilage is thinner than 2 mm, an adjustment is required.

   Hayes *et al.* proposed a theoretical solution that accounts for the thickness effect when stiffness measurements are made with indenter radius comparable to the cartilage thickness [115]. They proposed using a constant $\kappa$ which is dependent on the ratio between the radius of contact ($a$) and the cartilage thickness ($h$). The adjusted elastic modulus of cartilage was then obtained using Equation 4.13

$$E_{adj} = \frac{1-\nu^2}{2\kappa}\sqrt{\frac{\pi}{A_c}}\frac{dP}{dh} \tag{4.13}$$

   where $\kappa$ values were found in Hayes *et al.* [115].

   Following these points the mean elastic modulus at each test point was calculated (and adjusted) from the mean stiffness at the corresponding point.

### 4.2.1 Analysis of Elastic Modulus

Statistical analysis was performed on the elastic modulus results and distribution throughout the tibial plateaux. In the first instance the repeatability of the elastic modulus values measured by repeated indentation tests at each point was performed. The variability distribution over the tested locations on the same knee was determined.

Then, mean elastic modulus values were grouped into various regions of clinical relevance and compared.

1. **Repeatability**

   Indentation tests at each of the testing points were repeated five times on five tibial plateaux. Indentation tests for specimen S1 were only performed once, therefore this specimen was not taken into consideration for this statistical analysis.

   Repeatability was calculated using the coefficient of variation (CV) between the repeated indentation tests on each knee. The CV is defined as the standard deviation (SD) within each point divided by the mean of the point (Equation 4.14) [270].

$$CV = \frac{SD_{within \quad each \quad test \quad point}}{Mean_{test \quad point}} * 100 \tag{4.14}$$

   The CV for each point was calculated using Equation 4.14. Additionally, in order to obtain the CV value for each tibial plateau, the CV of each point was squared and the CV of the specimen calculated was the root square of the average of the squared CV of each point (Equation 4.15).

$$CV_{specimen} = \sqrt{\sum_{i=1}^{n} (CV)_i)^2} \tag{4.15}$$

   where $i$ is the testing point number.

2. **Variability of Elastic Modulus Distribution**

   Elastic modulus variability over each tibial plateau was represented using a box plot of all the elastic moduli measurements for each point. The box plots show the spread of elastic modulus measurements for each point over the tibial plateau.

3. **Regional Elastic Modulus Distribution Analysis**

   Further analysis of the elastic modulus distribution was attempted. Elastic modulus values were grouped into different regions (by compartments, by half

compartments and by Modified Michigan Regions (MMR)) in order to better understand the variations across the tibial plateau.

- ***Medial and Lateral Compartments***

  Elastic modulus mean values were grouped according to the compartment they belonged to, medial or lateral. Statistical analysis was then performed to compare means.

- ***Four Regions***

  Here the tibial plateau was divided into four regions (Lateral-Anterior (LA), Lateral-Posterior (LP), Medial-Anterior (MA) and Medial-Posterior (MP)) (Figure 4.6). elastic modulus means in each region were then compared.

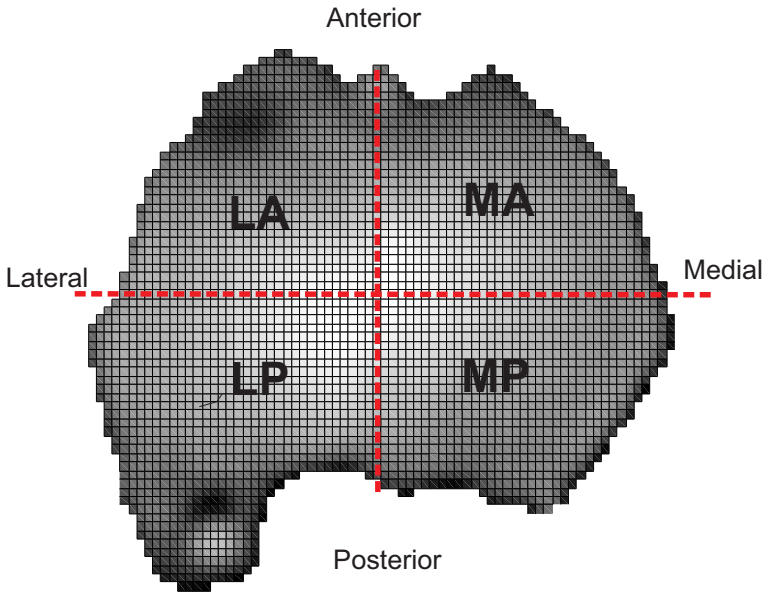


**Figure 4.6:** Division of tibial plateau in 4 regions

- ***Regional Analysis Using Modified Michigan Regions***

  Many authors have shown that there are significant differences between cartilage variables in areas covered by the menisci and areas uncovered by the menisci [3, 23, 89, 103, 271]. Most of these studies have restricted their analyses to these two regions in each compartment.

  Recently, a study [2] was published proposing regions for the analysis of mechanical properties. This study used the classic separation between "covered" and "uncovered" by the menisci, but divided the covered area into 3 smaller regions: II - anterior external, III - central external and IV - posterior

external. Region I is not covered by the meniscus [2] (Figure 4.7). These regions will be referred to as the Michigan Regions (MR), as the study originated from University of Michigan, Michigan, USA.

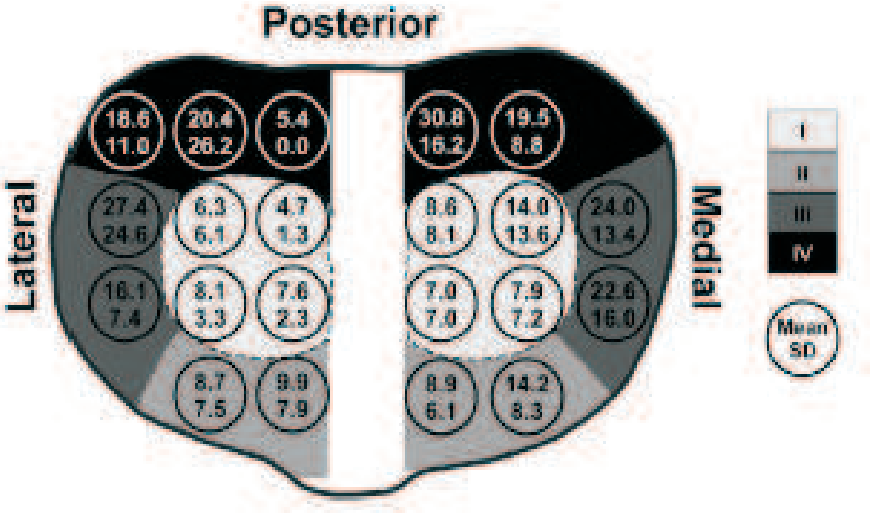


**Figure 4.7:** Michigan regions [2]. Reproduced with permission of John Wiley and Sons.

In this work, a new region selection, based on the MR, was carried out with the aim of adapting these MR to the work performed here. The new regions will be referred to as Modified Michigan Regions (MMR). Changes included enlarging the regions to a bigger area of the tibial plateau, separation of the regions between compartments (rather than assuming that mirror regions behave similarly), adapting uncovered menisci area to porcine specimens (Figure 4.8).

For the identification of the MMR regions, an image of the whole tibial plateau, before menisci removal, was taken (Figure 4.9.A). (1) The menisci location was identified on this image. This divided the tibial plateau in an area covered by the menisci and one uncovered by the menisci. (2) The menisci were removed from the tibial plateau and a second image was taken (Figure 4.9.B). (3) The area covered by the menisci was divided into 3 parts: the anterior quarter became region II, the middle part corresponded to region III and the posterior quarter was region IV. Region V corresponded to areas uncovered by the menisci on the external rim. (4) The topographical

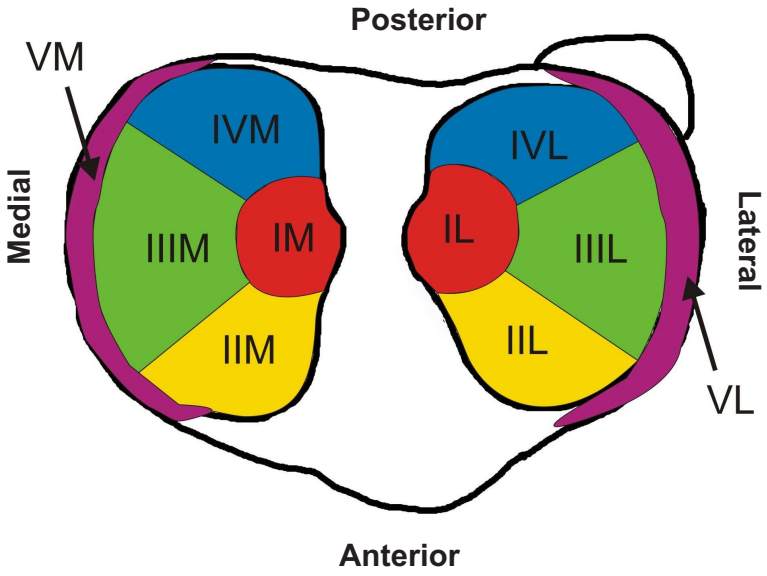


**Figure 4.8:** Modified Michigan regions used for data analysis. Region I was the area uncovered by the menisci in the central area of the tibial plateau on the medial (IM) and lateral (LM) compartment. Area uncovered by the menisci and located in the external rim of the medial and lateral rim where separated into a new region VM and VL respectively. The area covered by the menisci was divided into 4 parts. The two middle parts corresponded to region III, the posterior quarter was region IV and the anterior quarter became region II.

surface of the corresponding tibial plateau (obtained in Chapter 4, Section 4.1.3) was superimposed on the previously acquired image. (5) Test points on each tibial plateau were grouped into the regions they were located (Figure 4.9.C).

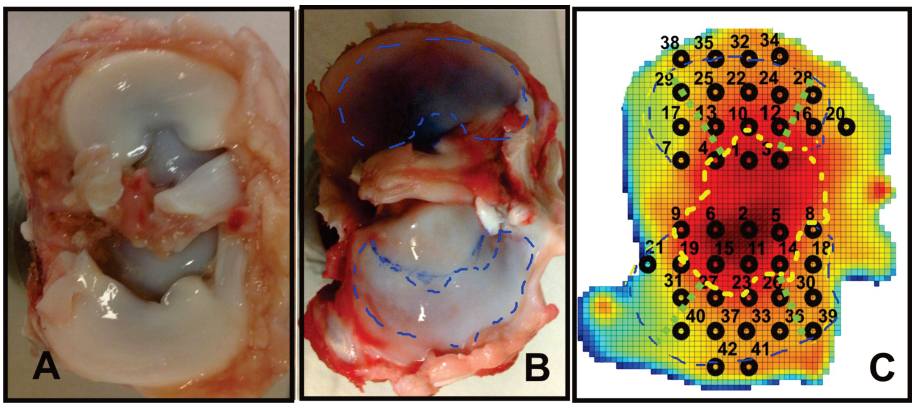


**Figure 4.9:** Identification of MMR on each tibial plateau. (A) Shows the image of the whole tibial plateau previous to menisci removal. (B) shows the image of the tibial plateau posterior to image removal with area covered by the menisci and area uncovered by the menisci identified. (C) Topographical map was compared to tibial plateau and test points were grouped in four regions according to location.

Mean values for each region were analysed using statistical analysis (described as follows).

***Statistical Analysis***

Mean comparison statistical analysis of elastic modulus variable over topographical regions was conducted to evaluate the null hypothesis: "*there is no difference between the elastic modulus means in different regions of the tibial plateau*".

Equal distribution of variance was tested by performing Levene's test for homogeneity. ANOVA was used to examine the overall difference between groups. Post-hoc paired groups difference was assessed by using a least squares difference (LSD) approach. Finally, the effect size described by Cohen, 1988 [272] was calculated and used to assess the obtained results. This value is important since it reveals how much difference there is between groups.

Cohen's theory proposes to calculate the proportion of variance ($\eta^2$) by dividing sum squares between groups by the total sum of squares (Equation 4.16). $\eta^2$ values are in the range of 0 to 1, 1 signifies a very big difference between the groups and 0 no difference.

$$\eta^2 = \frac{SS \quad between \quad Groups}{SS_{total}} \tag{4.16}$$

## 4.3 Cartilage Thickness Measurement

Cartilage thickness over the six tibial plateaux specimens was measured non-invasively with an ultrasound probe and by an invasive optical method using the light microscope to observe histologically prepared samples.

### 4.3.1 Measurement of thickness using ultrasound

In Chapter 2, Section 2.3.4 a background on the use of US was presented. With the aim of acquiring the thickness measurements of articular cartilage at each testing point an ultrasound transducer was used. An A-mode ultrasound pen-like transducer, (V312, Panametrics, Olympus, MA, USA) and (V313, Panametrics, Olympus, MA, USA), with a centre frequency of 10 MHz, a diameter of 6 mm and bandwidth of -6 dB was used. The output was connected observed through a virtual oscilloscope.

The ultrasound was adjusted (screwed) into the indenter position. The US was positioned perpendicular to the surface tested for thickness. The rotation and translation angles calculated previously for indentation normal to the surface (Section 4.1.3) were used for the US positioning. A layer of gel (Parker Laboratories Inc, New Jersey, USA) over the cartilage surface was placed in AOI previous to measurements.

The thickness of articular cartilage was calculated using the time of flight, calculated from the time between two peaks observed from the amplitude of the output signal. The first peak observed corresponding to the gel-articular surface interface and the 2nd peak corresponding to the articular cartilage - subchondral bone interface. Between these two peaks, but closer to the articular cartilage - subchondral bone interface peak, a peak with lower amplitude is observed, which corresponds to the tidemark [108].

To calculate cartilage thickness, time of flight was multiplied by the speed of sound in articular cartilage (1760 $ms^{-1}$ [273]).

The aim of this section was to measure the thickness in all testing points non-destructively previous to performing the mechanical tests. In order for this to be practical, it was important that measurements were accurate and reliable each time. Moreover, cartilage thickness measurements obtained using US were then compared with those obtained by the optical method described below.

### 4.3.2 Histology and Safranin O staining

In Chapter 2, Section 2.7.3 histology and staining of cartilage were introduced. The staining procedure used was first described by Klymkowsky and Hanken to stain amphibious samples with Alizarin Red. This procedure was modified for staining of thin sections with Safranin O (No. S-2255, Basic Red 2, Sigma Companies Group Pty Ltd, Perth, Western Australia) [274].

#### 4.3.2.1 Materials and Methods

Each tibial plateau was divided into 4 mm diameter plugs which were then divided into 3 sections (Figure 4.13). The middle section of each plug (centred on each testing point described in Chapter 4, Section 4.4.4.4) was decalcified by immersing the plug

in 8% formic acid for 72 hours. Samples were then placed in 10% neutral buffered formalin solution for 5 days. The sections were then snap-frozen with liquid nitrogen and placed in a -80 $^{\circ}C$ freezer for at least 2 hours.

The cartilage plug sections were then sliced into 6 $\mu$m thick slices at -30 $^{\circ}C$ using a cryo-microtome (2800 Frigocut-E, Reichert-Jung, Reichert Tech, Munich, Germany). Cuts were made perpendicular to articular surface, so each slice contained both cartilage and bone. Histological sections were placed on identified adherent microscopic glass slides and stained with Safranin O dye by the following protocol described below:

***Staining Protocol:***

- Safranin O was prepared by combining 100 mg Safranin O and 100 ml acetic acid in 100 ml distilled water ($dH_2O$).
- Histological sections were dehydrated by placing them in a series of graded concentrations of alcohol solutions for intervals of 2 minutes. Sections went from through different concentrations of alcohol (Xylene/Clearene x 2, 70%, 90%, 100%, 100%).
- Histological sections were then immersed in Safranin O dye for 5 minutes.
- Further, dehydration was performed by passing the sections though increasing concentrations of alcohol (70%, 90%, 100%, 100%, clearing x 2) in 1 minute intervals.
- Finally, sections were mounted using resinous medium and covered with a cover-slip.

Sections were observed in a light microscope (BX40F4, Olympus, Tokyo, Japan) at 400x magnification and 200x magnification. Digital images (two fields per magnification value) were recorded (camera U-READB 60X, Olympus, Tokyo, Japan). The scale was displayed on each image (Figure 4.10).

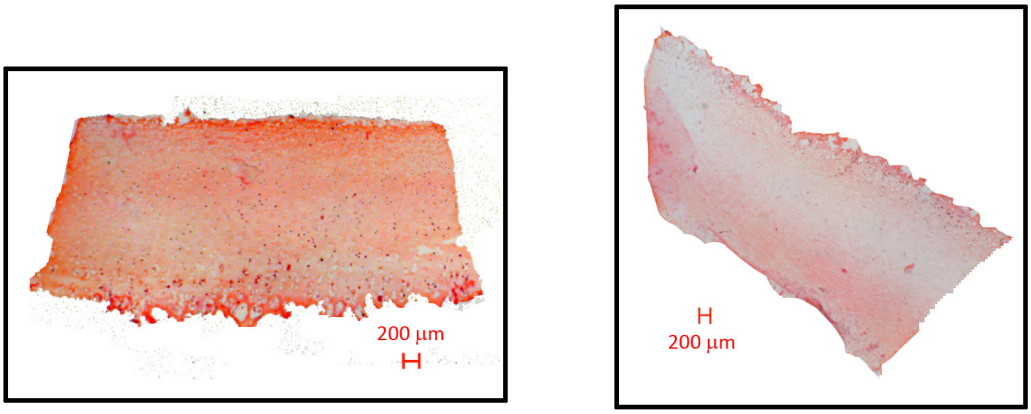


**Figure 4.10:** Safranin O stained histological sections with microscopical scale on the side.

#### 4.3.2.2 Acquisition of Thickness Through Histology

A custom program, was developed in Matlab, to allow the measurement of the cartilage thickness for the histological sections. The program used the scale to convert image coordinates into millimetres and then allowed the measurement of the cartilage thickness.

To obtain cartilage thickness distribution, thickness measurements were performed for different slices of the same plug section. From four to eight slices on each plug section were obtained. The measurements of each plug were then averaged for each plug. Thickness measurements were then plotted at their corresponding location of the cartilage surface.

### 4.3.3 Statistical Analysis

A more comprehensive understanding of cartilage thickness distribution was sought and therefore a series of statistical analyses were performed on the cartilage thickness measurement data.

- **Repeatability**

  Repeatability of thickness measurements made on the histological slices for each plug was tested by calculating CV within measurements on the same plug section. Repeatability was carried out on five specimens, since measurements on S6 were performed only once for each plug due to time limitations.

- **Variability of Thickness Distribution**

  Variability of thickness distribution over each tibial plateau was assessed. Box plotting allowed the visualization of variation of measurements within the same point as well as over the whole tibial surface.

- **Regional Analysis of Thickness Distribution**

  Cartilage thickness measurements were compared over different regions using statistical analysis outlined earlier (Chapter 4, Section 3). First, the mean cartilage thickness of each compartment was compared. Second, the mean cartilage thickness of the LA, LP, MA and MP regions were calculated and compared. Finally, cartilage thickness means were grouped into the MMR's.

For the statistical analysis the independent variable was the region it belonged to (Lateral and Medial for first case, LA, LP, MA, MP for the second and MMR for the third). The dependent variable was the mean cartilage thickness at each testing point.

## 4.4 Matrix Constitution

A non-destructive method for GAG quantification in whole tibial plateaux was attempted. This was part of a number of ongoing preliminary tests for future clinical applications involving early OA detection. The use of fluoroscopes for GAG quantification is advantageous due to low running costs and widespread access. To the author's knowledge quantifying GAG in this way has never been done previously.

Whole undamaged tibial plateaux were immersed in a cationic contrast agent (CA4+) for 24h. Tibial plateaux were then imaged using a 3D fluoroscope (3D-RX, BV Pulsera 12", Philips Medical Systems, Veenpluis, The Netherlands). The attenuation (gray) values at each test point were obtained by segmenting the 3D fluoroscopy image sequences using Mimics (Materialise, Leuven, Belgium) and extracting the gray values at each test point. In order to complete the non-destructive method for quantifying GAG, attenuation values were correlated to GAG content in test point. GAG quantification at test points was carried out by extracting osteochondral plugs from test points and performing DMMB assay on cartilage at each location. A calibration curve

was produced showing the relationship between attenuation of CA4+ in the fluoroscope volumes with GAG content measured by the DMMB assay.

Unfortunately the nature of the relationship between the gray values and GAG content was not predictable and therefore the GAG quantification obtained by DMMB assays were used for GAG analysis at each point in all specimens.

### 4.4.1 Contrast Enhanced 3D Radiographical Imaging

Non-invasive methods to detect GAG concentration by combining imaging methods with contrast agents were discussed in Section 2.7. Bansal *et al.* studied the effect of different anionic and cationic contrast agents in the detection of GAG through contrast enhanced computed tomography (CECT) [275, 276, 277]. After a series of comparisons between several contrast agents, it was found that cationic contrast agents perform better than their anionic counterpart by comparing similar charges [277]. These studies showed that cationic contrast agents achieve higher X-ray attenuation values using less concentration of contrast agent than the commercially available anionic contrast agents [276, 277]. Additionally, cationic contrast agents have shown to have a high specificity regarding attachment to GAG, which was demonstrated by the observation of expected GAG distribution throughout cartilage layers [276, 277]. A contrast agent with four positive charges (CA4+) was found to have the best performance compared to one or two charges [276, 277]. It was demonstrated that CA4+ concentrations significantly correlated with GAG content and the attenuation coefficient accounted for 83% of the GAG content changes in articular cartilage [276]. The contrast agent CA4+, provided by Prof. Mark Grinstaff's group at Boston University, was used with the aim of developing a non-destructive method to quantify GAG in articular cartilage.

#### 4.4.1.1 Optimization of Fluoroscopic Image Acquisition Variables

The CA4+ contrast agent was previously tested in combination with $\mu$CT imaging [275, 276, 277]. The use of $\mu$CT provides great advantages regarding high image resolution ("70 mm in plane resolution and 1 mm inter-slice distance" [275]) and short amounts of time for image acquisition compared to other imaging techniques such as MRI [275,

277]. However, for clinical applications, the use of devices that allow *in vivo* imaging is essential. The fluoroscopes are low radiation devices and they are readily available in clinical settings, thus it was relevant to test the CA4+ using this device.

The 3D fluoroscope used in this study (3D-RX, BV Pulsera 12", Philips Medical Systems, Veenpluis, The Netherlands) consists of a rotational C-arm, with the X-ray source and detector placed on opposite sides. The BV Pulsera software allows volume capture and reformatting to create a rectangular capture volume, similar to that produced by a CT scan.

The use of the fluoroscope requires the operator to wear a lead apron and stand at least 2 m away from X-ray tube and behind a leaded screen while acquiring the image. Additionally, specific training on radiation safety and use of fluoroscope was carried out. Local rules and protocols for fluoroscope use were developed in conjunction with a Nuffield Orthopaedic Centre radiologist for its use.

Image acquisition was carried out using the 3D Rotational X-Ray (3D-RX) setting on the fluoroscope. This setting required the selection of the frame frequency (3,8 or 15 frames per second (fps)) and the image size (diameter of 16.3/12.4/9.3 cm). The number of fps resulted in different number of images for each scan (90, 225 or 450 images per scan respectively).

***Materials and Methods***

Two tibial plateaux were scanned with different amounts of soft tissue (before dissection and after dissection) and in different media (air, water, saline solution) and different containers (polyethylene bag, plastic container, pyrex glass). By alternating conditions, optimal variables were obtained. These settings were used for all posterior imaging.

The use of the fluoroscope required several steps:

- Position of rotation axis of the fluoroscope was adjusted so the C-arm could rotate without colliding with the floor or with the table on which the specimen was placed. Additionally, rotation axis was adjusted so the specimen was aligned with the X-ray source. These adjustments were tested by taking low radiation 2D images after each adjustment.

- Once the correct position was obtained, the image was acquired in an arc spanning 200° around the specimen. The acquired image series had a default resolution of $256^3$ voxels and a reconstruction volume of 2.3/1/0.4 litres depending on the sphere diameter chosen when the image was acquired.
- The acquired image series were reconstructed in a 3D volume resolution of $128^3$, $256^3$ or $512^3$ voxels and exported in DICOM format.
- This image data was then imported into Mimics (v14.1, Materialise, Netherlands), reconstructed and segmented using a semi-automated threshold based segmentation to produce a 3D geometry.

#### 4.4.1.2 Preparation of CA4+ Solution

It was established by observation that a minimum of 50 ml of CA4+ solution was needed for complete immersion of one average size tibial plateau. This was determined by measuring different volumes of solution required to completely submerge the tibial plateau. The solution was prepared by following these steps:

- 1.5 g of CA4+ were mixed with 50 ml of deionidised water.
- 25 mg of proteinase inhibitor cocktail (P214-1BTL, Sigma-Aldrich, MO, USA) was added to the solution.
- pH of solution was set to 7.4 by adding NaOH. pH was measured using pH meter (Mettler Toledo Seven Easy, Mettler-Toledo Inc, Columbus, USA).

#### 4.4.1.3 Estimation of Diffusion Time of Contrast Agent in the Tibial Plateau

The diffusion of the contrast agent through the cartilage layers and throughout the whole tibial plateau was essential for the acquisition of accurate measurements of GAG content. Previously, the performance of CA4+ was studied using small (diameter $\leqslant 7$ mm) cartilage plugs [275, 276, 277]. Given that the current study utilised whole tibial plateaux, it was important to determine the time of diffusion.

- Five porcine knee joints were dislocated, soft tissue was removed and joints were dissected.
- The five tibial plateaux were immersed in 50 ml of CA4+ solution at room temperature.
- Imaging of each sample and CA4+ was performed at 0, 2, 4, 6, 8, 10 and 24 hours of immersion using the 3D fluoroscope under optimised settings (see Chapter 4, Section 4.4.1.1).
- Image sequences obtained were segmented using Mimics software and reconstructed into a 3D volumes (see Chapter 4, Section 4.4.1.4).
- Bansal *et al.* proposed the use of the contrast agent uptake ratio (CUR) to calculate the attenuation per unit of GAG [276]. CUR is the ratio between the attenuation value of the cartilage and the attenuation value of the CA4+. Grey values of cartilage volume at each time point were extracted. CUR values at each time step were calculated from gray values of the segmented cartilage volume and gray values of CA4+.
- A curve representing CUR value in reference to acquisition time of image was constructed.
- CUR values for each specimen were fitted into a curve of the type $1 - A * exp^{-(\frac{T}{\tau})}$. $\tau$ value for each specimen was obtained. The $\tau$ value described the time required to reach 65% of the maximum attenuation. Assuming linearity between 65% and 100% contrast agent penetration, time for full penetration was calculated by interpolating $\tau$.
- Optimal time needed for full diffusion of contrast agent was calculated by the identifying the minimal time at which the CUR value plateaued.

#### 4.4.1.4 Segmentation: Development of Attenuation vs. GAG Concentration Curve

DICOM image sequences obtained from the 3D fluoroscope at different time points, were imported into Mimics software. The aim of the segmentation was to acquire the cartilage volume at each time point, in order to be able to compare the CUR value of each specimen at different time points. To achieve this the following segmentation steps were carried out:

- Using semi-automatic thresholds in combination with manual segmentation, cartilage and bone surfaces were acquired. Segmentation was done up to the growth plate line, instead of whole bone, for two reasons: (1) more efficient segmentation, (2) more accurate subsequent registration. This segmentation will be referred to as *"bone and cartilage"*.
- Segmentations of *"bone and cartilage"* were reconstructed into 3D volumes.
- The final *"bone and cartilage"* volume, the corresponding to image sequence obtained last (i.e. left the longest in the CA4+) was used for reference volume. This volume will be referred to as *"bone and cartilage Tf"* (Tf refers to final time).
- *"bone and cartilage"* volumes of all other time points were registered to *"bone and cartilage Tf"*. Registered volumes were converted into masks.
- As mentioned previously cartilage is not visible in X-ray imaging without the use of a contrast agent. Therefore, it was hypothesized that cartilage was fully visible at the mask corresponding to *"bone and cartilage Tf"* and non-existent at the mask corresponding to the image sequence previous to immersion in CA4+ (*"bone and cartilage 0 h"*). Further, the cartilage volume was calculated by subtracting these two bone and cartilage volumes (Equation 4.17).

$$Cartilage_{Volume} = (bone \quad and \quad cartilage \quad Tf) - (bone \quad and \quad cartilage \quad 0h) \tag{4.17}$$

- Gray values at each time point were extracted from the cartilage volume using boolean operations.
- Gray values of a standard CA4+ volume and deionised water volume were also extracted in order to calculate CUR and Hounsfield Units (HU) at each time point.
- The CUR value for each time point was calculated by dividing the average gray value of the cartilage by the CA4+ average gray value.

This procedure was repeated for all five tibial plateaux.

### 4.4.2 Fluoroscope X-ray Attenuation vs GAG Content Curve

A curve that correlated fluoroscope attenuation at each testing point and GAG quantity obtained by DMMB assay (Chapter 4, Section 4.4.4) was desired. The objective was to create a reference table/curve for GAG quantification estimation through intensity values, thus non-destructively.

In order to construct this curve it was necessary to obtain intensity values at each testing point (Chapter 4, Section 4.4.3).

### 4.4.3 Acquisition of Intensity Values at Each Test Point

Six tibial plateaux specimens were immersed in CA4+ for the period of time considered optimal for diffusion and penetration of CA4+ (Chapter 4, Section 4.4.1.3). Specimens were imaged at 0 h and optimal time (estimated to be  24 h). Image sequences were segmented and cartilage volume were acquired following the procedure to that explained in Chapter 4, Section 4.4.1.4.

In Chapter 4, Section 4.4.1.1 an average attenuation value for each specimen was obtained, however for the construction of the attenuation vs GAG concentration curve it was necessary to extract the attenuation values at each testing point.

Gray values of the whole cartilage volume were extracted. Attenuation values were combined with STereoLithography (STL) file of the cartilage volume by using a custom Matlab program.

The gray values of the cartilage surfaces were registered to the topographical data obtained from the laser scanning. Registration was performed using an iterative closest point algorithm which allowed only rigid registration. Once registration was achieved, a grid of testing points (obtained in Chapter 4, Section 4.1.3) was used to identify testing points on the cartilage surface.

A comparison between intensity values extracted from the cartilage surface and GAG content obtained from 4 mm plugs using DMMB was carried out. The kd-tree algorithm was used to identify all the points inside a cylindrical volume of the indenter radius centred on each testing point. Intensity values over this cylindrical area were averaged at each point and compared to corresponding GAG content measured by DMMB assay.

This procedure was repeated for all six tibial plateaux.

### 4.4.4 1,9-Dimethylmethylene Blue Colorimetric Assay (DMMB)

The general principle of this method was described in Chapter 2, Section 2.7.3. In summary, GAG content can be quantified in solution due to the binding properties of GAG to DMMB, which causes changes in the spectrum of the dye [191]. The DMMB assay consists of several steps including preparation of 2 reagents, development of a standard curve, preparation of the samples and analysis of the data.

#### 4.4.4.1 Preparation of DMMB Colour Reagent

***Reagents [100 ml]:***

- 304 mg of 40.55 mM glycine
- 237 mg of 40.55 mM NaCl (Sodium Chloride)
- 9.5 ml of 9.5 mM 0.1M HCl (Hydrogen Chloride)
- 1.6 mg of 0.0016 % (w/v) DMMB at pH 3.0,

***Preparation:***

Ingredients were adjusted for 1 litre of reagent. The DMMB colour reagent was prepared by dissolving 16 mg DMMB in 1000 ml of water containing 3.04 g glycine, 2.37

g NaCl and 95 ml 0.1 M HCl. The solution was adjusted to pH 3.0 and the reagent was then left for 2 hours to mix. The reagent was then covered with aluminium-foil to protected it from the light and stored at room temperature. It has been reported that DMMB reagent lasts up to 3 months under these conditions [191].

#### 4.4.4.2 Preparation of Papain Digestion Buffer

***Ingredients [100 ml]:***

- 328 mg of 20 mM sodium phosphate buffer (pH 6.8) . pH was adjusted using NaOH.
- 29.24 mg of 1 mM EDTA (Ethylenediaminetraacetic acid)
- 200 $\mu l$ of 1 M DTT (2 mM dithiothreitol)
- 30 mg of 300$\mu g/ml$ papain

Given that DTT and papain should be added near to the time of use, 500 ml of sodium phosphate and EDTA solution were prepared and stored at room temperature for future use.

***Preparation:***

Sodium phospate was mixed with 400 ml of distilled and deionized water (milli-Q grade) and was left to mix for 1 hour after which pH was adjusted to 6.8 by adding NaOH. EDTA was then added to the solution and mixed for 1 minute. DTT and papain in corresponding proportions were added just before carrying out experiment. Solutions were stored in a fridge for a maximum of 7 days.

#### 4.4.4.3 Preparation of the Standard Curve

The standard curve for GAG quantification is a plot constructed by combining chondroitin sulphate, which is one of the main constituents of GAG, and papain buffer. These two components have a linear relationship at certain concentrations, the aim was to use the linear part of this curve to calculate the amount of GAG in a cartilage sample. This calculation is done by fitting the absorbance of the sample onto the graph to acquire the GAG (chondroitin sulphate) concentration.

***Preparation:***

Taking the previously prepared sodium phosphate/ EDTA solution, (Chapter 4, Section 4.4.4.2), 5 mg of chondroitin sulphate was added to 10 ml of the solution and left to mix for 1 hour in the fridge. Then, DTT and papain were also added.

The standard curve solutions were placed in a transparent 96 well-plate in different concentrations (Table 4.1).

**Table 4.1:** Proportions of chondroitin sulfphate solution, papain buffer and DMMB for an standard curve. The first column represents the concentration of GAG that corresponds to the combination presented in the respective row. ChS refers to the chondroitin sulphate solution, Buffer refers to the papain buffer and DMMB refers to the DMMB reagent.

| $\mu g/ml$ | ChS $[\mu l]$ | Buffer $[\mu l]$ | DMMB $[\mu l]$ |
|---|---|---|---|
| 0.000 | 0 | 40.0 | 100 |
| 0.025 | 0.2 | 39.8 | 100 |
| 0.050 | 0.4 | 39.6 | 100 |
| 0.075 | 0.6 | 39.4 | 100 |
| 0.100 | 0.8 | 39.2 | 100 |
| 0.250 | 2.0 | 38.0 | 100 |
| 0.500 | 4.0 | 36.0 | 100 |
| 0.750 | 6.0 | 34.0 | 100 |
| 1.000 | 8.0 | 32.0 | 100 |
| 2.500 | 20.0 | 20.0 | 100 |
| 5.000 | 40.0 | 0.0 | 100 |

The DMMB reagent was added as close as possible to the reading of the absorbance given that the reagent is highly photosensitive and therefore exposure to light might alter the values. Measurement of the the standard curve solutions were repeated three times.

Further dilutions to the solution were made in order to fit the linear portion of the relationship between the GAG concentration measured by chondroitin sulfate and the absorbance. Absorbance was measured by using a microplate spectrophotometer (SpectraMax 384 Plus, 4A, 50-60 H Molecular Devices, California, USA) in combination with software SoftMax Pro 6.2.1 (Molecular Devices, California, USA) at 520 nm wavelength.

#### 4.4.4.4 Sample Preparation

Once the dilution with best fit for the standard curve was found, the analysis of cartilage plugs was carried out. For this purpose samples were prepared by following several steps presented below:

***Protocol for Sample Preparation:***

1. After finalising the imaging section of the experiments (Chapter 4, Section 4.4.1), mechanical tests were repeated once more. Indian ink was placed on the tip of the indenter so that the position of the testing points was known. Since the tibial plateau was demounted from the sample holder to be imaged, it was necessary to re-assess the re-mounted tibial plateau position in order to obtain the same testing points:
    - Re-mounted tibial plateau was scanned using the high resolution laser
    - Both scans were registered: the one taken previous to the addition of contrast agent analysis and the one taken after re-mounting (following the addition of contrast agent)
    - The resulting transformation matrix from the registration was used to find new re-mounted positions of the indentation points
    - Rotation angles for WASIM were recalculated for remounted points
    - Mechanical testing was carried out applying ink periodically to the tip of the indenter (Figure 4.11)

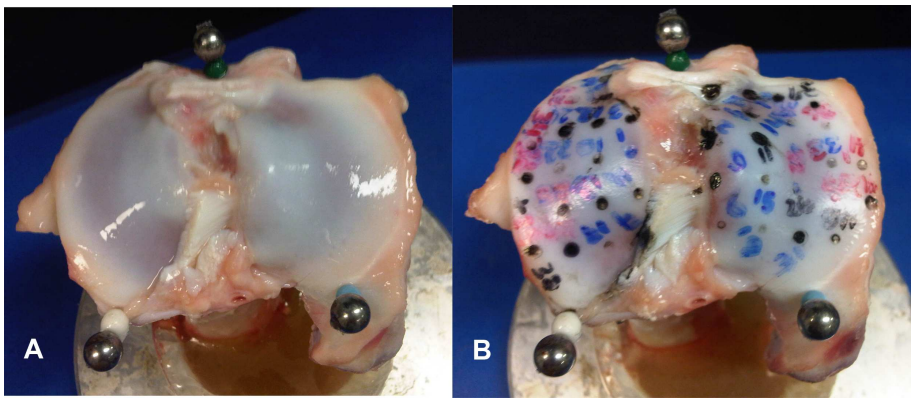


**Figure 4.11:** A. Tibial plateau after scan. B. Tibial plateau with test points identified on the surface.

2. Using a 4 mm diameter mosaicplasty circular osteotome, cartilage plugs were centre on the selected test points and extracted (Figure 4.12). Approximately 40 points from each of six tibial plateaux were prepared for DMMB testing. Plugs were stored in a small test tube identified with the specimen number and position number according to the indentation schematic location.

**Figure 4.12:** Four millilitre plugs to be used in DMMB assays extracted from tibial plateau

3. Each plug was separated into three parts (Figure 4.13). A middle section of about 0.5 mm was destined for histological and staining analysis (Chapter 4, Section 4.3.2), and the other two parts were used for DMMB tests.

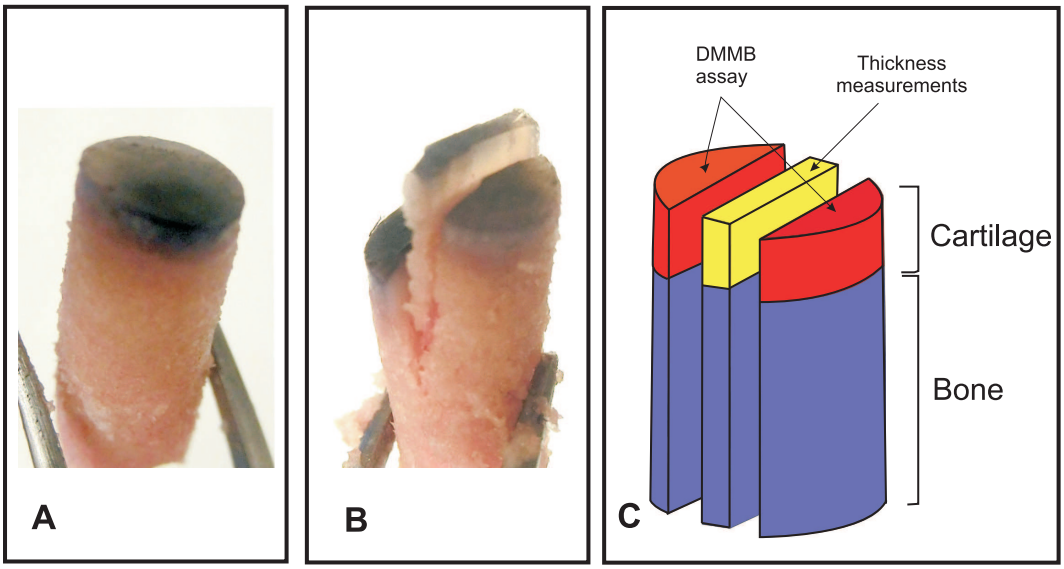


**Figure 4.13:** Separation of cartilage plug (A) into 3 parts (B). The two external sections were used for DMMB, while the middle section was used for thickness measurements (C)

4. Empty identified vertex tubes were weighed.

5. Two outer sections of each cartilage plug were cut into small pieces and placed

into the corresponding empty tube.

6. Tubes with chopped pieces of cartilage were weighed. This measure gave the wet weight.

7. Tubes of chopped cartilage were freeze-dried following procedure described in Chapter 4, Section 4.4.4.5.

8. 1 ml of papain buffer was added to each tube and then placed in an incubator at 60 $^{\circ}C$ overnight.

9. Tubes were assessed for remaining pieces of cartilage. The cartilage should have been completely digested. Otherwise, more papain buffer was added and the tube was left in the incubator again for a few hours. Finally, all tubes were filled with 2 ml of papain solution and mixed for a few seconds.

***Sample Readings:***

Sample solution in different dilutions and a standard curve solutions were placed in a transparent 96 well-plate. Both the standard curve and the sample solution were placed with replicates (x3, x5 respectively). Dilutions used are given in Table 4.2 and points used for the standard curve are given in Table 4.3.

**Table 4.2:** Preparation of commonly used dilutions of the sample. The first column represents the sample dilution, the second column represents the concentration of the sample solution, the third column represents the proportion of papain buffer and the final column refers to the DMMB reagent.

| Sample Dilution | Sample Sln $[\mu l]$ | Buffer $[\mu l]$ | DMMB $[\mu l]$ |
|---|---|---|---|
| Non-diluted | 40 | 0 | 100 |
| 1 in 2 Diluted | 20 | 20 | 100 |
| 1 in 5 Diluted | 8 | 32 | 100 |
| 1 in 10 Diluted | 4 | 36 | 100 |

Absorbance of the 96 samples in the well-plate were measured using a Molecular Devices microplate reader at 520 nm wavelength. DMMB tests were repeated at least eight times for each testing point. Given the sensitivity of the assay to pipetting error and photo-sensitivity, extreme outliers were excluded, leaving at least five samples per point. GAG content was then normalized by wet and dry weight (Chapter 4, Section

**Table 4.3:** Standard curve preparation. The first column represents the concentration of GAG that corresponds to the combination presented in the respective row. ChS refers to the chondroitin sulphate solution, Buffer refers to the papain buffer and DMMB refers to the DMMB reagent.

| $\mu g/ml$ | ChS $[\mu l]$ | Buffer $[\mu l]$ | DMMB $[\mu l]$ |
|---|---|---|---|
| 0 | 0 | 40 | 100 |
| 5 | 4 | 36 | 100 |
| 7.5 | 6 | 34 | 100 |
| 10 | 8 | 32 | 100 |
| 25 | 20 | 20 | 100 |
| 50.0 | 40 | 0 | 100 |

4.4.4.5).

#### 4.4.4.5 Freeze-Drying Technique

The freeze drying technique, also known as lyophilization, consisted of the dehydration of a frozen material. This procedure was completed by using an apparatus that, by creating a vacuum, induces sublimation of frozen water inside the tissue into its gas phase.

Freeze-drying completion required the following steps:

- Samples were frozen overnight in -80 $^{\circ}C$ freezer.
- The container was half filled with isopropanol and the other half filled with dry ice.
- Lids of sample tubes were opened and covered with parafilm membrane. Using a needle, small holes were made in the parafilm.
- Samples were placed in the sample holder (vacuum).
- Generator was turned on and vacuum valve released.
- After five hours, samples were taken out of the freeze-drying apparatus and weighed. Then samples were placed again to freeze-dry for one more hour after which they were re-weighed again. If the weight had not changed during that hour, it was concluded that the samples were dry, otherwise it was left for one

more hour and the procedure was repeated.

- The weight recorded after this procedure corresponded to the dry weight of the sample.

#### 4.4.4.6 Analysis of Data

A custom program was developed in Matlab to process the data; readings extracted from microplate spectrophotometer were matched to concentrations of standard curve cartilage plugs and sample ID. GAG content was calculated by interpolating the absorbance values into standard curve of respective plate. GAG concentration values inside the curve were considered as valid and further calculations were performed on them. GAG concentration values outside the linear range of the standard curve were not considered valid and were excluded from analysis.

Valid GAG concentration values were adjusted to one by multiplying it by the dilution. GAG content per milligram wet/dry weight as a function of chondroitin sulphate concentration was calculated by dividing the GAG content by wet weight and dry weight respectively. The difference between the weight after freeze-drying and the empty tube constituted the dry weight, and the difference between the chopped cartilage and the empty tube constituted the wet weight. The analysis of GAG per milligram of both wet and dry weight, allowed an examination of the effect of water content in GAG distribution.

Further, GAG concentration values over the six tibial plateaux were analysed and statistically tested.

- **Repeatability**

  Different measures of GAG concentration at the same point were tested for repeatability. Similar to repeatability analysis performed for elastic modulus (Chapter 4, Section 4.2.1), repeatability was assessed through the calculation of CV within measurements of absorbance within the same plug.

- **Variability of GAG Distribution**

  Mean GAG content values at each testing point were plotted at the corresponding

location on the tibial plateaux. This allowed visualisation of the distribution of GAG over each tibial surface. The variability of repeated measurements at the same point and across the tibial plateau were assessed with boxplots.

- **Regional GAG Distribution Analysis**

  Similar to regional analysis performed in elastic modulus values, GAG concentration means were also grouped into the different regions. Statistical analysis of mean comparison was performed in all tibial plateaux.

  Firstly, the tibial plateau was divided into the lateral and medial compartment. GAG content between compartments was compared. Second, the tibial plateau was divided into four equal parts and GAG concentration mean for each region was compared. Finally, analysis of GAG content over MMR was carried out.

  Mean comparison statistical analysis was performed using similar procedure than mentioned in Chapter 4, Section 3. The independent variable was the region the GAG concentration belonged to (Lateral and Medial for first case, LA, LP, MA, MP for the second and MMR clusters for the third). The dependent variable was the mean GAG content.

## 4.5 Correlating of Cartilage Variables: Thickness, GAG Concentration and Elastic Modulus

In previous sections (Chapter 4, Sections 4.1, 4.3, 4.4) a scattered distribution of material properties (Elastic Modulus), GAG content and thickness was obtained independently. This presented an opportunity to study an overall view of variables (elastic modulus, GAG and thickness) distribution. However it was difficult to compare variables between the different tibial plateaux since the location of testing points on each knee was not exactly the same.

In this section the objective was to obtain a continuous distribution of cartilage variables over each tibial plateau. This allowed better visualization of variable distribution over the tibial plateaux. Two types of comparisons were performed: point-matched and site-matched comparison of cartilage variables on the same knee and over the six

tibial plateaux.

### 4.5.1 Continuous Cartilage Variables Distribution

Linear interpolation of mean variables between scattered testing points was performed in the X and Y directions independently. This process was achieved by using a custom Matlab routine developed by the author, and was repeated for each material property measured (elastic modulus, GAG content and thickness) over the six specimens.

A continuous distribution of each of the cartilage variables in the six tibial plateaux was obtained.

### 4.5.2 Extraction of Cartilage Variables from Continuous Surfaces

Using the continuous distribution of cartilage variables obtained in the previous Section, cartilage variables over six tibial plateaux were compared. The objective was to obtain approximately the same point on each sample, in order to compare tibial plateaux accurately. To achieve this three steps were followed: (1) Tibial plateaux were registered to one selected tibial plateau (S1), (2) A new grid of points to extract the cartilage variables from was obtained by calculating the smallest intersection between the original grids of testing points for all tibial plateaux. (3) Values of all variables from all samples were obtained at the new grid testing points. Further details of each step are given in the following sections.

#### 4.5.2.1 Registration of Surfaces

In the previous sections cartilage variables were measured on testing points obtained from fitting a 6 mm spaced grid over the topographical map of each tibial plateau. In this section topographical maps were registered to S1, which was chosen as the reference topology. In the first instance tibial plateaux were assessed for orientation. Right and left knees were tested, therefore orientation was flipped to match the S1 orientation. Once all samples had the same orientation, topographical surfaces were registered to S1 using an iterative closest point (ICP) affine registration algorithm. This registration

allowed rotation, translation and also size adjustment. As a result a transformation matrix was obtained.

#### 4.5.2.2 Selection of Extraction Points

Previously, a 6 mm spaced grid was used to obtain testing points, this was because there needed to be enough space between testing points for physical extraction of 4 mm plugs. In this section variable values were obtained from an interpolated surface of measured variables, therefore the grid could have a smaller separation. Testing points used previously for each specimen were multiplied by the transformation matrix (obtained in Chapter 4, Section 4.5.2.1) for registration. Testing points were superimposed and the minimum area bounding all the test points from all six specimens was selected. Following the procedure described in Chapter 4, Section 4.1.3, a grid of 1 mm space between points was fitted into this area and filtered to ROI. The resulting points constituted the new points for extraction of variable values. These points were referred to as the extraction points. Approximately 100 points for each tibial plateau were obtained.

#### 4.5.2.3 Extraction of Variable Values from Surfaces

Cartilage mechanical, physical and biological properties of each knee were multiplied by the transformation matrix obtained from ICP registration for the respective tibial surface (Chapter 4, Section 4.5.2.1) . This allowed cartilage variables to be in the same position as the corresponding registered surface.

Kd-tree algorithm was used to identify neighbouring points inside a circular area equal to the indenter radius and centred on each extraction point. Variable values inside the circular area were averaged and recorded as the variable value at that extraction point. This process was repeated for each extraction point at each tibial plateau for each of the variables tested.

This section allowed the acquisition of cartilage material properties (elastic modulus), cartilage geometrical properties (cartilage thickness) and cartilage biological properties (GAG), over six tibial plateaux in exactly the same points. Consequently point-

matched and site-matched comparison was carried out between knees.

### 4.5.3 Point-matched Comparison Between Variables on Each Tibial Plateau

Correlation between cartilage variables at the same corresponding point on each tibial plateau was performed using Spearman correlation. Further, interaction analysis using a series of multi-regression tests was carried out in order to observe the effect of a third variable on the other two.

### 4.5.4 Point-matched Comparison Between Variables Distribution Over Each Tibial Plateaux

Similarly, correlation of cartilage variable distribution over the six tibial plateaux was assessed by calculating Spearman correlation. Values of GAG concentration, elastic modulus and cartilage thickness at each extraction point were correlated.

A point-matched comparison of each variable over the six tibial plateaux was obtained. It was, thus possible to form conclusions about the similarity of cartilage variable distribution over the six tibial plateau.

### 4.5.5 Regional Analysis of Variables Between Tibial Plateaux

Regional comparisons of variables of the same tibial plateau and cartilage variables distribution across different tibial plateaux were performed. The aim of this analysis was to identify regional effects in variables distribution. Cartilage variables obtained from the extraction points were grouped into MMR for this analysis.

#### 4.5.5.1 Region-match Comparison of Each Variable Over Six Tibial Plateau

Using MMR regions, region-matched regional comparisons of each variable across different tibial plateaux were carried out. The means of each region were compared over all tibial plateaux.

#### 4.5.5.2 Region-match Comparison of Cartilage Variables Over Each Tibial Plateau

Correlation of mean cartilage mechanical, physical and biological properties values grouped by MMR regions was performed. Regional effect was assessed by evaluating the interaction between these three variables.

## 4.6 Summary

In this chapter the methodology used to measure elastic modulus, GAG concentrations and cartilage thickness was presented and the results are shown and discussed in the next two chapters. Additionally, the methodology for the analysis of the correlation between measured variables was presented and results are shown in Chapter 6.

# Chapter 5

# MECHANICAL PROPERTIES AND GAG CONTENT

In this chapter mechanical properties, cartilage thickness and GAG content of the articular cartilage on six whole porcine tibial plateaux, at approximately 40 points on each and with repeated measurements, are reported. It was considered that the study of material properties, cartilage thickness and GAG content over the tibial plateau would provide an understanding of the behaviour of the articular cartilage under load.

Several studies have been published suggesting that articular cartilage adapts to the loading patterns it is subjected to [19, 21, 271, 278]. In particular, studies have shown that cartilage adapts to gait loading patterns [18, 19, 21]. These studies show that articular cartilage develops a material property distribution that is related to the loading patterns it is subjected to. Furthermore, these results are supported by the other independent facts such as (1) material properties in neo-natal cartilage does not exhibit this heterogeneity [271], (2) Knee lesions [19, 279] or malignancies [174, 280] create a sudden shift in load to areas of articular cartilage unprepared to support stress, therefore creating new pathways for initiation of OA.

The evolution and adaptation of the knee joint to load has been observed through the heterogeneity that the tibial plateau displays in its material properties and thickness distribution over the surface [18]. There have been several studies that have measured

the material properties over the tibial plateau, however most have only tested a few points on the surface [278]. Others that have tested more points have used a mix of healthy and OA or defective cartilage [30, 157, 281]. Additionally, many of the studies have measured the material properties of cartilage using cartilage plugs [2, 278] which could alter the matrix constituents.

Thickness has been shown to be a relevant parameter in understanding the distribution of material and biological properties of cartilage [18, 27, 282, 283, 284]. Therefore, it is an important variable to take into account.

GAG content throughout the tibial plateaux has been investigated in a number of studies [23, 32, 59]. Variations in GAG distribution over the articular cartilage have been reported between healthy and degraded cartilage [32, 282, 285]. In degraded cartilage the GAG concentration is low. However, GAG distribution in healthy cartilage has been little studied and conflicting results have been reported. Some authors have found negligible differences over an articular surface [32] while others have reported significant regional differences [89, 278, 286]. The majority of studies on healthy specimens have taken into consideration small number of cartilage samples from different regions of the specimen, and this is a major limitation. In order to gain a better understanding of GAG distribution across tibial plateaux, GAG concentration must be measured over more points.

In the present work it was aimed to find a non-destructive method for quantification of GAG, measurement of mechanical properties and cartilage thickness. For the measurement of mechanical properties indentation was used, for the measurement of cartilage thickness, US was attempted and optical measurements were used. Finally, for GAG quantification a method which attempted the development of a calibration curve that correlated attenuation of fluoroscopic images after tissue was immersed in CA4+ for 24h with GAG content in a defined area was used.

## 5.1 Mechanical Properties

The mechanical properties of articular cartilage of porcine knees were obtained following several steps. Results of each step are presented as follows.

### 5.1.1 Topography Maps and Test Points

**Topographical Maps:**

The topographical maps for each specimen were constructed from a point cloud of approx 660,000 points, representing the height of the surface at each X,Y position. The colours represent the height of the topographical surface (Figure 5.1 and topography of the six tibial plateaux can be found in Appendix A, Figure A.1).

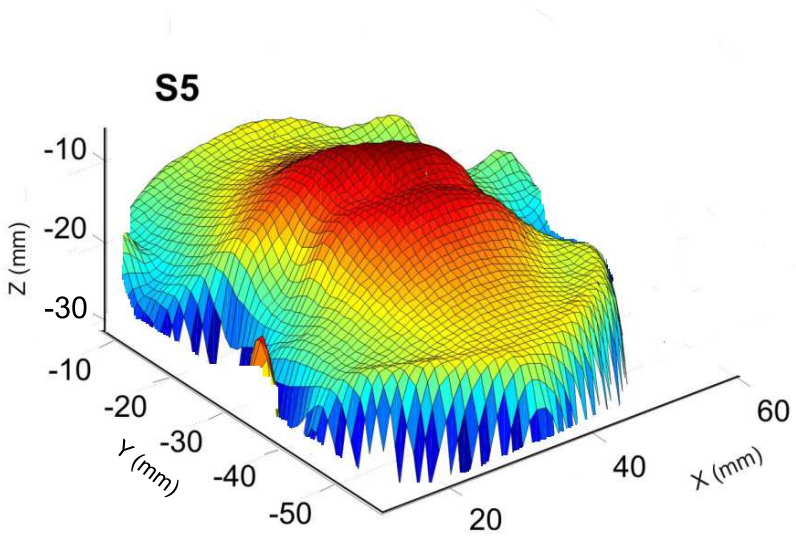


**Figure 5.1:** Topography of tibial plateau obtained from scan using high resolution laser. The colors represent the height of the topographical surfaces of the different specimen S5

In this figure it is possible to observe that the highest part of the tibial surface was given by the tibial plateau eminence which divides the medial and lateral compartment on each knee. Both compartments on all knees exhibited a concave shape. In all six tibial plateaux it was observed that the lateral compartment was flatter than the medial compartment. The medial compartment in all six specimens was concave by comparison. This difference between lateral and medial compartments is consistent with the morphology described in Chapter 2, Section 2.1.

**Selection of Test Points:**

Test points over which the material properties, cartilage thickness and GAG concentration were measured, were selected using the topography maps (Chapter 4, Section 2).

The location of test points at each tibial plateau is shown in Figure 5.2. The numeration of the points represents the identification (ID) of each point and was preserved for all tests performed. Test points at each tibial plateau were different, due to the algorithm used to generate them (see Chapter 4, Section 2). Selection of test points for all six tibial plateaux is shown in Appendix A, Figure A.2.

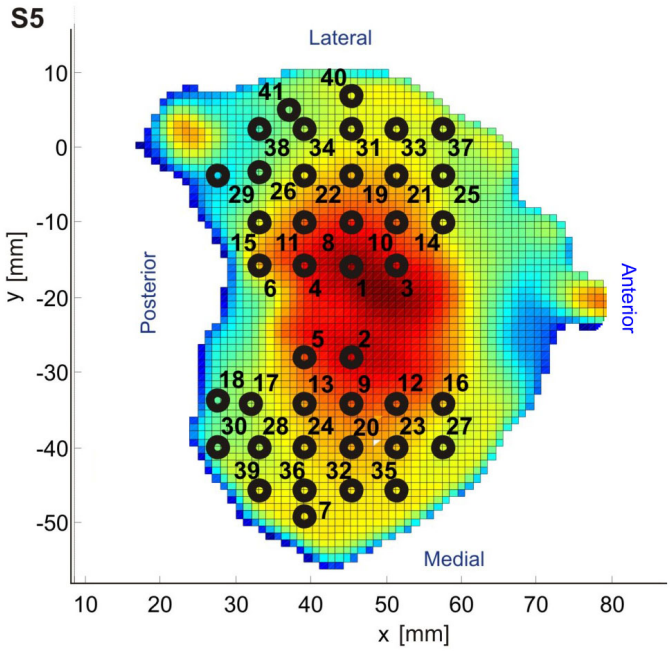


**Figure 5.2:** Test points in specimen S5

### 5.1.2 Measurement of Mechanical Properties

Mechanical properties were measured by using indentation normal to the surface. This was accomplished by calculating the normal vector at each test point, and aligning this vector with the indenter position. The elastic modulus was calculated, taking into account the cartilage thickness at each test point.

**Calculation of Normal Vectors at Each Test Point**

Normal vectors of all points, inside an area of interest (AOI) for each testing point were calculated and averaged. Normal vectors at each test point are presented in Figure 5.3

for a representative specimen.

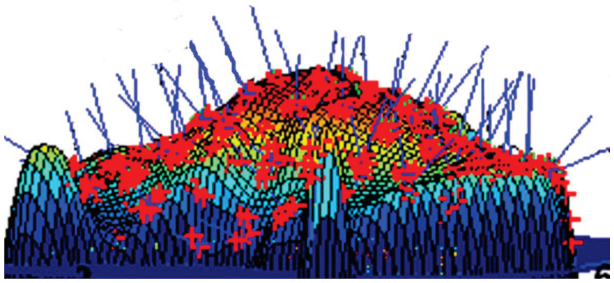

**Figure 5.3:** Normal vectors at each testing point for a representative specimen

As observed in Figure 5.3, normal vectors at each test point have different inclination due to the undulating topography of the tibial plateau. Therefore, different rotation angles were necessary to achieve indentation normal to the surface for each test point.

#### 5.1.2.1 Indentation Measurements

Force and displacement data were obtained for each testing point by performing normal indentation. Displacement controlled tests were carried out at a rate of 10 percent per second.

The unloading part of the P-h plot was fitted with a curve of the type $P = B(h - h_f)^m$ (Figure 5.4). Stiffness was obtained by calculating the 1st derivative of the fitted curve (Equation 4.7) and elastic moduli were obtained from the stiffness and thickness of each test point (Equation 4.13).

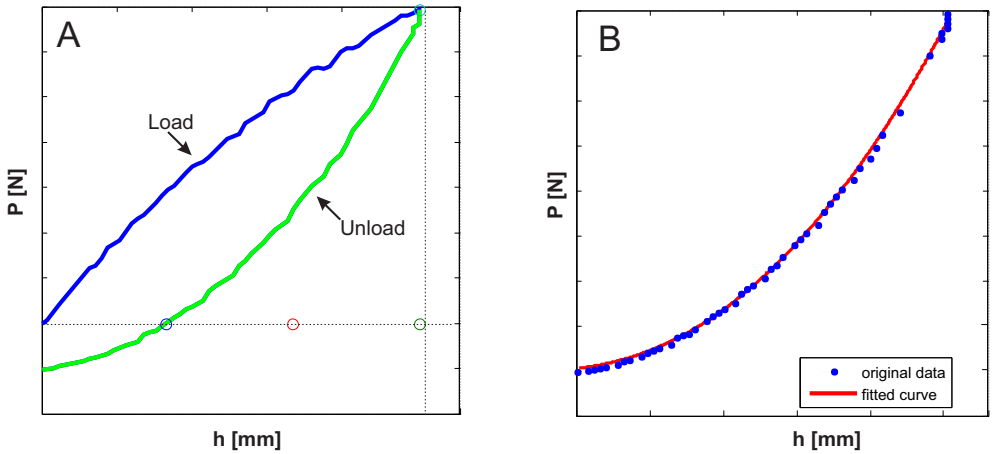


**Figure 5.4:** (A)Typical load and unload curve. (B) Unload curve and fitted curve of the type $P = B(h - h_f)^m$.

In Figure 5.4 it can be observed that there was a good fit ($R^2 > 0.9$) between experimental data and the fitted curve. This procedure was repeated for each one of

the indentation tests performed (approximately 1000 tests). Indentation tests were repeated five times at each test point on five tibial plateaux (40 points x 5 tests x 5 specimens).

#### 5.1.2.2 Elastic Moduli Distribution

Elastic modulus at each test point over the six tibial plateaux was calculated as explained in Chapter 4, Section 4.2. The mean elastic modulus was calculated from the mean stiffness at each test point and it is presented in Figure 5.5 for one tibial. The colour of each testing point represents the mean elastic modulus of the test point in the corresponding position. The mean stiffness of all tibial plateaux is shown in Appendix A, Figure A.3.

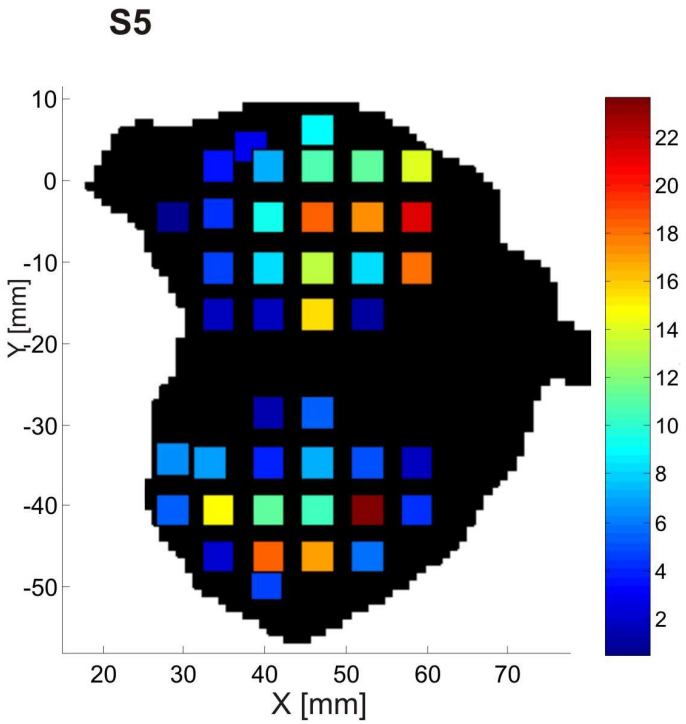


**Figure 5.5:** Elastic modulus distribution at each test point in specimen S5. Values of E are shown in MPa units. Colours of each test point represent the values of E at each point. Red corresponds to the highest values while blue are the lowest.

The Elastic modulus distribution over the tibial plateau showed higher elastic moduli values at the center of both the medial and lateral compartment. Elastic moduli values range from 1 MPa to values over 20 MPa. The average elastic moduli over all six tibial plateaux was approximately 10 MPa.

As it can be observed in Figure A.3, the rim locations for both compartments had

points of low elastic modulus (blue), while there was a concentration of points with higher elastic moduli (yellow, orange and red) in the central part of both compartments. These differences in elastic moduli values suggest a large variability in the distribution of mechanical properties over the tibial plateau. Additionally, concentration of high stiffness in the central areas of each compartment suggests that this region would respond differently to load than the surrounding areas.

#### 5.1.2.3 Repeatability of Elastic Modulus Within Each Point and Variability Across Each Specimen

The repeatability of the elastic modulus measurements was represented using boxplots. The boxplots had two aims: (1) to show the variability of the elastic modulus mean across each tibial plateau and (2) to show the repeatability of elastic modulus within each point.

Figure 5.6 shows the spread of elastic moduli at each point and the location of the test points on specimen S5. The spread of elastic moduli at each point in all six tibial plateaux is shown in Appendix A, Figures A.4 and A.5. In these figures it can be observed that the elastic moduli distribution has a high variability. It was also possible to see that higher elastic modulus values were located in central areas of each compartment. Overall, the average spread of elastic modulus values at each testing point was low (average SD of 0.96, 1.80, 1.84, 0.61, 1.81 MPa for specimens S2, S3, S4, S5 and S6 respectively) for all tibial plateaux. Nevertheless, at least a few points on each tibial plateau showed a high spread (SD $\geq$ 4 MPa).

The average elastic moduli for the six tibial plateaux was between 5.8 to 8.7 MPa ($\overline{E}$ = 6.7 MPa). Moreover, most mean elastic moduli values varied between 0.4 to 24 MPa, although only one specimen (S6) showed elastic moduli values over 25 MPa. The SD of the mean values, over the whole specimen, for all specimens was around 9 MPa, except for S6 for which a higher SD was observed (Table 5.1). Less than 45% of the points were within $\pm$1 SD of the mean elastic modulus of the specimen they belonged to, which further indicates variability.

The reliability of elastic modulus obtained by indentation was examined by calculating

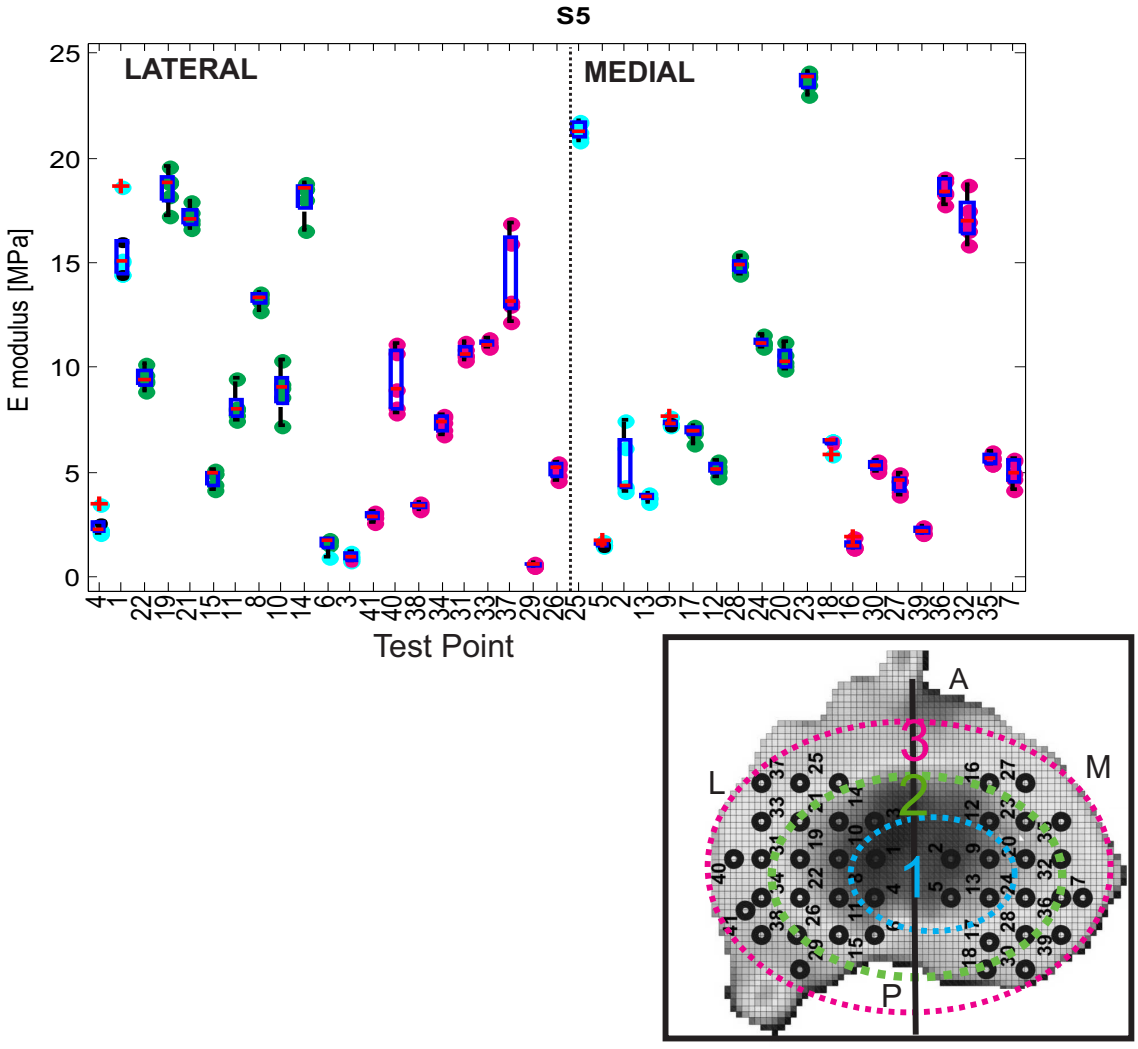


**Figure 5.6:** Boxplot distribution of specimen S5. This plot presents the different values of elastic modulus calculated from the repeated indentation tests at each point. Points are classified according to their position. To the left of the dotted line are the points located in the lateral compartment and to the right of the dotted line the medial compartment. The colours represent the ring the test points are located in: cyan the inner ring, pink the most external ring and green the middle ring. On top of the scattered points a boxplot that highlights the mean elastic modulus value of each point and the upper and lower boundaries for repeated measurements is shown. Beside each boxplot a map of the tibial plateau with the location of the test points is shown.

CV for each testing point. The average CV (S2, S3, S4, S5, S6) was 3.72%, 8.92%, 8.24%, 6.38%, 8.37% respectively. Obtained CV values demonstrated that stiffness measurements obtained by indentation were repeatable within ±9% in all specimens.

**Table 5.1:** Maximum and minimum elastic moduli values for specimens S2, S3, S4, S5, S6. Mean value and SD for each specimen.

| Specimen | Elastic modulus Range Means MPa | Mean MPa | SD MPa |
|---|---|---|---|
| S2 | 0.30 - 14.91 | 8.80 | 3.62 |
| S3 | 2.00 - 20.05 | 8.76 | 4.45 |
| S4 | 1.50 - 22.36 | 9.86 | 5.53 |
| S5 | 0.60 - 24.10 | 8.83 | 6.18 |
| S6 | 1.82 - 42.38 | 13.72 | 9.45 |

Even though the tibial plateaux showed heterogeneous elastic moduli distribution, there were many points with similar values. This suggested that there might be regions significantly different to others in terms of their mean elastic modulus. Therefore, regional analysis of elastic modulus distribution was performed by grouping points according to their location.

### 5.1.3 Elastic Moduli Regional Analysis

With the aim of understanding elastic moduli distribution over the tibial plateaux, material properties distribution was analysed by grouping values into the (1) lateral and medial compartment, (2) half compartments (dividing each compartment in four) and (3) MMR.

Statistical tests to compare mean values over these groups were performed.

#### 5.1.3.1 Elastic Moduli Variations in Medial and Lateral Compartments

The difference between mean elastic modulus on the lateral and the medial compartments was evaluated for each tibial plateaux. The mean values for each compartment were compared for the six tibial plateaux. The independent variable was the compartment the point belonged to i.e. which included two groups: Lateral or Medial. The dependent variable was defined as the mean elastic moduli values.

Results are summarized in Table 5.2. This table presents mean elastic modulus and SD of each compartment. Additionally, the total number of points tested for each tibial plateau (N) and the number of points in each compartment ($n_l$ and $n_m$ for lateral and medial compartment respectively). Also the p values for the mean comparison test which was obtained from the one way ANOVA or Welch test depending on the homogeneity of variance results (Chapter 4, Section 3). The effect size between mean elastic modulus of regions is also shown in the last column.

**Table 5.2:** Values of mean elastic moduli in medial and lateral compartments in the six tibial plateaux. The first column corresponds to the specimen tested, N is the total number of points, $\overline{E_l}$ is the mean elastic moduli in the lateral compartment and its standard deviation ($SD_l$), $n_l$ is the number of points located in the lateral compartment. Similarly, $\overline{E_m}$ is the mean elastic moduli in the medial compartment and its standard deviation ($SD_m$), $n_m$ is the number of points located in the medial compartment. p is the statistical significance between medial and lateral compartments calculated from ANOVA or Welch test, on each specimen, depending on homogeneity of variance. The last column represents the effect size between mean elastic modulus of each compartment.

| Specimen | N | Elastic Modulus | | | | | | p | Effect size |
|---|---|---|---|---|---|---|---|---|---|
| | | Lateral | | | Medial | | | | |
| | | $\overline{E_l}$ MPa | $SD_l$ MPa | $n_l$ | $\overline{Em}$ MPa | $SD_m$ MPa | $n_m$ | | |
| S1 | 42 | 6.82 | 3.98 | 23 | 9.73 | 6.10 | 19 | 0.045 | 0.100 |
| S2 | 40 | 10.52 | 2.45 | 20 | 7.33 | 3.89 | 20 | 0.008 | 0.170 |
| S3 | 39 | 8.55 | 4.15 | 21 | 9.01 | 4.89 | 18 | 0.724 | 0.003 |
| S4 | 42 | 9.52 | 5.29 | 23 | 10.40 | 6.05 | 19 | 0.470 | 0.130 |
| S5 | 41 | 9.33 | 6.27 | 22 | 8.24 | 6.19 | 19 | 0.609 | 0.006 |
| S6 | 40 | 14.41 | 11.22 | 22 | 12.88 | 6.92 | 18 | 0.431 | 0.016 |

Mean elastic moduli values of the lateral compartment were between 6 to 15 MPa, while the mean elastic moduli values of the medial compartment were between 7 to 13 MPa. The mean elastic moduli of specimens is similar, although the mean elastic modulus of S6 is slightly higher than all the other specimens. S1 and S3 were right knees, while all other specimens were left knees. The right knees showed a slightly higher mean elastic modulus in the medial compartment. The left knees showed slightly higher mean elastic modulus in the lateral compartment with the exception of S4.

The comparison of mean elastic moduli between compartments showed no significant differences in mean elastic moduli between the medial and lateral compartment in four of the six tibial plateaux. Only for S1 and S2, the elastic moduli were significantly

different between compartments. Nevertheless, the calculated effect size in these specimens was small.

#### 5.1.3.2 Elastic Moduli Distribution in Four Compartments

A common practice in clinical settings is to divide the articular cartilage in four quarters for the description of the location of defects or lesions on the tibial plateau. Therefore, elastic moduli values were grouped in four quarters according to their location (Figure 4.6). Mean elastic modulus of each region was calculated and compared statistically (Section 3).

A summary of the mean distribution of elastic moduli on six tibial plateaux grouped in four regions is summarized in Figure 5.7. Mean elastic modulus in the LA region ($\overline{E_{LA}}$) was between 9 to 14.5 MPa ($\overline{E_{LA}}$ = 12.3 MPa), mean elastic modulus in the LP region ($\overline{E_{LP}}$) ranged between 4 to 19 MPa ($\overline{E_{LP}}$ = 8.9 MPa), mean elastic modulus in the MA region ($\overline{E_{MA}}$) ranged between 9 to 14 MPa ($\overline{E_{MA}}$ = 12.3 MPa), mean elastic modulus in the MP region ($\overline{E_{MP}}$) ranged between 5.5 to 10 MPa ($\overline{E_{MP}}$ = 8.1 MPa).

Mean comparison of the elastic moduli grouped in four regions showed significant differences between at least two regions in three tibial plateaux (S1, S2, S5) and non-significant differences in the other three tibial plateaux (S3, S4, S6). However, the anterior regions consistently seemed to have higher elastic moduli than the posterior regions. The only exception to this was observed in S2, where LP was significantly higher than MP.

From these results, higher elastic moduli were observed for the anterior region of both compartments. However, the high SD within regions suggests that there might be another selection of regions that could give a better insight into elastic modulus distribution. Therefore, a further analysis was carried out using MMR.

#### 5.1.3.3 Elastic Modulus Variability Within MMR

As mentioned in Chapter 4, Section 4.2.1, the Michigan Regions (MR) were modified to be more appropriate to the specimens used in this study. Three changes were made to the MR: (1) Meniscus area was modified from human menisci to porcine menisci.

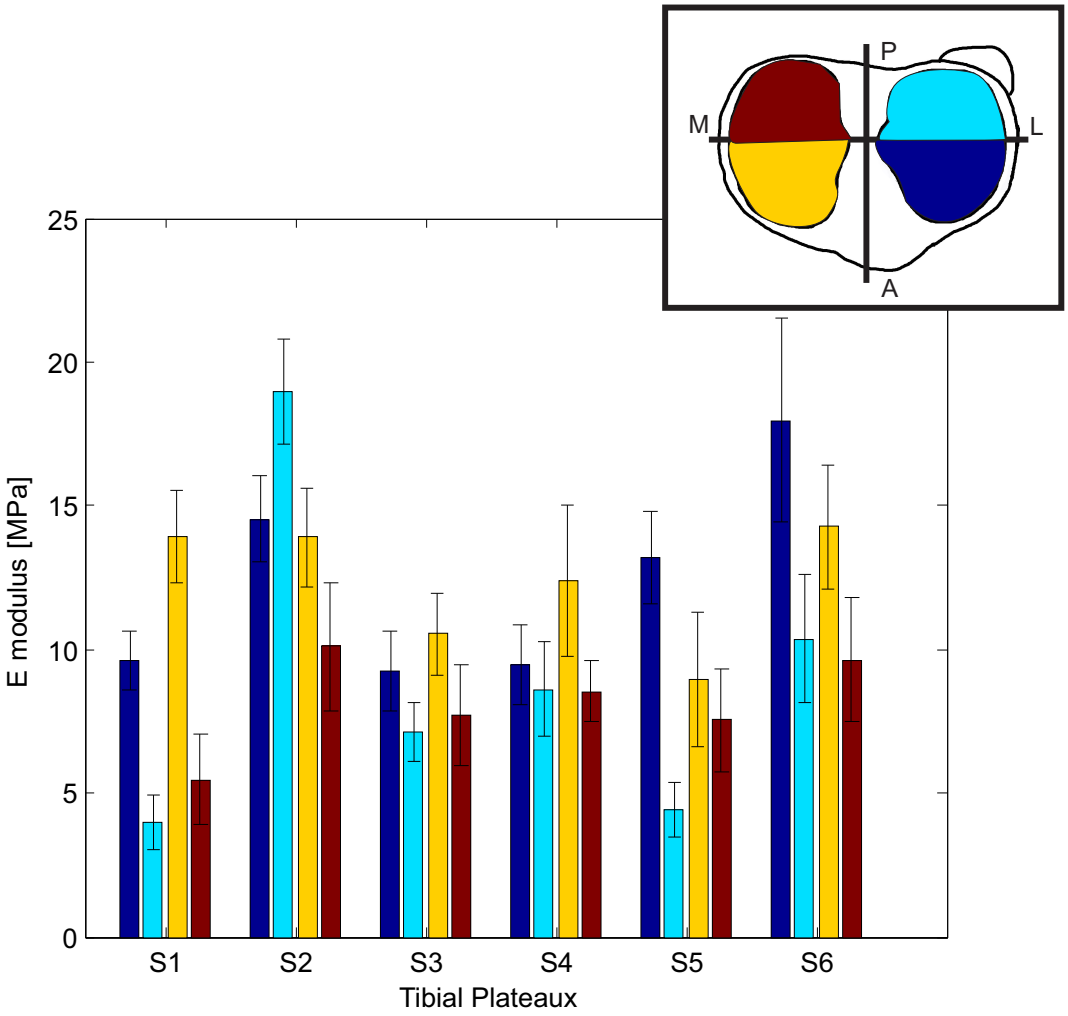


**Figure 5.7:** Mean elastic moduli distribution in each half compartment LA, LP, MA, MP. Bar colours represent the various regions of the tibial plateau which are described by the inset figure.

Porcine menisci covers a bigger portion of the articular cartilage compared to human cartilage [287]. Porcine menisci is also able to carry 30% more load than human menisci [287]. (2) The second change was regarding the size of the area tested on the tibial plateau. The area tested for cartilage variables in the present study was larger than the areas ordinarily tested. In particular in this study, many points were tested at the very edge of the tibial plateaux, which ordinarily is not taken into consideration in other studies. This area, uncovered by the menisci and located in the external rim of the medial and lateral rim were separated into a new region (V). (3) The medial and lateral compartment have different topographies (the medial is concave, while the lateral is flat or convex). Moreover, it has been reported that loading patterns over compartments are not symmetrical [18, 288, 289]. Finally, the meniscus in each compartment has a slightly different size. Considering all these factors, it was decided that there was not sufficient evidence to assume that variable distribution over both compartments would be equivalent, therefore symmetrical regions over each compartment were separated into medial (M) or lateral (L) accordingly and were tested separately. The Modified Michigan Regions (MMR) used in the current study are shown in Figure 5.8.

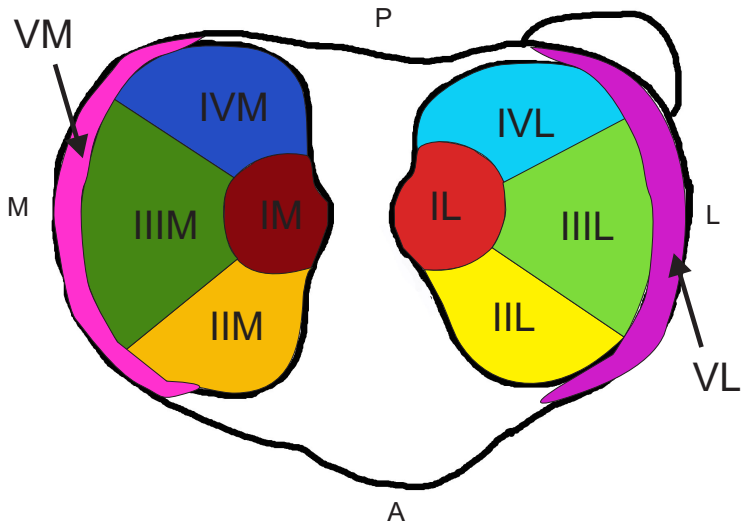


**Figure 5.8:** Modified Michigan Regions (MMR) used for data analysis. Region I was the area uncovered by the menisci in the central area of the tibial plateau on the medial (IM) and lateral (LM) compartment. Area uncovered by the menisci and located in the external rim of the medial and lateral rim was separated into a new region VM and VL respectively. The area covered by the menisci was divided into 4 parts. The two middle parts corresponded to region III, the posterior quarter was region IV and the anterior quarter became region II.

The mean elastic modulus values for the various test points which lay in the MMR regions were grouped (Figure 5.8), and were compared for each tibial plateau. Results

are summarized in Figure 5.9.

Figure 5.9 shows the mean elastic modulus for each region over each tibial plateau displayed using colour bars. In this figure each colour represents a different region which can be found in the MMR colour map displayed in the top right corner of the figure.

In this figure it can be observed that in four of the six tibial plateaux VM had the lowest elastic moduli. In the medial compartment regions IVL or VL had the lowest elastic moduli. The highest elastic moduli were observed in region IIIL in the lateral compartment of five of the six tibial plateaux. On the medial side the highest elastic moduli varied between IIM and IIIM in all tibial plateaux except S2. In general the mean elastic moduli of regions IIIL and IIIM were consistently within the highest elastic modulus values of the tibial plateaux. It can be observed that regions IIIL and IVL were significantly different in all specimens. In the medial compartment IIIM and IVM showed significant differences in four of the six tibial plateaux. Moreover, regions IIL and IIIL showed a similar elastic modulus in five of the six specimens. In the medial compartment, regions IIM and IIIM showed more variability, in S1, S2 and S6 no significant differences were found ($p > 0.05$), while in the other three specimens these regions were significantly different ($p \leq 0.05$). These observations show that mirror regions in the lateral and medial compartment were not identical.

Additionally, region I (IL and IM) was consistently lower than region III (IIIL and IIIM) except for IIIM in S2. These differences were only significant in two of the six (S4 and S6) specimens for both compartments.

On the other hand, region V in both compartments (VL and VM) was lower than most regions in the same compartment in five of the six tibial plateaux (S1, S2, S3, S4, S5). This supports the region selection used by MMR, since it gave relevant information about the elastic moduli distribution over the tibial plateau.

These results suggest that, in general, there was a trend for areas uncovered by the menisci to show a lower elastic modulus than areas covered by the menisci.

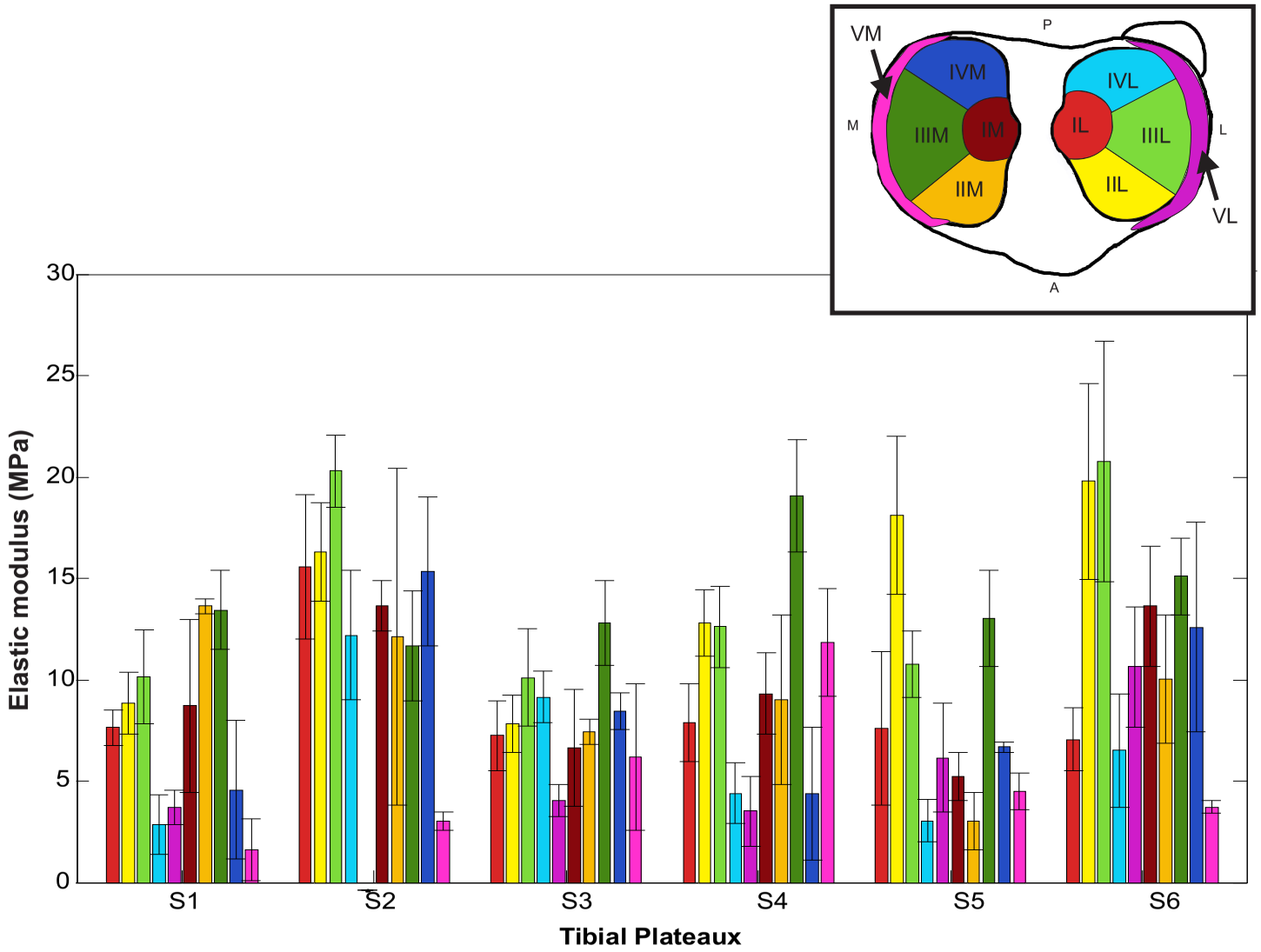


**Figure 5.9:** Mean elastic modulus over MMR on each tibial plateau. Colours of the bars represent a different MMR region. Colour map is displayed in the top right corner of the figure.

## 5.2 Cartilage Thickness

Initially measurement of thickness of articular cartilage was attempted using an US probe. The aim of this procedure was to obtain the thickness measurements automatically using the algorithms developed for indentation tests. The US was attached in the indenter position.

It was expected to observe three peaks from the ultrasound, in order to identify the two boundaries (gel-cartilage and cartilage-subchondral bone) in order to calculate the cartilage thickness. However, preliminary tests performed in a few points showed inconsistent results. The first peak was always observed, however second and third peaks were not consistently detected. Even manual adjustment of the US to obtain 2nd or 3rd peak did not produce consistent positive results. This made it very difficult to carry out the measurement of cartilage thickness at each point, and even more complicated to incorporate this procedure into an automated routine.

Therefore, cartilage thickness measurements were calculated from histological sections (cartilage and bone) obtained from the middle section of cartilage plugs (Chapter 4, Figure 4.13) at each test point (at least 200 measurements were performed on each tibial plateau).

### 5.2.1 Cartilage Thickness Distribution

Mean cartilage thickness measurements at each point in S5 are shown in Figure 5.10. The colour at each test point represents the cartilage thickness, where blue is the least thick and red is the thickest. The colour scale bar is given in millimetres.

Low cartilage thickness was observed in central areas of both compartments while higher cartilage thickness was observed in the external rim. A similar cartilage thickness distribution was observed in all tibial plateaux (Appendix A, Figure A.6). Values of cartilage thickness were between 1.8 and 5 mm in all specimens.

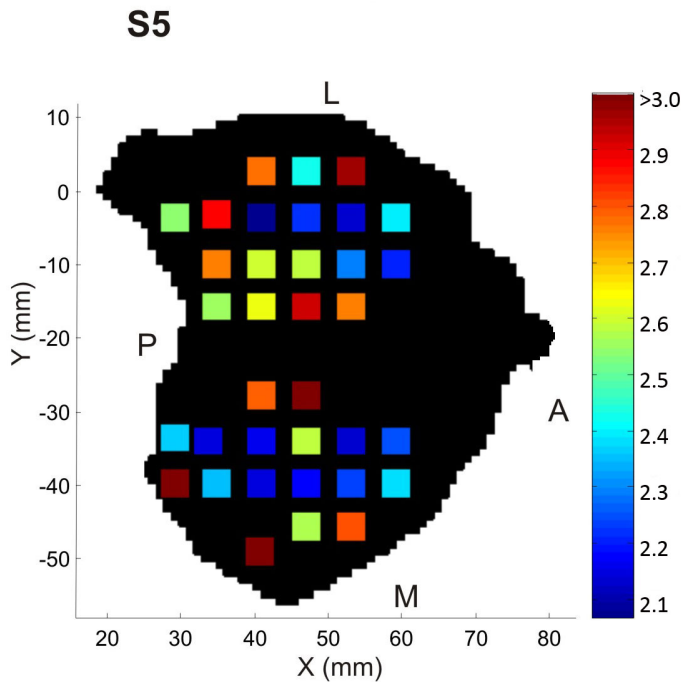


**Figure 5.10:** Thickness measured by histological method at testing points in samples S5. The colour at each test point represents the cartilage thickness at corresponding position, where blue is the least thick and red is the thickest. The colour scale bar is given in millimetres.

### 5.2.2 Repeatability of Cartilage Thickness Measurements Within Each Point and Variability Across Each Specimen

The repeatability of cartilage thickness measurements within each test point and the variability of cartilage thickness across each tibial plateaux were studied. Figure 5.11 shows cartilage thickness across each test point of specimen S5. The distribution of cartilage thickness for all specimens is shown in Appendix A, Figures A.7 and A.8. Additionally, repeatability within each point at each specimen was assessed through CV calculations.

The average spread (given by SD) within cartilage thickness measurements at each point was found to be similar for all tibial plateaux and it was 239.7 $\mu$m, 244.6 $\mu$m , 262.6 $\mu$m, 292.1 $\mu$m , 255.7 $\mu$m for specimens S1, S2, S3, S4 and S5 respectively.

Highest variability within repeated measurements was normally found at points located in the external rim, which also, in general had higher curvature and thickness. The lowest variability in repeated measurements was found in points located in the central areas of the compartments, normally with less curvature and with lower mechanical properties.

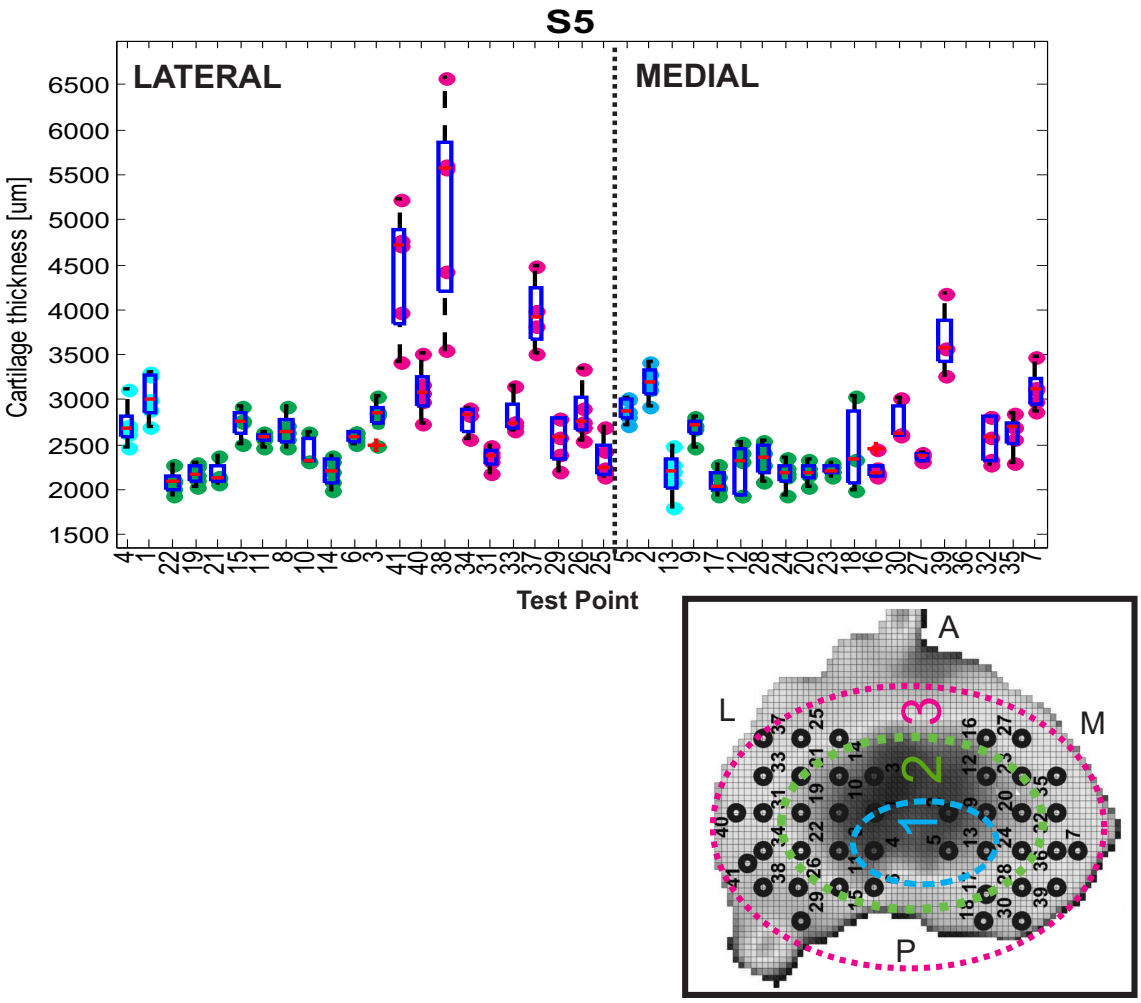


**Figure 5.11:** Cartilage thickness values of repeated measurements and mean value at each test point in specimen S5. Points are classified according to their position. To the left of the dotted line are the points located in the lateral compartment and to the right of the dotted line the medial compartment. The colours represent the ring the test points are located in: cyan the inner ring, pink the most external ring and green the middle ring. On top of the scattered points a box plot that highlights the mean elastic modulus value of each point and the upper and lower boundaries for repeated measurements is shown. Beside each boxplot a map of the tibial plateau with the location of the test points is shown.

Moreover, average CV of each specimen (S1, S2, S3, S4 and S5) were 16.4%, 17.3%, 14.9%, 17.5% and 15.2% respectively. These results show that measurements of cartilage thickness were repeatable within ±20%. This repeatability was lower than reported cartilage thickness measurements performed with US [111], but it was higher than the reported repeatability of cartilage thickness performed with a needle probe [1].

In general a high variation in cartilage thickness values was observed across all specimens (Table 5.3), however more than half of the measurements were within ± 1 SD of the mean thickness of any given specimen.

The variability of cartilage thickness distribution was lower than the variability of the mechanical properties.

**Table 5.3:** Maximum and minimum cartilage thickness values for specimens S1, S2, S3, S4, S5. Mean value and SD for each specimen.

| | Cartilage Thickness | | |
|---|---|---|---|
| Specimen | Range Means $\mu$m | Mean $\mu$m | SD $\mu$m |
| S1 | 1873.6 - 5061.6 | 2598.6 | 614.1 |
| S2 | 2122.0 - 3928.3 | 2586.5 | 393.2 |
| S3 | 2190.8 - 4863.3 | 2903.2 | 653.0 |
| S4 | 2147.4 - 3979.9 | 2743.0 | 439.8 |
| S5 | 2067.5 - 5055.9 | 2704.9 | 623.5 |

Heterogeneous distribution of cartilage thickness was found. However more than half of the points had similar values. Regional analyses of cartilage thickness were performed by grouping the points according to their location.

### 5.2.3 Cartilage Thickness Regional Analysis

Cartilage thickness distribution was analysed over different regions of the tibial plateau. First, the mean cartilage thickness of the medial and lateral compartment were compared. Second, the mean cartilage thickness over half compartments (four regions) were compared. Finally, the cartilage thickness was compared over the MMR regions.

#### 5.2.3.1 Cartilage Thickness Variation in Medial and Lateral Compartments

Cartilage thickness values over each tibial plateau were grouped according to their location within the medial or lateral compartment. Statistical mean comparison was performed.

Table 5.4 summarizes results from mean comparison between the medial and lateral compartment. This table presents mean cartilage thickness and SD of each compartment. Additionally, the total number of points tested on each tibial plateau (N) and the number of points on each compartment ($n_l$ and $n_m$ for lateral and medial compartment respectively). Also, p value for the mean comparison test which was obtained from the one way ANOVA or Welch test depending on the homogeneity of variance results (Chapter 4, Section 3). The effect size between the lateral and medial compartment mean cartilage thickness is also shown.

**Table 5.4:** Values of mean cartilage thickness ($T$) in medial and lateral compartments in six tibial plateaux. The first column corresponds to the specimen tested, N is the total number of points, $\overline{T_l}$ is the mean cartilage thickness in the lateral compartment and its standard deviation ($SD_l$), $n_l$ is the number of points located in the lateral compartment. Similarly, $\overline{T_m}$ is the mean cartilage thickness in the medial compartment and its standard deviation ($SD_m$), $n_m$ is the number of points located in the medial compartment. p is the significant difference between compartments calculated from ANOVA between groups or Welch test depending on homogeneity of variance. The last column represents the effect size between the lateral and medial compartment mean cartilage thickness.

| Specimen | N | Cartilage Thickness | | | | | | p | Effect size |
|---|---|---|---|---|---|---|---|---|---|
| | | Lateral | | | Medial | | | | |
| | | $\overline{T_l}$ $\mu$m | $SD_l$ $\mu$m | $n_l$ | $\overline{Tm}$ $\mu$m | $SD_m$ $\mu$m | $n_m$ | | |
| S1 | 42 | 2759.40 | 720.60 | 23 | 2404.1 | 389.20 | 19 | 0.610 | 0.008 |
| S2 | 38 | 2641.73 | 438.55 | 19 | 2448.00 | 480.19 | 19 | 0.202 | 0.04 |
| S3 | 37 | 2945.39 | 700.25 | 20 | 2853.48 | 610.14 | 17 | 0.676 | 0.05 |
| S4 | 38 | 2829.10 | 416.55 | 24 | 2620.15 | 456.97 | 16 | 0.143 | 0.007 |
| S5 | 40 | 2821.64 | 725.45 | 22 | 2574.41 | 454.00 | 18 | 0.216 | 0.004 |
| S6 | 40 | 2574.92 | 1417.60 | 22 | 2443.00 | 873.71 | 18 | 0.732 | 0.007 |

In Table 5.4 it can be observed that the lateral compartment was consistently thicker than the medial compartment, however these differences were not significant. As it was confirmed by the effect size, difference between compartments were small in all tibial plateaux. The SD for the lateral compartment was higher than that for the medial

compartment in all tibial plateaux except for S4. Moreover, mean stiffness of the lateral compartment was found to be between 2600 to 2950 $\mu$m, while mean thickness of the medial compartment was found to be between 2400 to 2850 $\mu$m.

In general, no significant difference in cartilage thickness was found between the medial and lateral compartments, although a repeatable pattern of thickness distribution was observed (lateral compartment was higher than medial).

#### 5.2.3.2 Cartilage Thickness Distribution in Four Compartments

The tibial plateaux were divided into quarters and mean cartilage thickness in these regions was compared. A mean comparison statistical test was performed.

A summary of cartilage thickness mean distribution over the six tibial plateaux grouped into four regions is shown in Figure 5.12. In this figure it can be observed that the mean cartilage thickness in the LA region ($\overline{T_{LA}}$) was between 2350 to 3250 $\mu$m ($\overline{T_{LA}}$ = 2779 $\mu$m). The mean cartilage thickness in the LP region ($\overline{T_{LP}}$) was between 2700 to 3100 $\mu$m ($\overline{T_{LP}}$ 2900 $\mu$m). The mean cartilage thickness in the MA region ($\overline{T_{MA}}$) was between 2400 to 2800 $\mu$m ($\overline{T_{MA}}$ = 2600 $\mu$m) and the mean cartilage thickness in the MP region ($\overline{T_{MP}}$) was between 2400 to 3000 $\mu$m ($\overline{T_{MP}}$ 2650 $\mu$m).

Overall, cartilage thickness in LP had slightly higher thickness values than LA in four of the six tibial plateaux (S1, S2, S3 and S4). Additionally, cartilage thickness in MA was slightly lower than MP in four of the six tibial plateaux (S1, S3, S4 and S5). However, no significant differences between regions were found.

Analysis of cartilage thickness over four compartments showed a repeatable pattern that was consistent over most tested specimens, however the differences between the four compartments were not significant. Therefore, regional analysis using the MMR was performed in order to obtain a better understanding of cartilage thickness distribution.

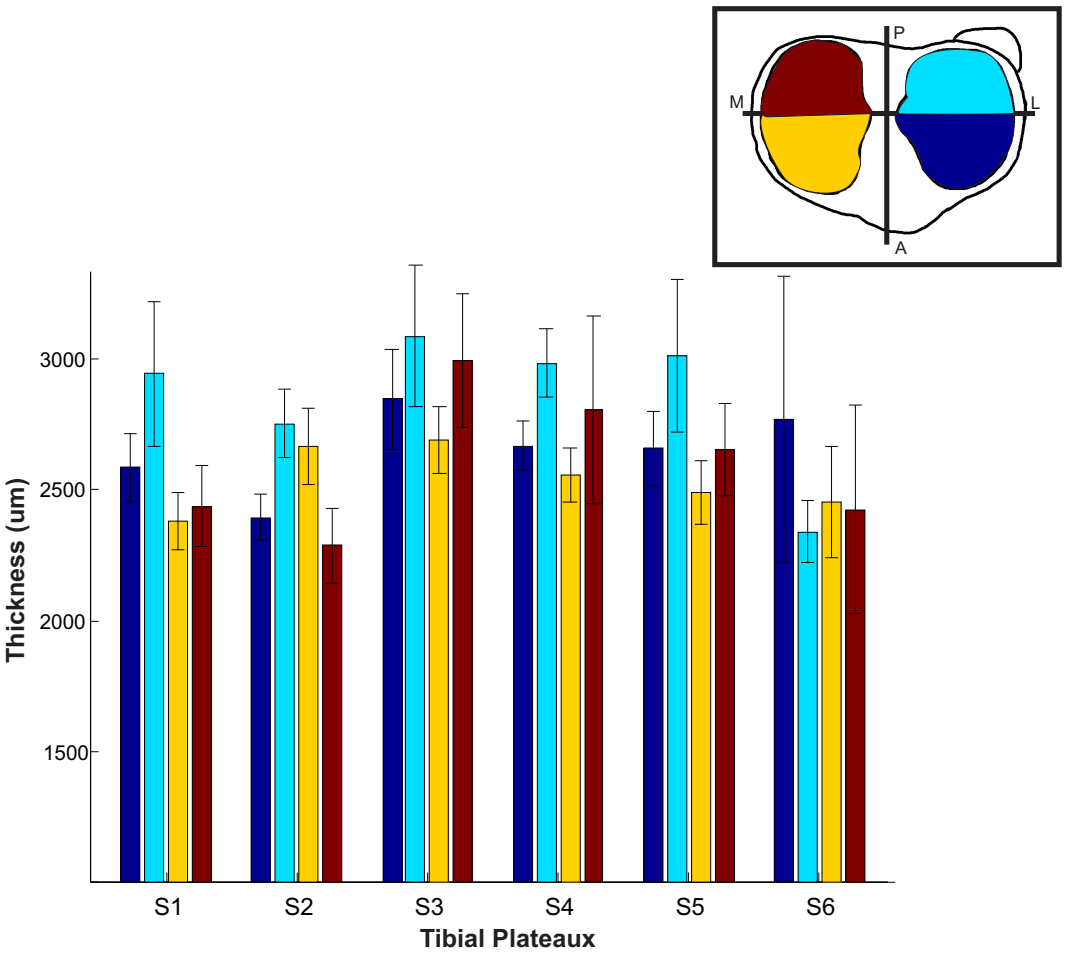


**Figure 5.12:** Mean thickness distribution four regions LA, LP, MA, MP. Bar colours represent a different region of the tibial plateau which is described by the inset map located on the right corner.

#### 5.2.3.3 Cartilage Thickness Variability for the MMR

The tibial plateaux were divided according to the MMR regions (see Figure 4.8). Comparison of mean cartilage thickness at each MMR region was performed on each tibial plateau.

The mean cartilage thickness and SD grouped by MMR at each tibial plateau are presented in Figure 5.13. In this figure it can be observed that the average thickness varies slightly between specimens within the same region. However, a similar trend was observed in cartilage thickness distribution between specimens. Regions V (VM and VL), located at the external rim, showed the highest cartilage thickness. Cartilage thickness of regions II, III and IV of both compartments were similar for all tibial plateaux and showed low cartilage thickness. These regions were all covered by the menisci.

In the lateral compartment, regions IL and IVL showed a similar value in all tibial plateaux (Figure 5.13). In addition, excluding the external rim (regions V), the region which had the highest cartilage thickness was region I (IM and IL) in five of the six specimens. Specimen S6 showed a higher cartilage thickness values than the other specimens and showed a slightly different trend.

Moreover, significant differences were observed between mirror regions in lateral and medial compartments in some of the specimens (i.e. region III in S2 and S6 and IV in S2, S5 and S6) suggesting that both compartments are not identical in cartilage thickness distribution.

## 5.3 Matrix Distribution and Quantification of GAG

GAG concentration throughout the tibial plateaux has been investigated in a number of studies [23, 32, 59]. Variations in GAG concentration distribution over the articular region have been reported between healthy and degraded cartilage [32, 282, 285]. In degraded cartilage the GAG concentration is low. However, GAG distribution in healthy cartilage has been little studied and conflicting results have been reported. Some authors have found negligible differences over an articular surface [32] while others have

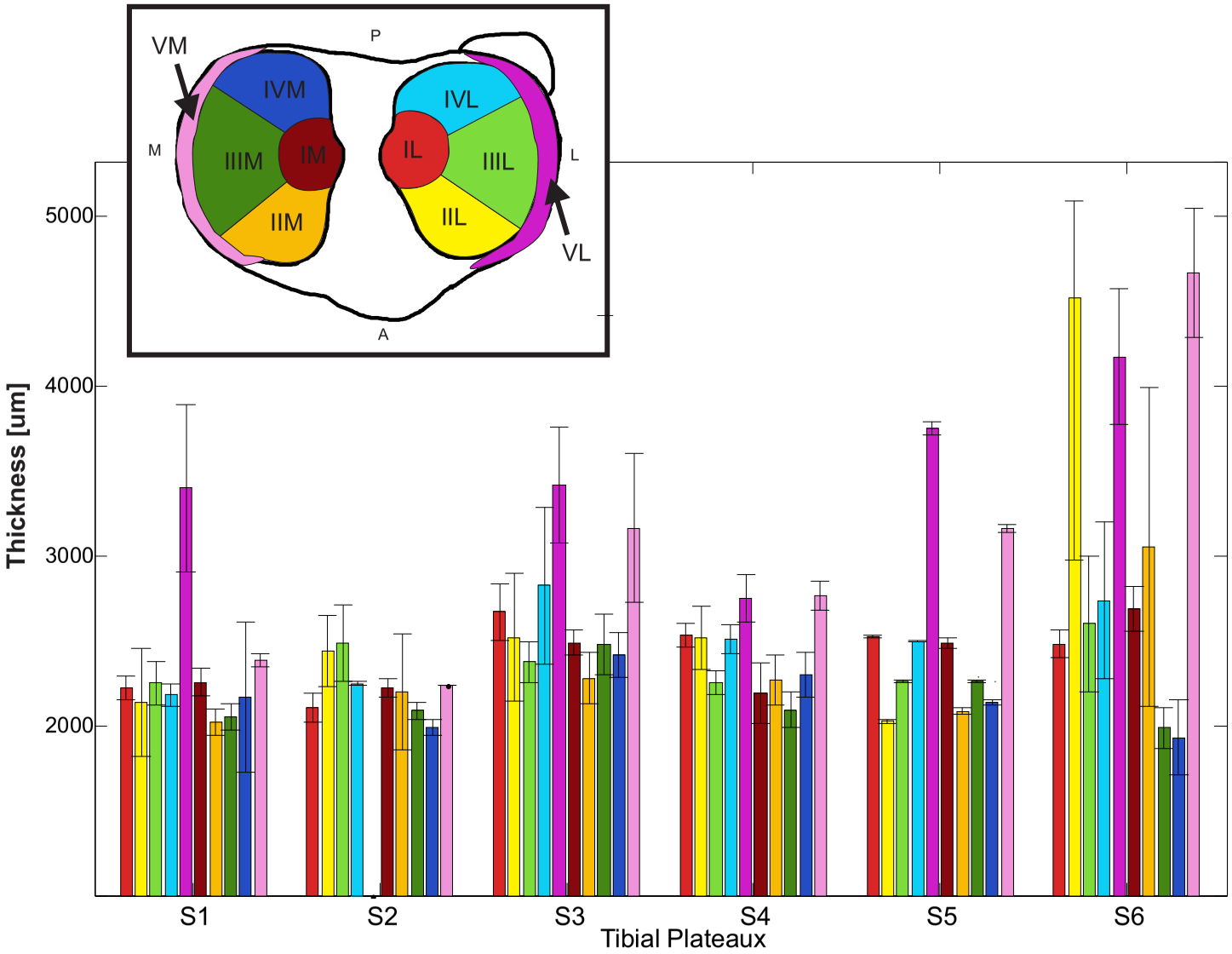


**Figure 5.13:** Mean cartilage thickness over MMR on each tibial plateau. Colours of the bars represents a different MMR region. Colour map is displayed in the top right corner of the figure.

reported significant regional differences [89, 278, 286]. The majority of studies on healthy specimens have taken small number of cartilage samples from different regions of the specimen, and this is a major limitation. In order to gain a better understanding of GAG distribution across tibial plateaux, GAG concentration must be measured over more points.

In the present work the distribution of GAG concentration in six porcine tibial plateaux, at approximately 40 points on each, was assessed by two methods: a non-destructive method which detected GAG concentration through the use of a contrast agent and fluoroscopy imaging, and a second destructive method which measured GAG concentration in cartilage plugs using the DMMB assay.

The non-destructive method required the definition of an optimal time of immersion of tibial plateaux in the contrast agent (CA4+). Additionally, attenuation values at each test point were extracted and correlated with the GAG concentrations obtained from the DMMB assay, in order to obtain a reference curve for quantification of GAG concentration in a non-destructive way.

The second method of quantifying GAG concentration at each test point, was performed through using the DMMB assay, in order to obtain: (a) GAG concentration maps for the six tibial plateaux and (b) carry out analysis of regional variations in GAG concentration for each plateau.

## 5.4 GAG Quantification

GAG quantification was obtained through two methods with the aim of correlating the two in order to construct a non-destructive GAG quantification curve. The first method (non-destructive method) required the definition of an optimal time of immersion of tibial plateaux in the contrast agent (CA4+). Then immersing the whole intact porcine knee in CA4+ and imaging it using a 3D fluoroscope after 24h. The second method of quantifying GAG concentration at each test point, was performed through using the DMMB assay, in order to obtain: (a) GAG concentration maps for the six tibial plateaux and (b) carry out analysis of regional variations in GAG concentration for

each plateau.

Furthermore, a curve that related both methods was created. Attenuation values at each test point were extracted from 3D reconstructed images. On the other hand, GAG content in the same test points was quantified by extracting osteochondral plugs and performing DMMB assay in the articular cartilage at each plug.

### 5.4.1 Quantification of GAG Through Imaging Techniques

A non-destructive method using a 3D fluoroscope (Chapter 4, Section 4.4.1.1) in combination with a cationic contrast agent (Chapter 4, Section 4.4.1.2) was used to quantify GAG. The optimal time of immersion of the tibial plateaux in the contrast agent was calculated first (Chapter 4, Section 4.4.1.3). The results of the experiments to determine the optimal time of immersion for extraction of intensity values are presented here.

#### 5.4.1.1 Optimal Configuration Parameters for Fluoroscope Imaging

After imaging specimens in different conditions (i.e. air, gel, water, frozen and non-frozen, mounted and demounted from sample holder, with and without metal markers), it was found that the quality of the image was unaffected by immersion media (gel, water or air). Images of non-frozen specimens had slightly better quality. Moreover, the use of dense metal, either metal markers or the metal sample holder, while imaging the specimen produced high scattering, which deteriorated the quality of the image significantly. Therefore, non-frozen specimens were imaged in air with no metal markers, specimens were removed from the sample holder before imaging.

Acquisition of images was performed at 15 fps, using an aperture size of 17 cm. Four hundred and fifty sequential linear images of the cartilage were acquired by these settings. Images were reconstructed with 512 $mm^3$ resolution. Five hundred and twelve sequential images were exported into DICOM.

The DICOM image sequences were then imported into Mimics for segmentation. Segmentation was performed using a semi-automated threshold based segmentation algorithm. All the acquired images met the minimum quality requirements for segment-

ation (cartilage with a thickness of 2 voxels).

#### 5.4.1.2 Optimal Time of Immersion in CA4+

Sequential 3D images of each sample were taken at 0, 2, 4, 6, 8, 15, 24 h. The cartilage volume at 24 h was obtained. Mean attenuation values of the cartilage volume at different time points were calculated and fitted with a curve of the type $1 - A * exp(\frac{-t}{\tau})$ (Figure 5.14). The time required to reach 65% of the maximum attenuation was obtained (from $\tau$ value) and the time for full attenuation was calculated by linear interpolation.

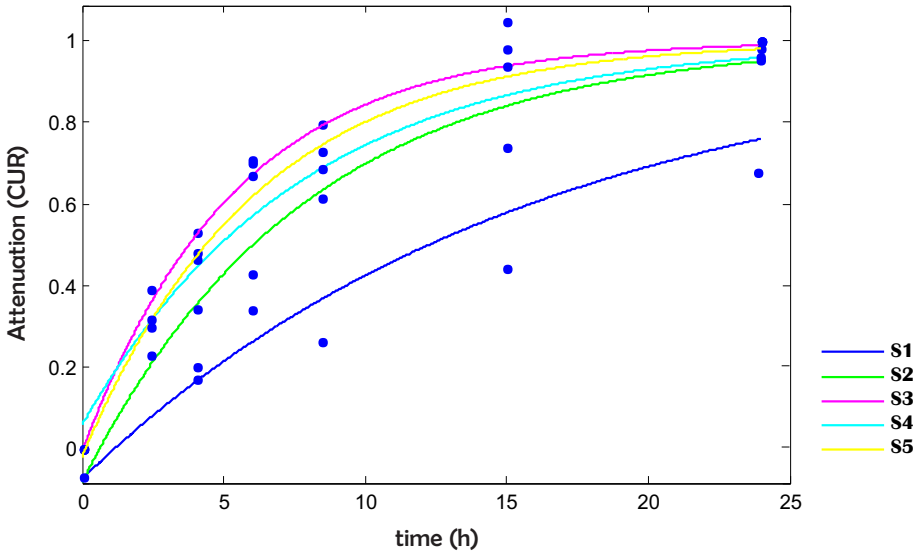


**Figure 5.14:** Contrast agent uptake ratio (CUR) of five samples at different time points. This curve shows the optimal time of immersion of tibial plateaux in CA4+

The resulting $\tau$ values and interpolated full penetration time, as well as equation parameters and the errors associated with the curve fitting (Sum Square Error (SSE) and R squared ($R^2$) are shown in Table 5.5.

**Table 5.5:** The Tau ($\tau$) value for optimal time of immersion of the tibial plateau in CA4+.

| Sample | $\tau$ [h] | A | SSE | $R^2$ | Interp. Max Att. [h] |
|---|---|---|---|---|---|
| S1 | 16.048 | 1.074 | 0.156 | 0.793 | 24.69 |
| S2 | 7.856 | 1.081 | 0.039 | 0.958 | 12.09 |
| S3 | 5.390 | 1.007 | 0.193 | 0.823 | 8.29 |
| S4 | 7.700 | 0.942 | 0.074 | 0.885 | 11.85 |
| S5 | 7.700 | 1.020 | 0.011 | 0.986 | 9.44 |

Most specimens had reached maximum attenuation before 24 h with the exception of S1 which showed maximum attenuation slightly after 24 h.

These results suggest that by 24 h, the contrast agent CA4+ had fully penetrated the tibial plateaux. These results provided the basis for the next step which assessed the correlation of attenuation with GAG concentration.

### 5.4.2 Attenuation Versus GAG Content Curve

In order to quantify GAG content in a non-destructive way, the correlation between GAG concentration (obtained by DMMB assay) and the attenuation values (obtained at each test point after specimens were submerged in CA4+ for 24 h) were identified. Figure 5.15 shows the relationship between mean attenuation and GAG concentration at each test point. Linear regression was used to examine the relationship between these two variables. Results of the goodness of curve fit ($R^2$) are shown in Table 5.6.

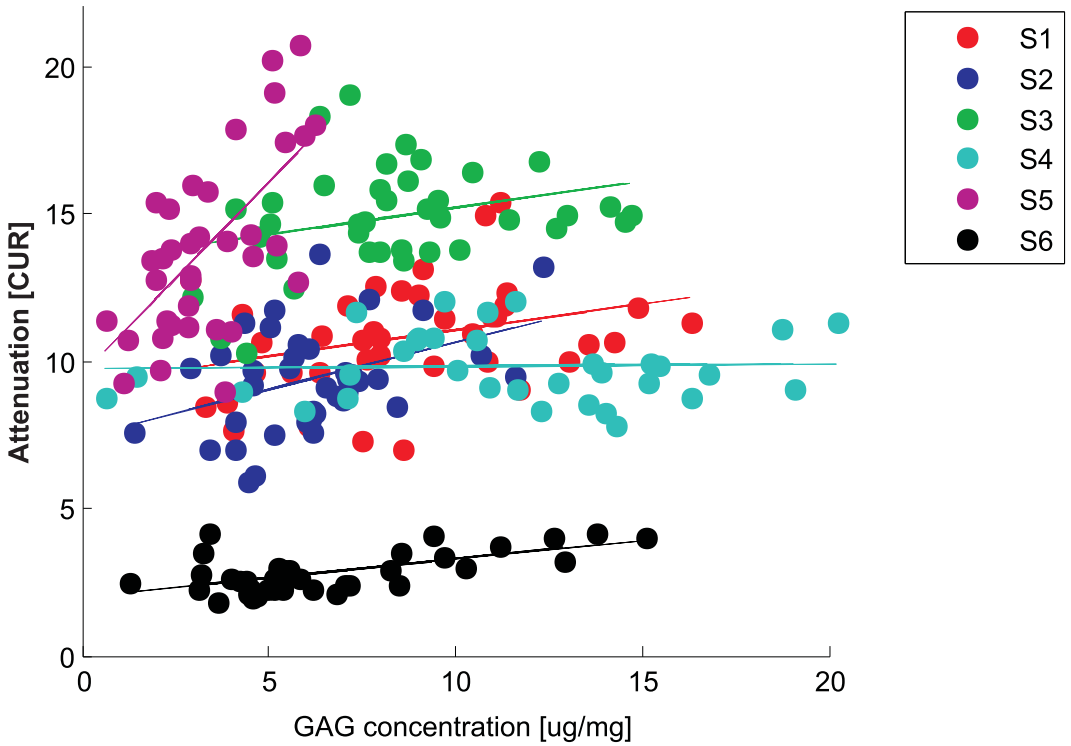


**Figure 5.15:** Correlation between mean attenuation of each testing point versus respective GAG concentration in all test points over specimens S1, S2, S3, S4, S5 and S6. CUR (contrast agent uptake ratio)

The correlation found between these two parameters was highly variable between specimens (Table 5.6). Moreover, the goodness of fit was very low ($R^2 < 0.2$) for four of the six specimens and below 0.45 for all specimens. The highest $R^2$ values were found

**Table 5.6:** Linear relationship between fluoroscope attenuation and GAG content

| Sample | slope | constant | $R^2$ |
|---|---|---|---|
| S1 | 0.178 | 9.29 | 0.101 |
| S2 | 0.319 | 7.45 | 0.161 |
| S3 | 0.182 | 13.40 | 0.097 |
| S4 | 0.0001 | 9.84 | 0.0001 |
| S5 | 1.305 | 9.56 | 0.414 |
| S6 | 0.129 | 2.00 | 0.393 |

in specimens S5 and S6 ($R^2 = 0.41$ and $R^2 = 0.39$ respectively). These results, were low compared to those previously reported in the literature [141, 290]

Results presented in Table 5.6 in combination with difference in fitted lines showed in Figure 5.15, suggest no clear correlation between fluoroscope attenuation and GAG content. Therefore, it was concluded that this method would not be a reliable method to measure GAG content in a non-destructive way.

### 5.4.3 DMMB Assay

GAG quantification was performed using the well established and accepted 1,9 - dimetrylmethylene blue (DMMB) assay. GAG content was measured at each of the testing points over six specimens (Chapter 4,Section 4.4).

#### 5.4.3.1 Comparison Between Wet and Dry Weight

GAG content was normalized by wet and dry weight of the sample. Dry weight was obtained by freeze-drying the sample for more than 6 h, while wet weight corresponds to the weight of the hydrated cartilage. The correlation between wet and dry weight was assessed (Figure 5.16). A high linear correlation ($R^2 = 0.73$) between GAG content normalized by dry weight was observed.

This result suggests that similar results would be obtained using either GAG content normalized by wet weight or GAG content normalized by dry weight. GAG content normalized per wet weight was used.

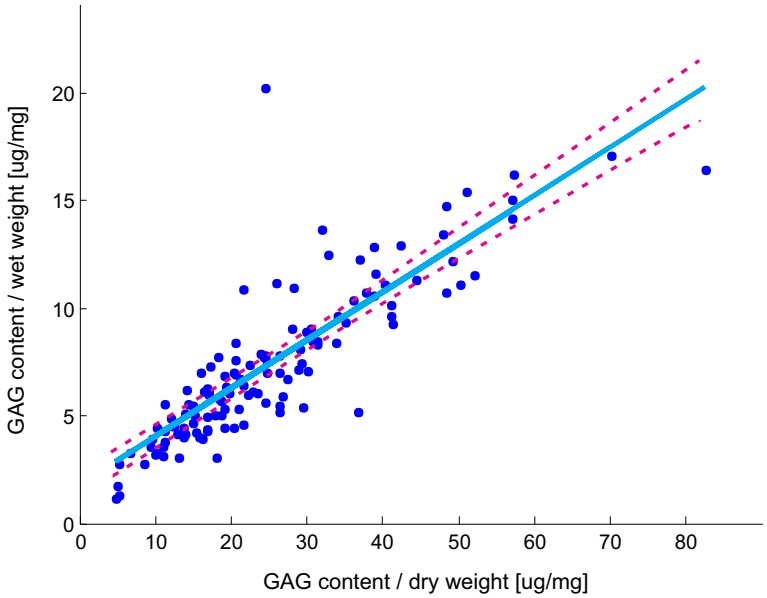


**Figure 5.16:** Relation between GAG content normalized by wet weight and GAG content normalized by dry weight

### 5.4.4 GAG Distribution

GAG concentration was measured for cartilage plugs extracted at each test point from the two external sections (Chapter 4, Figure 4.13). Mean GAG concentration values at each test point over six tibial plateaux were plotted at the locations from which they were taken (Figure A.9). The colour of each testing point represents the mean GAG content normalized per wet weight, where blue corresponds to the lowest GAG concentration and red corresponds to the highest.

In Figure 5.17 shows GAG concentration distribution over specimen S5. In Appendix A, Figure A.9 the distribution of mean GAG concentration over the six tibial plateaux is shown. The identification of patterns in GAG concentration distribution over the six tibial plateaux is not as clearly defined as the other measured variables reported previously. However, careful observation shows areas of high GAG concentration located consistently in, but not restricted to, central areas near the tibial eminence in all specimens. Although other areas of high GAG concentration were observed, these are less consistent over the six tibial plateaux.

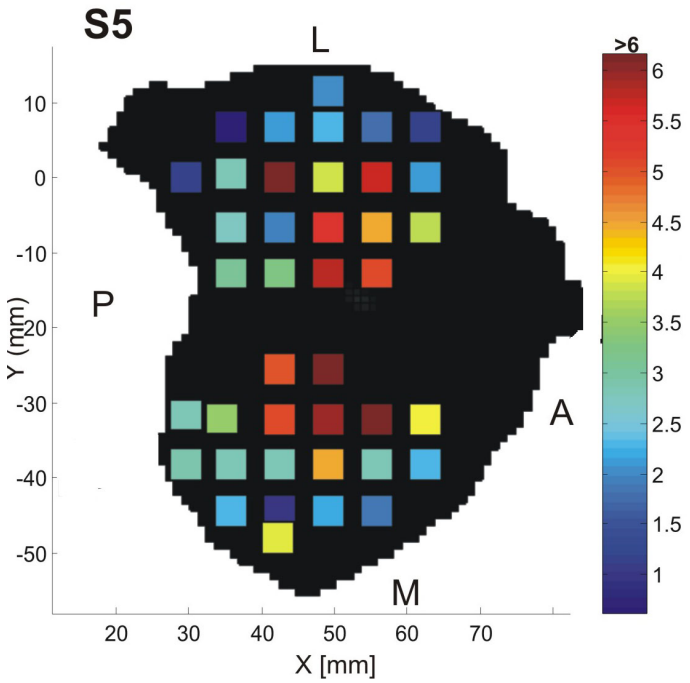


**Figure 5.17:** GAG distribution at testing points in samples S5

#### 5.4.4.1 Repeatability of GAG Concentration Within Each Point and Variability Across Each Specimen

The repeatability of GAG concentration measured at each test point through DMMB assays was assessed. The variability of GAG concentration values over approximately 40 points on each tibial plateaux was represented using boxplots (Figures A.10 and A.11).

In general, GAG concentration values ranged between 1 and 20 $\mu$g/mg. The mean repeatability (SD) within measurements at each test point on each tibial plateaux was 0.53 $\mu$g/mg, 0.57 $\mu$g/mg, 0.48 $\mu$g/mg, 0.90 $\mu$g/mg, 0.21 $\mu$g/mg, 0.43 $\mu$g/mg for specimens S1, S2, S3, S4, S5 and S6 respectively. Moreover, repeatability assessed by CV calculations (7.36%, 9.08%, 5.79%, 7.32%, 5.70%, 6.03% for specimens S1, S2, S3, S4, S5 and S6) showed repeatability of GAG concentration was within $\pm$10%.

In Figures 5.18 the distribution of GAG concentration in specimen S5 is presented. The distribution of GAG concentration in all six specimens is shown in Appendix A, Figures A.10 and A.11. The low spread of GAG concentration within each point is evident for almost all test points. Only a few points had a higher spread (greater than 4 $\mu$g/mg) driven by outliers.

S5 showed an interesting pattern between points. This specimen showed a clear division of mean GAG concentration between points near the tibial eminence and externally located points.

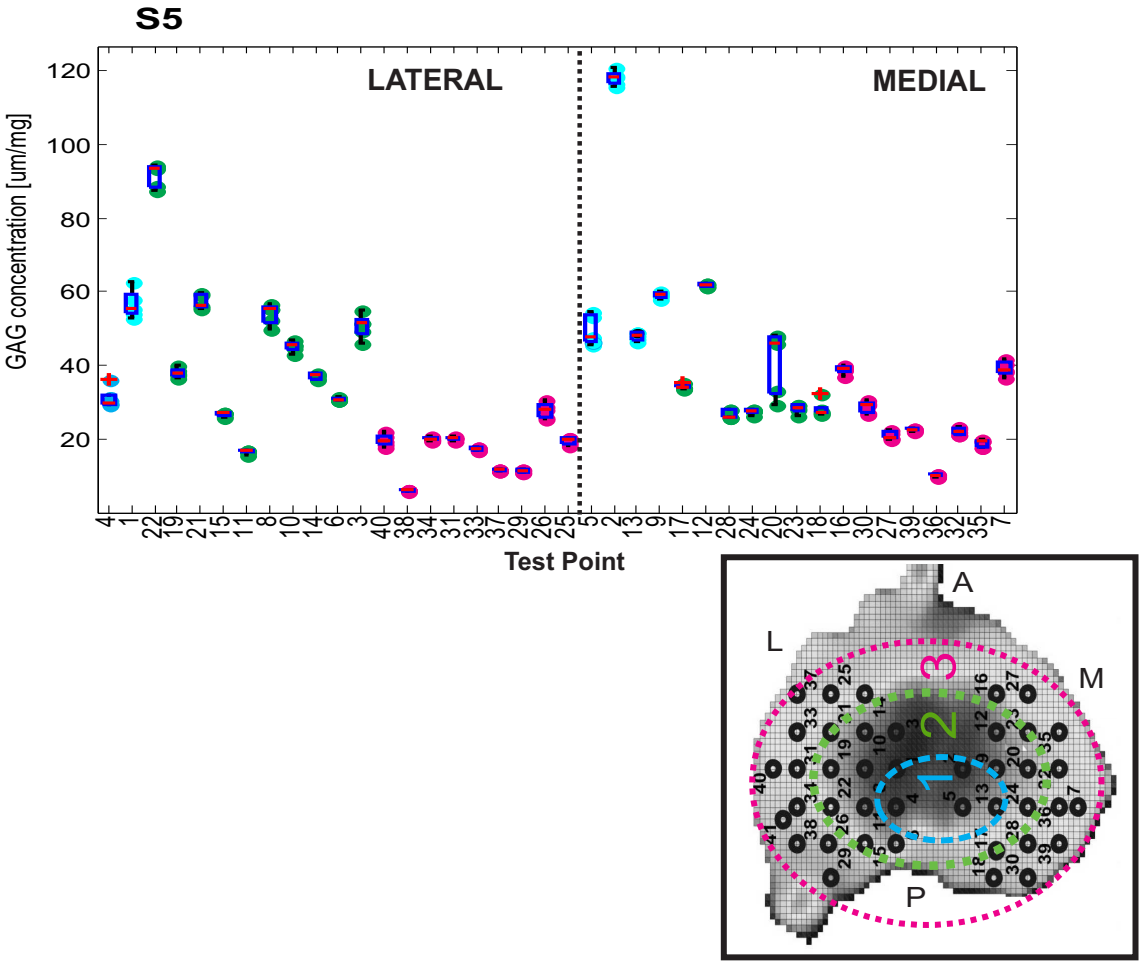


**Figure 5.18:** Boxplot of the distribution of GAG concentration in specimen S5. This plot presents the different values of GAG concentration calculated from DMMB assay at each point. Red are the highest GAG concentration values and blue are the lowest. On top of the scattered points a box plot that highlights the mean GAG concentration value of each point and the upper and lower boundaries for repeated measurements is shown. Beside each plot there is a map of the tibial plateau with the location of the test points.

Table 5.7 shows the range of GAG concentration values, the mean GAG concentration for each specimen and the SD. Overall, it can be observed that there was a relatively high variability of GAG concentration in terms of the difference between the maximum and minimum values observed for each specimen (an order of magnitude difference between lowest and highest values in most specimens). Mean GAG concentration for all specimens was around 7 $\mu$g/mg. However, 40% of test points were outside $\pm 1$ SD of the mean GAG concentration of each specimen.

A heterogeneous distribution of GAG on six tibial plateaux was found. However,

**Table 5.7:** Maximum and minimum GAG concentration values for specimens S1, S2, S3, S4, S5, S6. Mean value and SD for each specimen.

| Specimen | GAG Concentration | | |
|---|---|---|---|
| | Range Means [$\mu$g/mg] | Mean [$\mu$g/mg] | SD [$\mu$g/mg] |
| S1 | 2.85 - 17.18 | 8.88 | 3.53 |
| S2 | 1.38 - 16.50 | 6.29 | 2.79 |
| S3 | 2.91 - 14.66 | 8.27 | 2.99 |
| S4 | 0.59 - 28.46 | 12.25 | 5.85 |
| S5 | 0.62 - 16.50 | 3.93 | 2.95 |
| S6 | 1.22 - 20.26 | 7.09 | 4.09 |

around 60% of GAG concentration values were within ±1 SD of the mean GAG concentration of each specimen. These results suggest that there may be homogeneous GAG concentrations within regions on the tibial plateaux. A regional analysis was carried out by grouping GAG concentration values by location.

### 5.4.5 GAG Regional Analysis

Test points were grouped into different regions and mean GAG concentrations were compared using statistical analysis. The first mean comparison was performed between the medial and lateral compartment. Then, each compartment was divided in half, and four compartments were compared. Finally, test points were grouped into the MMR.

#### 5.4.5.1 GAG Variation Between Medial and Lateral Compartments

Mean GAG concentration values were classified into the medial and lateral compartment according to the location of the test points. Statistical analysis was performed to compare means.

Table 5.8 shows the mean GAG concentration in the lateral and medial compartment.

Mean values of GAG concentration in the lateral compartment were between 4 and 11 $\mu$g/mg ($\overline{GAG_l}$ = 7.6 $\mu$g/mg), while mean values of GAG concentration in the medial compartment were between 4 and 14 $\mu$g/mg ($\overline{GAG_m}$ = 8.0 $\mu$g/mg). Higher concentrations of GAG were found in the lateral compartment in four of the six tibial plateaux. However, the difference between compartments was not significant in any

**Table 5.8:** Values of mean GAG concentration ($GAG$) in medial and lateral compartments in six tibial plateaux. The first column corresponds to the specimen tested, N is the total number of points, $\overline{GAG_l}$ is the mean GAG concentration in the lateral compartment and its standard deviation ($SD_l$), $n_l$ is the number of points located in the lateral compartment. Similarly, $\overline{GAG_m}$ is the mean GAG concentration in the medial compartment and its standard deviation ($SD_m$), $n_m$ is the number of points located in the medial compartment. p is the significant difference between compartments calculated from ANOVA between groups or Welch test depending on homogeneity of variance. The last column represents the effect size between mean GAG concentration of each compartment.

| Specimen | N | GAG Concentration | | | | | | p | Effect size |
|---|---|---|---|---|---|---|---|---|---|
| | | Lateral | | | Medial | | | | |
| | | $\overline{GAG_l}$ $\mu$g/mg | $SD_l$ $\mu$g/mg | $n_l$ | $\overline{GAG_m}$ $\mu$g/mg | $SD_m$ $\mu$g/mg | $n_m$ | | |
| S1 | 42 | 9.59 | 3.93 | 23 | 8.02 | 2.85 | 19 | 0.154 | 0.050 |
| S2 | 40 | 6.16 | 2.38 | 20 | 5.92 | 2.26 | 20 | 0.744 | 0.003 |
| S3 | 39 | 7.14 | 2.21 | 21 | 9.60 | 3.29 | 18 | 0.009 | 0.172 |
| S4 | 39 | 11.02 | 5.92 | 24 | 14.23 | 5.33 | 15 | 0.096 | 0.073 |
| S5 | 41 | 3.95 | 3.43 | 22 | 3.90 | 2.36 | 19 | 0.952 | <0.001 |
| S6 | 40 | 7.49 | 4.55 | 22 | 6.61 | 3.50 | 18 | 0.505 | 0.012 |

of the specimens, with the exception of S3. In S3, the medial compartment showed significantly higher GAG concentration than the lateral compartment (p = 0.009).

The magnitude of the SD values relative to their corresponding means indicated large variability in GAG concentration within the medial and lateral compartments of each plateau. Once again this suggested that there might be sub-regions within each compartment where the variability was lower.

#### 5.4.5.2 GAG Concentration Distribution in Four Compartments

Each tibial plateau was divided into four regions (LA, LP, MA and MP) (Figure 4.6). The mean GAG concentrations for each region were compared in each specimen using statistical analysis.

A summary of mean GAG concentration distribution over six tibial plateaux grouped in four equal regions is shown in Figure 5.12. The mean GAG concentration in the LA region for the six tibial plateaux ($\overline{GAG_{LA}}$) was between 5.5 - 9 $\mu$g/mg ($\overline{GAG_{LA}}$ = 6.8 $\mu$g/mg). The mean GAG concentration in the LP region ($\overline{GAG_{LP}}$) was between 4 - 10.5 $\mu$g/mg ($\overline{GAG_{LP}}$ = 8.4 $\mu$g/mg). On the medial side the mean GAG concentration ($\overline{GAG_{MA}}$) was between 4.5 - 10 $\mu$g/mg ($\overline{GAG_{MA}}$ = 8.3 $\mu$g/mg) and the mean GAG

concentration in the MP region ($\overline{GAG_{MP}}$) was between 3 - 9.5 $\mu$g/mg ($\overline{GAG_{MP}} = 8.1$ $\mu$g/mg).

The mean GAG concentration in the LP region was slightly higher than the LA region in four of the six tibial plateaux (S1, S2, S5, S6). In the medial compartment, slightly higher GAG concentration was observed in the MA compartment compared to the MP compartment in five of the six tibial plateaux (S2, S3, S4, S5, S6). However, no significant differences were found between regions in any of the specimens. This was confirmed by the small effect size in all specimens. A graphical representation of GAG concentration means is presented in Figure 5.19.

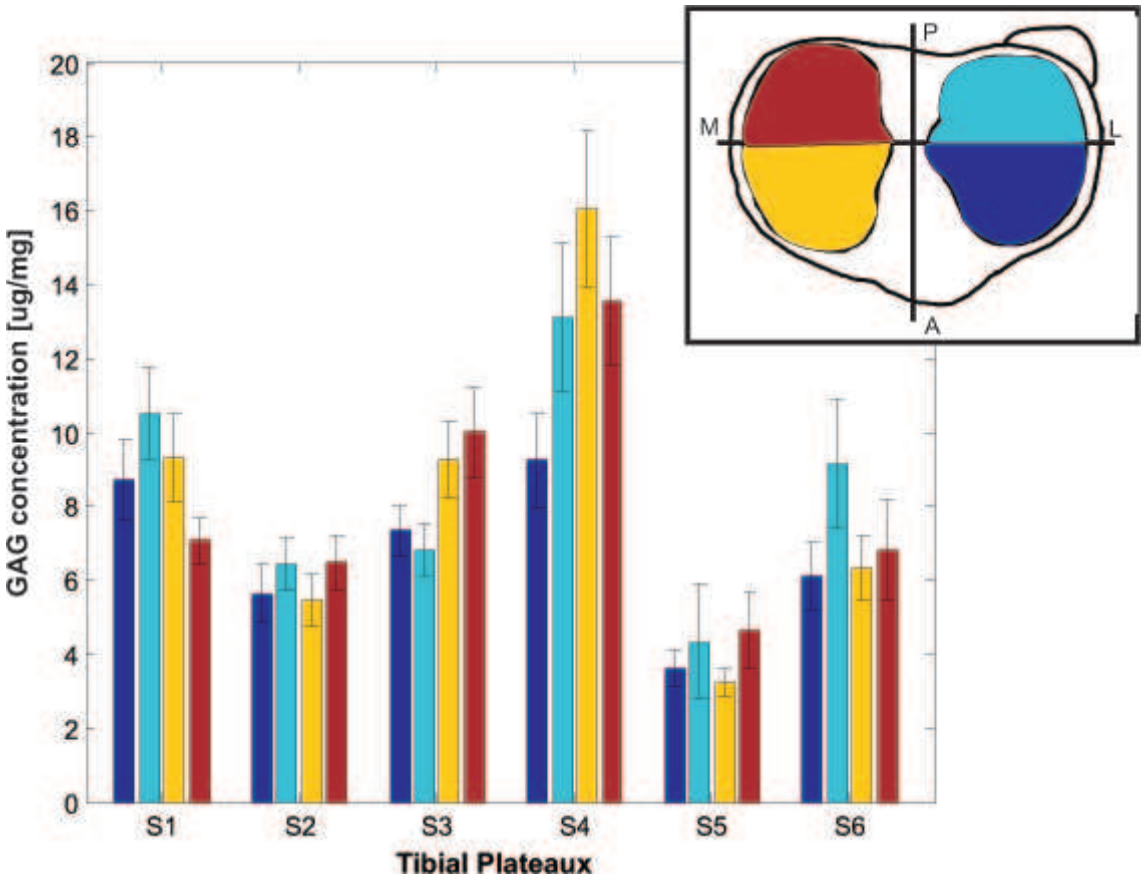


**Figure 5.19:** Mean GAG concentration distribution grouped four regions LA, LP, MA, MP. Bar colours represent a different region of the tibial plateau which is described by the inset map located on the right corner.

Overall, relatively consistent patterns in GAG concentration distribution were observed for half compartments in four specimens (S1, S2, S5, S6). Anterior regions (LA and MA) showed slightly lower GAG concentration than their posterior counterparts (LP and MP). However, these differences were not significant in any of the specimens. The SD of each region on all tibial plateaux was relatively high compared to the mean

values.

#### 5.4.5.3 GAG Concentration Variability Within The MMR

The GAG concentration at all test points (approximately 1000) were grouped according to location into the MMR for each tibial plateau. Mean comparison of GAG concentrations between regions was carried out for each tibial plateau. Figure 5.20 shows the mean GAG concentration and SD for each MMR region on each specimen and the p value obtained from mean comparison statistical test between regions.

Mean GAG concentrations for the MMR regions were 8.0 $\pm$ 2.5 [$\mu$g/mg]. Significant differences between at least two regions were observed in all specimens except for S1.

In the lateral compartment region IL had consistently the highest GAG concentration (except for S6 where IL was the 2nd highest after VL). In the medial compartment IM had the highest GAG concentrations in four of six specimens (S2, S3, S5, S6). Region V in both compartments was also notable for high GAG concentrations in most specimens. On the other hand the lowest GAG concentrations were generally found in regions II, III or IV depending on the specimen.

Significant differences were found between region IL and region IIIL in five of the six tibial plateaux (S1, S3, S4, S5, S6). In the medial compartment significant differences between region IM and IVM were observed in all the specimens with the exception of S1. Regions III and IV in both compartments had similar GAG concentrations in all specimens.

Results obtained by analysis of GAG concentration distribution over six tibial plateaux grouped by MMR regions, showed that higher GAG concentrations were found in region I in both compartments (IM and IL), followed by region V (VM and VL). These results indicate that GAG concentration distribution is highest in areas uncovered by the menisci. Moreover, areas with lowest GAG concentration were normally found between regions II, III and IV; all areas which are covered by the menisci. Significant differences were found between mirror regions in lateral and medial compartment in some of the specimens (i.e. regions IM and IL and regions IVM and IVL in S2, IIIM

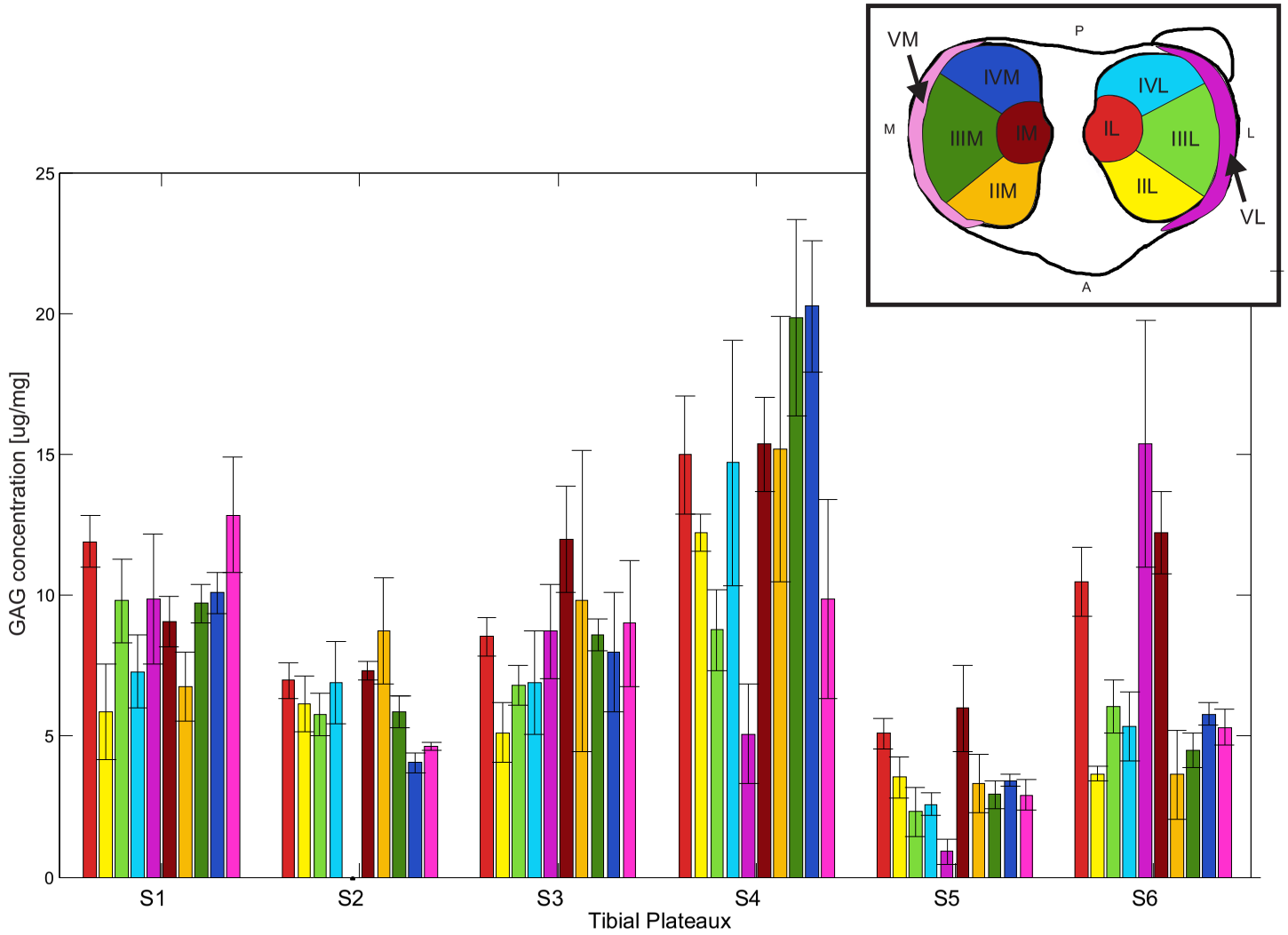


**Figure 5.20:** Mean GAG concentration over MMR on each tibial plateau. Colours of the bars represents a different MMR region. Colour map is displayed in the top right corner of the figure.

and IIIL in S3).

Results of GAG concentration distribution suggest a high correlation between GAG concentration and the location of the menisci.

### 5.4.6 Discussion

In this chapter, topographical maps (Figure A.1) showed the expected characteristics of tibial plateaux such as the curvature of compartments, the tibial eminence, position of fibula.

An average of 40 test points on each tibial plateau were identified (Figure A.2) to measure mechanical properties, cartilage thickness and GAG concentration. These test points covered all areas of the tibial plateaux excluding the tibial eminence, since this area has no cartilage, but including the external rim ordinarily not included. Although measurements of mechanical properties of articular cartilage have been reported by several authors [2, 23, 28, 278], in the present work at least double the amount of test points previously reported were measured for mechanical, physical and biological properties. This allowed a higher resolution of the distribution of variables to be obtained.

Topographical variations of GAG content over the tibial plateau had been studied previously [23, 24, 141, 290]. The majority of papers focus on GAG distribution between cartilage layers (from surface to deep) rather than mapping spatial distribution over a whole articular surface. One of the most successful methods for GAG mapping has been achieved through the use of imaging methods. In particular, dGEMRIC technique is a well accepted method for this purpose [23]. Similarly, there has been some effort to validate qQCT techniques for the assessment of GAG distribution [141, 290].

Heterogeneity of the distribution of mechanical properties, cartilage thickness and GAG content was observed in all specimens.

Less than 20% of the mechanical property values were within $\pm 1$ SD of the mean of the specimen in all tibial plateaux. Cartilage thickness showed less variability than the mechanical properties (55% of the cartilage thickness values were within $\pm 1$ SD of the

mean of the specimen), however variability in mean thickness was from approximately 2 to 5 mm. Heterogeneity of mechanical properties and thickness distribution over the tibial plateau is in agreement with the literature [18, 27, 30, 70, 83, 231, 284]. Moreover, the heterogeneity of the GAG concentration across six porcine tibial plateaux was demonstrated. Approximately 70% of values were within ±1 SD of the mean of each specimen.

The distribution of mechanical properties over the articular cartilage showed areas of higher elastic modulus in central regions of both medial and lateral compartments, surrounded by areas of lower elastic modulus. Moreover the distribution of cartilage thickness over the articular cartilage in porcine tibial plateaux showed low cartilage thickness values in the central regions of both lateral and medial compartments, surrounded by areas of higher cartilage thickness. These distribution patterns of both the mechanical properties and cartilage thickness suggest a relationship between the two variables.

Regional analysis of the mechanical properties and cartilage thickness showed that (1) the lateral compartment was slightly thicker than the medial compartment and no significant differences in mechanical properties between compartments were found. In the literature, there are conflicting results regarding the thickness distribution over compartments. Significant difference in thickness between compartments ($p < 0.002$), the medial being the thickest [157, 206] were reported. However, Koo *et al* [289], suggested that thickness was related to contact geometry between the articular surfaces and found that the lateral compartment was thicker than the medial compartment. (2) The four region analysis showed that posterior regions of both lateral and medial compartments were slightly thicker than the anterior regions and had a lower elastic modulus. These results showed an inverse relationship between elastic modulus and cartilage thickness distribution.

A more detailed analysis of the distribution of these two variables was performed using the MMR division. MMR regions were developed based on the work reported by Deneweth [2]. These regions differentiate the areas uncovered by the menisci (IM and IL in the centre of the tibial plateau, near the tibial crescent and VM and VL in the

external rim of the tibial plateau) and the areas covered by the menisci (IIL and IIM - on the anterior region, IIIL and IIIM - middle area and IVL and IVM - on the posterior region). Results of the mechanical properties and cartilage thickness distribution using MMR confirmed the negative relationship between these two variables. Region V on both compartments (VM and VL) showed the highest thickness and lowest elastic modulus. Region I in both compartments (IM and IL) showed the second highest thickness and mechanical properties which were lower than for regions III (IIIM and IIIL). Region II and III showed the highest elastic modulus and the lowest cartilage thickness. Moreover regions III were significantly different than regions IV in most specimens.

Negative correlation between cartilage thickness and mechanical properties is in line with results reported in the literature [222, 291].

In the literature higher stiffness in areas covered by the menisci in comparison with areas uncovered by the menisci have been found [103, 278]. These areas were also related to load-bearing areas when knee is near full extension [21, 278]. Additionally, several authors have reported that cartilage thickness was highly correlated with load patterns [18, 21, 231, 281, 284]. Therefore, cartilage was the thickest in menisci-uncovered areas, where there was "cartilage-to-cartilage contact" [18, 19, 21, 282, 284]. Nevertheless, some authors disagree with this [27, 30, 231]. In the work presented here, it was found that the mechanical properties values were the highest in areas covered by the menisci, in agreement with Bevill [278] and Barker [103]. Moreover, the thickness distribution presented in this chapter is in agreement with findings that state that cartilage is the thickest in menisci-uncovered areas. Comparison of thickness with data reported in literature, required an adjustment of the area tested in this study. Here a larger area of the tibial plateau was assessed (normal vector of test points located in the external rim of the lateral and medial compartment had angles greater than $40^{\circ}$ relative to the $Z_W$ axis indenter). Therefore, it is important to exclude the most external rim located in the external lateral and medial side for comparisons. Taking this into account, the thickness distribution was consistent with results reported in the literature [282].

Comparison of the mechanical properties analysed by the MMR, with the work results of Deneweth *et al.* [2] showed some discrepancies. Deneweth *et al.* found significant differences in the mechanical properties of region II, compared to regions III and IV, which had similar mechanical properties. In the present work significant differences between regions III and IV were found, while mechanical properties of regions II were similar to those found in regions III. Nevertheless, both works found similar mechanical properties between regions I and II. The differences in results could be explained by the species used. Deneweth *et al.* performed experiments on human cartilage while the current work was performed using porcine specimens. The literature suggests that these patterns would depend on animal specific gait patterns [289]. Additionally, Deneweth *et al.* measured the elastic modulus at 10% strain over several points in the tibial plateau, while in the present work the deformation was not consistently 10% of cartilage thickness, but varied over the tibial plateau dependent on the thickness of the cartilage. The elastic modulus values obtained in the present work are in good agreement with those reported by Deneweth *et al.* [2, 253].

On the other hand, GAG concentration distribution on six tibial plateaux showed high GAG concentrations in central areas near the tibial eminence. Later, regional analysis confirmed that high GAG concentrations were consistently found in areas uncovered by the menisci. These results were in agreement with findings reported in the literature [23, 89, 282].

A group in Boston University headed by Prof. M. Grinstaff, developed a contrast agent (CA4+) and quantified GAG content using $\mu$CT imaging techniques [141, 154, 290, 292]. This group found high correlations ($p > 0.7$) between GAG content measured by $\mu$CT and GAG concentration measurements by DMMB assays. In the present work it was aimed to reproduce these experiments using a 3D fluoroscope (instead of a $\mu$CT) and a whole knee (instead of plugs of cartilage), nevertheless small correlations ($0.1 \leq R^2 \leq 0.45$) between these two measurements were found. The discrepancies between the results obtained by Grinstaff's group and this work could be attributed to some changes between experiments settings (size of the sample and resolution of the imaging device), these are discussed below.

(a) Grinstaff's group performed the experiments in 4 to 7 mm diameter plugs. The size of the plug affects the time of penetration and distribution of the CA4+ into the articular cartilage. The time of maximum penetration obtained by Grinstaff's group was between 1 to 3 h, $\tau = 2.22$ h [293], nevertheless plugs were left in the CA4+ for 24 h. It was unclear in the literature whether it was necessary to leave the sample this extra time, however further discussion of these results was carried out with members of Grinstaff's group and it was suggested that repetition of the experiment leaving the specimens for 5 to 6 times the amount of time given by $\tau$ would improve the outcome. In the current work, whole tibial plateaux were immersed in the CA4+ and the time of maximum penetration obtained were in general between 10 to 12 h. Leaving the specimens 5 to 6 times the maximum values would imply that for whole specimens 50 to 60 h of submersion in CA4+ (at room temperature) would be necessary. Even though protease inhibitors are added with the contrast agent, tests must be carried out to evaluate the integrity of the sample after this amount of time at room temperature. The literature suggests that changes in cartilage properties can be found after 40 h at room temperature [27, 47]. These results would suggest that to be able to use a contrast agent in whole specimens, it would be necessary to use a contrast agent with a higher diffusion rate.

(b) Bansal *et al.* [275] imaged the samples with a $\mu$CT, which had a resolution of 30 to 50 voxels through the tissue depth. This allowed a high level of detail of intensity values to be measured throughout the cartilage layers. Lower resolution, such as the one obtained with the fluoroscope (2 to 3 voxels) could lead to lower accuracy in the measurement of intensity values, since there are less voxels to average and some of those might contain partial volume artifacts.

Samosky *et al.* [23] studied the spatial GAG distribution in knees using dGEMRIC. The author tried to correlate GAG distribution to biomechanical properties of cartilage. He found that correlation between properties was achieved when only the first 700 $\mu$m were taken from dGEMRIC values. Otherwise, when values over the whole thickness were taken into account, the correlation ceased to exist.

The analysis of GAG distribution throughout the full thickness cartilage of six tibial

plateaux was carried out. GAG distribution was analysed using mean comparison of different regions. As discussed in Chapter 2, cartilage is composed of different layers, each of which has distinct structural components. In particular, GAG content varies between layers and distinguishes them [61]. In the present chapter, an average of GAG concentration over the full thickness volume of the cartilage plug tested was taken.

The difference in GAG concentration between OA regions and non-OA regions has been shown using the DMMB assay [282, 285, 294], however it was not clear whether the assay is sensitive enough to detect differences in normal cartilage [32]. In this chapter significant differences between GAG concentration distribution were found. These results demonstrate that the DMMB assay has the potential to show significant differences in GAG concentration in normal articular cartilage. To the knowledge of the author this is a new finding.

In this work, mechanical tests were performed using in-situ indentation with periodic hydration using saline solution. In the past, some authors have suggested that samples indented in air (instead of saline solution) did not reach complete recovery [295] and, therefore, indentation tests in tissue should be carried out in a solution chamber. Repeatability of results obtained in this work suggests that periodic hydration of specimens with saline solution is sufficient when using whole specimens. Testing whole tibial plateaux may have a different effect on hydration compare to testing plugs, due to the access and release of fluids to the tissue. When working with plugs, fluids have direct access to all layers of the tissue. When working with whole specimens the fluids have to pass through the most superficial layer to get inside the tibial plateau. Therefore, it is possible that whole knees have a better retention of fluids when indentation is being performed, as in whole specimens the retention of fluid is superior than in plugs.

Moreover, in this chapter two GAG quantification methods were presented in order to develop a predicting calibration curve that would allow non-destructive GAG quantification. Nevertheless, the correlation curve gave no predicting results and low correlation. Therefore GAG distribution analysis was performed solely based on quantification of GAG obtained from DMMB assay.

Measurements of cartilage thickness were attempted using two methods: using an US probe and an optical method. It was not possible to obtain consistent and reliable results using the US probe. In the literature the use of US for cartilage thickness measurements has had conflicting results. Rushfeldt et al. [296] and Modest et al. [108] were successful acquiring cartilage thickness measurements using an US system developed in-house. However, other groups that have used commercial US probes have reported less successful results [1, 297]. Additionally, the optimal US frequency to be used for cartilage thickness measurements is not clear.

The repeatability of the thickness measurements were within ±20%. This repeatability is lower than the thickness measurements performed using a needle probe [157]. Due to conflicting results on the repeatability of cartilage thickness using US reported in the literature [1, 107, 111, 267], it was difficult to compare obtained results with this technique. All techniques for the measurement of cartilage thickness present advantages and disadvantages. One of the limitations of the measurement of thickness through histological sections is being able to obtain plug extraction normal to the surface at every point of the whole tibial plateau. In the present work, care was taken in plug extraction reward normal to the surface, however it was possible that there were errors since normality was accessed optically.

The repeatability of mechanical properties measurements was within ±9% and repeatability of GAG content was within ±10%. This was within the repeatability values reported in the literature using similar techniques [27, 157].

### 5.4.7 Conclusions

- Differences in the flatness or concavity of tibial compartments, as well as their relative inclination were identified on the topographical maps. Small changes in the topography of each specimen was observed. The overall topography was consistent with expected tibial plateau topography.
- In the present work an indenter size of 1.35 mm radius was used, therefore elastic modulus measurements correspond to local elastic behaviour of articular cartilage in an indented region.

- The repeatability of mechanical properties and cartilage thickness measurements were within ±9% and ±20% respectively.
- Heterogeneity of mechanical properties and cartilage thickness distribution was shown.
- Regional analysis of mechanical properties and cartilage thickness values showed an inverse relationship. The thickest areas were the regions uncovered by the menisci, which were the areas located in the external rim and central areas located near the tibial crescent. Furthermore, the highest elastic modulus were found in areas covered by the menisci.
- Regional analysis using MMR division showed significant differences in elastic modulus between regions III and IV of both compartments and between V and II, III and IV in both compartments. Moreover, significant difference in cartilage thickness grouped by MMR regions was found between regions V and II, III and IV, and between I and III and IV in both compartments. This tibial plateau division was the most useful to understand mechanical properties and cartilage thickness distribution. This supports the notion of changes in material properties between areas covered and uncovered by the menisci.
- The elastic modulus values in six tibial plateaux were in the range of 0.5 to 25 MPa in five of the six tibial plateaux. Cartilage thickness values were in the range of approximately 2000 to 5000 $\mu$m.
- Comparison of normalized GAG concentrations by wet and dry weight showed high correlation between measurements.
- Heterogeneity of the GAG concentration across six porcine tibial plateaux was found and its concentration of GAG over the six tibial plateau varied from 1 to 20 $\mu$g/mg.
- Repeatability of GAG concentration measured by DMMB was within ±10% and the spread of measurements within points was around 0.5 $\mu$g/mg in all specimens.
- Regional analysis of mean GAG concentration between the medial and lateral

compartment showed no significant differences. Moreover, assessment of mean GAG concentration over four regions showed lower GAG concentrations in the anterior regions compared to their posterior counterparts. Although, again these differences were not significant.

- Regional analysis of GAG concentrations through MMR regions, showed patterns of high GAG concentrations in areas uncovered by the menisci (near the tibial eminence and in the external rim). Moreover, areas covered by the menisci showed low GAG concentrations. Significant differences between areas covered and uncovered by the menisci were found.

- Whole tibial plateaux submerged in CA4+ reached maximum attenuation by 24h. This suggested that CA4+ had fully penetrated the cartilage by this time point. Nevertheless, correlations between mean attenuation at each test point and corresponding GAG concentration (measured by DMMB), showed low values (0.01 to 0.45) compared to those reported in the literature [141, 154, 290, 292]. Therefore, it was concluded that under the conditions used in this work (i.e. whole specimens, 3D fluoroscope imaging and CA4+), specimens should be left for a longer period of time in the contrast agent. As this could negatively affect the integrity of the tissue, it would be best to use a contrast agent with a higher diffusion rate.

# Chapter 6

# RELATIONSHIP BETWEEN MECHANICAL PROPERTIES, CARTILAGE THICKNESS AND GAG CONCENTRATION

Osteoarthritis is a multifactorial disease with a complex pathway in terms of its initiation and development. In particular, the development of the disease is not well understood. Moreover, the understanding of the interaction between key variables in healthy cartilage is limited. To facilitate a better understanding of the initiation and development of OA, the relationships between mechanical, biological and structural properties such as elastic modulus, GAG concentration and cartilage thickness must be determined in healthy cartilage.

In the previous chapters the mechanical properties, cartilage thickness and GAG concentration were obtained and described for six porcine tibial plateaux and the distribution of each variable was analysed independently. In this chapter the results of investigations into the relationship between these variables are reported. Published studies suggest strong correlations between stiffness and thickness [21, 115, 281, 289, 291]. Correlation between GAG and mechanical properties has also been studied [21, 23, 32,

83, 271, 298], however, the findings in healthy cartilage are less consistent than those for diseased cartilage.

In Chapter 5, mechanical properties, GAG concentration and cartilage thickness were measured at test points defined on each tibial plateau specimen independently. These test points were not identical for each specimen, i.e. they were not located in the same position. Thus, in order to compare the variables distribution over the six tibial plateaux on the same points, it was necessary to obtain a higher resolution distribution of each variable. This would, therefore, allow an extraction of all variables values using the same grid of points mapped on to all tested specimens.

The overall aim of this chapter was to investigate the correlation of the measured variables within the same specimen and to also identify any consistent distribution patterns over the different tibial plateaux. It was envisaged that these relationships may provide insight into understanding the development of OA.

## 6.1 High Resolution Distribution Maps of Measured Variables

High resolution distribution maps of mechanical properties, GAG concentration and cartilage thickness were obtained and they are presented in Figures 6.1, 6.2 and 6.3. High resolution distribution maps for six tibial plateaux are shown in Appendix A, Figures A.12, A.13 and A.14 respectively. These figures were obtained by linear interpolation between measured values of each variable.

The high resolution elastic modulus distribution maps over the six tibial plateaux (Appendix A, Figure A.12) showed similar patterns. The highest elastic moduli were located on the central crescent-shaped area of each compartment, while the periphery and central areas of the whole tibial plateau (near the tibial eminence) had lower values (Figure 6.1). This crescent-shaped area changed in size and location between the tibial plateaux, but in general a central location of high elastic modulus was observed over all specimens.

The high resolution GAG concentration distribution maps over the six tibial plateaux

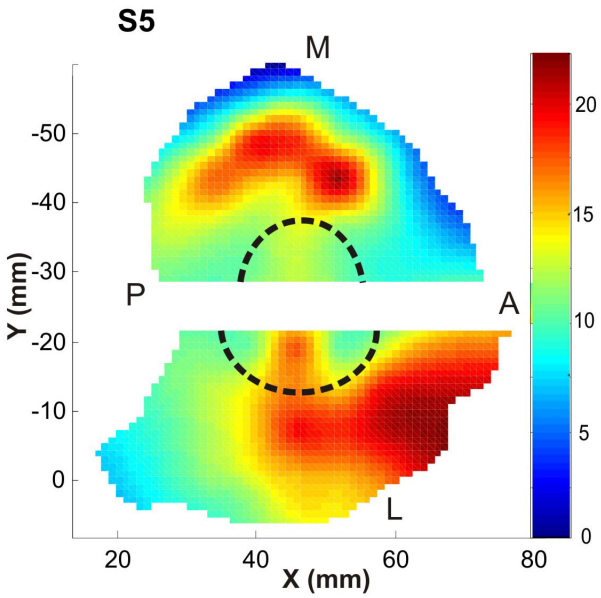


**Figure 6.1:** Continuous elastic modulus distribution maps for specimens S5. Colour bar shows the elastic modulus values in MPa, where red represents the highest elastic modulus values and blue the lowest. The dashed line represents the location of the menisci. The tibial eminence is blank since no points were tested in this area.

(Figure A.13) showed high GAG concentrations in the areas located near the tibial eminence. This pattern was consistent in most specimens. S4 showed a slightly different pattern to the rest of the tibial plateaux. The highest GAG concentration for this specimen (S4) was not centred on the tibial eminence but was slightly more posterior. As observed in previous chapters the high GAG concentration observed near the centre of the tibial eminence is highly correlated with the absence of menisci in this location (Figure 6.2).

The high resolution cartilage thickness distribution maps over the six tibial plateaux (Figure A.14) showed repeatable patterns in terms of distribution. The thinnest cartilage was located in a crescent-shaped area in the middle of both compartments. The surrounding areas, especially towards the periphery, became increasingly thicker (Figure 6.3).

The qualitative comparison of the high resolution maps of the three variables show an apparent inverse relationship between cartilage thickness and elastic modulus located in areas covered by the menisci. High concentrations of GAG were found in areas uncovered by the menisci.

When comparing cartilage parameters using these high resolution maps, it is important

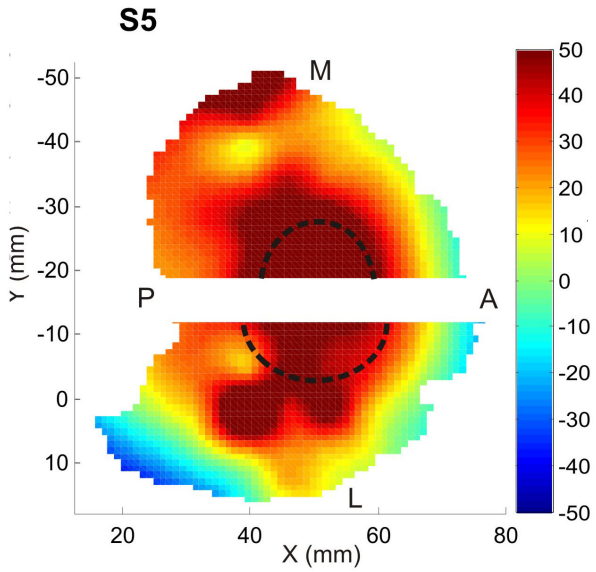


**Figure 6.2:** High resolution GAG concentration distribution maps of specimens S5. Colour bar shows the GAG concentration values in $\mu$m/mg, where red represent the highest GAG concentration values and blue the lowest. The tibial eminence is blank since no points were tested in this area.

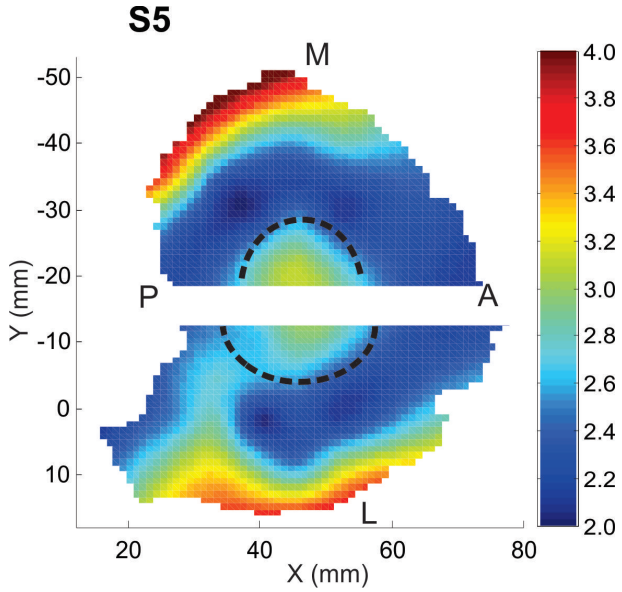


**Figure 6.3:** High resolution cartilage thickness distribution maps of specimens S5. Colour bar shows the cartilage thickness values in millimetres, where red represents the highest cartilage thickness values and blue the lowest. The tibial eminence is blank since no points were tested in this area.

to remember that linear interpolation was carried out between testing points, beyond these measured points (at the periphery) extrapolation took place. Thus, those values located at the rim of the tibial plateau should be regarded as not reliable.

### 6.1.1 Registration of Surfaces

The 3D datasets of the six specimens' topographical maps were superimposed and aligned to the same coordinate system (S1) using affine registration. The transformation matrices obtained from the affine registration (translation, rotation and size adjustment) were applied to all distribution maps of each tibial plateau for the different variables (Figure 6.4).

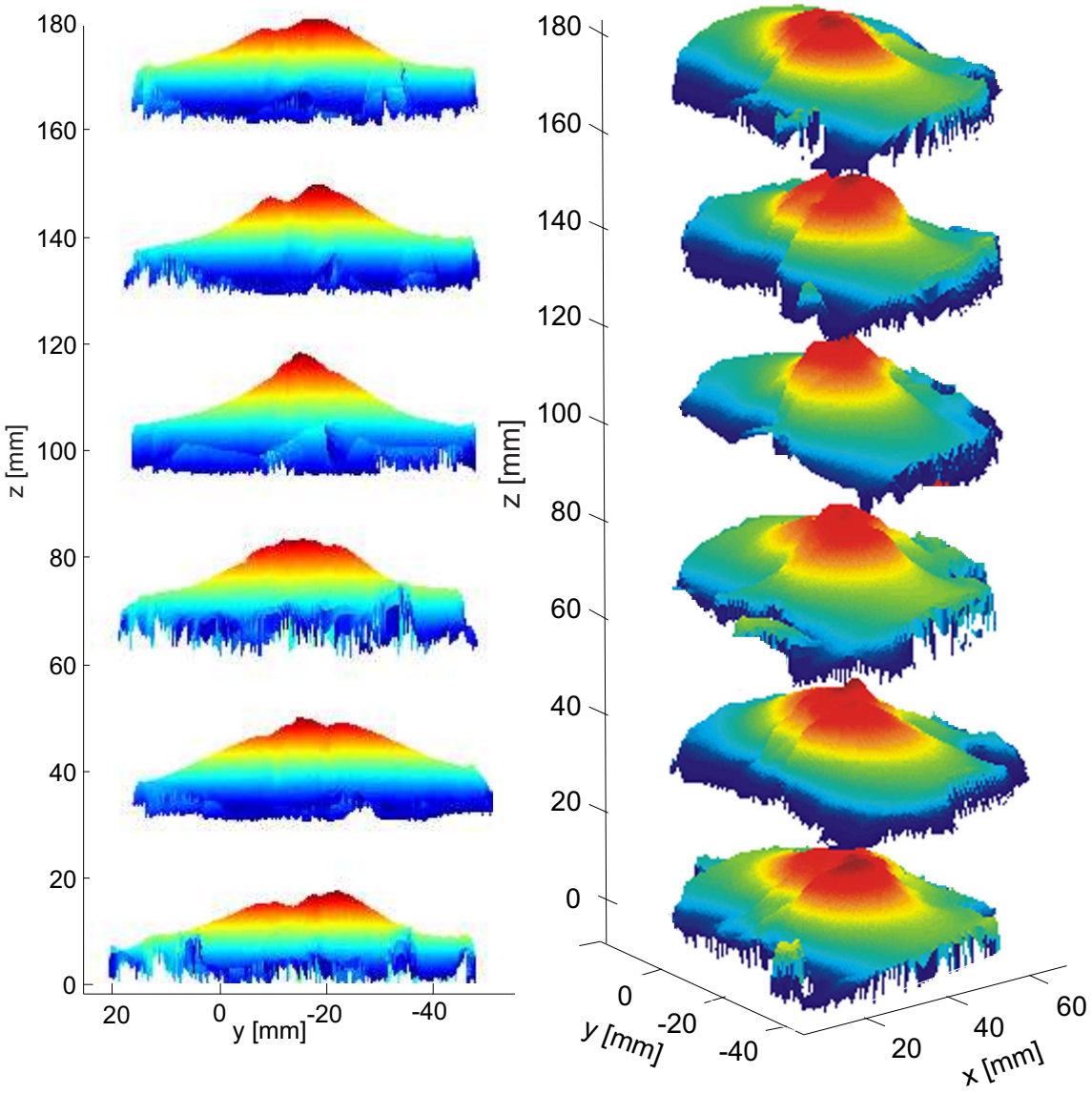


**Figure 6.4:** 3D view and anterior posterior view of registered high resolution surfaces S1, S2, S3, S4, S5, S6 at different heights.

In Figure 6.4 the superimposed registered surfaces are presented at different heights for visual purposes. Two views (3D and coronal) are presented in this figure. It can be observed that the size, rotations and translations were adjusted to obtain good alignment between the tibial plateaux. The main differences between tibial plateaux are observed in the central areas indicated by the dotted line in Figure 6.5. Inside the dotted area several ligament attachments are located, therefore differences observed in these areas are artefacts of ligaments removal rather than an intrinsic characteristic of the tibial plateau. Nevertheless, no measurements were performed in these regions, as no cartilage is found in this area.

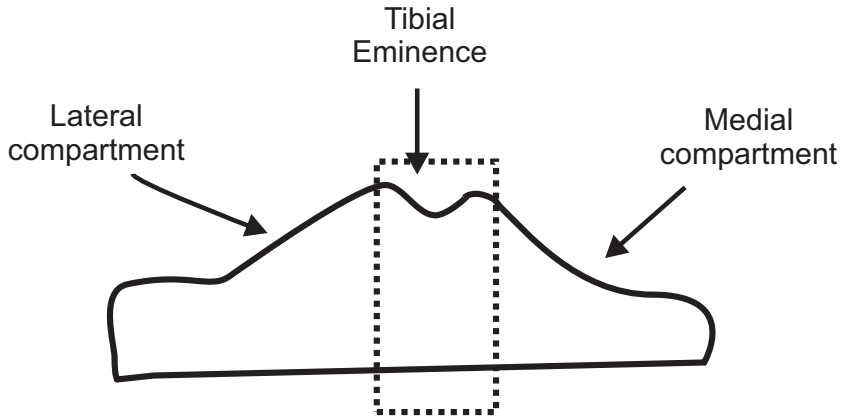


**Figure 6.5:** Sketch of posterior-anterior view of a tibial plateau. In the figure the lateral and medial compartment and tibial eminence are indicated. The dotted rectangle indicates the area where no measurements were taken.

A new grid was defined inside the area where measurements were taken from the six specimens. Elastic moduli, GAG concentration and cartilage thickness values were extracted from AOI (Chapter 4, Section 4.4.3) centred at points defined by the grid in the high resolution maps (extracting point). As all the surfaces were registered, it was possible to have the corresponding grid fitted to all surfaces.

Using the kd-tree algorithm, all points inside the AOI were obtained and averaged. Point-matched and region-matched comparisons were performed.

### 6.1.2 Point-match Analysis Between Tibial Plateaux

Two analyses were performed: (1) the correlation between the mechanical properties, cartilage thickness and GAG concentration for each one of the six tibial plateaux at each "extraction point", (2) the correlation between each variable value at each "extraction

point" over the six tibial plateaux.

#### 6.1.2.1 Point-matched Comparison Between Mechanical Properties, Cartilage Thickness and GAG Concentration at Each Tibial Plateau

Correlation of parameters (stiffness, GAG and thickness) for each tibial plateau was carried out. Results are summarized in Figure 6.6. Correlations were considered high when the correlation coefficient was above 0.4, moderate when the correlation coefficient was between 0.2 to 0.4 and low when the correlation coefficient was between 0 to 0.2.

Figure 6.6 shows the point-matched correlation between elastic modulus (E), GAG concentration (GAG) and cartilage thickness (T).

In Figure 6.6 it can be observed that GAG concentration and elastic modulus showed a consistent inverse correlation except for S3. Cartilage thickness and elastic modulus also showed a consistent inverse correlation in all specimens. Correlation between GAG concentration and cartilage thickness showed a direct correlation in all specimens except S4. Moreover, interaction between the three variables did not show any consistent trend compared to individual relationships. It is possible to observe that correlations found in this figure were low or moderate and in most cases, not statistically significant ($p>0.05$).

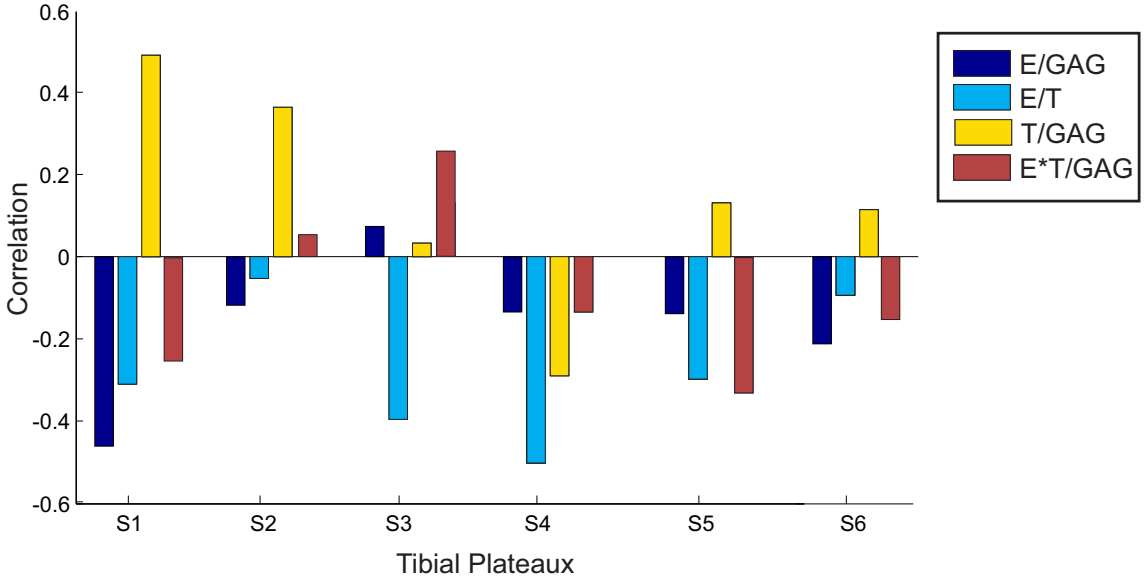


**Figure 6.6:** Point-matched correlation between elastic modulus (E), GAG concentration (GAG) and cartilage thickness (T) over specimens S1, S2, S3, S4, S5 and S6.

The inverse correlation between cartilage thickness and elastic modulus had been

already reported in Chapter 5, however, a new finding regarding the correlation between GAG concentration and elastic modulus had not been observed directly before. The inverse correlation between GAG concentration and elastic modulus suggests that the stiffness of the articular cartilage decreases with increasing GAG concentration.

#### 6.1.2.2 Point-matched Comparison of Each Variable Over the Six Tibial Plateaux

Point-matched correlation of each variable over the six tibial plateaux was performed. Spearman correlations were calculated for all combinations between specimens. Point-matched correlations of elastic modulus, GAG concentration and cartilage thickness are summarized in Tables 6.1, 6.2 and 6.3 respectively.

**Table 6.1:** Point-matched correlation of elastic modulus over six tibial plateau. ** is the correlation significance at the level of 0.01 (2-tailed), * is the correlation significance at the level of 0.05 (2-tailed)

| Specimen | S2 | S3 | S4 | S5 | S6 |
|---|---|---|---|---|---|
| S1 | -0.115 | 0.405 ** | 0.489 ** | 0.397 ** | 0.350 ** |
| S2 | | 0.253 ** | 0.356 ** | 0.396 ** | 0.314 ** |
| S3 | | | 0.592 ** | 0.656 ** | 0.523 ** |
| S4 | | | | 0.744 ** | 0.848 ** |
| S5 | | | | | 0.717 ** |

Moderate to high direct and significant correlations between elastic modulus distribution between all samples were found except S1 with S2 (Table 6.1). This indicates high consistency in elastic modulus distribution between all six tibial plateaux.

**Table 6.2:** Point-matched correlation of GAG over six tibial plateaux. ** is the correlation significance at the level of 0.01 (2-tailed), * indicates statistical significant correlation at the level of 0.05 (2-tailed)

| Specimen | S2 | S3 | S4 | S5 | S6 |
|---|---|---|---|---|---|
| S1 | 0.198 * | -0.005 | 0.112 | 0.183 | 0.301 ** |
| S2 | | 0.283 ** | -0.143 | 0.569 ** | 0.515 ** |
| S3 | | | 0.071 | 0.305 ** | 0.367 ** |
| S4 | | | | -0.317 ** | 0.220 * |
| S5 | | | | | 0.378 ** |

Table 6.2 presents the analysis of GAG concentration distribution over the six tibial

plateaux. It can be observed that there was moderate and high direct correlations in GAG concentration distribution between most specimens. Nevertheless, some exceptions were found such as the relationship between S4 and S5 which showed a significantly inverse correlation. These results suggest relatively high consistency in the GAG distribution between the six tested specimens.

**Table 6.3:** Point-matched correlation of cartilage thickness six tibial plateaux. ** is the correlation significance at the level of 0.01 (2-tailed), * is the correlation significance at the level of 0.05 (2-tailed)

| Specimen | S2 | S3 | S4 | S5 | S6 |
|---|---|---|---|---|---|
| S1 | 0.168 | 0.352 ** | 0.076 | 0.284 ** | -0.002 |
| S2 | | 0.119 | -0.072 | 0.062 | 0.248 ** |
| S3 | | | 0.609 ** | 0.614 ** | -0.065 |
| S4 | | | | 0.669 ** | -0.136 |
| S5 | | | | | 0.125 |

Table 6.3 presents the cartilage thickness distribution correlations over six tibial plateaux in a point-matched analysis. It can be observed that cartilage thickness distribution was less consistent than the distribution of the other two variables previously tested, however 60% of the measurements showed a direct correlation. Only one of the correlations between specimens (S4 with S5) was inverse, and this correlation was not significant. Moreover, five combinations showed a low correlation coefficient (non significant), suggesting that no correlation was found between these specimens.

In general, moderate and high direct correlations were found in variables distribution over the six tibial plateaux. Elastic modulus distribution was the most consistent over the six specimens, followed by GAG concentration distribution. The least consistent distribution was observed in cartilage thickness distribution.

### 6.1.3 Regional Analysis of Parameters Between Tibial Plateaux

Mechanical properties, GAG concentration and cartilage thickness grouped by the MMR's over six tibial plateaux were analysed.

Additionally, the topographical height which was obtained from the Z value of the topographical maps (Chapter4, Section 4.1.3) was also included in the analysis since it has been observed by some authors [289] that the geometry of the knee, influences

the contact area. This could affect the distribution of mechanical properties since the correlation between contact areas and elastic modulus has been reported [289].

Mean comparisons and correlations between the MMR regions over the six tibial plateaux were evaluated. Two types of analysis were performed: (1) comparison of mean values of mechanical properties, GAG concentration, cartilage thickness and topographical height between MMR regions for each specimen. (2) Comparison of each mean variable value at each region (MMR) over all specimens.

As mentioned in the methodology, the chosen grid for the analysis of the "extraction points" only covered areas where measurements had been obtained initially for all specimens (by superimposing test points), therefore new "extraction points" do not include the most external parts of the rim referred to as regions V in the MMR.

#### 6.1.3.1 Region-matched Comparison of Material Properties Distribution Across Six Tibial Plateaux Clustered by MMR

Region-matched comparison of topographical height, elastic modulus, GAG concentration and cartilage thickness distribution across six tibial plateaux was carried out by grouping extraction points into the various MMR's.

Topographical height distribution using MMR is shown (Figure 6.7). A high correlation of topographical height on MMR between specimens was obtained ($p > 0.79$ for all cross-correlations between specimens) (Table 6.4). This result suggests similar topographical distribution in the six tibial plateaux.

**Table 6.4:** Region-matched correlation of topographical height six tibial plateaux. ** is the correlation significance at the level of 0.01 (2-tailed), * is the correlation significance at the level of 0.05 (2-tailed)

| Specimen | S2 | | S3 | | S4 | | S5 | | S6 | |
|---|---|---|---|---|---|---|---|---|---|---|
| S1 | 0.851 | ** | 0.875 | ** | 0.737 | ** | 0.951 | ** | 0.945 | ** |
| S2 | | | 0.816 | ** | 0.915 | ** | 0.854 | ** | 0.937 | ** |
| S3 | | | | | 0.865 | ** | 0.904 | ** | 0.867 | ** |
| S4 | | | | | | | 0.791 | ** | 0.845 | ** |
| S5 | | | | | | | | | 0.913 | ** |

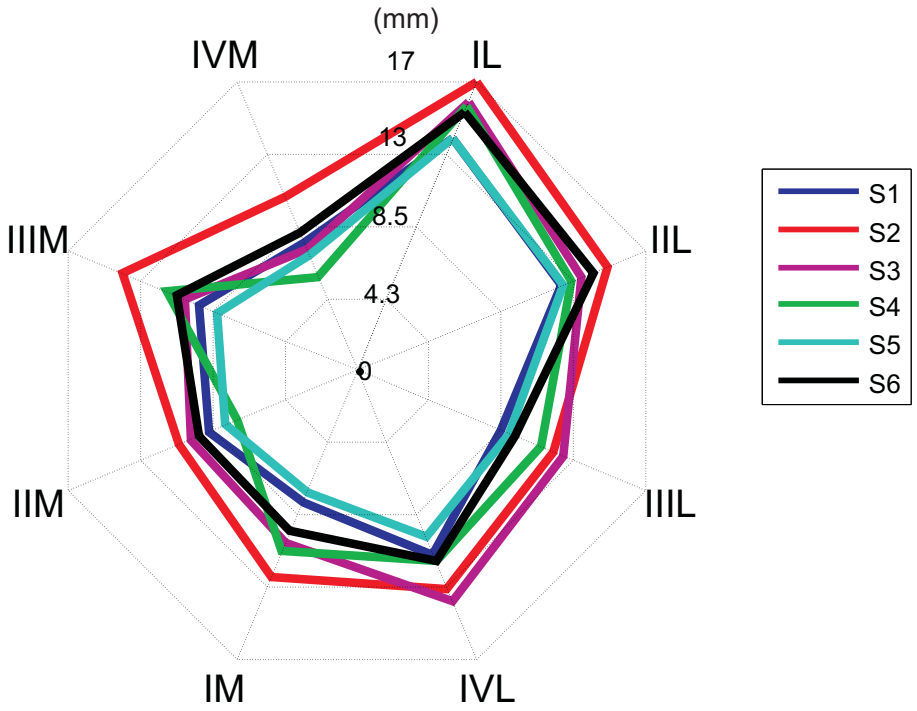


**Figure 6.7:** Region-based comparison of topographical height distribution grouped by MMR

- ***Elastic Modulus:***

  The elastic modulus distribution over the MMR on the six tibial plateaux is shown in Figure 6.8. In this figure it is possible to observe a similar trend in the lateral and medial compartments, where regions IIIM and IIIL show the highest values of elastic modulus in most specimens. Additionally, all specimens showed a similar patterns (S2 was the only exception). These similarities between trends in elastic modulus distribution can also be observed in Table 6.5 where all correlation coefficients were greater than 0.3.

**Table 6.5:** Region-matched correlation of elastic modulus over the six tibial plateaux. ** indicates statistically significant correlations at the level of 0.01 (2-tailed), * is correlation significance at the level of 0.05 (2-tailed)

| Specimen | Elastic Modulus Correlations | | | | | | | | | |
|---|---|---|---|---|---|---|---|---|---|---|
| | S2 | S3 | | S4 | | S5 | | S6 | | |
| S1 | -0.115 | 0.405 | ** | 0.489 | ** | 0.397 | ** | 0.350 | ** | |
| S2 | | 0.253 | ** | 0.356 | ** | 0.396 | ** | 0.314 | ** | |
| S3 | | | | 0.592 | ** | 0.656 | ** | 0.523 | ** | |
| S4 | | | | | | 0.744 | ** | 0.848 | ** | |
| S5 | | | | | | | | 0.717 | ** | |

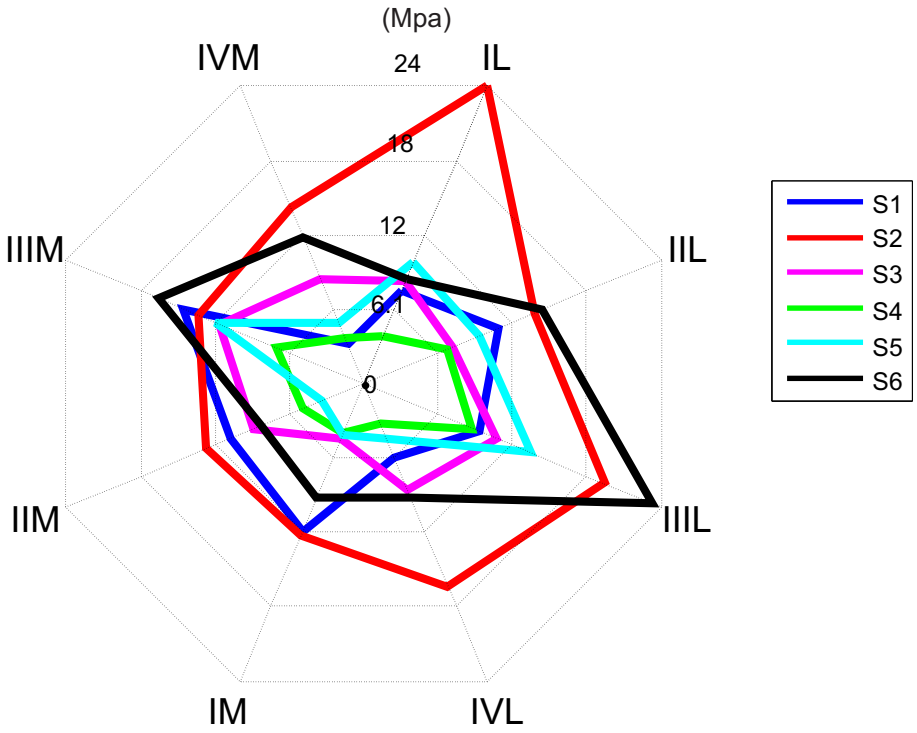


**Figure 6.8:** Region-based comparison of elastic modulus distribution over the six tibial plateaux grouped by MMR

- ***GAG:***

  Figure 6.9 presents the GAG concentration distribution over six tibial plateaux grouped by MMR. In this figure it can be observed that in the lateral compartment trends are highly similar between specimens. In the medial side there is slightly more variability, particularly in regions IIIM and IV medial.

  Table 6.6 summarizes the correlations between GAG concentration means grouped by MMR over the six specimens. In general correlations are consistently direct and significant, however S4 had a different distribution than the rest of the specimens.

**Table 6.6:** Region-matched correlation of GAG concentration six tibial plateaux. ** indicates statistical significant correlation at the level of 0.01 (2-tailed), * is correlation significance at the level of 0.05 (2-tailed)

| Specimen | GAG Concentration Correlations | | | | | | | | | |
|---|---|---|---|---|---|---|---|---|---|---|
| | S2 | | S3 | | S4 | S5 | | S6 | | |
| S1 | 0.198 | * | -0.005 | | 0.112 | 0.183 | | 0.301 | ** | |
| S2 | | | 0.283 | ** | -0.143 | 0.569 | ** | 0.515 | ** | |
| S3 | | | | | 0.071 | 0.305 | ** | 0.367 | ** | |
| S4 | | | | | | -0.317 | ** | 0.220 | * | |
| S5 | | | | | | | | 0.378 | ** | |

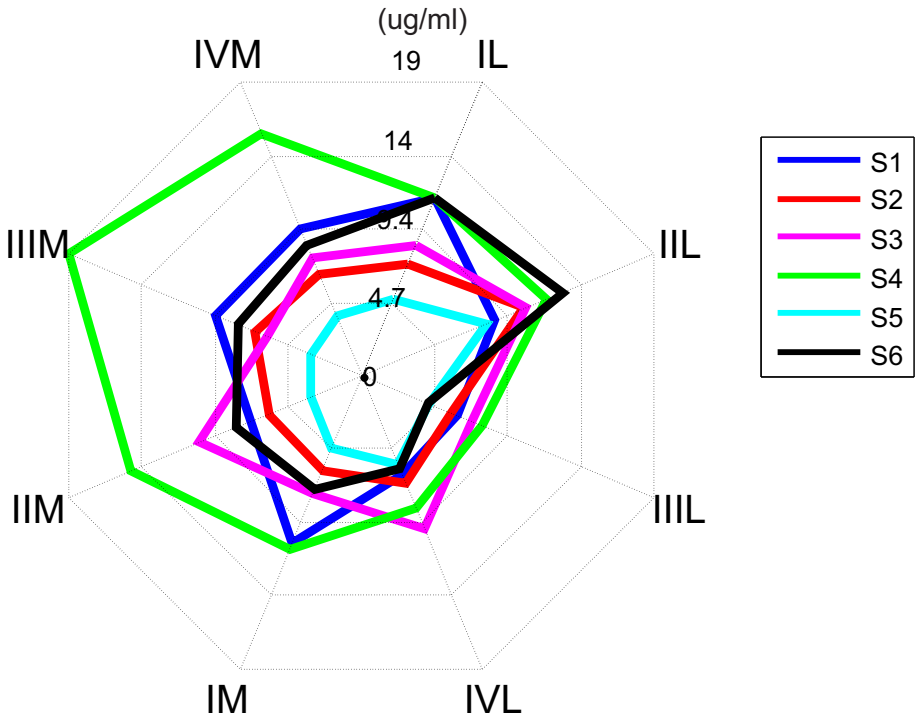


**Figure 6.9:** Region-based comparison of GAG concentration distribution over six tibial plateaux grouped by MMR

- ***Thickness:***

  Cartilage thickness of the six specimens grouped by MMR showed high variability between specimens (Figure 6.10). Additionally, there was no obvious mirror behaviour, regarding cartilage thickness trends, between the medial and lateral compartment. There were two different trends between specimens, S1, S2 and S3 were relatively similar, whereas S5 and S6 had a different pattern and were similar to each other. This variability among specimens was also reflected in the results of the statistical tests where significant direct correlations are only found in 50% of the cross-correlations (Table 6.7).

**Table 6.7:** Region-matched correlation of cartilage thickness six tibial plateaux. ** indicates statistical significant correlation at the level of 0.01 (2-tailed), * is correlation significance at the level of 0.05 (2-tailed)

| Specimen | Cartilage Thickness Correlations | | | | | | | | | | | |
|---|---|---|---|---|---|---|---|---|---|---|---|---|
| | S2 | | S3 | | | S4 | | | S5 | | | S6 | |
| S1 | 0.168 | | 0.352 | ** | | 0.076 | | | 0.284 | ** | | -0.002 | |
| S2 | | | 0.119 | | | -0.072 | | | 0.062 | | | 0.248 | ** |
| S3 | | | | | | 0.609 | ** | | 0.614 | ** | | -0.065 | |
| S4 | | | | | | | | | 0.669 | ** | | -0.136 | |
| S5 | | | | | | | | | | | | 0.125 | |

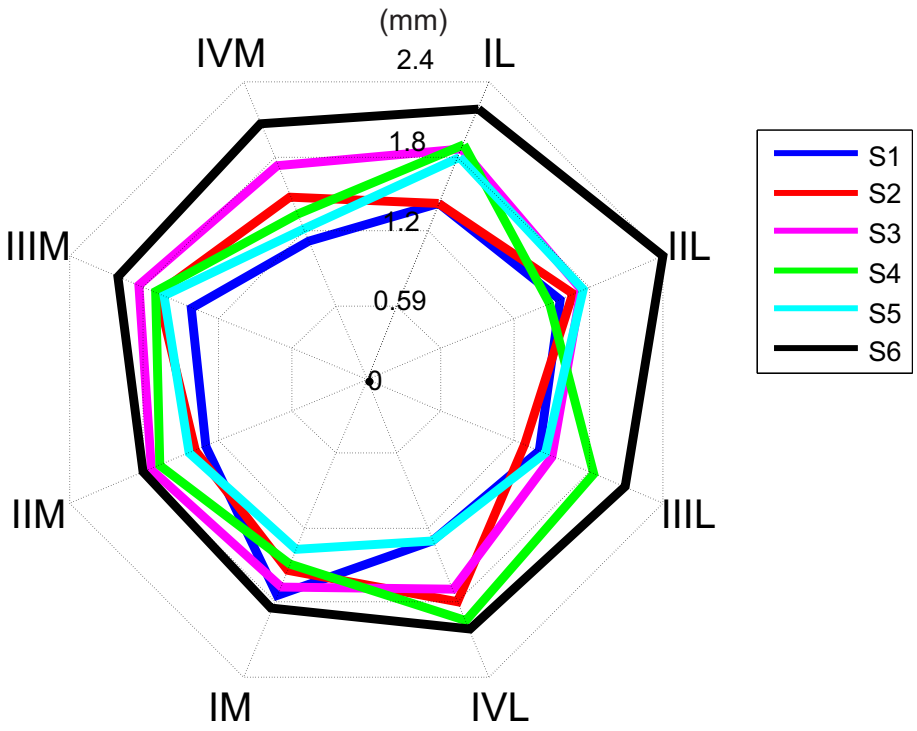


**Figure 6.10:** Region-based comparison of cartilage thickness distribution over six tibial plateaux grouped by MMR

Overall, correlation of variable distribution over the six tibial plateau grouped by MMR, showed consistent distribution in elastic modulus, GAG concentration and topographical height. The topographical height was highly consistent between specimens, followed by the elastic modulus and then the GAG concentrations. Cartilage thickness showed the most variability between specimens. Although similar trends were found between compartments, the distribution of the three measured variables is not mirror-like since magnitudes change between the medial and lateral side.

#### 6.1.3.2 Region-matched Comparison Between Variables Over Each Tibial Plateaux Grouped by MMR

Region-matched comparison of mechanical properties, GAG concentration, cartilage thickness and topographical height distribution over MMR region on each tibial plateaux was carried out. Spearman correlations between variables grouped by the MMR on each tibial plateau were calculated.

The correlations between the four variables for each tibial plateau was summarized in Figure 6.11. A consistent inverse correlation between elastic modulus (E) and GAG concentrations (GAG) was observed. Consistent direct correlation between topograph-

ical height (Topo) and thickness was also observed. Topographical height was also directly correlated with GAG concentrations in all specimens (except in S4). Moreover, GAG concentrations were directly correlated to cartilage thickness (except in S4). The elastic modulus and the cartilage thickness were inversely correlated in four of the six specimens, but in three of the specimens correlations were very small (correlation coefficient $< 0.1$). Similarly the elastic modulus was inversely correlated to the topographical height in four of the six specimens.

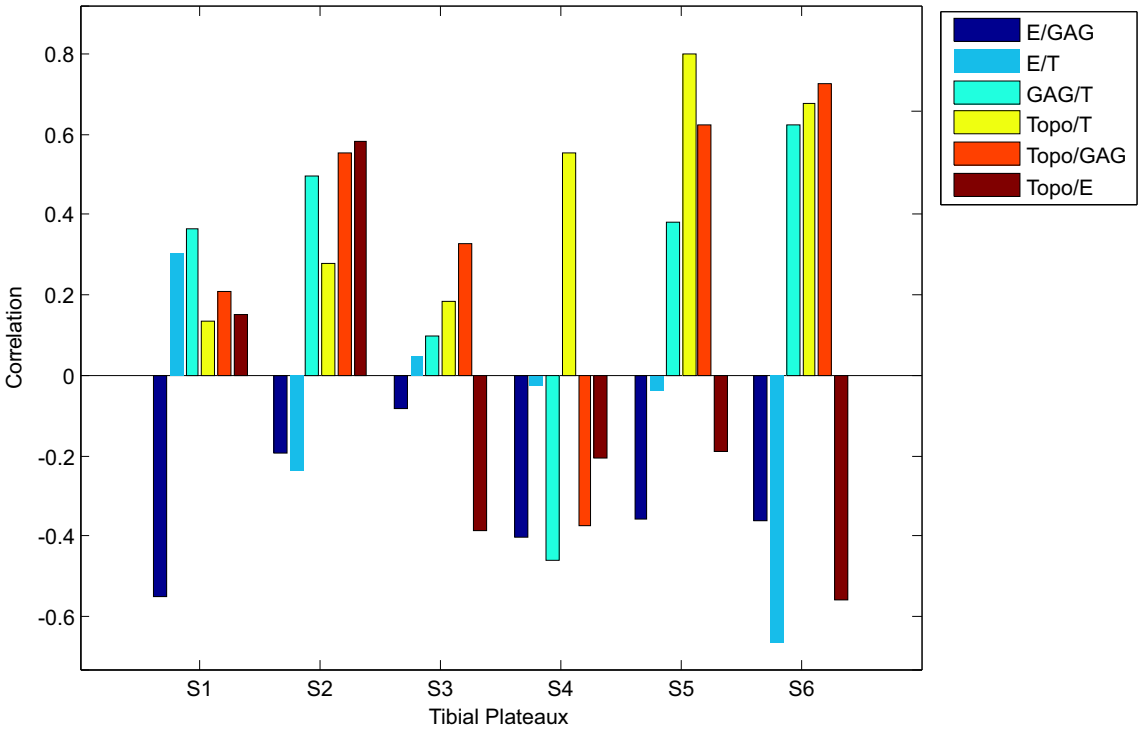


**Figure 6.11:** Region-matched correlation between elastic modulus (E), GAG concentration (GAG), cartilage thickness (T) and topographical height (Topo) over the six tibial plateaux grouped by MMR

Using the MMR regions, it was possible to observe variable trends in more detail and, therefore, correlations found previously were further examined. In Figure 6.12 the mean value of normalized elastic modulus, GAG concentration, cartilage thickness and topographical height on each MMR region are presented for specimen S5. In Appendix A, Figure A.16 the normalized values of these four parameters for each MMR region are shown for all six tibial plateaux. In these figures an inverse correlation between elastic modulus and topographical height was consistently found for the majority of

the regions (with the exception of region IVM for all specimens and regions IM in S1 and IL and IIL in S2).

The correlation between the elastic modulus and cartilage thickness was inverse for all specimens (except for S2). Variations in elastic modulus were more pronounced between regions compared to the variation of cartilage thickness.

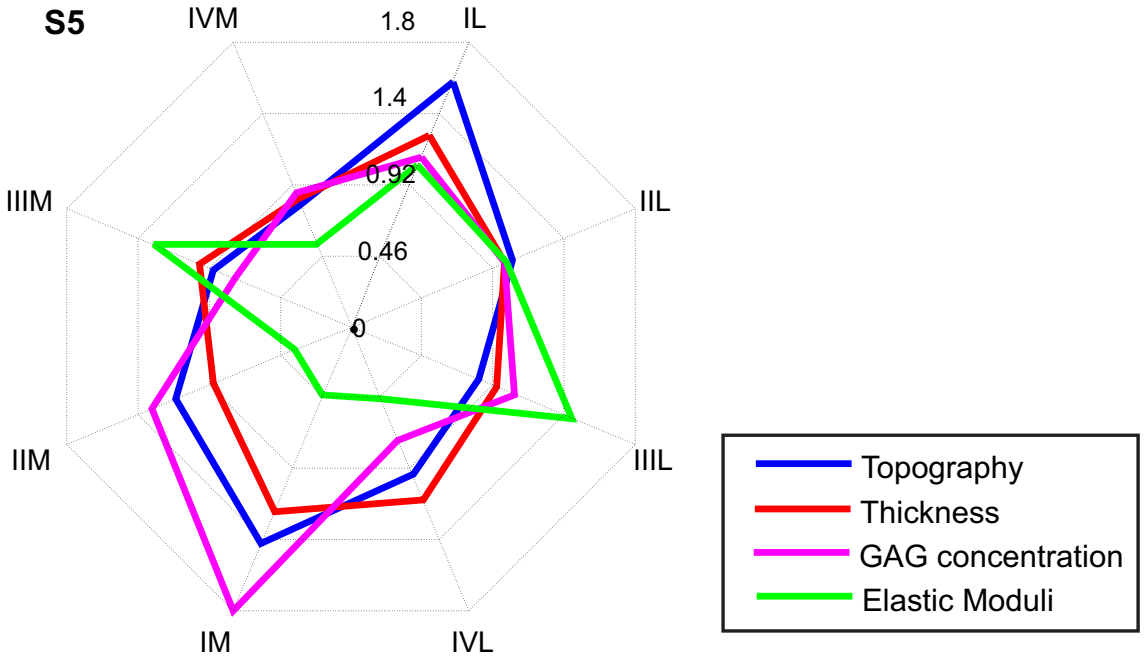


**Figure 6.12:** Means of mechanical properties (Elastic modulus), GAG concentration, cartilage thickness and topographical height on each MMR over tibial plateau S5.

In this section it was found that GAG concentrations were directly correlated to the cartilage thickness and topographical height and inversely correlated to the elastic modulus. Additionally, inverse correlation between elastic modulus and topographical height in most regions was observed. Finally, inverse correlations between elastic modulus and cartilage thickness were found.

## 6.2 Discussion

In this chapter the correlations between four variables: the elastic modulus, GAG concentration, cartilage thickness and topographical height were analysed at the same points (point-matched) and regions (region-matched) over the six tibial plateaux. This analysis was performed by comparison of (a) each variable for each tibial plateaux and (b) all variables over all six tibial plateaux.

An inverse correlation between GAG concentration and the elastic modulus, and a direct correlation between GAG concentration and cartilage thickness were found. Several authors have reported [17, 26, 47, 59, 99, 286] that areas subjected to high stress are thought to have the highest amount of GAG. Moreover, Kempson *et al.* found that degraded cartilage was softer and had lower GAG content than normal healthy cartilage [27]. However, in healthy cartilage these correlations are less obvious [32]. Very few authors have studied the relationship between GAG concentration and mechanical properties in healthy cartilage. Samosky et al., [23] studied the correlation between GAG concentrations and stiffness using dGEMRIC in combination with mechanical tests. These authors concluded that correlation between the two variables was found when only the top 700 $\mu$m of GAG concentration were taken and that when GAG concentration was taken as an average over the whole thickness this correlation disappeared. Kempson *et al.* found a direct correlation between GAG content and creep modulus [47]. On the contrary, Kiviranta *et al.* [235] found a inverse correlation between GAG concentration and mechanical properties of the articular cartilage.

In the present work, GAG concentrations were measured using biochemical analysis (DMMB), which gives an average of the GAG content of the whole plug. Using this method significant differences in GAG concentration distribution over healthy cartilage articular surfaces was observed. A direct correlation between GAG concentration and cartilage thickness was found. Additionally, an inverse correlation between GAG concentration and elastic modulus was observed.

Furthermore, in the present work inverse correlations between cartilage thickness and mechanical properties have been observed. These findings are in agreement with those reported in the literature [206, 291]. Significant differences were observed in all measured variables between areas covered and uncovered by the menisci. Therefore, the MMR regions appeared to be an appropriate way to analyse this type of data. Differences between regions covered and uncovered by the meniscus have been previously observed by several authors [28, 89]. Appleyard *et al.* found that the cartilage located under the meniscus was 2 to 5 times stiffer and thinner than that in uncovered areas in ovine tibial plateaux [28].

In Chapter 5 the menisci location was identified on each knee, therefore the MMR regions were knee-specific. In this chapter, a new grid consistently mapped across specimens was used for the variable comparison, therefore location of the menisci in MMR regions was the same for all tibial plateaux. In this work it was observed that although small variations were found between size and location of the menisci on each tibial plateau, general regional analysis performed in this chapter was consistent with the trends found in the knee-specific analyses. This suggests that there are patterns in the variable distribution which are consistent across the specimens. The relationships found on the point-matched analyses were increased in the region-matched analyses of parameters distribution over the six tibial plateaux presented in this chapter.

The relationship found overall between the distribution of the measured variables with the menisci location, has also been related to contact patterns. Contact patterns during stance in human tibial plateaux [19] and in quadrupeds [281] seem to be similar. The high resolution maps obtained for mechanical properties, GAG concentration and cartilage thickness, show a correlation with contact maps reported in the literature [3, 19, 62, 281, 299]. Additionally, correlation between topographical maps, mechanical properties and GAG was observed, which supports Koo and Andriacchi's observations [289]. They showed that in weight bearing areas contact plays an important role in the development of articular cartilage. It is generally accepted that biomechanics of the knee is an important factor in the development of OA. However, there must be conditioning of the articular cartilage to loads, since major differences have not been detected in cartilage parameters distribution between athletes and sedentary people [231]. Therefore, it seems that drastic changes in loading patterns, for example due to injury, would be a major risk for the development of OA.

In this study porcine tibial plateaux were used due to the similarities in basic structure and geometry with the human tibial plateaux [287]. One of the main differences between porcine tibial plateaux and human tibial plateaux is that the area covered by the porcine menisci is larger than for human knees, as a result it carries 75% of the load while human menisci only bears 45% of the load [287].

Fukubayashi and Kurosawa studied areas of the tibial plateau which were subjected

to high pressures during contact at stance phase with and without menisci [3]. It was observed that peak pressure locations in knees without menisci coincided with the unicompartmental knee OA (UKOA) lesion location (Figure 6.13).

In the high resolution maps of mechanical properties distribution obtained in the current work, it is possible to observe that under the area covered by the menisci, there are regions of high elastic modulus surrounded by regions of low elastic modulus. The interface between these two regions shows a high gradient (Figure A.17). This figure was obtained from the 2nd derivative of the elastic moduli in all specimens. The location of the highest variations in elastic modulus are shown in red and blue.

The dotted lines in Figure A.17 indicate areas of high contact pressures and common unicompartamental OA lesion locations according to the literature [3, 25] and are indicated in Figure 6.13.A and Figure 6.13.B. It is also possible to observe (by comparing Figure 6.13 and Figures 6.14 which shows the second derivative of the elastic moduli for specimen S5 and Figure A.17) located in Appendix A, which shows the second derivative of the elastic moduli for all six tibial plateaux. It can be observed in these figures that the maximum changes in elastic modulus occur in the regions of high contact pressure and where unicompartamental OA occurs. This suggests that the combination of localized high gradients in elastic modulus with high contact pressures may result in the initiation of damage of the articular cartilage at these locations which could result in the development of OA.

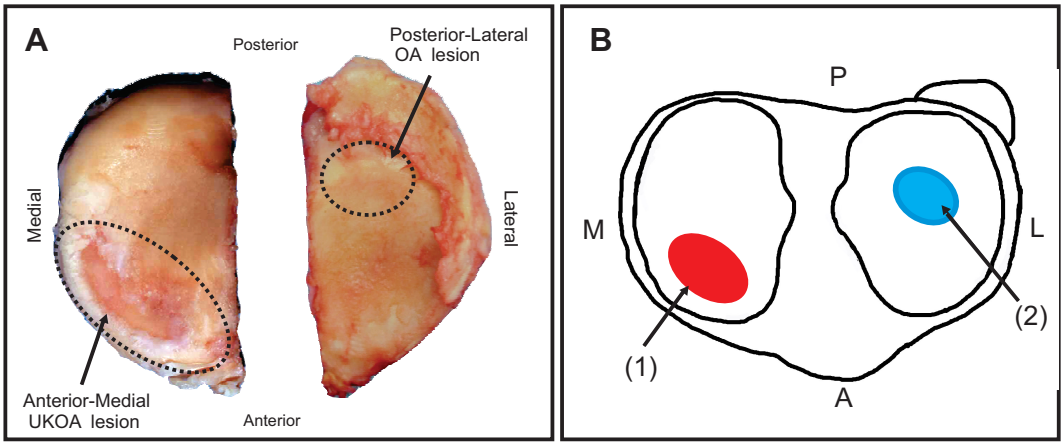


**Figure 6.13:** A. Common location of Unicompartmental Knee OA (UKOA) lesions in humans. In the lateral compartment the UKOA is located in the posterior lateral region while in the medial side is located anterior medially. B. High contact areas subjected to high pressures according to Fukubayashi and Kurosawa [3].

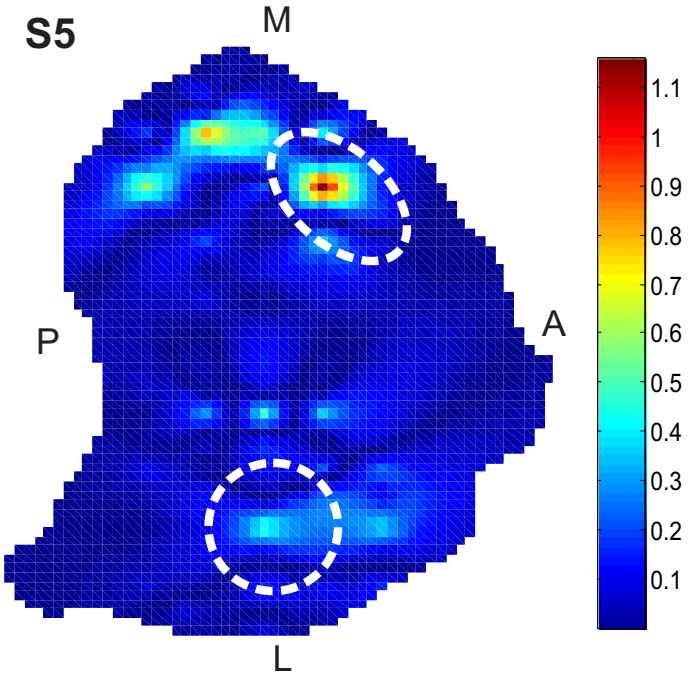


**Figure 6.14:** 2nd derivative of the high resolution maps of the elastic modulus distribution of tibial plateau S5

Although in this study, a low number of specimens were tested (n = 6), results were consistent over tested specimens. Nevertheless, this is a small number and extrapolating these results to a whole population must be carried out with caution.

## 6.3 Conclusions

- Point-matched and region-matched comparison of variable distributions showed consistent significant and direct correlations over six tibial plateaux, suggesting consistent distribution of variables in tested specimens.
- Point-matched comparison of thickness distribution between specimens showed more variability in cross-correlation between specimens than other variables. Nevertheless, 60% of cross-correlations between specimens were significantly and positively correlated.
- Region-matched comparison performed over the MMR's showed: (a) Consistent inverse correlation between GAG concentration and elastic modulus. (b) Inverse correlation between cartilage thickness and mechanical properties. (c) Direct correlation between GAG and thickness. (d) Direct correlation between cartilage thickness and topographical height and between GAG concentration and topo-

graphy. On the other hand, an inverse correlation between elastic modulus and topographical height was found.

- Through usage of high resolution maps and regional matched analyses, high correlation between the variables distribution and the location of the meniscus was observed. High GAG concentrations were found in regions uncovered by the menisci, while areas covered by the menisci had the highest elastic modulus and lowest thickness.

- High resolution maps provided a simple and reliable way to observe variables distribution over the tibial plateaux. Moreover, the comparison of these maps with contact pattern maps found in the literature [3, 19, 281] could provide insight into understanding the initiation of OA lesions in the knee.

# Chapter 7

# CONCLUSIONS

Although OA has been a topic of research for decades, how the disease progresses through its different stages is not well understood. In particular, many questions remain regarding its development and progression at its initial stages. While the majority of previous work has attempted to understand OA by studying diseased cartilage, there are fewer studies which have focussed on the properties of pre-disease (healthy) cartilage. It is, however, well accepted that OA is a multi-factorial disease, resulting from the interaction between cartilage properties and structure, external stimulus and genetic factors, among others. Studies that focus on the distribution of material properties and other variables of healthy cartilage over articular surfaces, such as the tibial plateau, should give insight into their interactions and, therefore, produce methods for detecting when these relationships change as the tissue transitions to a diseased state.

The relationship and interaction between the mechanical, biological and geometrical properties of articular cartilage on tibial plateaux has been investigated before, albeit in isolated points over their surfaces. Maps of the distribution and correlation of these properties over tibial plateaux with high resolution have never been previously produced. It was attempted to address these literature gaps in this thesis. The goal was to measure mechanical properties, GAG concentration and cartilage thickness distribution over six whole porcine tibial plateaux. It was hoped that by determining how these variables interact with one another it would be possible to gain insight into the initiation of knee OA.

To do this, high resolution maps of the distribution of GAG concentration, cartilage thickness and elastic modulus were obtained on six healthy porcine tibial plateaux, by a combination of experimental measurements and linear interpolation between test points. The spatial correlation of the measured variables was carried out. This work presents a new approach whereby the distribution of articular cartilage variables over the tibial plateau are visualized and correlated through the use of high resolution maps.

The following questions were addressed:

- Is the distribution of the elastic modulus, GAG concentration and cartilage thickness over healthy tibial plateaux heterogeneous?
- Is there a correlation between the distribution of these variables in terms of their location on the tibial plateau?
- Does the interaction between these variables provide insight into the location of lesions associated with unicompartmental knee OA?

## 7.1 Summary Findings

In this section the main findings are summarized relative to the above research questions.

***Potential of the WASIM:***

The WASIM is a novel and unique testing device with 5 DOF and with the capacity of interchanging and attaching several probes. This allows the study of articular cartilage and other tissues in a non-damaging way. In the work presented in this document, the WASIM was used to obtain topographical maps of whole undamaged tibial plateaux. These maps were also used to obtain the rotation angles necessary to align an AOI perpendicular to probes such as the indenter and ultrasound. This was particularly advantageous for the assessment of elastic modulus since load is applied in the direction that the tissue experiences load *in vivo*. Additionally, it is advantages for the collection of data in both indentation and US measurements. Mechanical tests were carried out using an indenter, which meant that the behaviour of the articular cartilage could be obtained in a realistic setting (as a whole specimen with subchondral bone and tibial

shaft). The cartilage thickness was attempted to be measured by using an US.

Additionally, a custom made routine was developed to allow the collection of the data necessary to acquire these three parameters in an automated manner. This routine allows the calculation of rotation angles necessary for perpendicular alignment of the cartilage surface with the probe. Additionally, it achieved the rotation and translation of the specimen in order to obtain this alignment, the downward movement of the probe until contact is reached and the collection of the data while test is carried out. This routines are highly adaptable to other probes which might be incorporated into the WASIM.

***Mechanical Properties and Thickness Distribution in Healthy Cartilage:*** Heterogeneity of the elastic modulus values over the tibial plateaux was demonstrated. Moreover, a consistent heterogeneous distribution was found between the six tibial plateaux. Crescent-shaped areas located in the central part of both the medial and lateral compartment showed high elastic modulus, compared to surrounding areas. The distribution of the elastic modulus seems to be associated with the location of the menisci; high elastic modulus values were found in areas covered by the menisci.

Similarly, heterogeneous distribution of cartilage thickness of the tibial plateaux was demonstrated. Distribution maps and regional analysis showed that cartilage was thicker in regions in the centre of the tibial plateau (near the tibial eminence). Once again this distribution was highly correlated with the position of the menisci; areas uncovered by the menisci were thicker than areas covered by the menisci. The differences in cartilage thickness between these regions were significant.

Furthermore, both elastic modulus and cartilage thickness distribution, in areas covered by the menisci, was not homogeneous. Within these regions, central areas were thinner with higher elastic modulus than the periphery.

Distribution of elastic modulus and cartilage thickness on the six tibial plateaux showed very similar patterns, suggesting high correlation between these variables.

***GAG Concentration Distribution in Healthy Cartilage:***

The qCTA methods were found not to be suitable for the quantification of GAG concentration in this project, since this method showed that the time ($\tau$) obtained via the optimal time curve required for full penetration and diffusion of the contrast agent into the articular cartilage was not sufficient when using whole tibial plateaux.

Nevertheless, the analysis of GAG concentration obtained through the use of the DMMB assay showed high consistency. Statistical analysis of point-matched and region-matched GAG concentrations over the six tibial plateaux demonstrated that the patterns for GAG concentration distribution were repeatable between specimens.

Heterogeneous distribution of GAG concentration over the tibial plateau was found. Distribution maps and regional analysis showed regions of high GAG concentration in the centre of the tibial plateau, near the tibial eminence, which corresponded with areas not covered by the menisci. Differences between areas covered and uncovered by the menisci were statistically significant.

***Correlation Between Elastic Modulus, GAG Concentration and Cartilage Thickness:***

High resolution distribution maps of elastic modulus, GAG concentration and cartilage thickness on healthy articular cartilage were obtained. These contour maps were extremely useful for visualization of the variable distribution. To the authors knowledge this is the first time that maps such as these have been obtained from so many measurements in healthy cartilage.

There was good consistency between tibial plateaux in point-matched and region-matched analyses of the three measured variables in healthy cartilage, nevertheless correlations between parameters were higher when parameters were compared within regions (region-analysis).

An inverse relationship between cartilage thickness and elastic modulus and between GAG concentration and elastic modulus was found, i.e. as cartilage thickness and GAG concentration increased elastic modulus decreased. Consequently, as expected, a direct relationship between GAG concentration and cartilage thickness was found. Further-

more, topographical height was also tested and it was found to be directly correlated with cartilage thickness and with GAG concentration and inversely correlated to the elastic modulus.

The heterogeneous distribution of mechanical properties and other variables over the tibial plateau could play a role in the behaviour of cartilage in response to load during activity. A study of the gradients of change in elastic modulus over the tibial plateau had not been carried out previously, to the knowledge of the author. The maximum gradient changes occurred at specific locations on the tibial plateaux that coincide with areas of high contact pressure reported by Fukubayashi and Kurosawa [3]. Areas subjected to high contact pressures in the absence of the meniscus were found to be in similar position to the common locations of unicompartmental knee OA lesions. These regions were also highly associated with areas where the elastic modulus gradient was steep (determined by calculating the 2nd derivative). These results suggest that when areas with high gradients in elastic moduli are subjected to high stresses they might be vulnerable to high loads, which could cause injury or lead to an OA lesion.

The high resolution maps were developed by linearly interpolating between measured values. Thus it is possible that small variations may exist between values of each point.

## 7.2 Implications of Findings

Consistent distribution patterns were found between the tested specimens for all measured variables and it was shown that the variable distribution is significantly different in the various regions of the tibial plateau, which highly relate to the position of the menisci. Contrary to what has commonly been suggested in the literature, areas covered by the menisci are not homogeneous in variable distribution. This suggests that the area covered by the menisci should be divided into smaller regions, such as MMR.

The heterogeneous distribution of the measured variables over the six tibial plateau, compared to reported homogeneity in neo-natal cartilage, supports the thesis that cartilage adapts to the loading patterns it is subjected to, and therefore a shift or dramatic change in loading patterns could initiate the process of degradation that leads

to OA. Nevertheless, sometimes OA develops in the absence of injury and abnormal load which could indicate a genetic predisposition, and this question remain to be answered.

Results obtained from penetration and diffusion of CA4+ into the articular cartilage, provides new information related to the use of this contrast agent for the measurement of GAG which was not in the literature up until now. Additionally, it suggests that when using whole tibial plateaux, a contrast agent with a higher diffusion rate is required. On the other hand, heterogeneity of GAG concentration detected through DMMB assay, validates the DMMB assay as a method for GAG quantification in healthy tibial plateaux, which up to now has not been clear in the literature.

The inverse relationship between GAG concentration and elastic modulus distribution in healthy cartilage, suggests that the interaction between articular cartilage variables changes once the deterioration process is initiated (since degraded cartilage has been characterised as being softer and containing less GAG in the literature). The change in the internal interactions between articular cartilage variables once degradation begins, is also supported by the fact that load stimulus improves cartilage structure (e.g. GAG content and cartilage thickness) in healthy cartilage, however, in diseased cartilage load accelerates the degradation of the tissue.

Heterogeneity in elastic modulus and cartilage thickness distribution suggests that different areas of the articular cartilage would respond differently to loading. Additionally, significant differences between regions and the surrounding areas creates transition zones where the gradient is highly steep. Since the position of the meniscus is not static, during movement these zones could be subjected to load in absence of the meniscus which could also make them more vulnerable to damage.

This work proposes a methodology to study the distribution of mechanical properties and biological components in tibial plateaux by using a novel testing machine. Further studies should be carried out in human specimens in order understand patterns and study the correlation of these high gradient areas to common location of knee OA. It is possible that by understanding the interactions between the distribution patterns in

healthy specimens, insight will be gained into the progression of the disease.

The potential of the WASIM for future research of the tibial plateau is tremendous, since it allows the measurement of several parameters in the same point over whole undamaged specimens. There are very few studies with these characteristics that are performed using the same device and at low cost. An example of a possible probe that would allow to acquire other parameters is a Raman spectrometer.

## 7.3 Limitations

- Indentation measurements were performed at a rate of 10 percent per second which translates to functional loading at 1 Hz. This is considered to be within the frequency of physiological load for slow walking [103]. However, indentation is ultimately a static measurement and cyclic loading would probably provide different results, which may be more relevant in the study of the cartilage material properties under physiologically conditions. Moreover, elastic behaviour was assumed; it is known that cartilage has a more complex behaviour. Additionally, cartilage thickness was measured after mechanical tests were performed. Therefore variation in percentage of displacement with respect to cartilage thickness at each point was unavoidable.

- Cartilage thickness was measured from plugs extracted manually at each test point. The normal axis for extraction of plugs was assessed optically. Although efforts were made to extract the cartilage plugs perpendicular to the surface, it is possible that all points on the surface were not the same distance from the bone due to the undulating shape of cartilage. This may have been the reason for the variation in measurements from the same plug.

- The measurement of cartilage thickness *a posteriori* to indentation is a common practice due to the lack of accurate techniques for the measurement of cartilage thickness in non-invasive, non-damaging and low cost ways. Nevertheless, elastic modulus could be influenced by the substrate material depending of depth of penetration and thickness of the sample. It is possible that results presented

are influenced by the subchondral bone. The development of better methods for measurement of cartilage thickness that could be incorporated into the WASIM or similar testing machines, is important.

- The DMMB method is relatively simple to set up, although the high sensitivity to light and to pipetting technique makes it difficult achieve a high degree of repeatability. Optimal results were obtained by always setting up a standard curve for each plate, taking special care when pipetting, placing dilutions of the same sample solution on the same plate, and adding the DMMB only seconds before reading of absorbency and if possible in absence of strong light.

- Experimental work in the present study was performed in healthy porcine specimens. Although similarities to human knees in terms of structure, geometry and contact patterns have been reported in the literature [281, 287], it is also known that porcine menisci cover a bigger area and are able to carry more load than human menisci. Additionally, locomotion in quadrupeds is significantly different than for humans. This suggests that it is possible that mechanical properties distribution are not identical between porcine and human knees and that unicompartmental knee OA lesions locations might not develop at the same locations.

- In this study mechanical properties, GAG concentration and cartilage thickness were measured in six porcine healthy tibial plateaux. Although high consistency in variable distribution between tibial plateaux suggest that there were reproducible patterns, this study was performed in a relatively small number of specimens which cannot be extrapolated to a whole population.

## 7.4 Recommendations for Future Research

In the future further efforts should be made to identify non-destructive methods for the measurement of the material, structural and biological properties of the tibial plateau. In particular, the measurement of cartilage thickness through non-destructive but accurate methods would represent a key step in this regard. Currently, this can be achieved using US or MRI. However, the accuracy of measurements of cartilage

thickness obtained by US has been widely debated and to date no consensus has been reached. The access to MRI is restricted and it is costly, therefore its use is not widespread. An inexpensive, non-destructive and accurate method for the measurement of cartilage thickness would in turn, allow more accurate calculations of cartilage mechanical properties using indentation, as it would be possible to measure cartilage thickness before performing the mechanical tests.

Further development is also required for non-destructive techniques to measure GAG concentrations over the tibial plateau. In particular the continuous development of contrast agents, such as CA4+ but with higher diffusion rates, would allow the detection of GAG accurately through CT imaging. This could lead to GAG quantification in human joints as a possible method for detection of OA in its very early stages. Another advantage of this method compared to other existing imaging methods such as dGEMRIC, is that CT is a much cheaper and more readily available imaging method compared to MRI.

Additionally, the next step of this project is to use the potential of the WASIM to incorporate other probes to investigate various parameters of articular cartilage in the same points over the tibial plateau or other joints. Moreover, it is possible to reproduce these experiments in normal healthy human cartilage and to investigate whether similar patterns of elastic modulus, GAG concentration and cartilage thickness to those in this thesis are found. It would also be interesting to obtain distribution maps of other cartilage variables such as collagen or other proteins that are thought to play a role in OA development. Additionally, more specimens should be tested.

## 7.5 Summary

In this study the proposed objectives were reached through experimental measurements. Moreover, a novel testing device with potential to collect reproducible data in non-damaging ways in whole specimens was introduced. A method to measure some of these variables was presented.

The type of high resolution maps obtained in this work for whole healthy tibial plateaux

are presented for the first time, as well as the correlation between variables. In addition the analysis of the gradient of mechanical properties over the tibial plateaux gave insight into steep changes in mechanical properties on the tibial plateau.

More work has to be carried out in order to understand the relationship between variable distribution and external stimuli in order to identify when deterioration begins, and therefore the interaction between the different variables that affect cartilage changes.

# CONFERENCE PROCEEDINGS

- Armengol, M., Brown, C.P., Hulley, P., Price. A.J., Gill, H.S. Mechanical properties of porcine tibial plateau cartilage correlates with position of expected osteoarthritic lesions. The Bone and Joint Journal, 96-B, Supplement 11, p 344, 2014. (Combined meeting of Orthopedic Research Societies (CORS), Venice, October 2013).
- Armengol. M., Gill, H.S., Hulley, P. Price, A.P. Matrix and material properties in porcine articular cartilage. European Orthopaedic Research Societies, Nantes, July 2014.
- Armengol, M., Brown, C.P., Price. A.J., Hulley, P., Gill, H.S. Measurement of mechanical properties throughout porcine tibial plateaux. Conference Proceedings Bone Research Society / British Orthopaedic Research Society Joint Meeting (BORS), Oxford, September 2013.
- Armengol, M., Brown, C.P., Price. A.J., Hulley, P., Gill, H.S. Measurement of mechanical properties throughout porcine tibial plateaux as a mechanism to understand early osteoarthritis. Conference Proceedings Bath Biomechanic Symposium 2012. Bath, September 2012.
- Armengol, M., Brown, C.P., Price. A.J., Hulley, P., Gill, H.S. Correlating material properties to matrix constitution of articular cartilage. Department of Engineering Science, Oxford University. September 2012.

# Bibliography


[1] J. S. Jurvelin, T. Rasanen, P. Kolmonen, and T. Lyyra, "Comparision of optical, needle probe and ultrasonic techniques for the measurement of articular cartilage thickness," *Journal of Biomechanics, Technical Note*, vol. 28, no. 2, pp. 231–235, 1995.

[2] J. M. Deneweth, *Mapping the Biomechanical Properties of Human Knee Cartilage*. PhD thesis, University of Michigan, 2013.

[3] T. Fukubayashi and H. Kurosawa, "The contact area and pressure distribution pattern of the knee. A study of normal and osteoarthrotic knee joints.," *Acta Orthopaedica Scandinavica*, vol. 51, pp. 871–9, dec 1980.

[4] World Health Organization, "Interesting facts about ageing," 2012.

[5] A. D. Woolf and B. Pfleger, "Burden of major musculoskeletal conditions.," *Bulletin of the World Health Organization*, vol. 81, pp. 646–56, jan 2003.

[6] D. Symmons, C. Mathers, and B. Pfleger, "Global burden of osteoarthritis in the year 2000," *World Health*, vol. 2002, no. 4, pp. 1–26, 2000.

[7] "World Health Organization (WHO) Report," tech. rep., 1997.

[8] H. J. Helminen, M. M. Hyrnnbnl, M. J. Lammi, J. P. A. Arokoski, T. Lapvetelainen, J. Jurvelin, I. Kiviranta, and M. I. Tammi, "Review and perspectives. Regular joint loading in youth assists in the establishment and strengthening of the collagen network of articular caartilage and contributes to the prevention of osteoarthrosis later in life: a hypothesis," *Journal Bone Mineral Metabolism*, vol. 18, pp. 245–257, 2000.

[9] D. T. Felson, R. C. Lawrence, P. A. Dieppe, R. Hirsch, C. G. Helmick, J. M. Jordan, R. S. Kington, N. E. Lane, M. C. Nevitt, Y. Zhang, M. Sowers, T. E. McAlindon, T. D. Spector, A. Robin Poole, S. Z. Yanovski, G. A. Ateshian, L. Sharma, J. A. Buckwalter, K. D. Brandt, and J. F. Fries, "Osteoarthritis : New Insights. Part I. The disease and its risk factors," *Annals of Internal Medicine*, vol. 133, no. 8, pp. 637–639, 2000.

[10] S. Kurtz, K. Ong, E. Lau, F. Mowat, and M. Halpern, "Projections of primary and revision hip and knee arthroplasty in the United States from 2005 to 2030.," *The Journal of Bone and Joint Surgery. American Volume*, vol. 89, pp. 780–5, apr 2007.

[11] "11th Annual Report National Joint Registry," Tech. Rep. December 2013, National Joint Registry, 2014.

[12] C. G. Armstrong and V. C. Mow, "Variations in the intrinsic mechanical properties of human articular cartilage with age, degeneration and water," *Journal of Bone and Joint Surgery*, vol. 64, no. 1, pp. 88–94, 1982.

[13] J. R. Parsons and J. Black, "The viscoelastic shear behavior of normal rabbit articular cartilage.," *Journal of Biomechanics*, vol. 10, pp. 21–9, jan 1977.

[14] J. P. A. Arokoski, M. M. Hyttinen, T. Lapveteläinen, P. Takács, B. Kosztáczky, L. Módis, V. Kovanen, and H. J. Helminen, "Decreased birefringence of the superficial zone collagen network in the canine knee (stifle) articular cartilage after long distance running training, detected by quantitative polarised light microscopy.," *Annals of the Rheumatic Diseases*, vol. 55, pp. 253–64, apr 1996.

[15] L. P. Li and W. Herzog, "The role of viscoelasticity of collagen fibers in articular cartilage: theory and numerical formulation.," *Biorheology*, vol. 41, no. 3-4, pp. 181–194, 2004.

[16] L. P. Li, W. Herzog, R. K. Korhonen, and J. S. Jurvelin, "The role of viscoelasticity of collagen fibers in articular cartilage: Axial tension versus compression," *Medical Engineering and Physics*, vol. 27, no. 1, pp. 51–57, 2005.

[17] I. Kiviranta, J. Jurvelin, M. Tammi, A.-M. Säämänen, and H. J. Helminen, "Weight bearing controls glycosaminoglycan concentration and articular cartilage thickness in the knee joints of young beagle dogs.," *Arthritis and Rheumatism*, vol. 30, pp. 801–9, jul 1987.

[18] T. P. Andriacchi, A. Mündermann, R. L. Smith, E. J. Alexander, C. O. Dyrby, and S. Koo, "A framework for the in vivo pathomechanics of osteoarthritis at the knee.," *Annals of Biomedical Engineering*, vol. 32, pp. 447–57, mar 2004.

[19] T. P. Andriacchi, S. Koo, and S. F. Scanlan, "Gait mechanics influence healthy cartilage morphology and osteoarthritis of the knee.," *The Journal of Bone and Joint Surgery. American Volume*, vol. 91 Suppl 1, pp. 95–101, feb 2009.

[20] I. Kiviranta, M. Tammi, J. Jurvelin, A. M. Säämänen, and H. J. Helminen, "Moderate running exercise augments glycosaminoglycans and thickness of articular cartilage in the knee joint of young beagle dogs.," *Journal of Orthopaedic Research*, vol. 6, pp. 188–95, jan 1988.

[21] A. C. Swann and B. B. Seedhom, "The stiffness of normal articular cartilage and the predominant acting stress levels: implications for the aetiology of osteoarthrosis.," *British Journal of Rheumatology*, vol. 32, pp. 16–25, jan 1993.

[22] J. T. Bingham, R. Papannagari, S. K. Van de Velde, C. Gross, T. J. Gill, D. T. Felson, H. E. Rubash, and G. Li, "In vivo cartilage contact deformation in the healthy human tibiofemoral joint.," *Rheumatology (Oxford, England)*, vol. 47, pp. 1622–7, nov 2008.

[23] J. T. Samosky, D. Burstein, W. Eric Grimson, R. Howe, S. Martin, and M. L. Gray, "Spatially-localized correlation of dGEMRIC-measured GAG distribution and mechanical stiffness in the human tibial plateau.," *Journal of Orthopaedic Research*, vol. 23, pp. 93–101, jan 2005.

[24] I. Kiviranta, M. Tammi, J. Jurvelin, and H. J. Helminen, "Topographical variation of glycosaminoglycan content and cartilage thickness in canine knee (stifle)

joint cartilage. Application of the microspectrophotometric method.," *Journal of Anatomy*, vol. 150, pp. 265–76, feb 1987.

[25] A. Gulati, R. Chau, D. J. Beard, A. J. Price, H. S. Gill, and D. W. Murray, "Localization of the full-thickness cartilage lesions in medial and lateral unicompartmental knee osteoarthritis.," *Journal of Orthopaedic Research*, vol. 27, no. 10, pp. 1339–1346, 2009.

[26] C. Hirsch and H. D. Frey, *A Contribution to the Pathogenesis of Chondromalacia of the Patella: A Physical, Histologic and Chemical Study*, vol. supp 83. Karolinska institutet, Stockholm: Kungl. Boktryckeriet, P. A. Norstedt & Söner, 1944.

[27] G. E. Kempson, C. J. Spivey, S. A. V. Swanson, and M. A. R. Freeman, "Patterns of cartilage stiffness on and degenerative femoral heads," *Journal of Biomechanics*, vol. 4, no. 3, pp. 597–609, 1971.

[28] R. C. Appleyard, M. V. Swain, S. Khanna, and G. A. C. Murrell, "The accuracy and reliability of a novel handheld dynamic indentation probe for analysing articular cartilage.," *Physics in Medicine and Biology*, vol. 46, pp. 541–50, feb 2001.

[29] J. P. A. Arokoski, M. M. Hyttinen, H. J. Helminen, and J. S. Jurvelin, "Biomechanical and structural characteristics of canine femoral and tibial cartilage.," *Journal of Biomedical Materials Research*, vol. 48, pp. 99–107, jan 1999.

[30] K. A. Athanasiou, M. P. Rosenwasser, J. A. Buckwalter, T. I. Malinin, and V. C. Mow, "Interspecies comparisons of in situ intrinsic mechanical properties of distal femoral cartilage.," *Journal of Orthopaedic Research*, vol. 9, pp. 330–40, may 1991.

[31] C. A. McDevitt, E. Gilbertson, and H. Muir, "An experimental model of osteoarthritis; early morphological and biochemical changes," *The Bone & Joint Journal*, vol. 59, no. 2, pp. 24–35, 1977.

[32] A. Maroudas, H. Evans, and L. Almeida, "Cartilage of the hip joint. Topographical variation of glicosaminoglycan content in normal and fibrillated tissue," *Annuals of the Rheumatic Diseases*, vol. 32, no. 1, pp. 1–9, 1973.

[33] R. K. Korhonen and S. Saarakkala, "Biomechanics and Modeling of Skeletal Soft Tissues," in *Theoretical Biomechanics* (K. D. Vaclav, ed.), pp. 113–132, InTech, 2011.

[34] E. a. Makris, P. Hadidi, and K. a. Athanasiou, "The knee meniscus: Structure-function, pathophysiology, current repair techniques, and prospects for regeneration," *Biomaterials*, vol. 32, no. 30, pp. 7411–7431, 2011.

[35] H. L. Birch, C. T. Thorpe, and A. P. Rumian, "Specialisation of extracellular matrix for function in tendons and ligaments," *Muscle, Ligaments and Tendons Journal*, vol. 3, no. 1, pp. 12–22, 2013.

[36] J. M. Mansour, "Biomechanics of Cartilage," in *Biomechanical Principles*, vol. 58, ch. Chapter 5, pp. 66–78, Eric Urbina Santibañez, jul 2003.

[37] R. Fujioka, T. Aoyama, and T. Takakuwa, "The layered structure of the articular surface.," *Osteoarthritis and cartilage / OARS, Osteoarthritis Research Society*, vol. 21, no. 8, pp. 1092–8, 2013.

[38] R. Shirazi and A. Shirazi-Adl, "Analysis of articular cartilage as a composite using nonlinear membrane elements for collagen fibrils," *Medical Engineering and Physics*, vol. 27, pp. 827–35, dec 2005.

[39] R. A. Stockwell, "Biology of cartilage cell," in *Biology Structure and Function*, Cambridge, England: Cambridge University Press, 1979.

[40] A. J. Sophia Fox, A. Bedi, and S. A. Rodeo, "The basic science of articular cartilage: structure, composition, and function.," *Sports Health*, vol. 1, pp. 461–8, nov 2009.

[41] J. Dudhia, "Aggrecan, aging and assembly in articular cartilage.," *Cellular and Molecular Life Sciences*, vol. 62, pp. 2241–56, oct 2005.

[42] J. A. Buckwalter, H. J. Mankin, and A. J. Grodzinsky, "Articular Cartilage and Osteoarthristis," *AAOS Instructional Course Lectures*, vol. 54, pp. 465–480, 2005.

[43] V. C. Mow, A. Ratcliffe, and A. R. Poole, "Cartilage and diarthrodial joints as paradigms for hierarchical materials and structures," *Journal of Biomaterials*, vol. 13, no. 2, pp. 67–97, 1992.

[44] C. T. Chen, M. Bhargava, P. M. Lin, and P. A. Torzilli, "Time, stress, and location dependent chondrocyte death and collagen damage in cyclically loaded articular cartilage.," *Journal of Orthopaedic Research*, vol. 21, pp. 888–98, sep 2003.

[45] J. S. Jurvelin, M. D. Buschmann, and E. B. Hunziker, "Optical and mechanical determination of Poisson's ratio of adult bovine humeral articular cartilage," *Journal of Biomechanics*, vol. 30, no. 3, pp. 235–241, 1997.

[46] R. M. Schinagl, D. Gurskis, A. C. Chen, and R. L. Sah, "Depth-dependent confined compression modulus of full-thickness bovine articular cartilage," *Journal of Orthopaedic Research*, vol. 15, no. 4, pp. 499–506, 1997.

[47] G. E. Kempson, H. Muir, S. A. V. Swanson, and M. A. R. Freeman, "Correlations between stiffness and the chemical constituents of cartilage on the human femoral head.," *Biochimica et Biophysica Acta*, vol. 215, pp. 70–7, jul 1970.

[48] S. Saarakkala, P. Julkunen, P. Kiviranta, J. Mäkitalo, J. S. Jurvelin, and R. K. Korhonen, "Depth-wise progression of osteoarthritis in human articular cartilage: investigation of composition, structure and biomechanics.," *Osteoarthritis and Cartilage / OARS, Osteoarthritis Research Society*, vol. 18, pp. 73–81, jan 2010.

[49] P. Julkunen, W. Wilson, J. S. Jurvelin, J. Rieppo, C.-J. Qu, M. J. Lammi, and R. K. Korhonen, "Stress-relaxation of human patellar articular cartilage in unconfined compression: prediction of mechanical response by tissue composition and structure.," *Journal of Biomechanics*, vol. 41, pp. 1978–86, jan 2008.

[50] W. Wilson, J. M. Huyghe, and C. C. Van Donkelaar, "Depth-dependent compressive equilibrium properties of articular cartilage explained by its composi-

tion," *Biomechanics and Modeling in Mechanobiology*, vol. 6, no. 1-2, pp. 43–53, 2007.

[51] A. R. Gannon, T. Nagel, and D. J. Kelly, "The role of the superficial region in determining the dynamic properties of articular cartilage," *Osteoarthritis and Cartilage*, vol. 20, no. 11, pp. 1417–1425, 2012.

[52] D. Eyre, "Collagen of articular cartilage," *Arthritis research*, vol. 4, no. 1, pp. 30–35, 2002.

[53] R. M. Aspden and D. W. Hukins, "Collagen organization in articular cartilage, determined by X-ray diffraction, and its relationship to tissue function.," *Proceedings of the Royal Society of London. Series B, Containing papers of a Biological character. Royal Society (Great Britain)*, vol. 212, no. 1188, pp. 299–304, 1981.

[54] B. L. Schumacher, J. A. Block, T. M. Schmid, M. B. Aydelotte, and K. E. Kuettner, "A novel proteoglycan synthesized and secreted by chondrocytes of the superficial zone of articular cartilage.," *Archives of Biochemistry and Biophysics*, vol. 311, pp. 144–52, may 1994.

[55] M. Wong and D. R. Carter, "Articular cartilage functional histomorphology and mechanobiology: a research perspective," *Bone*, vol. 33, pp. 1–13, jul 2003.

[56] S. Chegini and S. J. Ferguson, "Time and depth dependent Poisson's ratio of cartilage explained by an inhomogeneous orthotropic fiber embedded biphasic model.," *Journal of Biomechanics*, vol. 43, pp. 1660–6, jun 2010.

[57] H. Guo, S. a. Maher, and P. a. Torzilli, "A biphasic finite element study on the role of the articular cartilage superficial zone in confined compression," *Journal of Biomechanics*, vol. 48, no. 1, pp. 166–170, 2015.

[58] B. L. Wong, W. C. Bae, J. Chun, K. R. Gratz, M. Lotz, and R. L. Sah, "Biomechanics of cartilage articulation: effects of lubrication and degeneration on shear deformation.," *Arthritis and Rheumatism*, vol. 58, pp. 2065–74, jul 2008.

[59] F. Guilak, A. Ratcliffe, N. Lane, M. P. Rosenwasser, and V. C. Mow, "Mechanical and biochemical changes in the superficial zone of articular cartilage in canine

experimental osteoarthritis.," *Journal of Orthopaedic Research*, vol. 12, pp. 474–84, jul 1994.

[60] S. L. Y. Woo, P. Lubock, M. A. Gomez, G. F. Jemmotta, S. C. Kueia, and W. H. Akeson, "Large deformation nonhomogeneous and directional properties of articular cartilage in uniaxial tension.," *Journal of Biomechanics*, vol. 12, pp. 437–46, jan 1979.

[61] A. Benninghoghoff, "Form und bau der gelenkknorpel in ihren beziehungen zur function," *Zeitschrift für Zellforschung und Mikroskopische Anatomie*, vol. 2, no. 5, pp. 789–862, 1925.

[62] K. S. Halonen, M. E. Mononen, J. S. Jurvelin, J. Töyräs, and R. K. Korhonen, "Importance of depth-wise distribution of collagen and proteoglycans in articular cartilage - a 3D finite element study of stresses and strains in human knee joint.," *Journal of Biomechanics*, vol. 46, pp. 1184–92, apr 2013.

[63] M. Wong, P. Wuethrich, M. D. Buschmann, P. Eggli, and E. Hunziker, "Chondrocyte biosynthesis correlates with local tissue strain in statically compressed adult articular cartilage.," *Journal of Orthopaedic Research*, vol. 15, pp. 189–196, mar 1997.

[64] N. M. Barchrach, W. B. Valhmu, E. Stazzone, A. Ratcliffe, and M. Lai, "Changes in proteoglycan synthesis of chondrocytes in articular cartilage are associated with the time-dependent changes in their mechanical environment," *Journal of Biomechanics*, vol. 28, no. 12, pp. 1561–1569, 1995.

[65] F. Guilak, A. Ratcliffe, and V. C. Mow, "Chondrocyte deformation and local tissue strain in articular cartilage: a confocal microscopy study.," *Journal of Orthopaedic Research*, vol. 13, pp. 410–21, may 1995.

[66] B. K. Hall, *Bones and Cartilage Developmental and Evolutionary skeletal Biology*. Oxford: Academic Press, Inc., 2nd ed., 2015.

[67] Z. Xue-Xi, M. Zhi-Hua, Y. Jian-Hua, and X. Yang, "Determination of collagen and proteoglycan concentration in osteoarthritic and healthy articular cartilage

by Fourier transform infrared imaging and partial least square," *Vibrational Spectroscopy*, vol. 78, pp. 49–53, 2015.

[68] P. Kiviranta, J. Rieppo, R. K. Korhonen, P. Julkunen, J. Töyräs, and J. S. Jurvelin, "Collagen Network Primarily Controls Poisson's Ratio of Bovine Articular Cartilage in Compression," *Journal of Orthopaedic Research*, vol. 24, no. 4, pp. 690–699, 2006.

[69] M. Thibault, A. R. Poole, and M. D. Buschmann, "Cyclic compression of cartilage/bone explants in vitro leads to physical weakening, mechanical breakdown of collagen and release of matrix fragments.," *Journal of Orthopaedic Research*, vol. 20, pp. 1265–73, nov 2002.

[70] J. M. Clark, "Variation of collagen fiber alignment in a joint surface: a scanning electron microscope study of the tibial plateau in dog, rabbit, and man.," *Journal of Orthopaedic Research*, vol. 9, pp. 246–57, mar 1991.

[71] A. K. Williamson, A. C. Chen, K. Masuda, E. J. M. a. Thonar, and R. L. Sah, "Tensile mechanical properties of bovine articular cartilage: Variations with growth and relationships to collagen network components," *Journal of Orthopaedic Research*, vol. 21, no. 5, pp. 872–880, 2003.

[72] S. Inerot, D. Heinegård, L. Audell, and S. E. Olsson, "Articular-cartilage proteoglycans in aging and osteoarthritis.," *The Biochemical Journal*, vol. 169, pp. 143–56, jan 1978.

[73] A. Maroudas, H. Muir, and J. Wingham, "The correlation of fixed negative charge with GAG content of human articular cartilage," *Biochimica et Biophysica Acta*, vol. 177, no. 3, pp. 492–500, 1969.

[74] C. Canal Guterl, C. T. Hung, and G. A. Ateshian, "Electrostatic and non-electrostatic contributions of proteoglycans to the compressive equilibrium modulus of bovine articular cartilage," *Journal of Biomechanics*, vol. 43, no. 7, pp. 1343–1350, 2010.

[75] J. A. Buckwalter and N. E. Lane, "Athletics and Osteoarthritis," *The American Journal of Sports Medicine*, vol. 25, pp. 873–881, dec 1997.

[76] F. C. Linn and L. Sokoloff, "Movement and composition of interstitial fluid of cartilage," *Arthritis & Rheumatism*, vol. 8, no. 4, pp. 481–494, 1965.

[77] A. Maroudas and R. Schneiderman, "Free and exchangeable or trapped and non-exchangeable water in cartilage," *Journal of Orthopaedic Research*, vol. 5, no. 1, pp. 133–138, 1987.

[78] V. C. Mow, M. H. Holmes, and M. W. Lai, "Fluid Transport and Mechanical Properties of Articular Cartilage," *Journal of Biomechanics*, vol. 17, no. 5, pp. 377–394, 1984.

[79] F. Loix, F. M. F. Simões, and B. Loret, "Articular cartilage with intra and extrafibrillar waters - Simulations of mechanical and chemical loadings by the finite element method," *Computer Methods in Applied Mechanics and Engineering*, vol. 197, no. 51-52, pp. 4840–4857, 2008.

[80] A. C. Fischer-Cripps, *The IBIS Handbook of Nanoindentation.* Australia: Fischer-Cripps Laboratories Pty Ltd., oct 2010.

[81] X. L. Lu and V. C. Mow, "Biomechanics of articular cartilage and determination of material properties.," *Medicine and Science in Sports and Exercise*, vol. 40, pp. 193–9, feb 2008.

[82] F. Boschetti, G. Pennati, F. Gervaso, G. M. Peretti, and G. Dubini, "Biomechanical properties of human articular cartilage under compressive loads.," *Biorheology*, vol. 41, pp. 159–66, jan 2004.

[83] J. S. Jurvelin, J. P. Arokoski, E. B. Hunziker, and H. J. Helminen, "Topographical variation of the elastic properties of articular cartilage in the canine knee.," *Journal of Biomechanics*, vol. 33, pp. 669–75, jun 2000.

[84] J. E. Hale, M. J. Rudert, and T. D. Brown, "Indentation assessment of biphasic mechanical property deficits in size-dependent osteochondral defect repair.," *Journal of Biomechanics*, vol. 26, pp. 1319–25, nov 1993.

[85] V. C. Mow, S. C. Kuei, W. M. Lai, and C. G. Armstrong, "Biphasic creep and stress relaxation of articular cartilage in compression: Theory and experiments," *Journal of Biomechanical Engineering*, vol. 102, pp. 72–84, 1980.

[86] W. M. Lai and V. C. Mow, "Drag-induced compression of articular cartilage during a permeation experiment," *Journal of Biorheology*, vol. 17, no. 1-2, pp. 111–123, 1980.

[87] J. M. Haemer, D. R. Carter, and N. J. Giori, "The low permeability of healthy meniscus and labrum limit articular cartilage consolidation and maintain fluid load support in the knee and hip," *Journal of Biomechanics*, vol. 45, no. 8, pp. 1450–1456, 2012.

[88] D. R. Askeland and P. P. Phule, *The Science & Engineering of Materials*. Toronto, Canada: Thomson Canada Lmt., 5th ed., 2006.

[89] P. G. Bullough, P. S. Yawitz, L. Tafra, and A. L. Boskey, "Topographical variations in the morphology and biochemistry of Adult Canine Tibial Plateau articular cartilage," *Journal of Orthopeadic Research*, vol. 3, pp. 1–16, 1985.

[90] R. K. Korhonen, M. S. Laasanen, J. Töyräs, J. Rieppo, J. Hirvonen, H. J. Helminen, and J. S. Jurvelin, "Comparison of the equilibrium response of articular cartilage in unconfined compression, confined compression and indentation.," *Journal of Biomechanics*, vol. 35, pp. 903–9, jul 2002.

[91] R. K. Korhonen, M. Wong, J. Arokoski, R. Lindgren, H. J. Helminen, E. B. Hunziker, and J. S. Jurvelin, "Importance of the superficial tissue layer for the indentation stiffness of articular cartilage," *Medical Engineering and Physics*, vol. 24, no. 2, pp. 99–108, 2002.

[92] J. Rieppo, M. M. Hyttinen, E. Halmesmaki, H. Ruotsalainen, A. Vasara, I. Kiviranta, J. S. Jurvelin, and H. J. Helminen, "Changes in spatial collagen content and collagen network architecture in porcine articular cartilage during growth and maturation.," *Osteoarthritis and Cartilage / OARS, Osteoarthritis Research Society*, vol. 17, pp. 448–55, apr 2009.

[93] L. Rieppo, S. Saarakkala, J. S. Jurvelin, and J. Rieppo, "Prediction of compressive stiffness of articular cartilage using Fourier transform infrared spectroscopy," *Journal of Biomechanics*, vol. 46, no. 7, pp. 1269–1275, 2013.

[94] S. Akizuki, V. C. Mow, F. Muller, J. C. Pita, and D. S. Howell, "Tensile properties of human knee joint cartilage. II. Correlations between weight bearing and tissue pathology and the kinetics of swelling.," *Journal of Orthopaedic Research*, vol. 5, pp. 173–86, jan 1987.

[95] M. a. McLeod, R. E. Wilusz, and F. Guilak, "Depth-dependent anisotropy of the micromechanical properties of the extracellular and pericellular matrices of articular cartilage evaluated via atomic force microscopy," *Journal of Biomechanics*, vol. 46, no. 3, pp. 586–592, 2013.

[96] H. Jin and J. L. Lewis, "Determination of Poisson's ratio of articular cartilage in indentation test using different sized indenters," *Summer Bioengineering Conference, Key Biscayne, FL*, 2003.

[97] N. Hamann, G. P. Brüggemann, and A. Niehoff, "Topographical variations in articular cartilage and subchondral bone of the normal rat knee are age-related," *Annals of Anatomy*, vol. 196, no. 5, pp. 278–285, 2014.

[98] Z. A. Cohen, D. M. McCarthy, S. D. Kwak, P. Legrand, F. Fogarasi, E. J. Ciaccio, and G. A. Ateshian, "Knee cartilage topography, thickness, and contact areas from MRI: in-vitro calibration and in-vivo measurements.," *Osteoarthritis and Cartilage / OARS, Osteoarthritis Research Society*, vol. 7, pp. 95–109, jan 1999.

[99] G. G. Niederauer, G. M. Niederauer, L. C. Cullen, K. A. Athanasiou, J. B. Thomas, and M. Q. Niederauer, "Correlation of cartilage stiffness to thickness and level of degeneration using a handheld indentation probe.," *Annals of Biomedical Engineering*, vol. 32, pp. 352–9, mar 2004.

[100] E. Argentieri, D. Sturnick, M. DeSarno, M. Gardner-Morse, J. Slauterbeck, R. Johnson, and B. Beynnon, "Changes to the articular cartilage thickness pro-

file of the tibia following anterior cruciate ligament injury," *Osteoarthritis and Cartilage*, vol. 22, no. 10, pp. 1453–1460, 2014.

[101] T. Lyyra and J. Jurvelin, "Indentation instrument for the measurement of cartilage stiffness under arthroscopic control," *Medical Engineering and Physics*, vol. 17, no. 5, pp. 395–399, 1995.

[102] W. N. Newberry, D. K. Zukosky, and R. C. Haut, "Subfracture insult to a knee joint causes alterations in the bone and in the functional stiffness of overlying cartilage.," *Journal of Orthopaedic Research*, vol. 15, pp. 450–5, may 1997.

[103] M. K. Barker and B. B. Seedhom, "The relationship of the compressive modulus of articular cartilage with its deformation response to cyclic loading: does cartilage optimize its modulus so as to minimize the strains arising in it due to the prevalent loading regime?," *Rheumatology (Oxford, England)*, vol. 40, pp. 274–84, mar 2001.

[104] Y. Song, J. M. Greve, D. R. Carter, S. Koo, and N. J. Giori, "Articular cartilage MR imaging and thickness mapping of a loaded knee joint before and after meniscectomy.," *Osteoarthritis and Cartilage / OARS, Osteoarthritis Research Society*, vol. 14, pp. 728–37, aug 2006.

[105] C. Adam, F. Eckstein, S. Milz, E. Schulte, C. Becker, and R. Putz, "The distribution of cartilage thickness in the knee-joints of old-aged individuals measurement by A-mode ultrasound," *Clinical Biomechanics*, vol. 13, no. 1, pp. 1–10, 1998.

[106] J. Töyräs, T. Lyyra-Laitinen, M. Niinimäki, R. Lindgren, M. T. Nieminen, I. Kiviranta, and J. S. Jurvelin, "Estimation of the Young's modulus of articular cartilage using an arthroscopic indentation instrument and ultrasonic measurement of tissue thickness," *Journal of Biomechanics*, vol. 34, pp. 251–256, 2001.

[107] J. Töyräs, J. Rieppo, M. T. Nieminen, H. J. Helminen, and J. S. Jurvelin, "Characterization of enzymatically induced degradation of articular cartilage using high frequency ultrasound," *Physics in Medicine and Biology*, vol. 44, p. 2723, 1999.

[108] V. E. Modest, M. C. Murphy, and R. W. Mann, "Optical verification of a technique for in situ ultrasonic measurement of articular cartilage thickness," *Journal of Biomechanics*, vol. 22, no. 2, pp. 171–173, 1989.

[109] M. S. Laasanen, S. Saarakkala, J. Töyräs, J. Hirvonen, J. Rieppo, R. K. Korhonen, and J. S. Jurvelin, "Ultrasound indentation of bovine knee articular cartilage in situ," *Journal of Biomechanics*, vol. 36, pp. 1259–1267, sep 2003.

[110] S.-Z. Wang, Y.-P. Huang, S. Saarakkala, and Y.-P. Zheng, "Quantitative assessment of articular cartilage with morphologic, acoustic and mechanical properties obtained using high-frequency ultrasound.," *Ultrasound in medicine & biology*, vol. 36, no. 3, pp. 512–527, 2010.

[111] R. W. Mann, "Discussion: A technique for measuring the compressive modulus of articular cartilage under physiological loading rates with preliminary results," *Proceedings of the Institution of Mechanical Engineers, Part H: Journal of Engineering in Medicine*, vol. 215, pp. 123–124, jan 2001.

[112] S. Ohashi, I. Ohnishi, T. Matsumoto, M. Bessho, J. Matsuyama, K. Tobita, M. Kaneko, and K. Nakamura, "Evaluation of the Accuracy of Articular Cartilage Thickness Measurement by Conventional and Real-time Spatial Compound Ultrasonography," *Ultrasound in medicine & biology*, vol. 2, no. 38, pp. 324–334, 2012.

[113] F. Eckstein, H. Boeth, G. Diederichs, W. Wirth, M. Hudelmaier, S. Cotofana, M. Hofmann-Amtenbrink, and G. Duda, "Longitudinal change in femorotibial cartilage thickness and subchondral bone plate area in male and female adolescent vs. mature athletes.," *Annals of Anatomy*, vol. 196, pp. 150–7, may 2014.

[114] R. Y. Hori and L. F. Mockros, "Indentation tests of human articular cartilage," *Journal of Biomechanics*, vol. 9, no. 4, pp. 259–268, 1976.

[115] W. C. Hayes, L. M. Keer, G. Herrmann, and L. F. Mockros, "A mathematical analysis for indentation tests of articular," *Journal of Biomechanics*, vol. 5, no. December 1970, pp. 541–551, 1972.

[116] C. T. Chen, N. Burton-Wurster, G. Lust, R. A. Bank, and J. M. Tekoppele, "Compositional and metabolic changes in damaged cartilage are peak-stress, stress-rate, and loading-duration dependent.," *Journal of Orthopaedic Research*, vol. 17, pp. 870–9, nov 1999.

[117] P. Brammer, O. Bartier, X. Hernot, G. Mauvoisin, and S. S. Sablin, "An alternative to the determination of the effective zero point in instrumented indentation: Use of the slope of the indentation curve at indentation load values," *Materials & Design*, vol. 40, pp. 356–363, sep 2012.

[118] A. C. Fischer-Cripps, "Critical review of analysis and interpretation of nanoindentation test data," *Surface and Coatings Technology*, vol. 200, pp. 4153–4165, apr 2006.

[119] G. J. Miller and E. F. Morgan, "Use of microindentation to characterize the mechanical properties of articular cartilage: Comparison of biphasic material properties across length scales," *Osteoarthritis and Cartilage*, vol. 18, no. 8, pp. 1051–1057, 2010.

[120] X. Chen, B. K. Zimmerman, and X. L. Lu, "Determine the equilibrium mechanical properties of articular cartilage from the short-term indentation response," *Journal of iomechanics*, vol. 48, pp. 176–180, 2015.

[121] A. Gouldstone, N. Chollacoop, M. Dao, J. Li, A. M. Minor, and Y.-L. Shen, "Indentation across size scales and disciplines: Recent developments in experimentation and modeling," *Acta Materialia*, vol. 55, pp. 4015–4039, jul 2007.

[122] O. Franke, M. Göken, M. A. Meyers, K. Durst, and A. M. Hodge, "Dynamic nanoindentation of articular porcine cartilage," *Materials Science and Engineering*, vol. 31, pp. 789–795, may 2011.

[123] M. L. Oyen and R. F. Cook, "A practical guide for analysis of nanoindentation data.," *Journal of the Mechanical Behavior of Biomedical Materials*, vol. 2, pp. 396–407, aug 2009.

[124] M. Taffetani, M. Griebel, D. Gastaldi, S. M. Klisch, and P. Vena, "Poroviscoelastic finite element model including continuous fiber distribution for the simulation of nanoindentation tests on articular cartilage," *Journal of the Mechanical Behavior of Biomedical Materials*, vol. 32, pp. 17–30, 2014.

[125] E. M. Darling, R. E. Wilusz, M. P. Bolognesi, S. Zauscher, and F. Guilak, "Spatial mapping of the biomechanical properties of the pericellular matrix of articular cartilage measured in situ via atomic force microscopy.," *Biophysical Journal*, vol. 98, pp. 2848–56, jun 2010.

[126] K. Athanasiou, G. Constantinides, and D. R. Lanctot, "Arthroscopic cartilage evaluator and method for using the same," *US Patent 5,503,162*, 1996.

[127] N. K. Simha, H. Jin, M. L. Hall, S. Chiravarambath, and J. L. Lewis, "Effect of indenter size on elastic modulus of cartilage measured by indentation.," *Journal of Biomechanical Engineering*, vol. 129, pp. 767–75, oct 2007.

[128] A. E. Giannakopoulos and S. Suresh, "Determination of elastoplastic properties by instrumented sharp indentation," *Scripta Materialia*, vol. 40, pp. 1191–1198, apr 1999.

[129] W. C. Bae, C. W. Lewis, M. E. Levenston, and R. L. Sah, "Indentation testing of human articular cartilage: effects of probe tip geometry and indentation depth on intra-tissue strain.," *Journal of Biomechanics*, vol. 39, pp. 1039–47, jan 2006.

[130] M. Stolz, R. Raiteri, A. U. Daniels, M. R. VanLandingham, W. Baschong, and U. Aebi, "Dynamic elastic modulus of porcine articular cartilage determined at two different levels of tissue organization by indentation-type atomic force microscopy.," *Biophysical Journal*, vol. 86, pp. 3269–83, may 2004.

[131] V. C. Mow, "A numerical algorithm and an experimental," *Journal of Biomechanics*, vol. 22, no. 8/9, pp. 853–861, 1989.

[132] W. C. Oliver and G. M. Pharr, "An improved technique for determining hardness and elastic modulus using load and displacement sensing indentation experiments," *Material Research Society*, vol. 7, no. 6, pp. 1564–1583, 1992.

[133] J. S. Field and M. V. Swain, "A simple predictive model for spherical indentation," *Journal of Materials Research*, vol. 8, no. 2, pp. 297–306, 1993.

[134] W. C. Oliver and G. M. Pharr, "Measurement of hardness and elastic modulus by instrumented indentation: Advances in understanding and refinements to methodology," *Journal of Materials Research*, vol. 19, pp. 3–20, jan 2004.

[135] M. Sakamoto, G. Li, T. Hara, and E. Y. S. Chao, "A new method for theoretical analysis of static indentation test," *Journal of Biomechanics*, vol. 29, no. 5, pp. 679–685, 1996.

[136] M. A. Haider and M. H. Holmes, "A mathematical approximation for the solution of a static indentation test," *Journal of Biomechanics*, vol. 30, no. 97, 1997.

[137] R. K. Korhonen and J. S. Jurvelin, "Compressive and tensile properties of articular cartilage in axial loading are modulated differently by osmotic environment," *Medical Engineering and Physics*, vol. 32, no. 2, pp. 155–160, 2010.

[138] E. Tanaka, F. Pelayo, N. Kim, M. J. Lamela, N. Kawai, and A. Fernández-Canteli, "Stress relaxation behaviors of articular cartilages in porcine temporomandibular joint," *Journal of Biomechanics*, vol. 47, no. 7, pp. 1582–1587, 2014.

[139] A. D. Lopez and C. C. J. L. Murray, "The global burden of disease , 1990 2020," *Nature Medicine*, vol. 4, no. 11, pp. 1241–1243, 1998.

[140] T. Karachalios, A. Zibis, P. Papanagiotou, A. H. Karantanas, K. N. Malizos, and N. Roidis, "MR imaging findings in early osteoarthritis of the knee.," *European Journal of Radiology*, vol. 50, pp. 225–30, jun 2004.

[141] P. N. Bansal, N. S. Joshi, V. Entezari, M. W. Grinstaff, and B. D. Snyder, "Non-Invasive Diagnostic Methods to monitor the GAG content and biomechanical properties of articular cartilage," *Orthopedic Journal*, pp. 53–56, 2010.

[142] L. M. Verbrugge, "Women, men, and osteoarthritis.," *Arthritis Care and Research*, vol. 8, pp. 212–20, dec 1995.

[143] T. Lawson, A. Morrison, S. Blaxland, M. Wenman, C. G. Schmidt, and M. a. Hunt, "Laboratory-based measurement of standing balance in individuals with knee osteoarthritis: A systematic review," *Clinical Biomechanics*, vol. 30, no. 4, pp. 330–342, 2015.

[144] L. Brody Thein, "Knee osteoarthritis : Clinical connections to articular cartilage structure and function," *Physical Therapy in Sport*, pp. 1–16, 2014.

[145] N. B. Moreira, G. C. Vagetti, V. de Oliveira, and W. de Campos, "Association between injury and quality of life in athletes: A systematic review, 1980-2013," *Apunts Medicina de l'Esport*, vol. 49, no. 184, pp. 123–138, 2014.

[146] F. Roemer, M. Jarraya, J. Niu, J.-R. Silva, R. Frobell, and A. Guermazi, "Increased risk for radiographic osteoarthritis features in young active athletes: a cross-sectional matched caseâ€"control study," *Osteoarthritis and Cartilage*, vol. 23, no. 2, pp. 239–243, 2015.

[147] J. A. Martin and J. A. Buckwalter, "Roles of Articular Cartilage Aging and Chondrocyte Senecence in the Pathogenesis of Osteoarthristis," *The Iowa Orthopedic Journal*, vol. 21, no. 319, pp. 1–7, 2001.

[148] A. S. Anderson and R. F. Loeser, "Why is osteoarthritis an age-related disease?," *Best Practice & Research Clinical Rheumatology*, vol. 24, pp. 15–26, feb 2010.

[149] J.-C. Rousseau, E. Sornay-Rendu, O. Borel, C. Bertholon, P. Garnero, and R. Chapurlat, "Serum sclerostin is not associated with knee osteoarthritis prevalence and progression of Kellgrenlawrence score in women: The ofely study," *Osteoarthritis and Cartilage*, vol. 22, pp. S57–S489, 2014.

[150] T. Aigner, B. Kurz, N. Fukui, and L. Sandell, "Roles of chondrocytes in the pathogenesis of osteoarthritis," *Current Opinion in Rheumatology*, vol. 14, pp. 578–584, 2002.

[151] V. Silverwood, C. Jinks, J. L. Jordan, J. Protheroe, and K. P. Jordan, "Current evidence on risk factors for knee osteoarthritis in older adults : a systematic

review and meta-analysis," *Osteoarthritis and Cartilage*, vol. 23, no. 4, pp. 1–9, 2014.

[152] H. Muir, "Molecular approach to the understanding of osteoarthrosis," *Annals of the Rheumatic Diseases*, vol. 36, pp. 199–208, 1977.

[153] E. L. Radin, D. B. Burr, B. Caterson, and D. Fyhrie, "Mechanical determinants of osteoarthrosis," *Seminars in Arthritis and Rheumatism*, vol. 21, no. 3 Suppl 2, pp. 12–21, 1991.

[154] P. Patwari, D. M. Cheng, A. A. Cole, K. E. Kuettner, and A. J. Grodzinsky, "Analysis of the relationship between peak stress and proteoglycan loss following injurious compression of human post-mortem knee and ankle cartilage.," *Biomechanics and Modeling in Mechanobiology*, vol. 6, pp. 83–9, jan 2007.

[155] M. B. Ellman, D. Yan, D. Chen, and H.-j. Im, "Biochemical Mediators Involved in Cartilage Degradation and the Induction of Pain in Osteoarthritis," in *Principles of Osteoarthritis- Its Definition, Character, Derivation and Modality-Related Recognition* (B. M. Rothschild, ed.), ch. 15, pp. 367–398, Rijeka: InTech, 2012.

[156] M. J. Pond and G. Nuki, "Experimentally-induced Osteoarthritis in the Dog.," *Annals of Rheumatic Diseases*, vol. 59, no. B, pp. 24–35, 1970.

[157] D. H. Hoch, A. J. Grodzinsky, T. J. Koob, M. L. Albert, and D. R. Eyre, "Early changes in material properties of rabbit articular cartilage after meniscectomy.," *Journal of Orthopaedic Research*, vol. 1, pp. 4–12, jan 1983.

[158] A. J. Bollet and J. L. Nance, "Biochemical Findings in Normal and Osteoarthritic Articular Cartilage. II. Chondroitin Sulfate Concentration and Chain Length, Water, and Ash Content.," *The Journal of Clinical Investigation*, vol. 45, pp. 1170–7, jul 1966.

[159] H. J. Mankin and A. Z. Thrasher, "Water Content Osteoarthritic and Binding in Normal Cartilage," *Journal of Bone & Joint surgery*, vol. 57, no. 1, pp. 76–80, 1975.

[160] S. Tanaka, C. Hamanishi, H. Kikuchi, and K. Fukuda, "Factors related to degradation of articular cartilagein osteoarthritis: a review," in *Seminars in Arthritis and Rheumatism*, vol. 27, pp. 392–399, Elsevier, jun 1998.

[161] S. Hada, H. Kaneko, R. Sadatsuki, L. Liu, I. Futami, M. Kinoshita, A. Yusup, Y. Saita, Y. Takazawa, H. Ikeda, K. Kaneko, and M. Ishijima, "The degeneration and destruction of femoral articular cartilage shows a greater degree of deterioration than that of the tibial and patellar articular cartilage in early stage knee osteoarthritis : a cross-sectional study," *Osteoarthritis and Cartilage*, vol. 22, no. 10, pp. 1583–1589, 2014.

[162] S. Grenier, M. M. Bhargava, and P. a. Torzilli, "An in vitro model for the pathological degradation of articular cartilage in osteoarthritis," *Journal of Biomechanics*, vol. 47, no. 3, pp. 645–652, 2014.

[163] L. S. Wang, C. Du, W. S. Toh, A. C. a. Wan, S. J. Gao, and M. Kurisawa, "Modulation of chondrocyte functions and stiffness-dependent cartilage repair using an injectable enzymatically crosslinked hydrogelwith tunable mechanical properties," *Biomaterials*, vol. 35, no. 7, pp. 2207–2217, 2014.

[164] L. Lippiello, D. Hall, and H. J. Mankin, "Collagen synthesis in normal and osteoarthritic human cartilage.," *The Journal of Clinical Investigation*, vol. 59, pp. 593–600, apr 1977.

[165] J. Imgenberg, B. Rolauffs, a. J. Grodzinsky, M. Schünke, and B. Kurz, "Estrogen reduces mechanical injury-related cell death and proteoglycan degradation in mature articular cartilage independent of the presence of the superficial zone tissue," *Osteoarthritis and Cartilage*, vol. 21, no. 11, pp. 1738–1745, 2013.

[166] D. Périé, J. C. Iatridis, C. N. Demers, T. Goswami, G. Beaudoin, F. Mwale, and J. Antoniou, "Assessment of compressive modulus, hydraulic permeability and matrix content of trypsin-treated nucleus pulposus using quantitative MRI," *Journal of Biomechanics*, vol. 39, no. 8, pp. 1392–1400, 2006.

[167] N. Vasan, "Effects of physical stress on the synthesis and degradation," *Connect Tissue Research*, vol. 12, pp. 49–58, 1983.

[168] F. H. Silver, G. Bradica, and A. Tria, "Do changes in the mechanical properties of articular cartilage promote catabolic destruction of cartilage and osteoarthritis?," *Matrix Biology*, vol. 23, no. 7, pp. 467–476, 2004.

[169] D. T. Felson, R. C. Lawrence, M. C. Hochberg, T. McAlindon, P. A. Dieppe, M. A. Minor, S. N. Blair, B. M. Berman, J. F. Fries, M. Weinberger, K. R. Lorig, J. J. Jacobs, and V. Goldberg, "Osteoarthritis: new insights. Part 2: treatment approaches," *Annals of Internal Medicine*, vol. 133, no. 9, p. 726, 2000.

[170] E. H. Frank, A. J. Grodzinsky, T. J. Koob, and D. R. Eyre, "Streaming potentials: a sensitive index of enzymatic degradation in articular cartilage.," *Journal of Orthopaedic Research*, vol. 5, pp. 497–508, jan 1987.

[171] V. Juras, M. Bittsansky, Z. Majdisova, P. Szomolanyi, I. Sulzbacher, S. Gäbler, J. Stampfl, G. Schüller, and S. Trattnig, "In vitro determination of biomechanical properties of human articular cartilage in osteoarthritis using multi-parametric MRI," *Journal of Magnetic Resonance*, vol. 197, no. 1, pp. 40–47, 2009.

[172] J. A. Buckwalter and H. J. Mankin, "Articular Cartilage. Part II: Degeneration and Osteoarthrosis, Repair, Regeneration, and Transplantation," *Instr Course Lect.*, vol. 47, pp. 487–504, 1998.

[173] J. Yin and Y. Xia, "Spectrochimica Acta Part A : Molecular and Biomolecular Spectroscopy Proteoglycan concentrations in healthy and diseased articular cartilage by Fourier transform infrared imaging and principal component regression," *SPECTROCHIMICA ACTA PART A: MOLECULAR AND BIOMOLECULAR SPECTROSCOPY*, vol. 133, pp. 825–830, 2014.

[174] J. P. A. Arokoski, J. S. Jurvelin, U. Väätäinen, and H. J. Helminen, "Normal and pathological adaptations of articular cartilage to joint loading.," *Scandinavian Journal of Medicine & Science in Sports*, vol. 10, pp. 186–98, aug 2000.

[175] D. F. McWilliams, B. F. Leeb, S. G. Muthuri, M. Doherty, and W. Zhang, "Occupational risk factors for osteoarthritis of the knee: A meta-analysis," *Osteoarthritis and Cartilage*, vol. 19, no. 7, pp. 829–839, 2011.

[176] W. P. Chan, G.-S. Huang, S.-M. Hsu, Y.-C. Chang, and W.-P. Ho, "Radiographic joint space narrowing in osteoarthritis of the knee: relationship to meniscal tears and duration of pain.," *Skeletal Radiology*, vol. 37, pp. 917–22, oct 2008.

[177] F. Roemer and A. Guermazi, "Osteoarthritis Year in Review 2014: imaging," *Osteoarthritis and Cartilage*, vol. 22, no. 12, pp. 2003–2012, 2014.

[178] A. Williams, A. Gillis, C. McKenzie, B. Po, L. Sharma, L. Micheli, B. McKeon, and D. Burstein, "Glycosaminoglycan distribution in cartilage as determined by delayed gadolinium-enhanced MRI of cartilage (dGEMRIC): potential clinical applications.," *American Journal of Roentgenology*, vol. 182, pp. 167–72, jan 2004.

[179] Y. Shafieyan, N. Khosravi, M. Moeini, and T. M. Quinn, "Diffusion of MRI and CT contrast agents in articular cartilage under static compression.," *Biophysical journal*, vol. 107, no. 2, pp. 485–92, 2014.

[180] D. Burstein, J. Velyvis, K. T. Scott, K. W. Stock, Y. J. Kim, D. Jaramillo, R. D. Boutin, and M. L. Gray, "Protocol issues for delayed Gd(DTPA)(2-)-enhanced MRI (dGEMRIC) for clinical evaluation of articular cartilage.," *Magnetic Resonance in Medicine*, vol. 45, pp. 36–41, jan 2001.

[181] C. J. Tiderius, L. E. Olsson, P. Leander, O. Ekberg, and L. Dahlberg, "Delayed gadolinium-enhanced MRI of cartilage (dGEMRIC) in early knee osteoarthritis.," *Magnetic Resonance in Medicine*, vol. 49, pp. 488–92, mar 2003.

[182] A. S. Kallioniemi, J. S. Jurvelin, M. T. Nieminen, M. J. Lammi, and J. Töyräs, "Contrast agent enhanced pQCT of articular cartilage.," *Physics in Medicine and Biology*, vol. 52, pp. 1209–19, feb 2007.

[183] A. W. Palmer, R. E. Guldberg, and M. E. Levenston, "Analysis of cartilage matrix fixed charge density and three-dimensional morphology via contrast-enhanced

microcomputed tomography.," *Proceedings of the National Academy of Sciences of the United States of America*, vol. 103, pp. 19255–60, dec 2006.

[184] R. A. Stockwell and J. E. Scott, "Distribution of acid glycosamino-glycans in human articular cartilage," *Nature*, vol. 215, pp. 1376–1378, 1967.

[185] J. Arokoski, I. Kiviranta, J. Jurvelin, M. Tammi, and H. J. Helminen, "Long-distance running causes site-dependent decrease of cartilage glycosaminoglycan content in the knee joints of beagle dogs.," *Arthritis and Rheumatism*, vol. 36, pp. 1451–9, oct 1993.

[186] I. Kiviranta, J. Jurvelin, M. Tammi, A. M. Säämänen, and H. J. Helminen, "Microspectrophotometric quantitation of glycosaminoglycans in articular cartilage sections stained with Safranin O.," *Histochemistry*, vol. 82, pp. 249–55, jan 1985.

[187] M. J. Palmoski, R. A. Colyer, and K. D. Brandt, "Joint motion in the absence of normal loading does not maintain normal articular cartilage.," *Arthritis and Rheumatism*, vol. 23, pp. 325–34, mar 1980.

[188] L. Rosenberg, "Chemical Basis for the Histological Use of Safranin O in the Study of Articular Cartilage of Safranin of Articular for the Study Cartilage," *The Journal of Bone & Joint Surgery*, vol. 53-A, no. 1, pp. 69–82, 1971.

[189] D. J. Goldstein and R. W. Horobin, "Surface staining of cartilage by Alcian blue, with reference to the role of microscopic dye aggregates in histological staining.," *The Histochemical Journal*, vol. 6, pp. 175–84, mar 1974.

[190] K. B. Taylor and G. M. Jeffree, "A new basic metachromatic dye, 1,9-dimethyl methylene blue.," *The Histochemical Journal*, vol. 1, pp. 199–204, mar 1969.

[191] C. J. Handley, "Assay of proteoglycan degradation," *Methods in Enzymology*, vol. 248, pp. 47–58, 1995.

[192] R. W. Farndale, C. A. Sayers, and A. J. Barrett, "A direct spectrophotometric microassay for sulfated glycosaminoglycans in cartilage cultures.," *Connective Tissue Research*, vol. 9, pp. 247–8, jan 1982.

[193] V. J. Coulson-Thomas and T. F. Gesteira, "Dimethylmethylene Blue Assay (DMMB)," *Bio-Protocol*, vol. 4, pp. 18–21, 2014.

[194] J. S. Mort and Roughley Peter J, "Measurement of Glycosaminoglycan Release from Cartilage Explants," in *Arthritis Research. Methods and Protocols* (A. P. Cope, ed.), ch. 12, pp. 201–209, New Yersey: Humana Press, 2007.

[195] R. F. Loeser, "Osteoarthritis year in review 2013: biology," *Osteoarthritis and Cartilage*, vol. 21, no. 10, pp. 1436–1442, 2013.

[196] M. Z. C. Ruan, A. Erez, K. Guse, B. Dawson, T. Bertin, Y. Chen, M.-M. Jiang, J. Yustein, F. Gannon, and B. H. L. Lee, "Proteoglycan 4 expression protects against the development of osteoarthritis," *Science Translational Medicine*, vol. 5, no. 176, pp. 1–16, 2013.

[197] M. a. Fernandez-Yague, S. A. Abbah, L. Mcnamara, D. I. Zeugolis, A. Pandit, and M. J. Biggs, "Biomimetic approaches in bone tissue engineering: Integrating biological and physicomechanical strategies," *Advanced Drug Delivery Reviews*, 2014.

[198] W. Wilson, C. C. van Donkelaar, B. van Rietbergen, and R. Huiskes, "A fibril-reinforced poroviscoelastic swelling model for articular cartilage.," *Journal of Biomechanics*, vol. 38, pp. 1195–204, jun 2005.

[199] G. A. Ateshian and H. Wang, "A theoretical solution for the frictionless rolling contact of cylindrical biphasic articular cartilage layers," *Journal of Biomechanics*, vol. 28, no. 11, pp. 1341–1355, 1995.

[200] G. A. Ateshian, "The role of interstitial fluid pressurization in articular cartilage lubrication.," *Journal of Biomechanics*, vol. 42, pp. 1163–76, jun 2009.

[201] M. A. Soltz and G. A. Ateshian, "Experimental verification and theoretical prediction of cartilage interstitial fluid pressurization at an impermeable contact interface in confined compression.," *Journal of Biomechanics*, vol. 31, pp. 927–34, oct 1998.

[202] R. A. Bank, M. Soudry, A. Maroudas, J. Mizrahi, and J. M. TeKoppele, "The increased swelling and instantaneous deformation of osteoarthritic cartilage is highly correlated with collagen degradation.," *Arthritis and Rheumatism*, vol. 43, pp. 2202–10, oct 2000.

[203] G. A. Ateshian, C. R. Henak, and J. A. Weiss, "Toward patient-specific articular contact mechanics," *Journal of Biomechanics*, vol. 48, no. 5, pp. 779–786, 2015.

[204] P. J. Basser, R. Schneiderman, R. a. Bank, E. Wachtel, and a. Maroudas, "Mechanical properties of the collagen network in human articular cartilage as measured by osmotic stress technique.," *Archives of biochemistry and biophysics*, vol. 351, no. 2, pp. 207–219, 1998.

[205] A. Maroudas, "Physicochemical properties of cartilage in the light of ion exchange theory.," *Biophysical Journal*, vol. 8, pp. 575–95, may 1968.

[206] J. Jurvelin, I. Kiviranta, A. M. Säämänen, M. Tammi, and H. J. Helminen, "Indentation stiffness of young canine knee articular cartilage–influence of strenuous joint loading.," *Journal of Biomechanics*, vol. 23, pp. 1239–46, jan 1990.

[207] A. Oloyede, R. Flachsmann, and N. D. Broom, "The dramatic influence of loading velocity on the compressive response of articular cartilage.," *Connective tissue research*, vol. 27, no. 4, pp. 211–224, 1992.

[208] N. D. Broom and C. a. Poole, "Articular cartilage collagen and proteoglycans. Their functional interdependency.," *Arthritis and rheumatism*, vol. 26, no. 9, pp. 1111–1119, 1983.

[209] R. K. Korhonen, M. S. Laasanen, J. Töyräs, R. Lappalainen, H. J. Helminen, and J. S. Jurvelin, "Fibril reinforced poroelastic model predicts specifically mechanical behavior of normal, proteoglycan depleted and collagen degraded articular cartilage," *Journal of Biomechanics*, vol. 36, pp. 1373–1379, sep 2003.

[210] J. Rieppo, J. Töyräs, M. T. Nieminen, M. Hyttinen, H. J. Helminen, and J. S. Jurvelin, "Quantitative microscopical and mechanical analyses reveal sensitively structural and functional changes of articular cartilage after enzymatic degrada-

tion using collagenase," in *46th Annual Meeting, Orthopaedic Research Society*, pp. March 12–15, 2000.

[211] V. Mow, D. Fithian, and M. Kelly, "Fundamentals of articular cartilage and meniscus biomechanics," in *Articular cartilage and knee joint function: basic science and arthroscopy* (J. W. Ewing, ed.), pp. 1–18, New York: Raven Press, 1990.

[212] D. L. Bader, G. E. Kempson, J. Egan, W. Gilbey, and A. J. Barrett, "The effects of selective matrix degradation on the short-term compressive properties of adult human articular cartilage.," *Biochimica et Biophysica Acta*, vol. 1116, pp. 147–54, apr 1992.

[213] M. Laasanen, J. Töyräs, R. Korhonen, J. Rieppo, S. Saarakkala, M. Nieminen, J. Hirvonen, and J. Jurvelin, "Biomechanical properties of knee articular cartilage," *Biorheology*, vol. 40, no. 1-3, pp. 133–140, 2003.

[214] R. Shirazi, A. Shirazi-Adl, and M. Hurtig, "Role of cartilage collagen fibrils networks in knee joint biomechanics under compression," *Journal of biomechanics*, vol. 41, no. 16, pp. 3340–8, 2008.

[215] B. Cohen, W. Lai, and V. Mow, "A transversely isotropic biphasic model for unconfined compression of growth and chondroepiphysis," *Journal of Biomechanical Engineering2*, vol. 41, no. 16, pp. 3340–3348, 2008.

[216] L. P. Li, M. D. Buschmann, and A. Shirazi-Adl, "Strain-rate Dependent Stiffness of Articular Cartilage in Unconfined Compression," *Journal of Biomechanical Engineering*, vol. 125, no. 2, p. 161, 2003.

[217] C. Glaser and R. Putz, "Functional anatomy of articular cartilage under compressive loading Quantitative aspects of global, local and zonal reactions of the collagenous network with respect to the surface integrity," *Osteoarthritis and Cartilage*, vol. 10, no. 2, pp. 83–99, 2002.

[218] F. Guilak, W. R. Jones, H. P. Ting-Beall, and G. M. Lee, "The deformation behavior and mechanical properties of chondrocytes in articular cartilage.," *Osteoarth-*

*ritis and Cartilage / OARS, Osteoarthritis Research Society*, vol. 7, pp. 59–70, jan 1999.

[219] T. Aigner, S. Soder, P. Gebhard, A. McAliden, and J. Haag, "Mechanisms of Disease role of chondrocytes in the pathogenesis of OA - structure, caos and senescence," *Nature Clinical Practice Rheumatology*, vol. 3, pp. 391–399, 2007.

[220] L. Xie, A. S. P. Lin, R. E. Guldberg, and M. E. Levenston, "Nondestructive assessment of sGAG content and distribution in normal and degraded rat articular cartilage via EPIC-microCT.," *Osteoarthritis and Cartilage / OARS, Osteoarthritis Research Society*, vol. 18, pp. 65–72, jan 2010.

[221] D. H. Gershuni and S. C. Kuei, "Articular cartilage deformation following experimental synovitis in the rabbit hip.," *Journal of Orthopaedic Research*, vol. 1, pp. 313–8, jan 1984.

[222] G. Jones, M. Glisson, K. Hynes, and F. Cicuttini, "Sex and site differences in cartilage development: a possible explanation for variations in knee osteoarthritis in later life.," *Arthritis and Rheumatism*, vol. 43, pp. 2543–9, nov 2000.

[223] P. Julkunen, P. Kiviranta, W. Wilson, J. S. Jurvelin, and R. K. Korhonen, "Characterization of articular cartilage by combining microscopic analysis with a fibril-reinforced finite-element model.," *Journal of Biomechanics*, vol. 40, pp. 1862–70, jan 2007.

[224] A. Thambyah, J. C. H. Goh, and S. D. De, "Contact stresses in the knee joint in deep flexion.," *Medical Engineering and Physics*, vol. 27, pp. 329–35, may 2005.

[225] B. A. Rogers, C. L. Murphy, S. R. Cannon, and T. W. R. Briggs, "Topographical variation in glycosaminoglycan content in human articular cartilage.," *The Journal of Bone and Joint Surgery. British Volume*, vol. 88, pp. 1670–4, dec 2006.

[226] M. L. Roemhildt, K. M. Coughlin, G. D. Peura, G. J. Badger, D. Churchill, B. C. Fleming, and B. D. Beynnon, "Effects of increased chronic loading on

articular cartilage material properties in the Lapine tibio-femoral joint," *Journal of Biomechanics*, vol. 43, no. 12, pp. 2301–2308, 2010.

[227] M. O. Jortikka, R. I. Inkinen, M. I. Tammi, J. J. Parkkinen, J. Haapala, I. Kiviranta, H. J. Helminen, and M. J. Lammi, "Immobilisation causes longlasting matrix changes both in the immobilised and contralateral joint cartilage.," *Annals of the Rheumatic Diseases*, vol. 56, pp. 255–61, apr 1997.

[228] J. Jurvelin, I. Kiviranta, M. Tammi, and H. J. Helminen, "Effect of Physical Exercise on Indentation Stiffness of Articular Cartilage in the Canine Knee," *International Journal of Sports Medicine*, vol. 7, no. 2, pp. 106–110, 1986.

[229] H. J. Helminen, M. M. Hyttinen, M. J. Lammi, J. P. A. Arokoski, T. Lapvetelainen, J. Jurvelin, I. Kiviranta, and M. I. Tammi, "Regular joint loading in youth assists in the establishment and strengthening of the collagen network of articular cartilage and prevention of OA later in life," *Journal of Bone Mineral Metabolism*, vol. 18, pp. 245–257, 2000.

[230] J. Francuski, A. Radovanović, N. Andrić, V. Krstić, D. Bogdanović, V. Hadžić, V. Todorović, M. L. Macanović, S. S. Petit, S. Beck-Cormier, J. Guicheux, O. Gauthier, and M. K. Filipović, "Age-related Changes in the Articular Cartilage of the Stifle Joint in Non-working and Working German Shepherd Dogs," *Journal of Comparative Pathology*, vol. 151, no. 4, pp. 363–374, 2014.

[231] F. Eckstein, S. Faber, R. Mühlbauer, J. Hohe, K.-H. Englmeier, M. Reiser, and R. Putz, "Functional adaptation of human joints to mechanical stimuli.," *Osteoarthritis and Cartilage / OARS, Osteoarthritis Research Society*, vol. 10, pp. 44–50, jan 2002.

[232] J. Jurvelin, I. Kiviranta, M. Tammi, and J. Helminen, "Softening of Canine Articular Cartilage After Immobilization of the Knee Joint," *Clinical Orthopaedic and Related Research*, vol. 207, no. 6, pp. 246–252., 1986.

[233] A.-M. Säämänen, I. Kiviranta, J. Jurvelin, H. J. Helminen, and M. Tammi, "Proteoglycan and collagen alterations in canine knee articular cartilage following

20 km daily running exercise for 15 weeks.," *Connective Tissue Research*, vol. 30, pp. 191–201, jan 1994.

[234] C. B. Little, P. Ghosh, and R. Rose, "The strenuous versus moderate exercise on the metabolism of proteoglycans in articular cartilage from different weight-bearing regions of the equine third carpal," *Osteoarthritis and Cartilage*, vol. 5, no. 1997, pp. 161–172, 1997.

[235] I. Kiviranta, M. Tammi, J. Jurvelin, J. Arokoski, A. M. Säämänen, and H. J. Helminen, "Articular cartilage thickness and glycosaminoglycan distribution in the canine knee joint after strenuous running exercise.," *Clinical Orthopaedic and Related Research*, vol. 283, no. 10, pp. 302–308, 1992.

[236] R. Oettmeier, J. Arokoski, A. J. Roth, H. J. Helminen, M. Tammi, and K. Abendroth, "Quantitative study of articular cartilage and subchondral bone remodeling in the knee joint of dogs after strenuous running training," *Journal of Bone and Mineral Research*, vol. 7, no. S2, pp. 419–424, 1992.

[237] J. L. Coleman, M. R. Widmyer, H. a. Leddy, G. M. Utturkar, C. E. Spritzer, C. T. Moorman III, F. Guilak, and L. E. DeFrate, "Diurnal variations in articular cartilage thickness and strain in the human knee," *Journal of Biomechanics*, vol. 46, pp. 541–547, 2012.

[238] U. M. Kujala, J. Kettunen, H. Paananen, T. Aalto, M. C. Battié, O. Impivaara, T. Videman, and S. Sarna, "Knee osteoarthritis in former runners, soccer players, weight lifters, and shooters.," *Arthritis and Rheumatism*, vol. 38, pp. 539–46, apr 1995.

[239] R. U. Repo and J. B. Finlay, "Survival after of Articular Cartilage Controlled Impact," *Journal of Bone and Joint Surgery*, vol. 59A, no. 8, pp. 1068–1076, 1977.

[240] J. F. Nishimuta and M. E. Levenston, "Response of cartilage and meniscus tissue explants to in vitro compressive overload," *Osteoarthritis and Cartilage*, vol. 20, no. 5, pp. 422–429, 2012.

[241] S. Park, R. Krishnan, S. B. Nicoll, and G. A. Ateshian, "Cartilage Interstitial Fluid Load Support in Unconfined Compression," *Journal of Biomechanics*, vol. 36, no. 12, pp. 1785–1796, 2003.

[242] V. Morel and T. M. Quinn, "Cartilage injury by ramp compression near the gel diffusion rate.," *Journal of Orthopaedic Research*, vol. 22, pp. 145–51, jan 2004.

[243] R. A. Magnussen, F. Guilak, and T. P. Vail, "Cartilage degeneration in post-collapse cases of osteonecrosis of the human femoral head: altered mechanical properties in tension, compression, and shear.," *Journal of Orthopaedic Research*, vol. 23, pp. 576–83, may 2005.

[244] P. J. Atkinson and R. C. Haut, "Subfracture insult to the human cadaver patellofemoral joint produces occult injury," *Journal of Orthopaedic Research*, vol. 13, no. 6, pp. 936–944, 1995.

[245] E. J. Miller, R. F. Riemer, T. L. Haut Donahue, and K. R. Kaufman, "Experimental validation of a tibiofemoral model for analyzing joint force distribution.," *Journal of Biomechanics*, vol. 42, pp. 1355–9, jul 2009.

[246] L. J. Borrelli, P. A. Torzilli, R. Grigiene, and D. L. Helfet, "Effect of impact load on articular cartilage: development of an intra-articular fracture model," *Journal of Orthopeadic Trauma*, vol. 11, no. 5, pp. 319–326, 1997.

[247] A. C. Gelber, M. C. Hochberg, L. A. Mead, N.-Y. Wang, and F. M. Wigley, "Joint injury in young adults and risk for subsequent knee and hip osteoarthritis," *Annals of Internal Medicine*, vol. 133, no. 16, pp. 321–328, 2000.

[248] V. C. Mow, M. C. Gibbs, W. M. Lai, W. B. Zhu, and K. A. Athanasiou, "Biphasic indentation of articular cartilage - II. A numerical algorithm and an experimental study," *Journal of Biomechanics*, vol. 22, no. 8/9, pp. 853–861, 1989.

[249] S. Saber-Samandari and K. a. Gross, "Effect of angled indentation on mechanical properties," *Journal of the European Ceramic Society*, vol. 29, pp. 2461–2467, sep 2009.

[250] C. Shi, H. Zhao, H. Huang, L. Xu, L. Ren, M. Bai, J. Li, and X. Hu, "Effects of Indenter Tilt on Nanoindentation Results of Fused Silica: an Investigation by Finite Element Analysis," *Materials Transactions*, vol. 54, no. 6, pp. 958–963, 2013.

[251] T. Lyyra-Laitinen, M. Niinimäki, J. Töyräs, R. Lindgren, I. Kiviranta, and J. S. Jurvelin, "Optimization of the arthroscopic indentation instrument for the measurement of thin cartilage stiffness," *Physics in Medicine and Biology*, vol. 44, pp. 2511–2524, 1999.

[252] J. G. Swadener, E. P. George, and G. M. Pharr, "The correlation of the indentation size effect measured with indenters of various shapes," *Journal of the Mechanics and Physics of Solids*, vol. 50, pp. 681–694, 2002.

[253] M. K. Baker and B. B. Seedhom, "The relationship of the compressive modulus of articular cartilage with its deformation response to cyclic loading," *Rheumatology*, vol. 40, pp. 274–284, 2001.

[254] D. E. Shepherd and B. B. Seedhom, "A technique for measuring the compressive modulus of articular cartilage under physiological loading rates with preliminary results," *Journal of Engineering in Medicine. Proceedings of the Institution of Mechanical Engineers. Part H.*, vol. 2, no. 211, pp. 155–65, 1997.

[255] E. 48/85, "Just Rollers plc, UK,"

[256] J. Kunz and M. Studer, "Determining the Modulus of Elasticity in Compression via the Shore A Hardness Theoretical Background," *Kunststoffe international*, no. 2, pp. 1–3, 2006.

[257] E. Radin, I. Paul, and M. Lowy, "A comparison of the dynamic force transmitting properties of subchondral bone and articular cartilage," *The Journal of Bone and Joint Surgery. American Volume*, vol. 52, no. 3, pp. 444–456, 1970.

[258] S. L.-Y. Woo, B. R. Simon, S. C. Kuei, and W. H. Akeson, "Quasi-Linear Viscoelastic Properties of Normal Articular Cartilage," *Journal Biomechanical Engineering*, vol. 102, no. 2, pp. 85–90, 1980.

[259] H. Mankin, V. Mow, J. Buckwalter, J. Iannotti, and A. Ratcliffe, "Form and function of articular cartilage," in *In Orthopedic Basic Science* (S. Simon, ed.), Chicago, IL: American Academy of Orthopedic Surgeons, 1994.

[260] H. Buckle, "The Science of Hardness Testing and its Research Applications," in *Microindentation Techniques in Material Science and Engineering* (P. J. Blau and B. R. Lawn, eds.), 1973.

[261] A. P. C. Choi, *Estimation of Young's Modulus and Poisson's Ratio of Soft Tissue using Indentation.* PhD thesis, The Hong Kong Polytechnic University, 2008.

[262] M. R. DiSilvestro and J.-K. F. Suh, "A cross-validation of the biphasic poroviscoelastic model of articular cartilage in unconfined compression, indentation, and confined compression.," *Journal of Biomechanics*, vol. 34, pp. 519–25, apr 2001.

[263] Q. Wang, Y.-Y. Yang, H.-J. Niu, W.-J. Zhang, Q.-J. Feng, and W.-F. Chen, "An ultrasound study of altered hydration behaviour of proteoglycan-degraded articular cartilage.," *BMC musculoskeletal disorders*, vol. 14, p. 289, jan 2013.

[264] K. L. Johnson, *Contact Mechanics.* Cambridge University Press, 9th ed., 1987.

[265] I. Sneddon, "The relation between load and penetration in the axisymmetric Boussinesq problem for a punch of arbitrary profile," *International Journal of Engineering Science*, vol. 3, no. 1, pp. 47–57, 1965.

[266] G. M. Pharr, W. C. Oliver, and F. R. Brotzen, "On the generality of the relationship among contact stiffness, contact area, and elastic modulus during indentation," *Journal of Materials Research*, vol. 7, pp. 613–617, jan 2011.

[267] D. E. Shepherd and B. B. Seedhom, "The 'instantaneous' compressive modulus of human articular cartilage in joints of the lower limb.," *Rheumatology (Oxford, England)*, vol. 38, pp. 124–32, feb 1999.

[268] N. Waters, "The indentation of thin rubber sheets by spherical indentors," *British Journal of Applied Physics*, vol. 16, pp. 557–563, 1965.

[269] J. T. Samosky, *Spatially-localized correlation of MRI and mechanical stiffness to assess cartilage integrity in the human tibial plateau.* PhD thesis, Massachusetts Institute of Technology, 2002.

[270] J. M. Bland and D. G. Altman, "Measurement Error," *British Medical Journal*, vol. 312, no. 7047, p. 1654, 1996.

[271] C. Little and P. Ghosh, "Variation in proteoglycan metabolism by articular chondrocytes in different joint regions is determined by post-natal mechanical loading," *Osteoarthritis and Cartilage*, vol. 5, pp. 49–62, jan 1997.

[272] J. Cohen, *Statistical power analysis for the behavioral sciences.* New Jersey: Lawrence Erlbaum, 2nd ed. ed., 1988.

[273] P. D. Rushfeldt, *Human hip joint geometry and the resulting pressure distribution.* PhD thesis, Massachussetts Institute of Technology, 1978.

[274] M. W. Klymkowsky and J. Hanken, "Whole-Mount Staining of Xenopus and Other Vertebrates," in *Methods in Cell Biology* (B. K. Kay and H. B. Peng, eds.), vol. 36, ch. 22, pp. 419–428, 429–441, San Diego: Academic Press, Inc., 1991.

[275] P. N. Bansal, N. S. Joshi, V. Entezari, M. W. Grinstaff, and B. D. Snyder, "Contrast enhanced computed tomography can predict the glycosaminoglycan content and biomechanical properties of articular cartilage.," *Osteoarthritis and Cartilage / OARS, Osteoarthritis Research Society*, vol. 18, pp. 184–91, mar 2010.

[276] P. N. Bansal, N. S. Joshi, V. Entezari, B. C. Malone, R. C. Stewart, B. D. Snyder, and M. W. Grinstaff, "Cationic contrast agents improve quantification of glycosaminoglycan (GAG) content by contrast enhanced CT imaging of cartilage.," *Journal of Orthopaedic Research*, vol. 29, pp. 704–9, may 2011.

[277] N. S. Joshi, P. N. Bansal, R. C. Stewart, B. D. Snyder, and M. W. Grinstaff, "Effect of contrast agent charge on visualization of articular cartilage using computed tomography: exploiting electrostatic interactions for improved sensitivity.," *Journal of the American Chemical Society*, vol. 131, pp. 13234–5, sep 2009.

[278] S. L. Bevill, P. L. Briant, M. E. Levenston, and T. P. Andriacchi, "Central and peripheral region tibial plateau chondrocytes respond differently to in vitro dynamic compression.," *Osteoarthritis and Cartilage / OARS, Osteoarthritis Research Society*, vol. 17, pp. 980–7, aug 2009.

[279] T. P. Andriacchi and E. J. Alexander, "Studies of human locomotion: past, present and future.," *Journal of Biomechanics*, vol. 33, pp. 1217–24, oct 2000.

[280] L. Sharma, J. Song, D. T. Felson, S. Cahue, E. Shamiyeh, and D. D. Dunlop, "The role of knee alignment in disease progression and functional decline in knee osteoarthritis.," *The Journal of the American Medical Association*, vol. 286, pp. 188–95, jul 2001.

[281] W. H. Simon, "Scale effects in animal joints. I. Articular cartilage thickness and compressive stress.," *Arthritis and Rheumatism*, vol. 13, no. 3, pp. 244–56, 1970.

[282] R. C. Appleyard, D. Burkhanrd, P. Ghosh, M. Cake, M. V. Swain, and G. A. C. Murrell, "Topographical analysis of the structural, biochemical and dynamic biomechanical properties of cartilage in an ovine model of osteoarthritis," *Osteoarthritis and Cartilage*, vol. 11, pp. 65–77, jan 2003.

[283] D. R. Carter and M. Wong, "Modelling cartilage mechanobiology.," *Philosophical Transactions of the Royal Society of London. Series B, Biological Sciences*, vol. 358, pp. 1461–1471, sep 2003.

[284] G. Li, S. E. Park, L. E. DeFrate, M. E. Schutzer, L. Ji, T. J. Gill, and H. E. Rubash, "The cartilage thickness distribution in the tibiofemoral joint and its correlation with cartilage-to-cartilage contact.," *Clinical Biomechanics (Bristol, Avon)*, vol. 20, pp. 736–44, aug 2005.

[285] C. B. Little, P. Ghosh, and C. R. Bellenger, "Topographic variation in biglycan and decorin synthesis by articular cartilage in the early stages of osteoarthritis: an experimental study in sheep.," *Journal of Orthopaedic Research*, vol. 14, pp. 433–44, may 1996.

[286] S. Slowman and K. Brandt, "Composition and glycosaminoglycan metabolism of articular cartilage from habitually loaded and habitually unloaded sites," *Arthritis & Rheumatism*, vol. 29, no. 1, pp. 88–94, 1986.

[287] N. G. Shrive, J. J. O'Connor, and J. W. Goodfellow, "Load-bearing in the knee joint.," *Clinical Orthopaedics and Related Research*, no. 131, pp. 279–87, 1978.

[288] F. Eckstein, S. Muller, S. C. Faber, K.-H. Englmeier, M. Reiser, and R. Putz, "Side differences of knee joint cartilage volume, thickness, and surface area, and correlation with lower limb dominance an MRI-based study," *Osteoarthritis and Cartilage*, vol. 10, pp. 914–921, dec 2002.

[289] S. Koo and T. P. Andriacchi, "A comparison of the influence of global functional loads vs. local contact anatomy on articular cartilage thickness at the knee.," *Journal of Biomechanics*, vol. 40, pp. 2961–6, jan 2007.

[290] P. N. Bansal, N. S. Joshi, V. Entezari, B. C. Malone, R. C. Stewart, B. D. Snyder, and M. W. Grinstaff, "Cationic contrast agents improve quantification of glycosaminoglycan (GAG) content by contrast enhanced CT imaging of cartilage.," *Journal of Orthopaedic Research*, pp. 1–6, dec 2010.

[291] D. E. Shepherd and B. B. Seedhom, "Thickness of human articular cartilage in joints of the lower limb.," *Annals of the Rheumatic Diseases*, vol. 58, pp. 27–34, jan 1999.

[292] R. C. Stewart, P. N. Bansal, B. D. Snyder, and M. W. Grinstaff, "Electrostatic Attraction between Charged Contrast Agents and Glycosaminoglycans Improves CT Imaging of Articular Cartilage," *ORS 2011 Annual Meeting*, no. 63, pp. 2011–2011, 2011.

[293] P. N. Bansal, N. S. Joshi, V. Entezari, B. C. Malone, R. C. Stewart, B. D. Snyder, and M. W. Grinstaff, "Supporting Information - Cationic Contrast agent improve quantification of glycosaminoglycan (GAG) content by Contrast Enhanced CT imaging of cartilage," *Personal and Ubiquitous Computing*, 2010.

[294] R. Rout, S. McDonnell, R. Benson, N. Athanasou, A. Carr, H. Doll, H. S. Gill, D. W. Murray, P. A. Hulley, and A. J. Price, "The histological features of anteromedial gonarthrosis–the comparison of two grading systems in a human phenotype of osteoarthritis.," *The Knee*, vol. 18, pp. 172–6, jun 2011.

[295] S. M. Elmore, L. Sokoloff, G. Norris, and P. Carmeci, "Nature of "imperfect" elasticity of articular cartilage," *Journal of Applied Physiology*, vol. 18, no. 2, pp. 393–396, 1963.

[296] P. D. Rushfeldt, R. W. Mann, and W. H. Harris, "Improved techniques for measuring in vitro the geometry and pressure distribution in the human acetabulum–I. Ultrasonic measurement of acetabular surfaces, sphericity and cartilage thickness.," *Journal of biomechanics*, vol. 14, no. 1979, pp. 253–260, 1981.

[297] J. Q. Yao and B. B. Seedhom, "Ultrasonic measurement of the thickness of human articular cartilage in situ.," *Rheumatology (Oxford, England)*, vol. 38, pp. 1269–1271, 1999.

[298] T. Franz, E. M. Hasler, R. Hagg, C. Weiler, R. P. Jakob, and P. Mainil-Varlet, "In situ compressive stiffness, biochemical composition, and structural integrity of articular cartilage of the human knee joint.," *Osteoarthritis and Cartilage / OARS, Osteoarthritis Research Society*, vol. 9, pp. 582–92, aug 2001.

[299] G. Li, L. E. DeFrate, S. E. Park, T. J. Gill, and H. E. Rubash, "In Vivo Articular Cartilage Contact Kinematics of the Knee: An Investigation Using Dual-Orthogonal Fluoroscopy and Magnetic Resonance Image-Based Computer Models," *American Journal of Sports Medicine*, vol. 33, pp. 102–107, jan 2005.

# Appendices

# Appendix A

# FIGURES OF SIX TIBIAL PLATEAUX

In this section figures corresponding to measurements performed on the six tibial plateaux (S1, S2, S3, S4, S5 and S6) are presented. These are: topographical surfaces, testing points, elastic modulus distribution, cartilage thickness and GAG values at each test point, GAG and thickness distribution at testing points and high resolution GAG concentration and cartilage thickness distribution maps, means of elastic modulus, GAG concentration, cartilage thickness and topographical high on each MMR and the 2nd derivative of high resolution maps of the Elastic modulus distribution

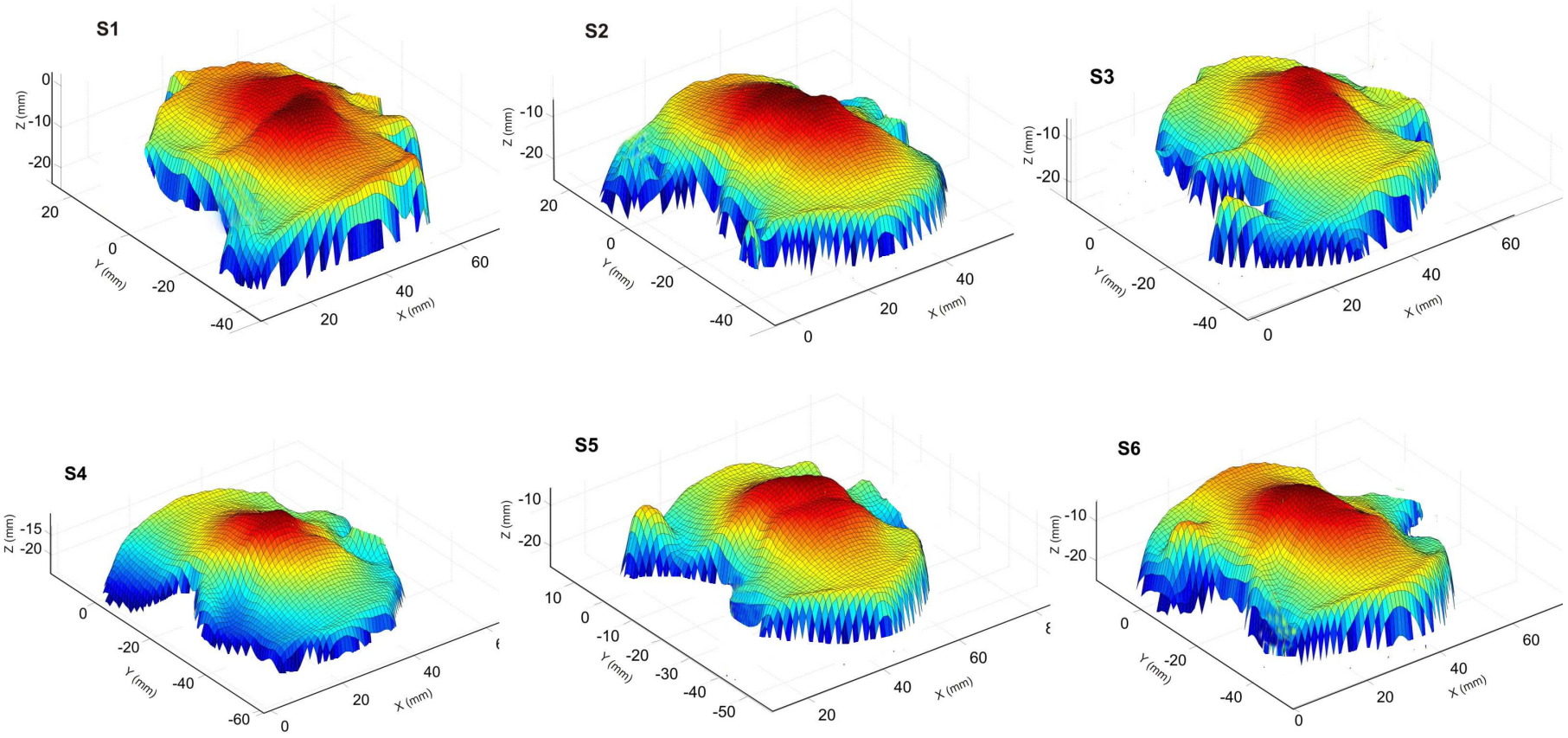


**Figure A.1:** Topography of tibial plateau obtained from scan using high resolution laser. The colors represent the height of the topographical surfaces of the different specimens: S1, S2, S3, S4, S5 and S6.

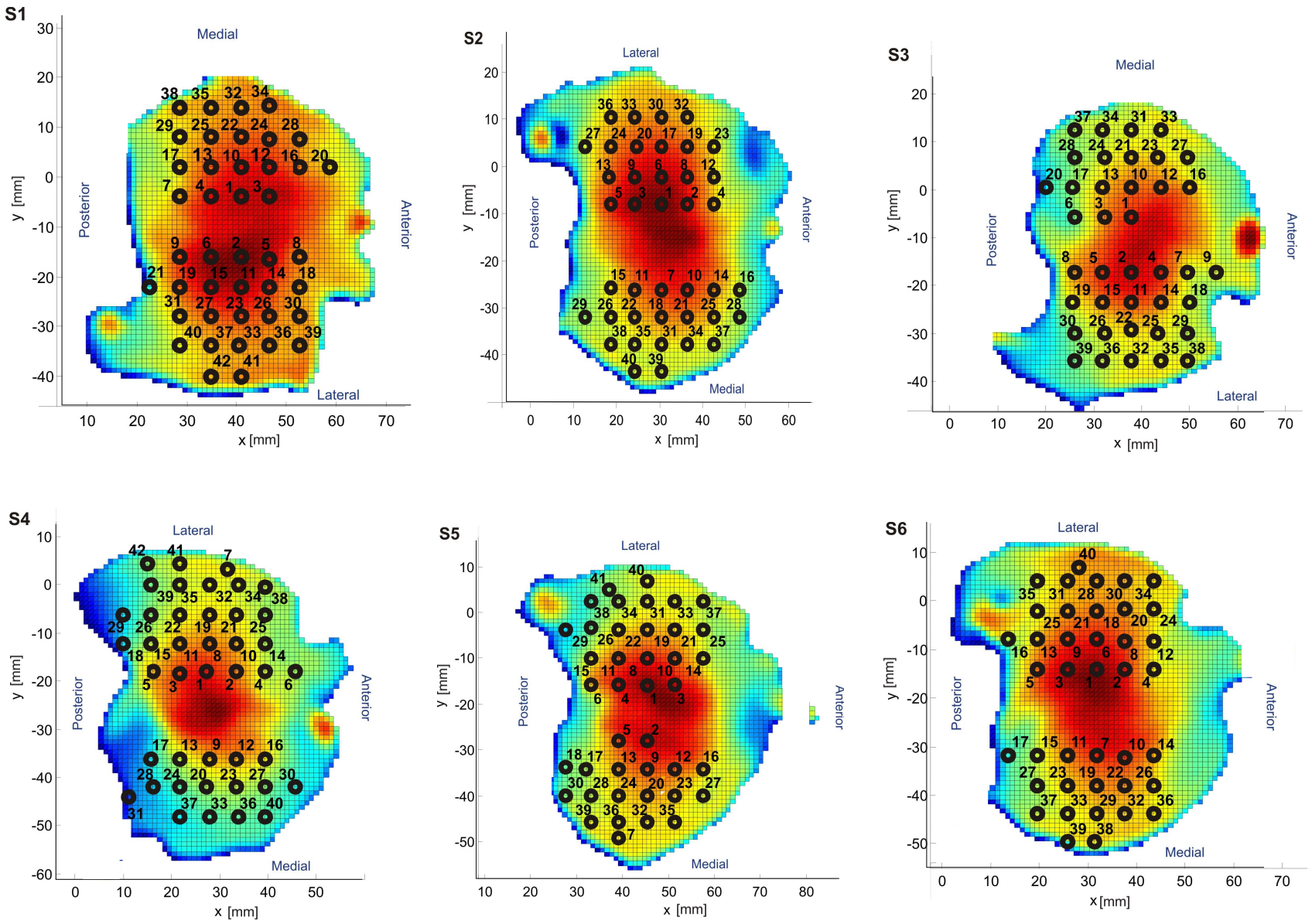


**Figure A.2:** Test points in specimens S1, S2, S3, S4, S5, S6. Four specimens (S2, S4, S5 and S6) were left knees, while S1 and S3 were right knees.

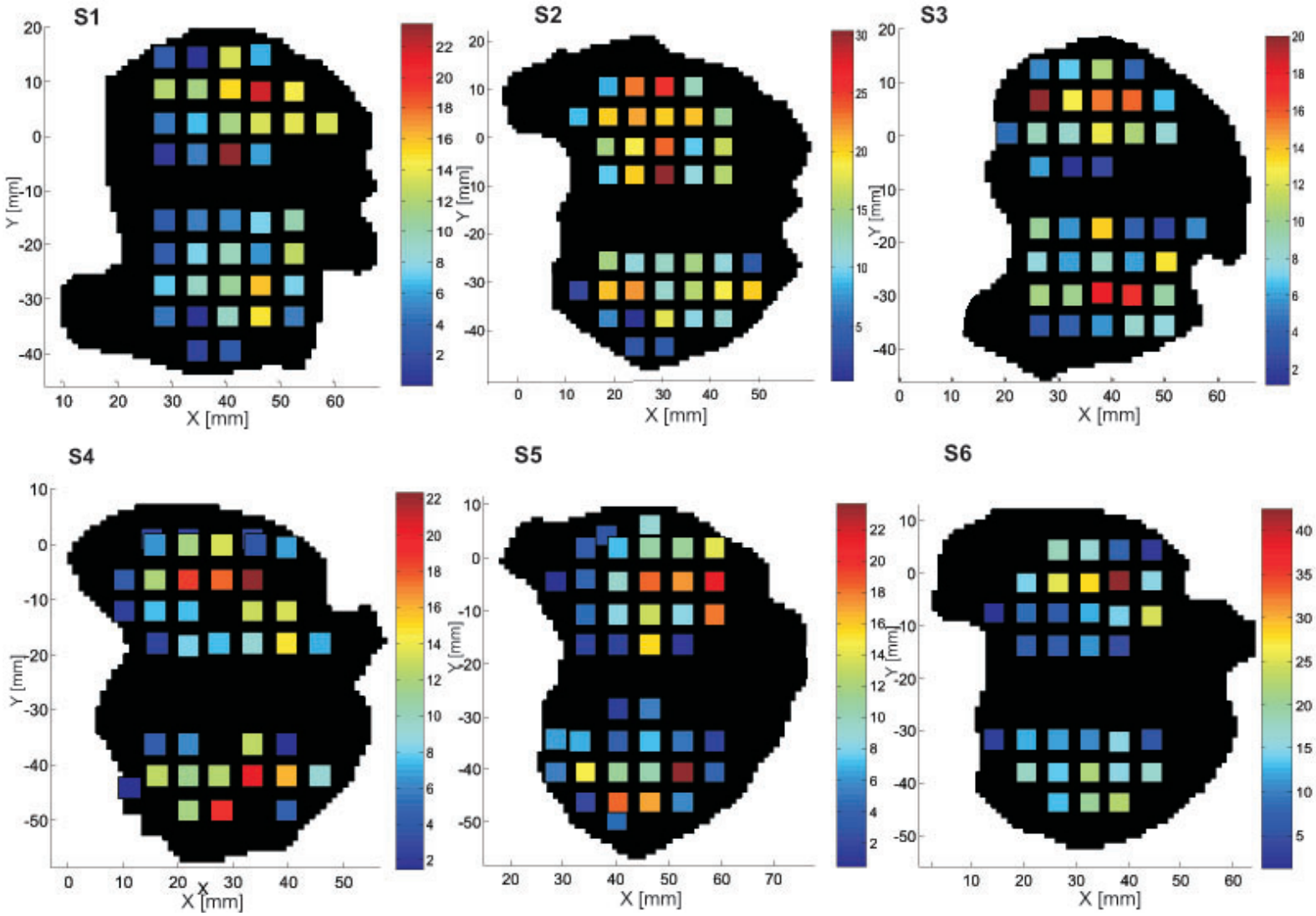


**Figure A.3:** Elastic modulus distribution at each test point in specimens S1, S2, S3, S4, S5. Values of E are shown in MPa units. Colours of each test point represent the values of E at each point. Red corresponds to the highest values while blue are the lowest.

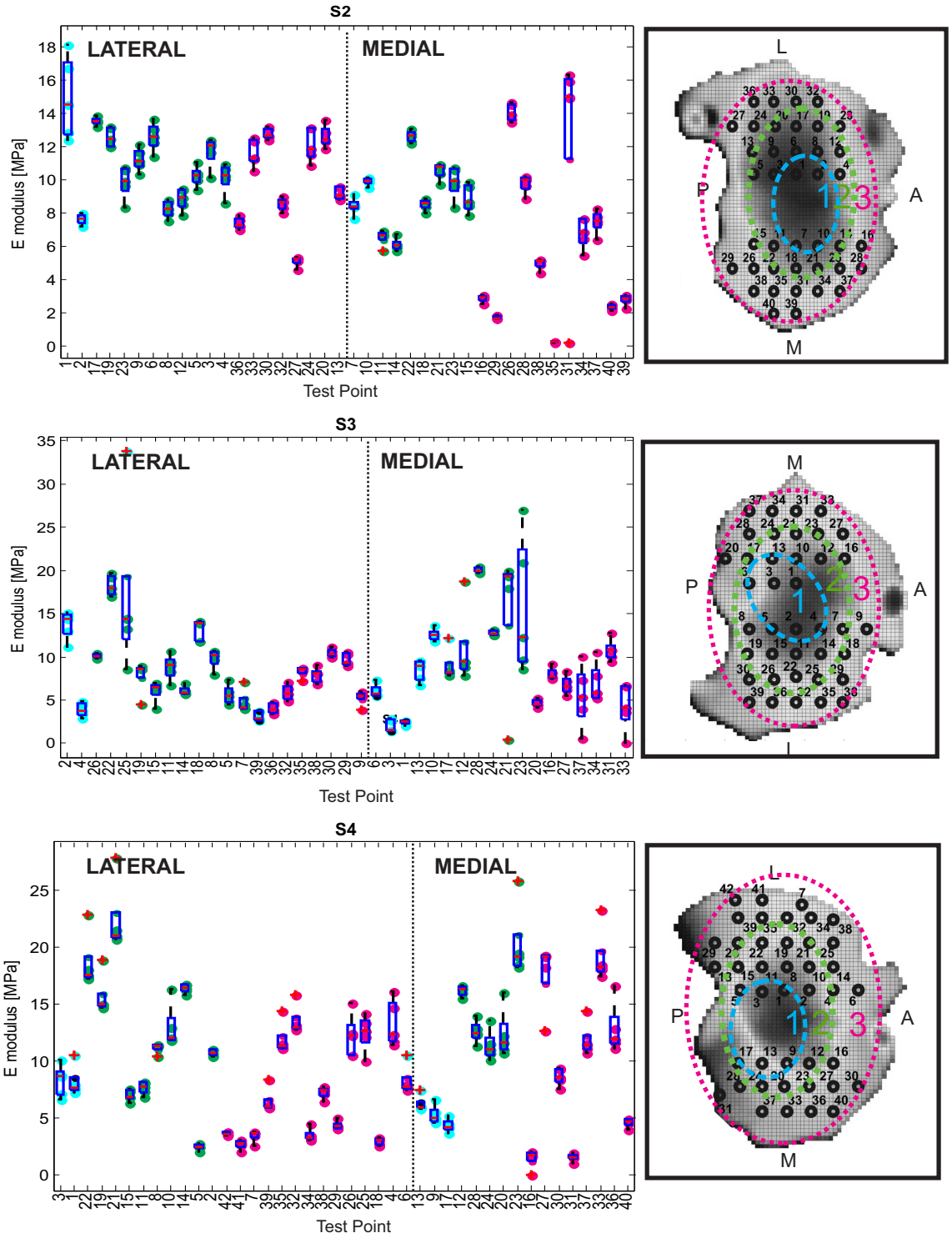


**Figure A.4:** Boxplot distribution of specimens S2, S3 and S4. This plot presents the different values of elastic modulus calculated from the repeated indentation tests at each point. Points are classified according to their position. To the left of the dotted line are the points located in the lateral compartment and to the right of the dotted line the medial compartment. The colours represent the ring the test points are located in: cyan the inner ring, pink the most external ring and green the middle ring. On top of the scattered points a box plot that highlights the mean elastic modulus value of each point and the upper and lower boundaries for repeated measurements is shown. Beside each boxplot a map of the tibial plateau with the location of the test points is shown.

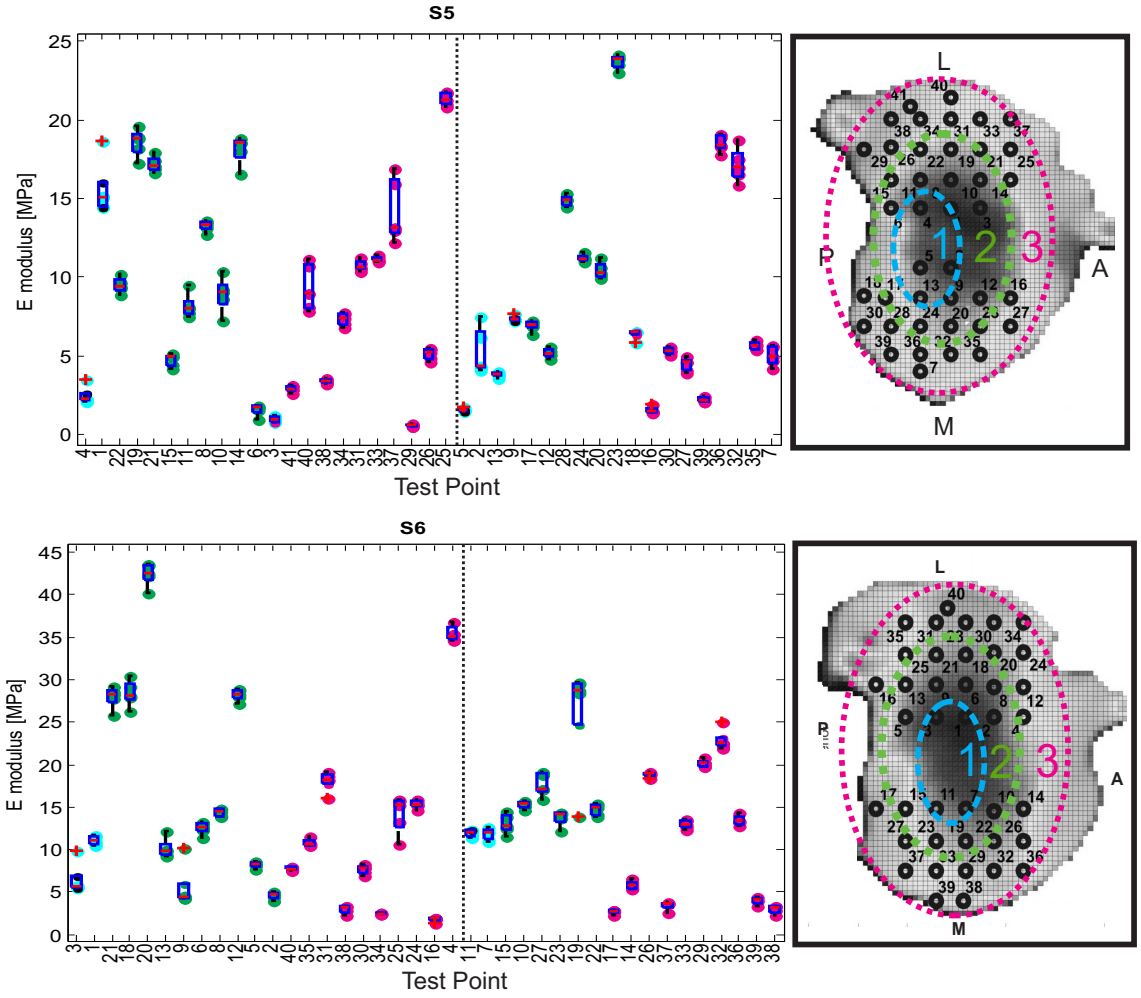


**Figure A.5:** Boxplot distribution of specimens S5 and S6. This plot presents the different values of elastic modulus calculated from the repeated indentation tests at each point. Points are classified according to their position. To the left of the dotted line are the points located in the lateral compartment and to the right of the dotted line the medial compartment. The colours represent the ring the test points are located in: cyan the inner ring, pink the most external ring and green the middle ring. On top of the scattered points a box plot that highlights the mean elastic modulus value of each point and the upper and lower boundaries for repeated measurements is shown. Beside each boxplot a map of the tibial plateau with the location of the test points is shown.

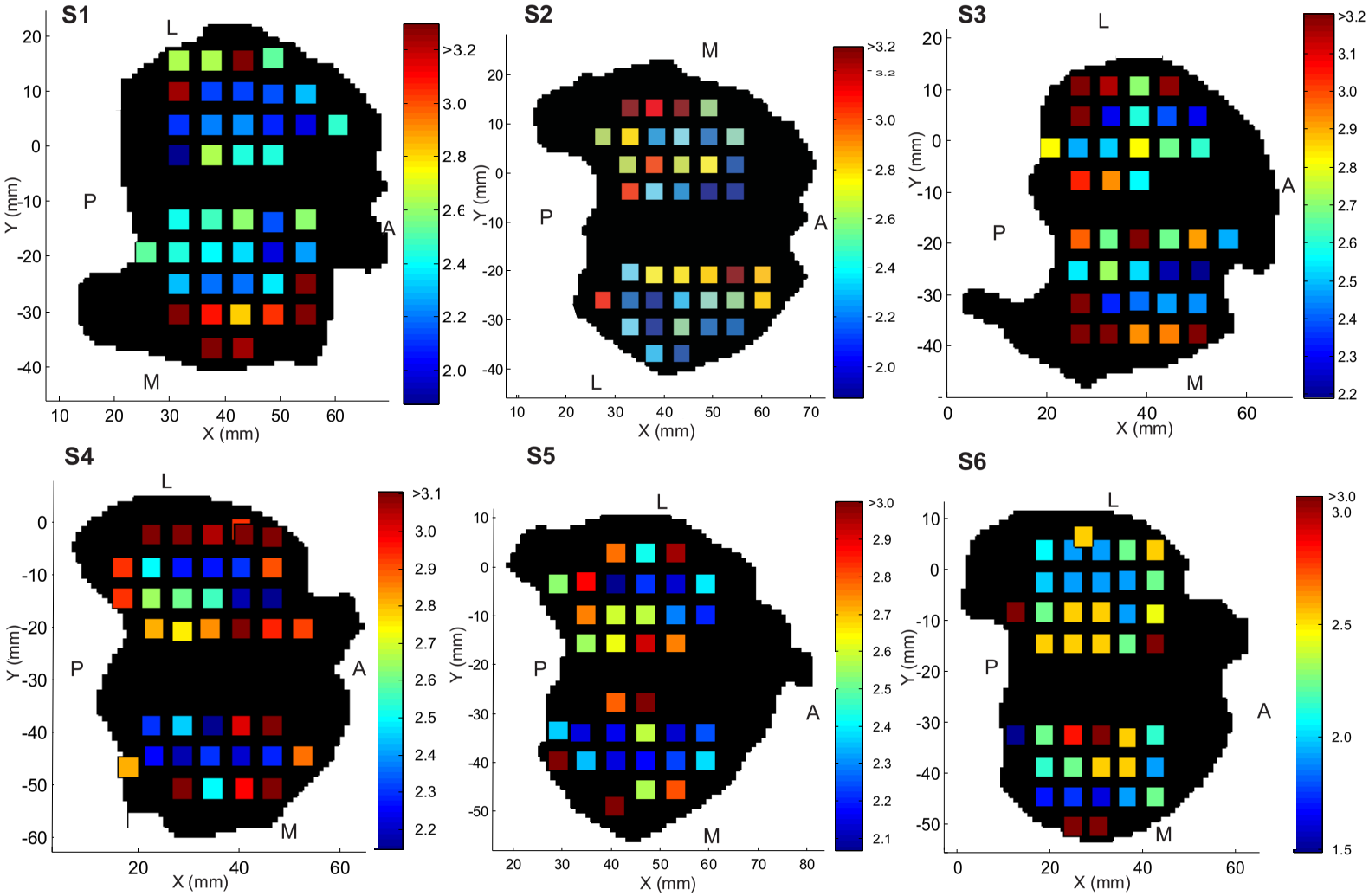


**Figure A.6:** Thickness measured by histological method at testing points in samples S1, S2, S3, S4, S5. The colour at each test point represents the cartilage thickness at corresponding position, where blue is the least thick and red is the thickest. The colour scale bar is given in millimetres.

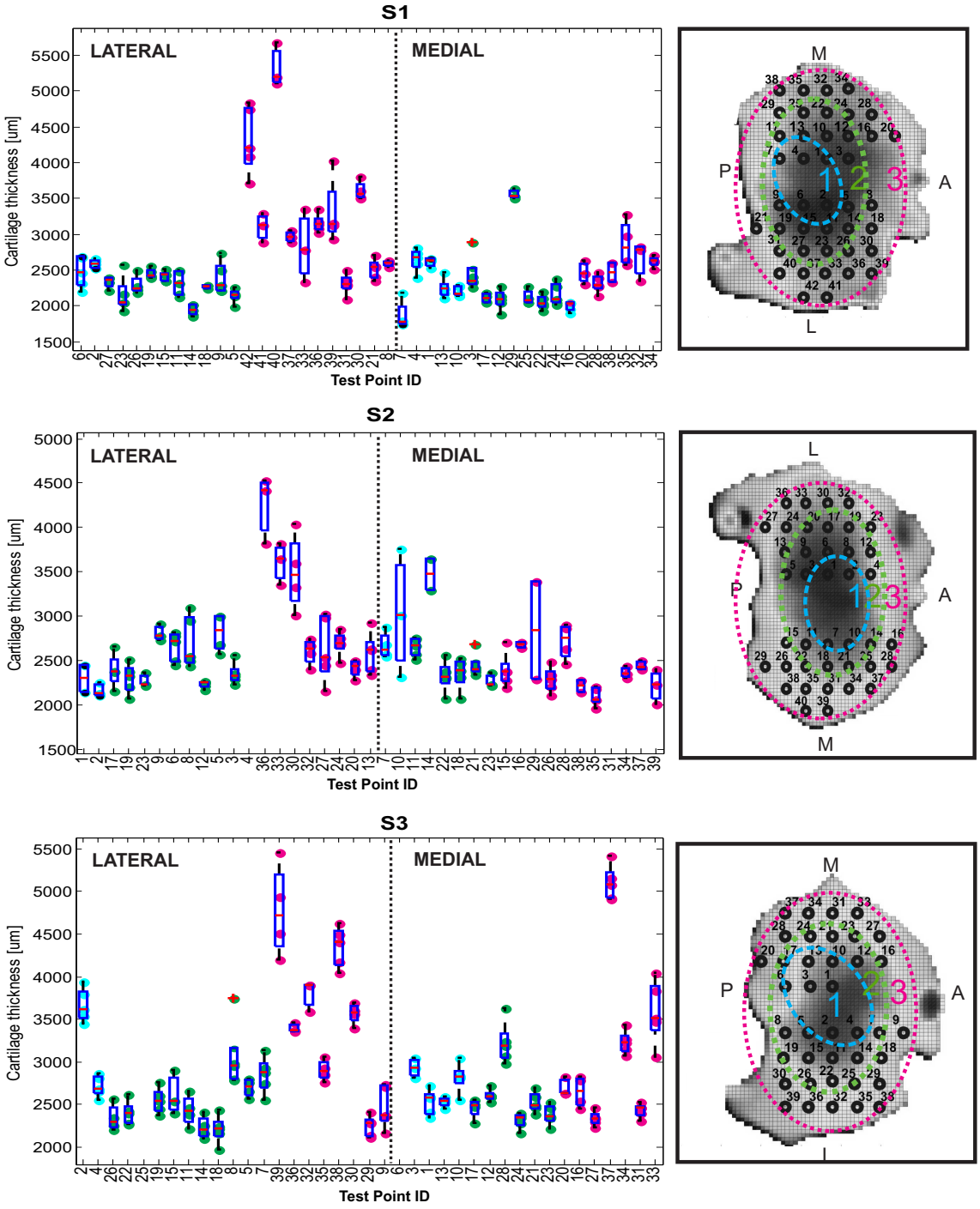


**Figure A.7:** Cartilage thickness values of repeated measurements and mean value at each test point in specimens S1, S2 and S3. Points are classified according to their position. To the left of the dotted line are the points located in the lateral compartment and to the right of the dotted line the medial compartment. The colours represent the ring the test points are located in: cyan the inner ring, pink the most external ring and green the middle ring. On top of the scattered points a box plot that highlights the mean elastic modulus value of each point and the upper and lower boundaries for repeated measurements is shown. Beside each boxplot a map of the tibial plateau with the location of the test points is shown.

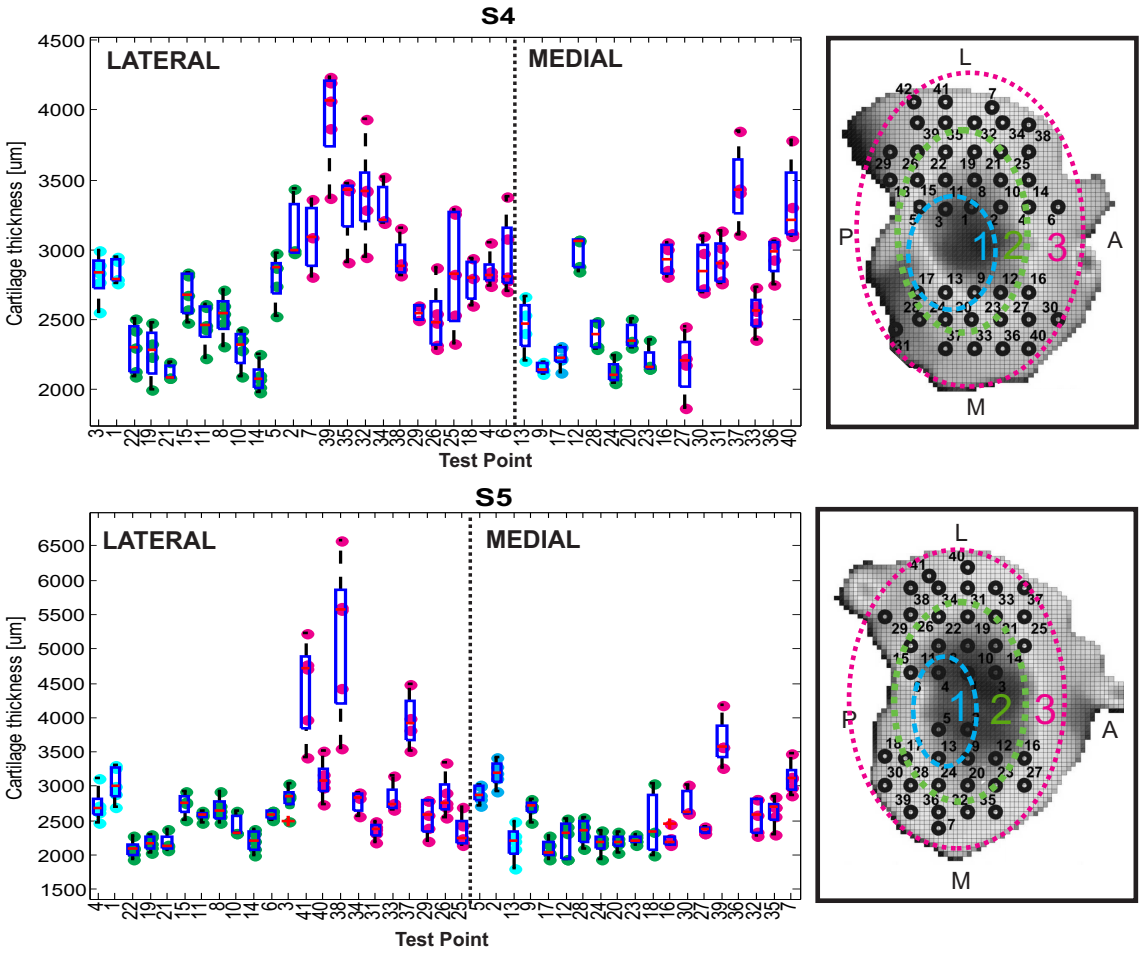


**Figure A.8:** Cartilage thickness values of repeated measurements and mean value at each test point in specimens S4 and S5. Points are classified according to their position. To the left of the dotted line are the points located in the lateral compartment and to the right of the dotted line the medial compartment. The colours represent the ring the test points are located in: cyan the inner ring, pink the most external ring and green the middle ring. On top of the scattered points a box plot that highlights the mean elastic modulus value of each point and the upper and lower boundaries for repeated measurements is shown. Beside each boxplot a map of the tibial plateau with the location of the test points is shown.

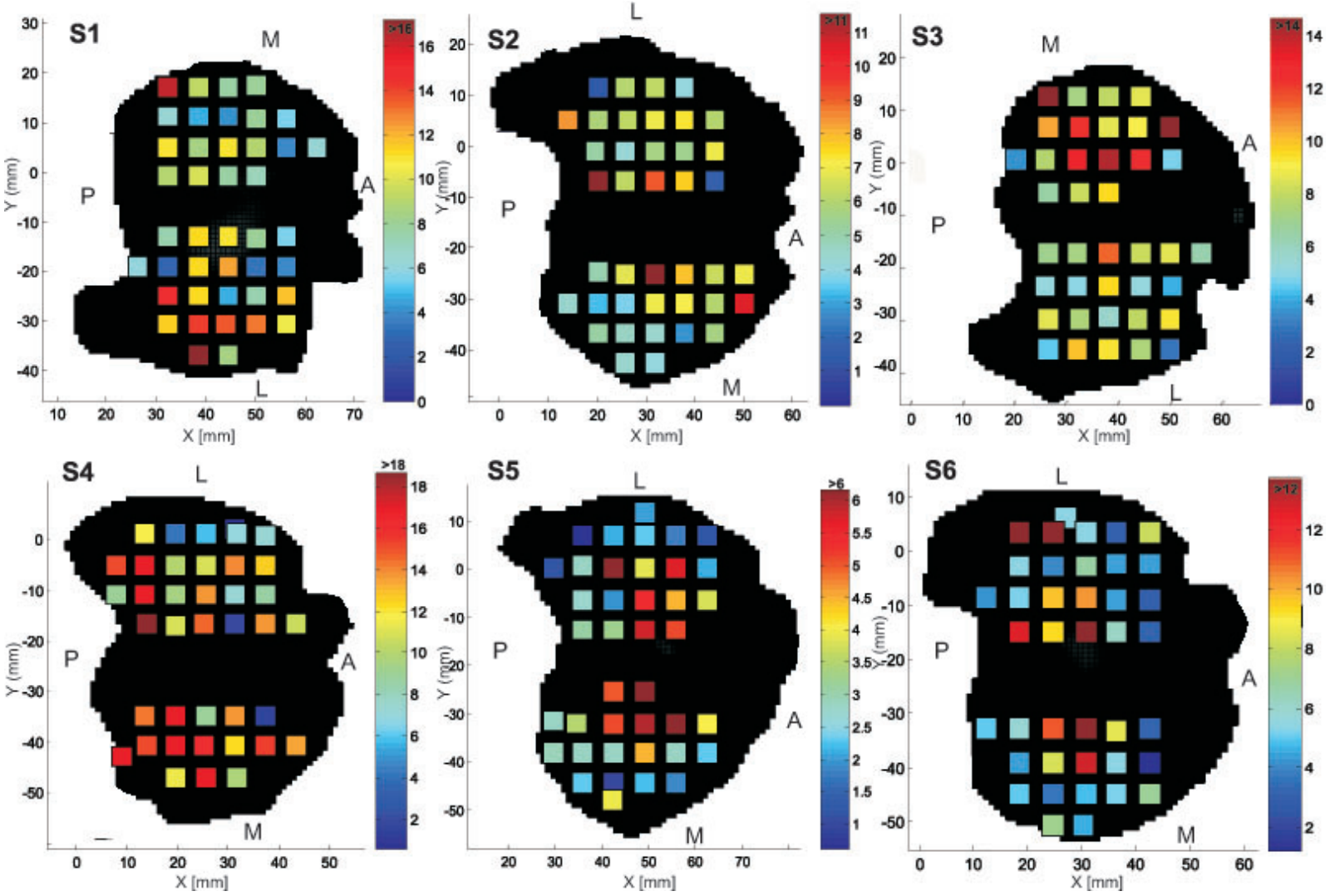


**Figure A.9:** GAG distribution at testing points in samples S1, S2, S3, S4, S5, S6

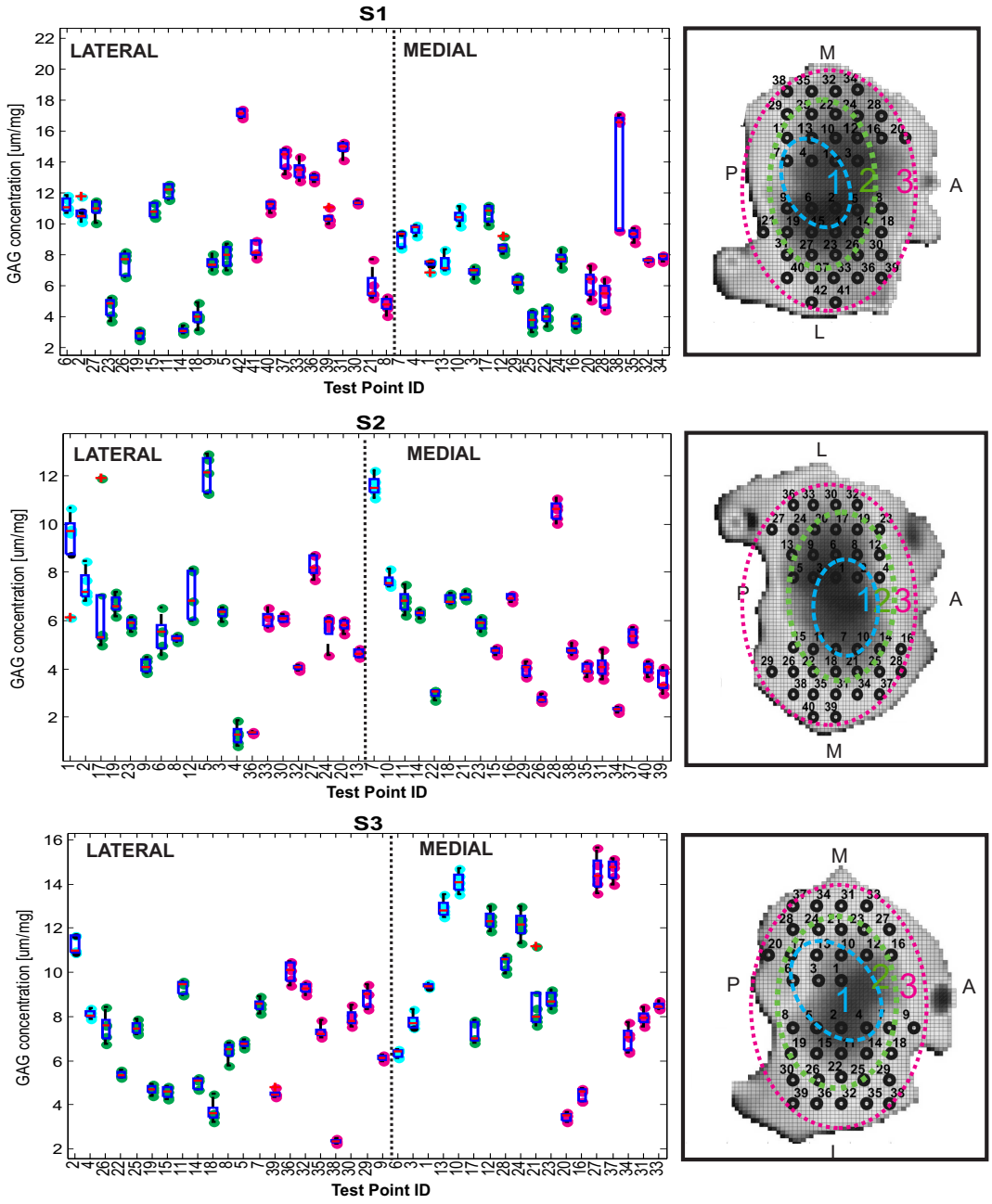


**Figure A.10:** Boxplot of the distribution of GAG concentration in specimens S1, S2 and S3. This plot presents the different values of GAG concentration calculated from DMMB assay at each point. Red are the highest GAG concentration values and blue are the lowest. On top of the scattered points a box plot that highlights the mean GAG concentration value of each point and the upper and lower boundaries for repeated measurements is shown. Beside each plot there is a map of the tibial plateau with the location of the test points.

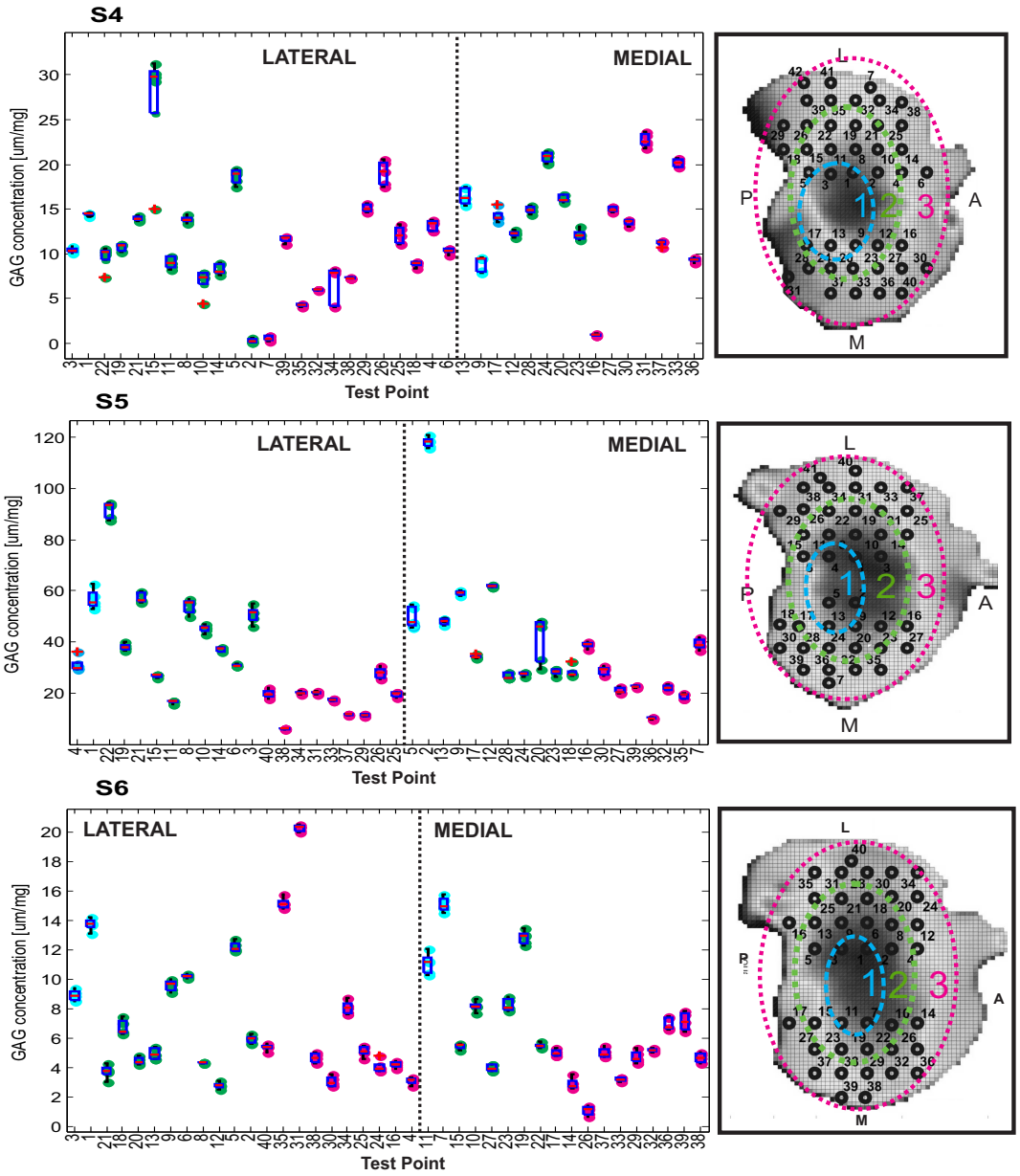


**Figure A.11:** Boxplot of the distribution GAG concentration in specimens S4, S5 and S6. This plot presents the different values of GAG concentration calculated from DMMB assay at each point. Red are the highest GAG concentration values and blue are the lowest. On top of the scattered points a box plot that highlights the mean GAG concentration value of each point and the upper and lower boundaries for repeated measurements is shown. Beside each plot there is a map of the tibial plateau with the location of the test points.

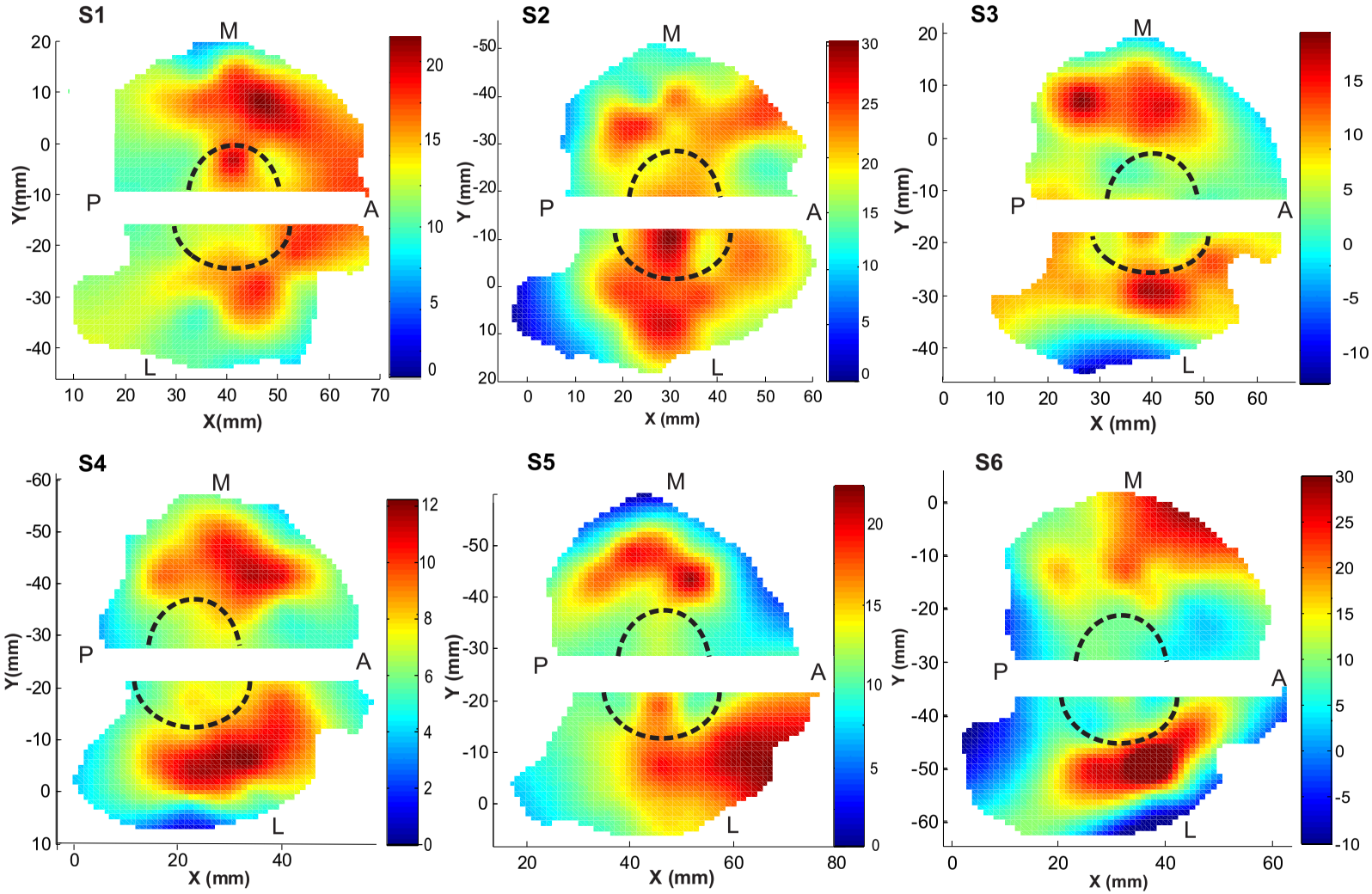


**Figure A.12:** Continuous elastic modulus distribution maps for specimens S1, S2, S3, S4, S5, S6. Colour bar shows the elastic modulus values in MPa, where red represents the highest elastic modulus values and blue the lowest. The dashed line represents the location of the menisci. The tibial eminence is blank since no points were tested in this area.

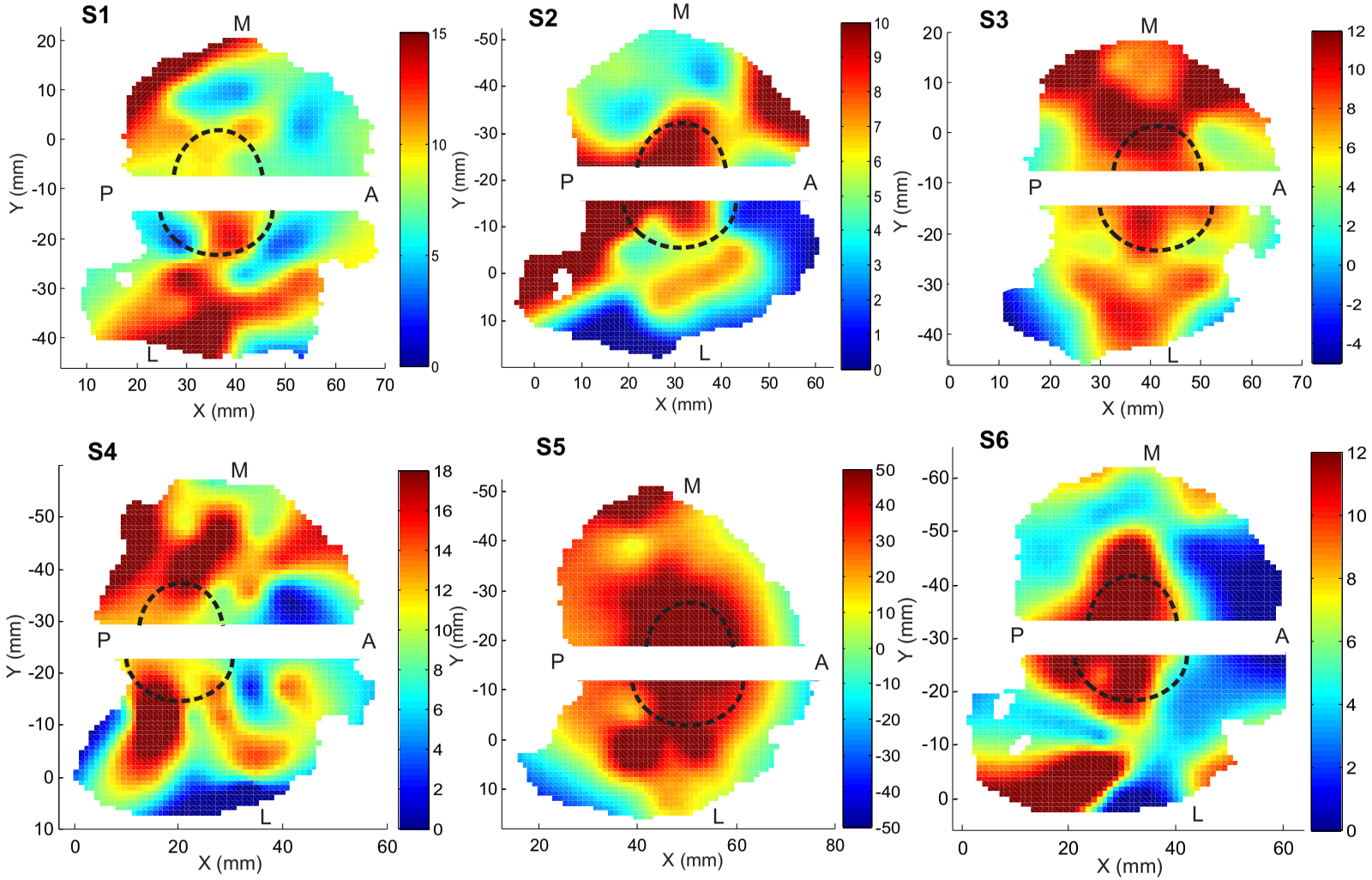


**Figure A.13:** High resolution GAG concentration distribution maps of specimens S1, S2, S3, S4, S5, S6. Colour bar shows the GAG concentration values in $\mu$m/mg, where red represent the highest GAG concentration values and blue the lowest. The tibial eminence is blank since no points were tested in this area.

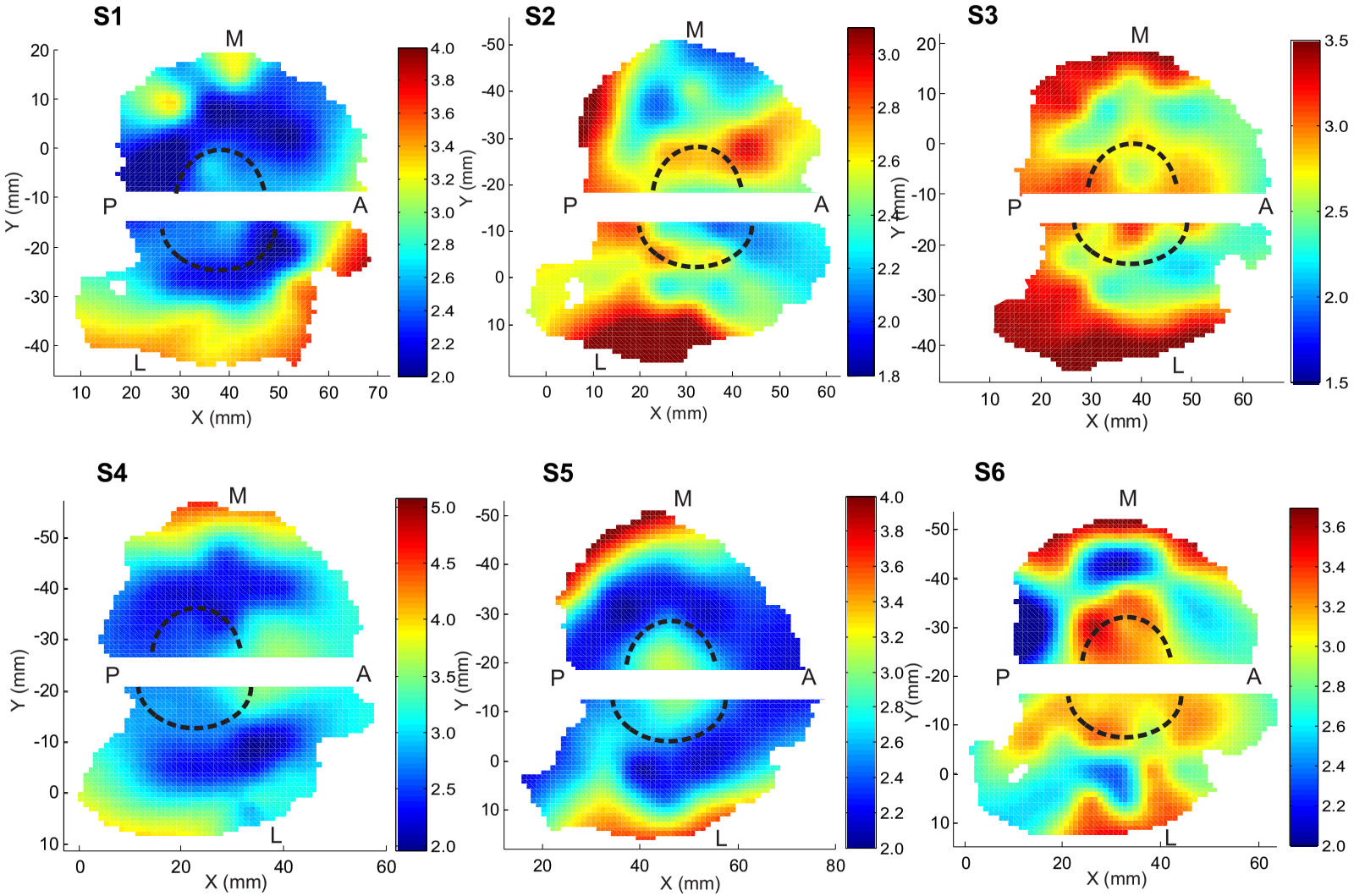


**Figure A.14:** High resolution cartilage thickness distribution maps of specimens S1, S2, S3, S4, S5, S6. Colour bar shows the cartilage thickness values in millimetres, where red represents the highest cartilage thickness values and blue the lowest. The tibial eminence is blank since no points were tested in this area.

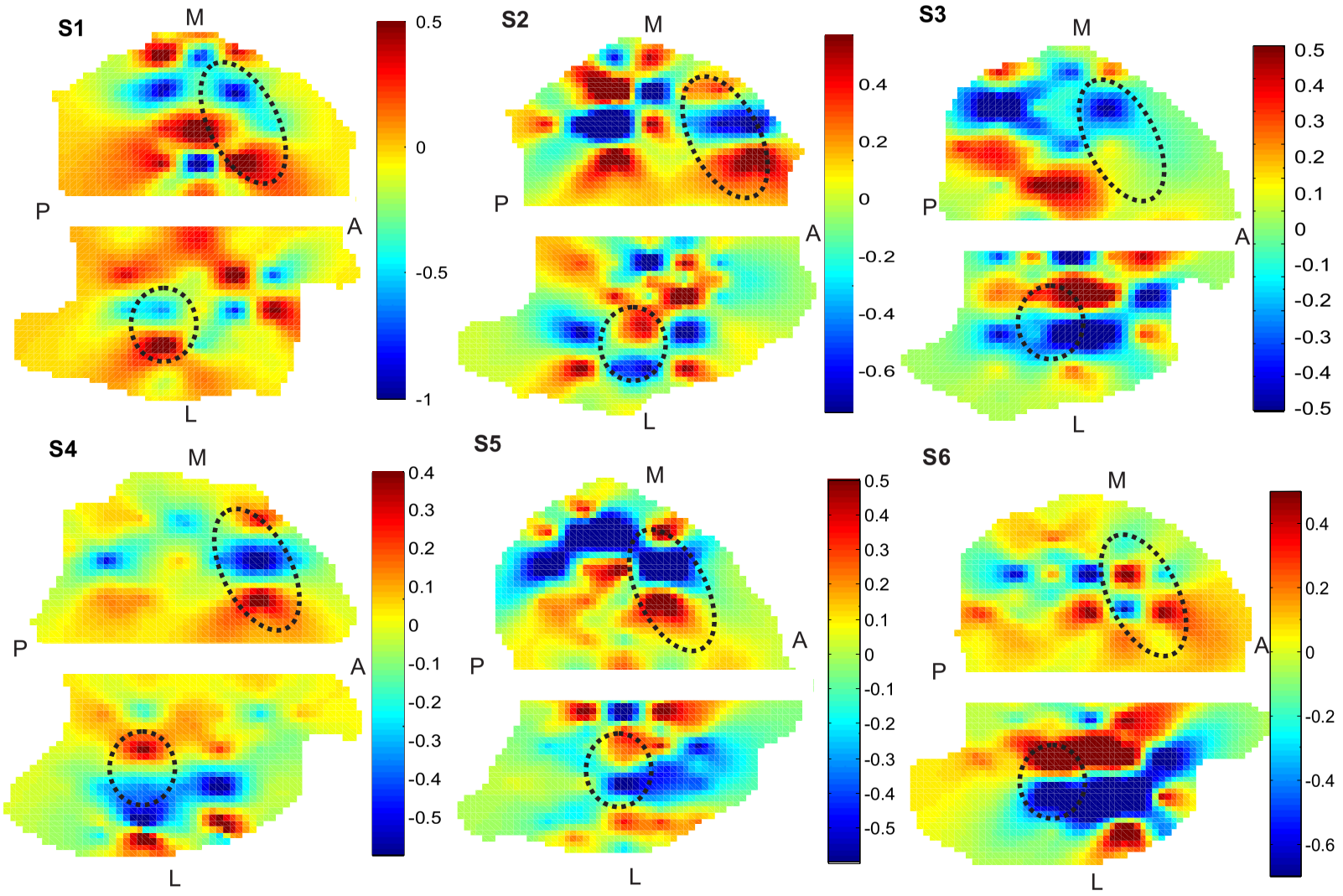


**Figure A.15:** 2nd derivative of the high resolution maps of the elastic modulus distribution of the six tibial plateaux

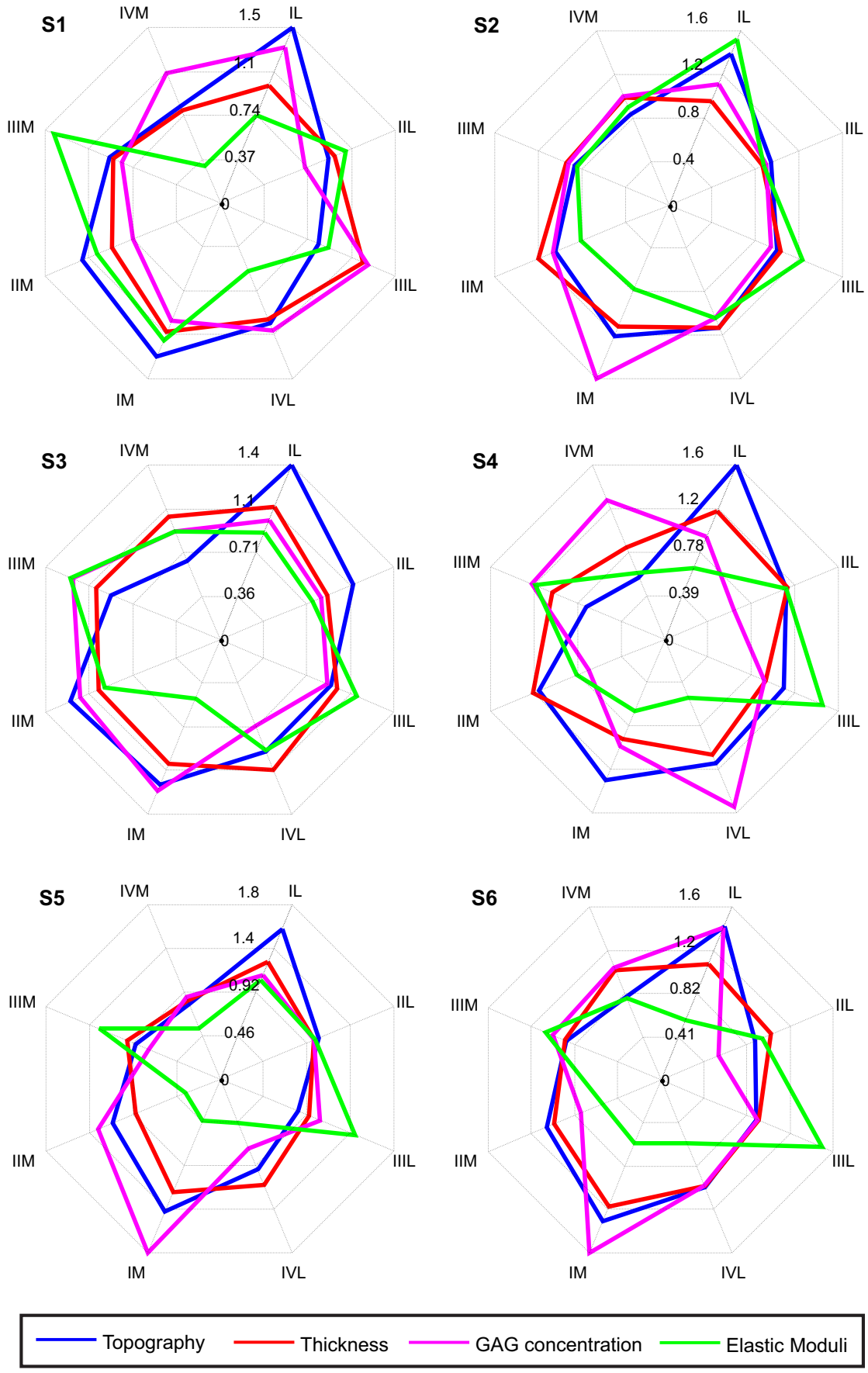


**Figure A.16:** Means of mechanical properties (Elastic modulus), GAG concentration, cartilage thickness and topographical height on each MMR over six tibial plateaux.

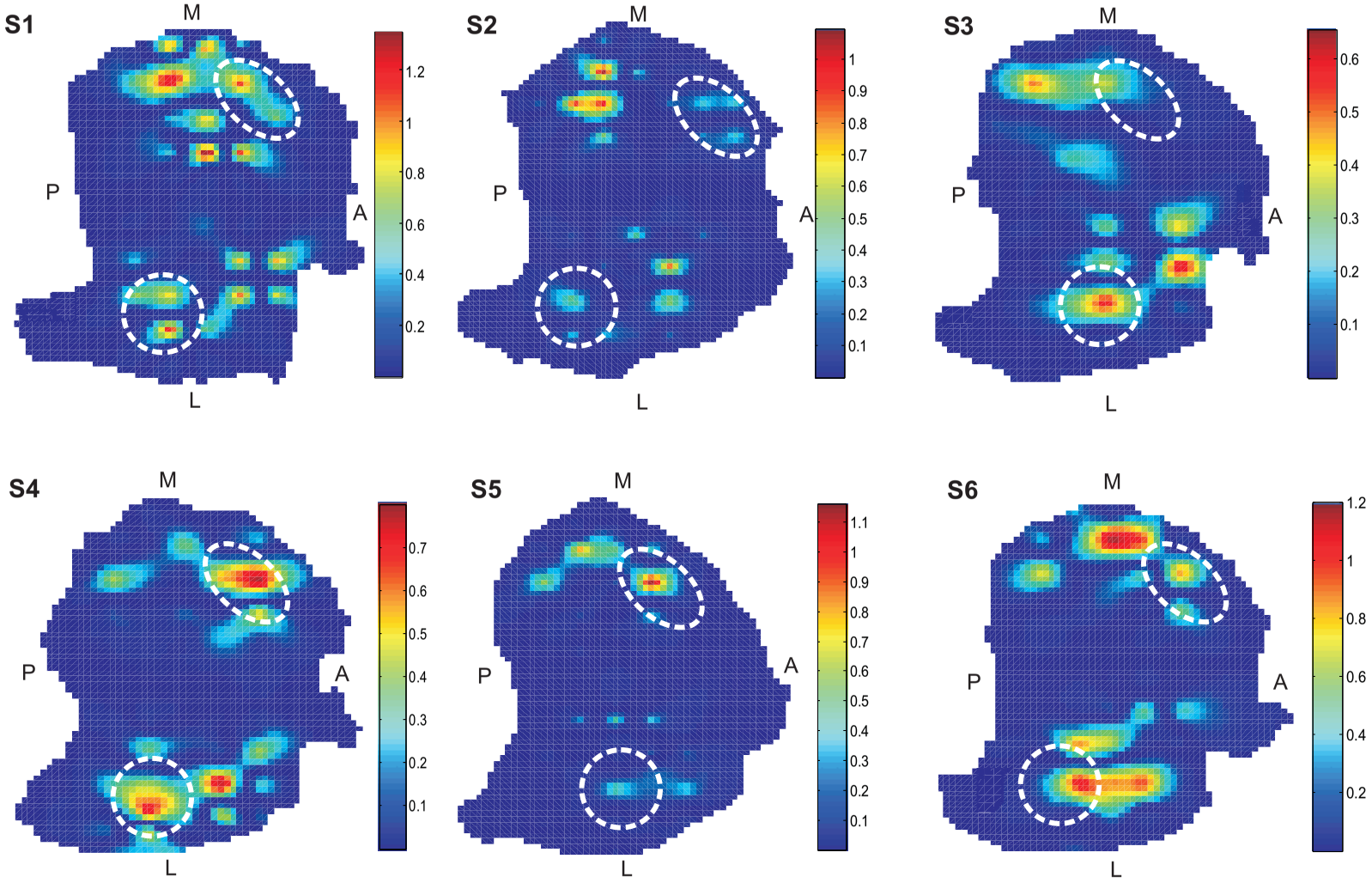


**Figure A.17:** 2nd derivative of the high resolution maps of the elastic modulus distribution of the six tibial plateaux

# Appendix B

# WASIM AUTOMATION CODE

In this section the routine developed by the author for automation of WASIM mechanical testing is presented. This code was written in C/C++.

```
#include "stdafx.h"
#include "extcode.h"
#include "fundtypes.h"
#include "platdefines.h"
#include "Tiab_base_level.h"
#include <windows.h>
#include <string>
#include <stdio.h>
#include <stdlib.h>
#include <fstream>
#include <iostream>
#include <strstream>
#include <sstream>
#include <string>
#include <vector>
#include <time.h>
#include <dos.h>


#using <system.dll>

using namespace System;
using namespace std;
using namespace System::Runtime::InteropServices;

typedef vector <double> record_t;
typedef vector <record_t> data_t;
typedef vector <string> record_st;
typedef struct{
  //vector <double*> AddX,AddY,AddZ,AddYaw,AddPitch;
  vector <double> x;
  vector <double> y;
  vector <double> z;
  vector <double> yaw;
  vector <double> pitch;
} AxisVectors;
```

```
public value class WASIM
{
public:
   static  HINSTANCE hGetProcIDDLL = LoadLibrary(L"Tiab_base_level.dll");
      //path to DLL;
   static  FARPROC lpfnGetProcessID= GetProcAddress(HMODULE
      (hGetProcIDDLL),"Tiab_open_connection"); //Get address for Function
      "Tiab_open_connection";
   static  FARPROC lpfnGetProcessID1 = GetProcAddress(HMODULE
      (hGetProcIDDLL),"Tiab_close_connection");
   //static   FARPROC lpfnGetProcessID2 = GetProcAddress(HMODULE
      (hGetProcIDDLL),"Tiab_write_scalar");
   static  FARPROC lpfnGetProcessID3 = GetProcAddress(HMODULE
      (hGetProcIDDLL),"Tiab_PID_set_setpoint");
   static  FARPROC lpfnGetProcessID4 = GetProcAddress(HMODULE
      (hGetProcIDDLL),"Tiab_PID_get_setpoint");
   static  FARPROC lpfnGetProcessID5 = GetProcAddress(HMODULE
      (hGetProcIDDLL),"Tiab_PID_get_modes");
   static  FARPROC lpfnGetProcessID6 = GetProcAddress(HMODULE
      (hGetProcIDDLL),"Tiab_PID_set_mode");
   static  FARPROC lpfnGetProcessID7 = GetProcAddress(HMODULE
      (hGetProcIDDLL),"Tiab_CL_config_mode"); //Select the mode of the
      replay & logging module.
   static  FARPROC lpfnGetProcessID8 = GetProcAddress(HMODULE
      (hGetProcIDDLL),"Tiab_CL_config_replay");
   static  FARPROC lpfnGetProcessID9 = GetProcAddress(HMODULE
      (hGetProcIDDLL),"Tiab_CL_config_logging"); //Configure data logging
      (output data)
   static  FARPROC lpfnGetProcessID10 = GetProcAddress(HMODULE
      (hGetProcIDDLL),"Tiab_CL_start");
   static  FARPROC lpfnGetProcessID11 = GetProcAddress(HMODULE
      (hGetProcIDDLL),"Tiab_CL_get_busy");
   static  FARPROC lpfnGetProcessID12 = GetProcAddress(HMODULE
      (hGetProcIDDLL),"Tiab_write_scalar");
   static  FARPROC lpfnGetProcessID13 = GetProcAddress(HMODULE
      (hGetProcIDDLL),"Tiab_read_scalar");
   static  FARPROC lpfnGetProcessID14 = GetProcAddress(HMODULE
      (hGetProcIDDLL),"Tiab_CL_config_log_channels");
   static  FARPROC lpfnGetProcessID15 = GetProcAddress(HMODULE
      (hGetProcIDDLL),"Tiab_read_analog_inputs");
   static  FARPROC lpfnGetProcessID16 = GetProcAddress(HMODULE
      (hGetProcIDDLL),"Tiab_CL_get_status");
   static FARPROC lpfnGetProcessID17 = GetProcAddress(HMODULE
      (hGetProcIDDLL),"Tiab_CL_start");
   static FARPROC lpfnGetProcessID19 = GetProcAddress(HMODULE
      (hGetProcIDDLL),"Tiab_CL_stop");
   static FARPROC lpfnGetProcessID20 = GetProcAddress(HMODULE
      (hGetProcIDDLL),"Tiab_PID_set_drive_gain");
   static  LVRefNum tiab;

//public:
   static int Connect();
```

```
   static void ConfReplayMd(char fileIn[]);
   static void ConfLoggin(char fileOut[]);
   static void ConfLogCh();
   static void ConfMd();
   static int ReadScalar();
   static int WASIM::WriteScalar(int32_t new_mode,char VariableName[]);
   static double ReadAnalogInp(int n); //n=0 for load cell and n=10 for laser
      A
   static void PIDSetPoint(int PID, double SetPoint, double RampTime);
   static double PIDGetPoint(int PID);
   static void PIDSetAmplitud(int PID, double Amplitud);
   static void SetModes(int PID, double Mode);
   static void SetAmplitud2One(double Mode);
   static void SetPID2Position(int i,int RampTime, AxisVectors coord);
   static void ConfigContinuousMode( char fileIn[],char fileOut[]);
   static int ZLaserIteration(int AValue);
   static int ZIndIteration(int AValue, int i, AxisVectors coord, int
      NumPoints);
   static void Start();
   static double GetBusy();
   static void Stop();
   static void Disconnect();
   static void GetStatus();
   static int CheckZRange(double zGetPoint);
   static void CheckMode(double Mode);
};


int WASIM::Connect(){

   //*************************************************************
   //*************** CONNECT ***********************************
    //*****************(WORKS!!! =) )*****************************
   //*************************************************************

   Console::WriteLine("Opening Tiab Connection");
   LVRefNum TiabTest;
   //Open connection to Tiab Software
   typedef int32_t (__cdecl * pICFUNC)(char[], uint16_t, LVRefNum*); //
      create typedef for "Tiab_open_connection"
   pICFUNC Tiab_open_connection = pICFUNC(lpfnGetProcessID); //Create a local
      function for the remote(dll) function
   char address[10] = "localhost"; //localhost or any ip address of the
      running Tiab Software
   int errorCode = Tiab_open_connection(address, 3364, &TiabTest);
      //(Address, port, Tiab program Handle) Returns error code
   Console::Write("Error returned from controller: " + errorCode + " \n" );
   if(errorCode){
      array<Byte>^msg = Text::Encoding::ASCII->GetBytes( "Connection failed"
         );
      //stream->Write(msg, 0, msg->Length);
   } else {
      array<Byte>^msg = Text::Encoding::ASCII->GetBytes( "Connection
```

```
         established" );
   //stream->Write(msg, 0, msg->Length);
   }
   tiab = TiabTest; // assign local ref to private ref.
   return errorCode;
}


void WASIM::ConfReplayMd(char fileIn[]){

   //*************************************************************
   //*************** CONFIGURE REPLAY MODE ***********************
   //*************************************************************
   //Config replay is one of the steps to configure the replay mode,
   //it is necesary to give the address of the replay file that will
   //be used. In order to choose the replay file, it's necesary to
   //know which procedure is going to be used.

      uint16_t FileType=0;

      Console::WriteLine("Writing Replay Mode");
      LVRefNum TiabTest = tiab; // assign private ref to local ref

      //int32_t __cdecl Tiab_CL_config_replay(LVRefNum *Handle, char
          String[], uint16_t FileType);
      typedef int32_t (__cdecl * pICFUNC8)(LVRefNum*, char[], uint16_t);

      //char String2[100]="C:\\Documents and Settings\\admin\\My
          Documents\\to_scan\\0-1mm_80x80_scan.txt";
      char String[100];
      strcpy(String,fileIn);

      pICFUNC8 Tiab_CL_config_replay;
      Tiab_CL_config_replay = pICFUNC8(lpfnGetProcessID8);

      double errorCode8 = Tiab_CL_config_replay (&TiabTest, String, FileType);
      Console::Write("Error returned from controller: " + errorCode8 + " \n"
          );
      if(errorCode8){
         array<Byte>^msg = Text::Encoding::ASCII->GetBytes( "" + errorCode8 +
             " setting motor position has failed" );
               //stream->Write(msg, 0, msg->Length);
      } else {
         array<Byte>^msg = Text::Encoding::ASCII->GetBytes( "In Path " +
             "strPath to String" + " set replay config \n ");
         Console::Write("Config Replay File: \n");
         //for (int i=0; i<=PathLen; i++){
         // Console::Write(strPath[i]);
         // //stream->Write(msg, 0, msg->Length);
         //}
      }

}
```

```
void WASIM::ConfLoggin(char fileOut[]){
   //Config Loggin is one of the steps to configure the replay mode,
   //Is necesary to give the address of the output(or loggin) file

   //*************************************************************
   //******************** CONFIG LOGGING ************************
   //*************************************************************

      uint16_t FileType=0;
      double FrequencyHz; //16MHz
      int32_t TimeS = 181; //Get seconds from file

      char CustomFile[250];
      strcpy(CustomFile,fileOut);

      //char CustomFile[120] = "C:\\Documents and Settings\\All
         Users\\Documents\\tiab_shared\\scanned\\test-120430.txt";

      Console::WriteLine("Configurating Loggin");
      LVRefNum TiabTest = tiab; // assign private ref to local ref

      //int32_t __cdecl Tiab_CL_config_logging(LVRefNum *Handle, uint16_t
         FileType, double FrequencyHz, int32_t TimeS, char CustomFile[]);
      typedef int32_t (__cdecl * pICFUNC9)(LVRefNum*, uint16_t, double,
         int32_t, char[]);

      //char strPath[24] = "C:\\tiab_data\\Waves.txt";

      pICFUNC9 Tiab_CL_config_logging;
      Tiab_CL_config_logging = pICFUNC9(lpfnGetProcessID9);

      double errorCode9 = Tiab_CL_config_logging (&TiabTest, FileType,
         FrequencyHz, TimeS, CustomFile);
      Console::Write("Error returned from controller: " + errorCode9 + " \n"
         );
      if(errorCode9){
         array<Byte>^msg = Text::Encoding::ASCII->GetBytes( "" + errorCode9 +
            " setting motor position has failed" );
              //stream->Write(msg, 0, msg->Length);
      } else {
         array<Byte>^msg = Text::Encoding::ASCII->GetBytes( "In Path " +
            "strPath to String" + " set replay config \n ");
              //stream->Write(msg, 0, msg->Length);
      }

}

void WASIM::ConfLogCh(){
   //Config Loggin Channels is one of the steps to configure the replay mode,
   //This bit doesnt work, however if the number of channels is preset before
   //starting, it is not necessary for it to work.
```

```
   //************************************************************
   //****************** CONFIG LOG CHANNELS *********************
   //************************************************************
   TD1Hdl Channels;

   Console::WriteLine("Configuring Log channels");
   LVRefNum TiabTest = tiab; // assign private ref to local ref

   typedef int32_t (__cdecl * pICFUNC14)(LVRefNum*, TD1Hdl);
   pICFUNC14 Tiab_CL_config_log_channels;
   Tiab_CL_config_log_channels = pICFUNC14(lpfnGetProcessID14);

   double errorCode14 = Tiab_CL_config_log_channels (&TiabTest, Channels);
   Console::Write("Error: " + errorCode14 + " \n" );
   if(errorCode14){
      array<Byte>^msg = Text::Encoding::ASCII->GetBytes( "error:" +
         errorCode14 + "\n");
      //stream->Write(msg, 0, msg->Length);
   } else {
      array<Byte>^msg = Text::Encoding::ASCII->GetBytes( "channel log
         configuration has been done \n" );
      //stream->Write(msg, 0, msg->Length);
   }
}

void WASIM::ConfMd(){
   //Config Mode is part of the replay system. It allows to tell the TIAB
      module
   //if you need a replay file, loggin file and the number of replays you want
   //to do (normally just 1)

   //************************************************************
   //************** CONFIG MODE - REPLAY AND CONFIG **************
   //************************************************************
   LVBoolean Replay = 1;
   LVBoolean Log= 1;
   uint32_t Replays = 1; //Number of time to repeat the file replay

   Console::WriteLine("Setting mode - replay and config");
   LVRefNum TiabTest = tiab; // assign private ref to local ref

   //int32_t __cdecl Tiab_CL_config_mode(LVRefNum *Handle, LVBoolean *Replay,
      LVBoolean *Log, uint32_t Replays);

   typedef int32_t (__cdecl * pICFUNC7)(LVRefNum*, LVBoolean*, LVBoolean*,
      uint32_t);
   pICFUNC7 Tiab_CL_config_mode;
   Tiab_CL_config_mode = pICFUNC7(lpfnGetProcessID7);
   //int PID = token[1]; // z-motor
   //double SetPoint = token[2]; // absolute position in mm (currently not
      calibrated)
   //double RampTime = token[3]; // tiem to get there (s)
   double errorCode7 = Tiab_CL_config_mode (&TiabTest, &Replay, &Log,
```

```
        Replays);
    Console::Write("Error returned from controller: " + errorCode7 + " \n" );
    if(errorCode7){
        array<Byte>^msg = Text::Encoding::ASCII->GetBytes( "error: " +
            errorCode7 + " \n" );
        //stream->Write(msg, 0, msg->Length);
    } else {
        array<Byte>^msg = Text::Encoding::ASCII->GetBytes( "Replay mode is on
            \n" );
        //stream->Write(msg, 0, msg->Length);
    }
}

void WASIM::GetStatus(){
    //*************************************************************
    //************************ GET STATUS ************************
    //*************************************************************
    TD2 Status;

    Console::WriteLine("Getting Status");
    LVRefNum TiabTest = tiab; // assign private ref to local ref

    //int32_t __cdecl Tiab_CL_get_status(LVRefNum *Handle, TD2 *Status);

    typedef int32_t (__cdecl * pICFUNC16)(LVRefNum*, TD2*);
    pICFUNC16 Tiab_CL_get_status;
    Tiab_CL_get_status = pICFUNC16(lpfnGetProcessID16);

    double errorCode16 = Tiab_CL_get_status (&TiabTest, &Status);
    Console::Write("Error: " + errorCode16 + " \n" );
    if(errorCode16){
        array<Byte>^msg = Text::Encoding::ASCII->GetBytes( "error:" +
            errorCode16 + "\n");
        //stream->Write(msg, 0, msg->Length);
    } else {
        array<Byte>^msg = Text::Encoding::ASCII->GetBytes( "status is? \n" );
        //Console::Write("Status: " + *Status + "\n");
        //stream->Write(msg, 0, msg->Length);
    }
}

int WASIM::ReadScalar(){
    //used to get the current mode in z motor (PID)

    //*************************************************************
    //*************** READ SCALAR VALUE ***************************
    //************ ALTERNATIVE TO GET MODES ************************

    char VariableName[20] = "_act_feedbk_mode_"; //For get modes
    //char VariableName[20] = "_act_input_"; //For get load cell values
    uint16_t VectorIndex= 0; //PID number = 1 #z motor
    uint16_t mode = 0; //mode 0 for read
    int32_t Value; //Get value
```

```
   Console::WriteLine("Reading scalar MODES to controller");
   LVRefNum TiabTest = tiab; // assign private ref to local ref

   //Call Method on Tiab Software - Write to scalar DSP Value

   //int32_t __cdecl Tiab_read_scalar(LVRefNum *Handle, char VariableName[],
       uint16_t VectorIndex, uint16_t mode, int32_t *Value);
   typedef int32_t (__cdecl * pICFUNC13)(LVRefNum*, char[], uint16_t,
       uint16_t, int32_t*);
   pICFUNC13 Tiab_read_scalar;
   Tiab_read_scalar = pICFUNC13(lpfnGetProcessID13);
   int errorCode13 = Tiab_read_scalar (&TiabTest, VariableName, VectorIndex,
       mode, &Value);
   Console::Write("Error returned from controller: " + errorCode13 + " \n" );
   if(errorCode13){
      array<Byte>^msg = Text::Encoding::ASCII->GetBytes( "" + errorCode13 + "
          Write scalar has failed" );
      //stream->Write(msg, 0, msg->Length);
   } else {
      int* Value2 = &Value;
      array<Byte>^msg = Text::Encoding::ASCII->GetBytes( "scalar value is
          mode: " + Value + " in actuator number: " + VectorIndex +"\n");
      Console::Write("Value2: " + *Value2 + " Value: " + Value + "\n");
      //stream->Write(msg, 0, msg->Length);
      //this->lblScalarWriteError->Text = "" + writeValue + " scalar
          successfully written to _test1";
   }
   return Value;

}

int WASIM::WriteScalar(int32_t new_mode,char VariableName[]){
   //used to get the current mode in z motor (PID)
   //char VariableName[20];

   //if(command == 1){
   // char VariableName[20] = "_act_feedbk_mode_";
   //}else{
   // char VariableName[10] = '_act_catch';
   //}

   //use it as:
   //Tiab_write_scalar("act_feedbk_mode_new_", act_index, new_mode);
   //Tiab_write_scalar("_act_catch", act_index, 1<<act_index);
   //act_index = the actuator index that you want to change modes for 0 =
       Actuator 1
   //new_mode = the mode that you require it to change to
   //1<<actuator index = Left shift by the actuator number
   //_act_catch will catch the actuator at its current feedback and switch
       mode to the mode specified in _act_feedback_mode_new_

   uint16_t act_index = 0; //actuator/PID that you want to change the mode
```

```
        of. PID1=2^0=1 #z motor
    uint16_t mode = 2; //mode always 2
    //int32_t new_mode; //Mode you want to change to

    Console::WriteLine("Writting scalar to mode "+ new_mode);
    LVRefNum TiabTest = tiab; // assign private ref to local ref

    //Call Method on Tiab Software - Write to scalar DSP Value

    //int32_t __cdecl Tiab_write_scalar(LVRefNum *Handle, int32_t Value,char
        VariableName[], uint16_t VectorIndex, uint16_t mode);
    typedef int32_t (__cdecl * pICFUNC12)(LVRefNum*, int32_t,char[], uint16_t,
        uint16_t);
    pICFUNC12 Tiab_write_scalar;
    Tiab_write_scalar = pICFUNC12(lpfnGetProcessID12);
    int errorCode12 = Tiab_write_scalar(&TiabTest, new_mode, VariableName,
        act_index, mode);
    Console::Write("Error returned from controller: " + errorCode12 + " \n" );
    if(errorCode12){
       array<Byte>^msg = Text::Encoding::ASCII->GetBytes( "" + errorCode12 + "
          Write scalar has failed" );
       //stream->Write(msg, 0, msg->Length);
    } else {
       Console::Write("Changed mode to :"+ new_mode+ "\n");
       //stream->Write(msg, 0, msg->Length);
       //this->lblScalarWriteError->Text = "" + writeValue + " scalar
          successfully written to _test1";
    }
    return errorCode12;

}

double WASIM::ReadAnalogInp(int n){
    //Used to read the load cell - //n=0 for load cell and n=10 for laser A

    //************************************************************
    //*************** READ ANALOGUE INPUTS ***********************
    //************************************************************
       LVRefNum TiabTest = tiab; // assign private ref to local ref
       typedef int32_t (__cdecl * pICFUNC15)(LVRefNum*, double[], uint16_t);

       pICFUNC15 Tiab_read_analog_inputs;
       Tiab_read_analog_inputs = pICFUNC15(lpfnGetProcessID15);
       int32_t AValuesLen = 12;
       //double* AValues = new double[AValuesLen];
       double AValues[12];

       double errorCode15 = Tiab_read_analog_inputs (&TiabTest, AValues,
           AValuesLen);
       Console::Write("Error returned from controller: " + errorCode15 + " \n"
           );
       if(errorCode15){
          array<Byte>^msg = Text::Encoding::ASCII->GetBytes( "" + errorCode15
```

```
            + " setting motor position has failed" );
              //stream->Write(msg, 0, msg->Length);
      } else {
         array<Byte>^msg = Text::Encoding::ASCII->GetBytes( "In Path " +
            "strPath to String" + " set replay config \n ");
         //for (int i=0; i<=AValuesLen; i++){
            Console::Write("Avalues: " + n + ": "+ AValues[n] + " \n" );
              //stream->Write(msg, 0, msg->Length);
         //}
      }
      return AValues[n];
}

double WASIM::PIDGetPoint(int PID){
   //Used to use the position of the motors (PID)

      Console::WriteLine("Getting setpoint from PID");
      LVRefNum TiabTest = tiab; // assign private ref to local ref
      //Call Method on Tiab Software - Write to scalar DSP Value
      typedef int32_t (__cdecl * pICFUNC4)(LVRefNum*, int32_t, double*);
      pICFUNC4 Tiab_PID_get_setpoint;
      Tiab_PID_get_setpoint = pICFUNC4(lpfnGetProcessID4);
      int value =0;
      //int PID = 1; // z-motor
      double SetPoint; // absolute position in mm (currently not calibrated)
      int errorCode4 = Tiab_PID_get_setpoint (&TiabTest, PID, &SetPoint);
      Console::Write("Error returned from controller: " + errorCode4 + " \n"
          );
      if(errorCode4){
         array<Byte>^msg = Text::Encoding::ASCII->GetBytes( "" + errorCode4 +
            " getting motor position has failed" );
//       stream->Write(msg, 0, msg->Length);
      } else {
         array<Byte>^msg = Text::Encoding::ASCII->GetBytes( "motor " + PID +
            " is at position: " + SetPoint + "" );
//       stream->Write(msg, 0, msg->Length);
      }
      return SetPoint;
}

void WASIM::PIDSetPoint(int PID, double SetPoint, double RampTime){
   //used to move the motors to a position. You have to specify the motor in
       PID
      //int PID = Int32::Parse(token[1]);
      //double SetPoint = Double::Parse(token[2]);
      //double RampTime = Double::Parse(token[3]);

      Console::WriteLine("Writing setpoint to PID");
      LVRefNum TiabTest = tiab; // assign private ref to local ref

      typedef int32_t (__cdecl * pICFUNC3)(LVRefNum*, int32_t, double,
         double);
      pICFUNC3 Tiab_PID_set_setpoint;
```

```
      Tiab_PID_set_setpoint = pICFUNC3(lpfnGetProcessID3);

      double errorCode3 = Tiab_PID_set_setpoint (&TiabTest, PID, SetPoint,
          RampTime);
      Console::Write("Error returned from controller: " + errorCode3 + " \n"
          );
      if(errorCode3){
         array<Byte>^msg = Text::Encoding::ASCII->GetBytes( "" + errorCode3 +
             " setting motor position has failed" );
         //stream->Write(msg, 0, msg->Length);
      } else {
         array<Byte>^msg = Text::Encoding::ASCII->GetBytes( "motor " + PID +
             " moving to " + SetPoint + "" );
         //stream->Write(msg, 0, msg->Length);
      }
}

void WASIM::PIDSetAmplitud(int PID, double Amplitud){
   //used to move the motors to a position. You have to specify the motor in
       PID
      //int PID = Int32::Parse(token[1]);
      //double SetPoint = Double::Parse(token[2]);
      //double RampTime = Double::Parse(token[3]);

      Console::WriteLine("Writing set amplitud to PID");
      LVRefNum TiabTest = tiab; // assign private ref to local ref

      //int32_t __cdecl Tiab_PID_set_drive_gain(LVRefNum *Handle, int32_t
          PID, double Amplitude);
      typedef int32_t (__cdecl * pICFUNC20)(LVRefNum*, int32_t, double);
      pICFUNC20 Tiab_PID_set_drive_gain;
      Tiab_PID_set_drive_gain = pICFUNC20(lpfnGetProcessID20);

      double errorCode20 = Tiab_PID_set_drive_gain (&TiabTest, PID, Amplitud);
      Console::Write("Error returned from controller: " + errorCode20 + " \n"
          );
      if(errorCode20){
         array<Byte>^msg = Text::Encoding::ASCII->GetBytes( "" + errorCode20
             + " setting motor position has failed" );
         //stream->Write(msg, 0, msg->Length);
      } else {
         array<Byte>^msg = Text::Encoding::ASCII->GetBytes( "motor " + PID +
             " amplitud to 1 \n" );
         //stream->Write(msg, 0, msg->Length);
      }
}

void WASIM::Start(){
   //Start Replay mode!

      Console::WriteLine("Start Replay mode - Play");
      LVRefNum TiabTest = tiab; // assign private ref to local ref
```

```
      //int32_t __cdecl Tiab_CL_start(LVRefNum *Handle);
      typedef int32_t (__cdecl * pICFUNC17)(LVRefNum*);
      pICFUNC17 Tiab_CL_start;
      Tiab_CL_start = pICFUNC17(lpfnGetProcessID17);

      double errorCode17 = Tiab_CL_start (&TiabTest);
      Console::Write("Error returned from controller: " + errorCode17 + " \n"
          );
      if(errorCode17){
         array<Byte>^msg = Text::Encoding::ASCII->GetBytes( "" + errorCode17
             + " setting motor position has failed" );
         //stream->Write(msg, 0, msg->Length);
      } else {
         array<Byte>^msg = Text::Encoding::ASCII->GetBytes( "Replay started
             \n" );
         //stream->Write(msg, 0, msg->Length);
      }

}

void WASIM::Stop(){
   //Stop Replay mode!

      Console::WriteLine("Stop Replay mode - STOP");
      LVRefNum TiabTest = tiab; // assign private ref to local ref

      //int32_t __cdecl Tiab_CL_stop(LVRefNum *Handle);
      typedef int32_t (__cdecl * pICFUNC19)(LVRefNum*);
      pICFUNC19 Tiab_CL_stop;
      Tiab_CL_stop = pICFUNC19(lpfnGetProcessID19);

      double errorCode19 = Tiab_CL_stop (&TiabTest);
      Console::Write("Error returned from controller: " + errorCode19 + " \n"
          );
      if(errorCode19){
         array<Byte>^msg = Text::Encoding::ASCII->GetBytes( "" + errorCode19
             + " error stopping WASIM" );
         //stream->Write(msg, 0, msg->Length);
      } else {
         array<Byte>^msg = Text::Encoding::ASCII->GetBytes( "Replay stopped
             \n" );
         //stream->Write(msg, 0, msg->Length);
      }

}

double WASIM::GetBusy(){
   //Start Replay mode!
   LVBoolean CL_busy;
   int Busy = 0;
   Console::WriteLine("Is WASIM busy?");
   LVRefNum TiabTest = tiab; // assign private ref to local ref
```

```
   //Tiab_CL_get_busy(LVRefNum *Handle, LVBoolean *CL_busy);
   typedef int32_t (__cdecl * pICFUNC11)(LVRefNum*,LVBoolean*);
   pICFUNC11 Tiab_CL_get_busy;
   Tiab_CL_get_busy = pICFUNC11(lpfnGetProcessID11);

   double errorCode11 = Tiab_CL_get_busy(&TiabTest, &CL_busy);
   Console::Write("Error returned from controller: " + errorCode11 + " \n" );

   if(errorCode11){
      Console::Write( "" + errorCode11 + " Getting WASIM status has failed" );
     //stream->Write(msg, 0, msg->Length);
    } else {
     //stream->Write(msg, 0, msg->Length);
    }

    if(CL_busy == LVBooleanTrue){
      Console::Write( "Logging/Replay is Active\n" );
      Busy=1;
      //stream->Write(msg, 0, msg->Length);
    } else {
      Console::Write( "Logging/Replay is Inactive\n" );
      Busy=0;
     //stream->Write(msg, 0, msg->Length);
    }
   return Busy;
}

void WASIM::SetModes(int PID, double Mode){
   //Set the mode of a PID. Now only used for z (PID=1), from 1=displacement
       mode or 2=force mode
      //int PID = 1; //motor z
      //double Mode = 2; //Change mode to 2
      //int PID = token[1]; // z-motor
      //double Mode = token[2]; // absolute position in mm (currently not
          calibrated)
      Console::WriteLine("Writing set mode to PID");
      LVRefNum TiabTest = tiab; // assign private ref to local ref

      //int32_t __cdecl Tiab_PID_set_mode(LVRefNum *Handle, uint8_t PID,
          double Mode);
      typedef int32_t (__cdecl * pICFUNC6)(LVRefNum*, uint8_t, double);
      pICFUNC6 Tiab_PID_set_mode;
      Tiab_PID_set_mode = pICFUNC6(lpfnGetProcessID6);

      double errorCode6 = Tiab_PID_set_mode (&TiabTest, PID, Mode);
      Console::Write("Error returned from controller: " + errorCode6 + " \n"
          );
      if(errorCode6){
         array<Byte>^msg = Text::Encoding::ASCII->GetBytes( "" + errorCode6 +
             " setting motor position has failed" );
         //stream->Write(msg, 0, msg->Length);
      } else {
         array<Byte>^msg = Text::Encoding::ASCII->GetBytes( "motor " + PID +
```

```
            " moving to " + Mode + "" );
         //stream->Write(msg, 0, msg->Length);
      }

}


void WASIM::SetAmplitud2One(double Mode){
      Console::WriteLine("Put X,Y,Z amplitud in 1");
      if (Mode ==1){
         //Write z
         WASIM::PIDSetAmplitud(0, 0);
         //Write x
         WASIM::PIDSetAmplitud(3, 1);
         //Write y
         WASIM::PIDSetAmplitud(4, 1);
      }
      else{
         //Write z
         WASIM::PIDSetAmplitud(0, 1);
         //Write x
         WASIM::PIDSetAmplitud(3, 0);
         //Write y
         WASIM::PIDSetAmplitud(4, 0);
      }
}

void WASIM::SetPID2Position(int i,int RampTime, AxisVectors coord){
   //vector <double> x,vector <double> y,vector <double> yaw, vector <double>
       pitch
      Console::WriteLine("SetPID2Position...");
      // PID=motor;SetPoint=Final position;RampTime=Time to get there
      //1st move z up
      Console::WriteLine("Moving z up to 80");
      WASIM::PIDSetPoint(1, 80, RampTime);
      Sleep(3000);
      //now move yaw (rotate about z axis)
      Console::WriteLine("Moving yaw to : " + coord.yaw[i] + "\n");
      WASIM::PIDSetPoint(2, coord.yaw[i], RampTime);
      Sleep(3000);
      //Move pitch (rotate about y axis)
      Console::WriteLine("Moving pitch to : " + coord.pitch[i] + "\n");
      WASIM::PIDSetPoint(3, coord.pitch[i], RampTime);
      Sleep(3000);
      //Move x axis
      Console::WriteLine("Moving x to : " + coord.x[i] + "\n");
      WASIM::PIDSetPoint(4, coord.x[i], RampTime);
      Sleep(3000);
      //Move y axis
      Console::WriteLine("Moving y to : " + coord.y[i] + "\n");
      WASIM::PIDSetPoint(5, coord.y[i], RampTime);
}
```

```
void WASIM::ConfigContinuousMode(char fileIn[],char fileOut[]){
      Console::WriteLine("Configuring Replay Mode");
      WASIM::ConfReplayMd(fileIn);
      Console::WriteLine("Configuring Loggin");
      WASIM::ConfLoggin(fileOut);
      Console::WriteLine("Configuring Mode: Replay and Login");
      WASIM::ConfMd();
}

int WASIM::ZIndIteration(int AValue, int i, AxisVectors coord, int
    NumPoints){
      double RampTime = 2;
      double Mode = 2;
      //Move z axis down - iterate using load cell values
      double zoGetPoint = WASIM::PIDGetPoint(1); //Where is z?
      double iLoadCell = WASIM::ReadAnalogInp(AValue);
      double fLoadCell = iLoadCell;
      double CmpLoadCell = 0;
      double ZfInd = coord.z[i];
      double zPosition=zoGetPoint;
      double ZInd = zoGetPoint;
      double zGetPoint=0;
      int Error=1;
      int Ok=0;
      int Contact=0;
      RampTime = 3;
      double ZAverage = 0;
      int size = 0;

      //if(abs(iLoadCell)<=0.05){
      // CmpLoadCell = 0.1;
      //}
      //else{
      // //CmpLoadCell = 5*iLoadCell;
      // CmpLoadCell = iLoadCell+1;
      //}

      CmpLoadCell = iLoadCell+1.1;

      for (int i=0;i<NumPoints;i++){
         ZAverage = coord.z[i]+ZAverage;
      }
      ZAverage = ZAverage/NumPoints;

      //if(ZfInd<ZAverage-20){
      // Error =0;
      // //break;
      //}
      //else{

      while ((ZInd-ZfInd)>20){

         zPosition=zPosition-5;
```

```
   WASIM::PIDSetPoint(1, zPosition, RampTime);
   Sleep(5000);
   ZInd = WASIM::PIDGetPoint(1); //Where is z?
   Ok = CheckZRange(ZInd);
   if (Ok ==0) {
      WASIM::Stop();
      break;
   }
   else{
      fLoadCell = WASIM::ReadAnalogInp(AValue);
      Console::WriteLine( "fLoadCell: " + fLoadCell);
      Console::WriteLine( "iLoadCell: " + iLoadCell);
      Console::WriteLine( "CmpLoadCell: " + CmpLoadCell);
      if ((fLoadCell)>=(abs(CmpLoadCell))) {
      //if ((fLoadCell)>=(abs(5*CmpLoadCell)+CmpLoadCell)) {
      //if ((fLoadCell)<=(abs(iLoadCell-(0.01*iLoadCell)))) {
         Console::WriteLine( "LoadCell Difference: " +
             (fLoadCell-iLoadCell));
         Contact=1;
         Error =0;
         break;
      }
   }
}
if (Contact!= 1){
   RampTime = 1;
   while ((ZInd-ZfInd)>10){
      zPosition=zPosition-3;
      WASIM::PIDSetPoint(1, zPosition, RampTime);
      Sleep(5000);
      ZInd = WASIM::PIDGetPoint(1); //Where is z?
      Ok = CheckZRange(ZInd);
      if (Ok ==0) {
         WASIM::Stop();
         break;
      }
      else{
         fLoadCell = WASIM::ReadAnalogInp(AValue);
         Console::WriteLine( "fLoadCell: " + fLoadCell);
         Console::WriteLine( "iLoadCell: " + iLoadCell);
         Console::WriteLine( "CmpLoadCell: " + CmpLoadCell);
         if ((fLoadCell)>=(abs(CmpLoadCell))) {
         //if ((fLoadCell)<=(abs(iLoadCell-(0.01*iLoadCell)))) {
            Console::WriteLine( "LoadCell Difference: " +
                (fLoadCell-iLoadCell));
            Contact=1;
            Error =0;
            break;
         }
      }
   }
}
if (Contact!= 1){
```

```
   while (((ZInd-ZfInd)<=10)&&((ZInd-ZfInd)>1)){
      zPosition=zPosition-1;
      WASIM::PIDSetPoint(1, zPosition, RampTime);
      Sleep(5000);
      ZInd = WASIM::PIDGetPoint(1); //Where is z?
      Ok = CheckZRange(ZInd);
      if (Ok ==0) {
         WASIM::Stop();
         break;
      }
      else{
         fLoadCell = WASIM::ReadAnalogInp(AValue);
         Console::WriteLine( "fLoadCell: " + fLoadCell);
         Console::WriteLine( "iLoadCell: " + iLoadCell);
         Console::WriteLine( "CmpLoadCell: " + CmpLoadCell);
         if ((fLoadCell)>=(abs(CmpLoadCell))) {
         //if ((fLoadCell)>=(abs(5*iLoadCell)+iLoadCell)) {
         //if ((fLoadCell)<=(abs(iLoadCell-(0.01*iLoadCell)))) {
            Console::WriteLine( "LoadCell Difference: " +
                (fLoadCell-iLoadCell));
            Contact=1;
            Error =0;
            break;
         }
      }
   }
}

if (Contact!= 1){
   while ((ZInd-ZfInd)<=1){
      zPosition=zPosition-0.5;
      WASIM::PIDSetPoint(1, zPosition, RampTime);
      Sleep(5000);
      ZInd = WASIM::PIDGetPoint(1); //Where is z?
      Ok = CheckZRange(ZInd);
      if (Ok ==0) {
         WASIM::Stop();
         break;
      }
      else{
         fLoadCell = WASIM::ReadAnalogInp(AValue);
         Console::WriteLine( "fLoadCell: " + fLoadCell);
         Console::WriteLine( "iLoadCell: " + iLoadCell);
         Console::WriteLine( "CmpLoadCell: " + CmpLoadCell);
         if ((fLoadCell)>=(abs(CmpLoadCell))) {
         //if ((fLoadCell)>=(abs(5*iLoadCell)+iLoadCell)) {
         //if ((fLoadCell)<=(abs(iLoadCell-(0.01*iLoadCell)))) {
            Console::WriteLine( "LoadCell Difference: " +
                (fLoadCell-iLoadCell));
            Contact=1;
            Error =0;
            break;
         }
```

```
            }
         }
      }
   //} //End else
return Error;
}

int WASIM::ZLaserIteration(int AValue){
      double RampTime = 2;
      double Mode = 1;
      //Move z axis down - iterate using load cell values
      double zoGetPoint = WASIM::PIDGetPoint(1); //Where is z?
      double VoLaser= WASIM::ReadAnalogInp(AValue);
      double zPosition=zoGetPoint;
      double VLaser = VoLaser;
      double zGetPoint=0;
      int Error=0, Ok=0;
      RampTime = 3;
      while (VLaser>20){
         zPosition=zPosition-10;
         WASIM::PIDSetPoint(1, zPosition, RampTime);
         Sleep(5000);
         zGetPoint = WASIM::PIDGetPoint(1); //Where is z?
         Ok = CheckZRange(zGetPoint);
         if (Ok ==1) WASIM::Stop();
         VLaser = WASIM::ReadAnalogInp(AValue);
      }
      zPosition=zPosition-VLaser;
      WASIM::PIDSetPoint(1, zPosition, RampTime);
      VLaser = WASIM::ReadAnalogInp(AValue);

      if((VLaser<0.003)&&(VLaser>-0.003)){
         Error=0;
      }
      else{
         RampTime = 1;
         while ((VLaser<=-0.003)||(VLaser>=0.003)){
            zPosition=zPosition-VLaser;
            WASIM::PIDSetPoint(1, zPosition, RampTime);
            Sleep(5000);
            zGetPoint = WASIM::PIDGetPoint(1); //Where is z?
            Ok = CheckZRange(zGetPoint);
            if (Ok ==1) WASIM::Stop();
            VLaser = WASIM::ReadAnalogInp(AValue);
         }
         if((VLaser<0.003)&&(VLaser>-0.003)){
            Error=0;
         }
         else Error=1;
      }
return Error;
}
```

```
void WASIM::Disconnect(){

      Console::WriteLine("Closing Tiab Connection");
      LVRefNum TiabTest = tiab; // assign private ref to local ref
      //Close Connection to Tiab Software
      typedef int32_t (__cdecl * pICFUNC1)(LVRefNum*);
      pICFUNC1 Tiab_close_connection = pICFUNC1(lpfnGetProcessID1);
      char address[10] = "localhost"; //localhost or any ip address of the
          running Tiab Software
      int errorCode = Tiab_close_connection(&TiabTest);
      Console::Write("Error returned from controller: " + errorCode + " \n" );
      if (errorCode){
         array<Byte>^msg = Text::Encoding::ASCII->GetBytes( "Connection close
             has failed" );
         //stream->Write(msg, 0, msg->Length);
         //this->lblDisconnectionError->Text = "Error Code: " +
             Tiab_close_connection (&TiabTest);
      } else {
         array<Byte>^msg = Text::Encoding::ASCII->GetBytes( "Connection
             closed successfully" );
         //stream->Write(msg, 0, msg->Length);
         //this->lblDisconnectionError->Text = "Connection Closed";
         //this->lblConnectionError->Text = "";
      }

} //End Disconnect

int WASIM::CheckZRange(double zGetPoint){
   int Ok;

   if((zGetPoint>-85)&&(zGetPoint<85)){
      Ok=1;
   }
   else
      Ok=0;
   return Ok;
}

void WASIM::CheckMode(double Mode){
        Console::WriteLine("Read current mode");
        int RdMode = WASIM::ReadScalar();

        if (RdMode!=Mode){
           Console::WriteLine("Set Mode in: " + Mode);
           WASIM::WriteScalar(Mode,"_act_feedbk_mode_");
           WASIM::WriteScalar(Mode,"_act_catch");
           //WASIM::SetModes(1, Mode);
        }
}

AxisVectors CreateXYZVectors(data_t &data){
  unsigned max_record_size = 0;
  unsigned dataLen = 0;
```

```
  unsigned NumRows = data.size();

  int n=0;

  vector <double*>
      AddX(NumRows),AddY(NumRows),AddZ(NumRows),AddYaw(NumRows),AddPitch(NumRows);
  vector <double>
      x(NumRows),y(NumRows),z(NumRows),yaw(NumRows),pitch(NumRows);
  dataLen = data[ n ].size();

  for (unsigned n = 0; n < data.size(); n++){

       for (unsigned ColNum = 0; ColNum <data[ n ].size(); ColNum++){
         cout << "data[" << n << "][ " << ColNum << "]: " << data[ n ][
             ColNum ] << "\n";
         if (ColNum==0){
            AddX[n]= &data[ n ][ ColNum ];
            x[n]=*AddX[n];
         }
         if (ColNum==1){
            AddY[n]= &data[ n ][ ColNum ];
            y[n]=*AddY[n];
         }
         if (ColNum==2){
            AddZ[n]= &data[ n ][ ColNum ];
            z[n]=*AddZ[n];
         }
         if (ColNum==3){
            AddYaw[n]= &data[ n ][ ColNum ];
            yaw[n]=*AddYaw[n];
         }
         if (ColNum==4){
            AddPitch[n]= &data[ n ][ ColNum ];
            pitch[n]=*AddPitch[n];
         }
       }
  }

  AxisVectors coordinates = {x,y,z,yaw,pitch};

  return coordinates;
}

//---------------------------------------------------------------------------
// Let's overload the stream input operator to read a list of CSV fields
    (which a CSV record).
// Remember, a record is a list of doubles separated by commas ','.
istream& operator >> ( istream& ins, record_t& record )
  {

  // make sure that the returned record contains only the stuff we read now
  record.clear();
```

```
  // read the entire line into a string (a CSV record is terminated by a
     newline)
  string line;
  getline( ins, line );

  // now we'll use a stringstream to separate the fields out of the line
  stringstream ss( line );
  string field;
  while (getline( ss, field, ',' ))
    {
    // for each field we wish to convert it to a double
    // (since we require that the CSV contains nothing but floating-point
       values)
    stringstream fs( field );
    double f = 0.0; // (default value is 0.0)
    fs >> f;
   // add the newly-converted field to the end of the record
   record.push_back( f );
  }
  // Now we have read a single line, converted into a list of fields,
     converted the fields
  // from strings to doubles, and stored the results in the argument record,
     so
  // we just return the argument stream as required for this kind of input
     overload function.
  return ins;
  }

//--------------------------------------------------------------------------
// Let's likewise overload the stream input operator to read a list of CSV
   records.
// This time it is a little easier, just because we only need to worry about
   reading
// records, and not fields.
istream& operator >> ( istream& ins, data_t& data )
  {
  // make sure that the returned data only contains the CSV data we read here
  data.clear();

  record_t record;
  while (ins >> record)
    {
    data.push_back( record );
   }

  // Again, return the argument stream as required for this kind of input
     stream overload.
  return ins;
  }

////////////////////////////////////////////////////////////////////////////
istream& operator >> ( istream& ins, record_st& header )
  {
```

```
  // make sure that the returned record contains only the stuff we read now
  header.clear();

  // read the entire line into a string (a CSV record is terminated by a
      newline)
  string line;
  getline( ins, line );

  // now we'll use a stringstream to separate the fields out of the line
  stringstream ss( line );
  string field;
  while (getline( ss, field, ',' ))
    {
     // add the newly-converted field to the end of the record
   header.push_back( field );
  }
  // Now we have read a single line, converted into a list of fields,
      converted the fields
  // from strings to doubles, and stored the results in the argument record,
      so
  // we just return the argument stream as required for this kind of input
      overload function.
  return ins;
  }

//******************Convert string into Double*****************************
//*************************************************************************
double string_to_double( const string& s )
 {
   std::istringstream i(s);
   double x;
   if (!(i >> x))
     return 0;
   return x;
 }

//-------------------------------------------------------------------------

int main()
{
   static  HINSTANCE hGetProcIDDLL;
   static  FARPROC lpfnGetProcessID;
   static  FARPROC lpfnGetProcessID1;
   //static   FARPROC lpfnGetProcessID2;
   static  FARPROC lpfnGetProcessID3;
   static  FARPROC lpfnGetProcessID4;
   static  FARPROC lpfnGetProcessID5;
   static  FARPROC lpfnGetProcessID6;
   static  FARPROC lpfnGetProcessID7;
   static  FARPROC lpfnGetProcessID8;
   static  FARPROC lpfnGetProcessID9;
   static  FARPROC lpfnGetProcessID10;
```

```
static  FARPROC lpfnGetProcessID11;
static  FARPROC lpfnGetProcessID12;
static  FARPROC lpfnGetProcessID13;
static  FARPROC lpfnGetProcessID14;
static  FARPROC lpfnGetProcessID15;
static  FARPROC lpfnGetProcessID16;
static  FARPROC lpfnGetProcessID17;
static  FARPROC lpfnGetProcessID18;
static  FARPROC lpfnGetProcessID19;
static  FARPROC lpfnGetProcessID20;
static  LVRefNum tiab;

hGetProcIDDLL = LoadLibrary(L"Tiab_base_level.dll"); //path to DLL

   //Specify methods to be used
lpfnGetProcessID = GetProcAddress(HMODULE
    (hGetProcIDDLL),"Tiab_open_connection"); //Get address for Function
    "Tiab_open_connection"
lpfnGetProcessID1 = GetProcAddress(HMODULE
    (hGetProcIDDLL),"Tiab_close_connection");
//lpfnGetProcessID2 = GetProcAddress(HMODULE
    (hGetProcIDDLL),"Tiab_write_scalar");
lpfnGetProcessID3 = GetProcAddress(HMODULE
    (hGetProcIDDLL),"Tiab_PID_set_setpoint");
lpfnGetProcessID4 = GetProcAddress(HMODULE
    (hGetProcIDDLL),"Tiab_PID_get_setpoint");
lpfnGetProcessID5 = GetProcAddress(HMODULE
    (hGetProcIDDLL),"Tiab_PID_get_modes");
lpfnGetProcessID6 = GetProcAddress(HMODULE
    (hGetProcIDDLL),"Tiab_PID_set_mode");
lpfnGetProcessID7 = GetProcAddress(HMODULE
    (hGetProcIDDLL),"Tiab_CL_config_mode"); //Select the mode of the
    replay & logging module.
lpfnGetProcessID8 = GetProcAddress(HMODULE
    (hGetProcIDDLL),"Tiab_CL_config_replay");
lpfnGetProcessID9 = GetProcAddress(HMODULE
    (hGetProcIDDLL),"Tiab_CL_config_logging"); //Configure data logging
    (output data)
lpfnGetProcessID10 = GetProcAddress(HMODULE
    (hGetProcIDDLL),"Tiab_CL_start");
lpfnGetProcessID11 = GetProcAddress(HMODULE
    (hGetProcIDDLL),"Tiab_CL_get_busy");
lpfnGetProcessID12 = GetProcAddress(HMODULE
    (hGetProcIDDLL),"Tiab_write_scalar");
lpfnGetProcessID13 = GetProcAddress(HMODULE
    (hGetProcIDDLL),"Tiab_read_scalar");
lpfnGetProcessID14 = GetProcAddress(HMODULE
    (hGetProcIDDLL),"Tiab_CL_config_log_channels");
lpfnGetProcessID15 = GetProcAddress(HMODULE
    (hGetProcIDDLL),"Tiab_read_analog_inputs");
lpfnGetProcessID16 = GetProcAddress(HMODULE
    (hGetProcIDDLL),"Tiab_CL_get_status");
lpfnGetProcessID17 = GetProcAddress(HMODULE
```

```
        (hGetProcIDDLL),"Tiab_CL_start");
    lpfnGetProcessID19 = GetProcAddress(HMODULE
        (hGetProcIDDLL),"Tiab_CL_stop");
    lpfnGetProcessID20 = GetProcAddress(HMODULE
        (hGetProcIDDLL),"Tiab_PID_set_drive_gain");

//try{
 //Here is the data we want.
  data_t data;
  record_st header;

  const char * filename = "FilenameInput.csv";
  // Here is the file containing the data. Read it into data.
  ifstream infile( filename );
  infile >> header; //the 1st line is a header

  cout << "Your CSV file contains " << header.size() << " records.\n";

  string mode_h = header[0];
  double Mode = string_to_double(mode_h);
  string TestType = header[2];
  string strfileIn = header[1];
  string MaxTime_h = header[3];
  double MaxTime = string_to_double(MaxTime_h);
  double MaxTime1 = 0;
  string SampleNum = header[4];
  string strfileOut;

  //const char* fileIn;
  string PathIn = "C:\\Documents and Settings\\input";
  string PathOut = "C:\\Documents and Settings\\output";

  string TempfileIn = PathIn + strfileIn;
  char *fileIn = (char*)TempfileIn.c_str();

  // Complain if something went wrong.
  if (!infile.eof())
    {
    cout << "Rest of data\n";
   infile >> data;
    //return 1;
    }

  infile.close();

  // Otherwise, list some basic information about the file.
  cout << "Your CSV file contains " << data.size() << " records.\n";
  AxisVectors coord = CreateXYZVectors(data);

   WASIM::Connect();
   Console::WriteLine( "Connected!" );

   //Get mode to do: Scan=1/Indentation=2/US-raster=1
```

```
//int Mode = 1;

time_t secs=time(0);
struct tm * timeinfo;
char dateToday [80];

time(&secs);
timeinfo = localtime(&secs);
//tm *t=localtime(&secs);
strftime (dateToday,80,"%y%m%d",timeinfo);

//Move to middle point
int RampTime = 3;
int i;
stringstream files;
int NumPoints = data.size();
int AValue=10;
int Error=0;
int Contact = 0;
double Busy = 0;
//Get type of test -> to put name and get points

Console::WriteLine("Number of points to indent are: "+ NumPoints +"\n");

for(i=0;i<NumPoints;i++){
      //Convert i into a string to incorporated in the name
   ostringstream os;
   os << i+1;
   string istr = os.str();
   strfileOut = TestType + "-" + dateToday + "-" + SampleNum + "-T" + istr;
   string TempfileOut = PathOut + strfileOut;
   char *fileOut = (char*)TempfileOut.c_str();

   Console::WriteLine("Coordinates : " + coord.x[i] + "," + coord.y[i] +
       "," + coord.z[i] + "," + coord.yaw[i]+ "," + coord.pitch[i] + "\n");
   WASIM::SetPID2Position(i, RampTime, coord );
//vector <double> coord.x, vector <double> coord.y, vector <double>
    coord.yaw, vector <double> coord.pitch
//Mode 1 = Scan and Mode 2 = Indent
   if (TestType == "ind") { //If there is indentation
      AValue=0; //Read LoadCell
      Error = WASIM::ZIndIteration(0, i, coord,NumPoints);
      WASIM::SetAmplitud2One(2);
      Console::WriteLine("Config Continuos mode");
      WASIM::ConfigContinuousMode(fileIn,fileOut);

      if ((Contact ==1)||(Error==0)){
         if (Mode==1){ //Displacement controlled indentaion
            WASIM::CheckMode(Mode);
            WASIM::CheckMode(1);
         }

         if (Mode==2) {//Force controlled indentation
```

```
            WASIM::CheckMode(Mode);
            WASIM::CheckMode(2);
         }
      }
   }
   else{ //If scan
      Error = WASIM::ZLaserIteration(10);
      NumPoints=1; //Just in case
      WASIM::SetAmplitud2One(1);
      WASIM::ConfigContinuousMode(fileIn,fileOut);
   }

   Sleep(2000);
   if ((Contact ==1)||(Error==0)){
      WASIM::Start();
      Console::WriteLine("MaxTime" + MaxTime);
      MaxTime1=MaxTime*1000;
      Sleep(MaxTime1);
      Busy = WASIM::GetBusy();
      while (Busy==1){
         Sleep(1000);
         Busy = WASIM::GetBusy();
      }
      WASIM::CheckMode(1);
      Console::WriteLine("Moving z up to 80");
      WASIM::PIDSetPoint(1, 80, RampTime);
   }
   else{
      WASIM::Stop();
      Console::WriteLine("Error iterating z - out of range?");
   }
} //End For

Console::WriteLine("Moving z up to 80");
WASIM::PIDSetPoint(1, 80, RampTime); //Set Z up
Console::WriteLine("End");
Console::WriteLine("Press any key to continue...");
Console::ReadKey(true);
//}


}
```